MIT/WHOI 98-22

Massachusetts Institute of Technology
Woods Hole Oceanographic Institution

Joint Program in Oceanography/ Applied Ocean Science and Engineering

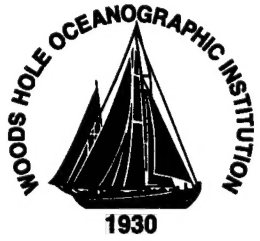

DOCTORAL DISSERTATION

The Fluvial Geochemistry of the Rivers of Eastern Siberia and Implications for the Effect of Climate on Weathering

by

Youngsook Huh

June 1998

MIT/WHOI

98-22

The Fluvial Geochemistry of the Rivers of Eastern Siberia and Implications for the Effect of Climate on Weathering

by

Youngsook Huh

Massachusetts Institute of Technology
Cambridge, Massachusetts 02139

and

Woods Hole Oceanographic Institution
Woods Hole, Massachusetts 02543

June 1998

DOCTORAL DISSERTATION

Funding was provided by the National Science Foundation Grants EAR-9304843 and EAR-9627613 and the Massachusetts Institute of Technology EAPS Student Research Fund.

Approved for publication; distribution unlimited.

Approved for Distribution:

Michael P. Bacon
Department of Marine Chemistry and Geochemistry

Paola Malanotte-Rizzoli
MIT Director of Joint Program

John W. Farrington
WHOI Dean of Graduate Studies

The Fluvial Geochemistry of the Rivers of Eastern Siberia and Implications for the Effect of Climate on Weathering

by

Youngsook Huh

B.S., Chemistry
Korea University, 1992

M.S., Physical Chemistry
Korea University, 1994

SUBMITTED IN PARTIAL FULFILLMENT OF THE REQUIREMENTS
FOR THE DEGREE OF

DOCTOR OF PHILOSOPHY

at the

MASSACHUSETTS INSTITUTE OF TECHNOLOGY

and the

WOODS HOLE OCEANOGRAPHIC INSTITUTION

June, 1998

Signature of Author _____
Joint Program in Oceanography/Applied Ocean Science and Engineering
Massachusetts Institute of Technology and Woods Hole Oceanographic Institution
May 1, 1998

Certified by _____
John M. Edmond
Professor of Geochemistry
Thesis Supervisor

Accepted by _____
Edward A. Boyle
Professor of Oceanography
Chair, Joint Committee for Chemical Oceanography

The Fluvial Geochemistry of the Rivers of Eastern Siberia and Implications for the Effect of Climate on Weathering

by

Youngsook Huh

Submitted to the Massachusetts Institute of Technology/Woods Hole Oceanographic Institution Joint Program in Oceanography/Applied Ocean Science and Engineering on May 1, 1998 in partial fulfillment of the requirements for the degree of Doctor of Philosophy.

Abstract

The dependence of weathering on climate (temperature and precipitation) forms the core of a negative feedback proposed to have maintained the Earth's atmospheric CO_2 within habitable limits for most of its history. This hypothesis has not been proven from field results. Data for chemical compositions and fluxes of periglacial rivers of the Russian Far East—the Lena, Yana, Indigirka, Kolyma, and Anadyr—were acquired and compared to the published dataset on tropical watersheds. Three broad geological divisions are made to facilitate the comparison—the stable basement shield, region of uplift and mountain building, and the sedimentary platform. In all three geologic regions no climatic effect on the rate of uptake of CO_2 by aluminosilicate weathering (ϕCO_2) was observed. This appears to be due to the unique non-glacial frost shattering processes which expose fresh rock surfaces and thus overcome the effect of temperature inhibition at high-latitudes. On the tropical shields, the lateritic cover builds up due to lack of topography, seals the weathering front from the climatic agents, and lowers weathering rates. There appear to be no primary climatic effects on weathering rates on the present Earth.

Thesis Supervisor: John M. Edmond
Title: Professor of Geochemistry

Acknowledgments

I would like to thank my advisor, John M. Edmond, and my committee members, Sam Bowring, Kathleen Ruttenberg, Karl Turekian, and Kelin Whipple, who have been completely supportive throughout my work with fresh insight and encouragement. Sam's generosity with access to his lab made the hundreds of Sr isotope measurement possible, which proved to be crucial to the data interpretation. Lui-Heung Chan taught me the art of measuring lithium isotope ratios and the rigor with which one should carry out scientific research. Paul E. Potter introduced me to the fascinating world of sandstone petrology and taught me a great deal about scientific writing and thinking.

Drew Coleman, Nancy Harris, Tom Blanchard, and Dave Senn helped me get adjusted to their labs. Mai-Yin Tsoi proved to be a great UROP student. Barry Grant rescued me from various laboratory problems. Alla Skorokhod patiently assisted with hectic travel arrangements, funding, and communication with the Russian colleagues.

The Joint Program offered me many research opportunities. Gera Panteleyev introduced us to the River Navigation Authority of Yakutia, and I deeply regret his loss on a separate expedition to the Ob. Mark Kurz provided access to his lab for initial Sr isotope measurements and chaired both my proposal exam and the thesis defense. Thanks also go to my fellow Joint Program students for their suggestions and care.

The increasingly sensitive analytical facilities enable one to measure almost anything one sets his/her mind to. The problem now is access to interesting field areas. The River Navigation Authority of Yakutia and their consultant Dr. Alexandr Zaitsev of Moscow State Univ. made the important expeditions to Siberia feasible, and I gratefully acknowledge their generosity and help. The research was carried out with National Science Foundation grants EAR-9304843 and EAR-9627613 and the EAPS Student Research Fund.

Finally I would like to thank my family for being so supportive and giving me the incentive to finish on time.

Table of Contents

List of Figures

List of Tables

Chapter 1

Introduction: Effect of Climate on Weathering as Represented in Fluvial Geochemistry

The Role of Weathering in the Geochemical Carbon Cycle

All the evidence indicates that most of the world experienced a significant, if not monotonic, net cooling over the last 50 Ma. It was remarked on as early as a hundred years ago from fossil records of land animals and plants (Rayner, 1995) but is most clearly shown by the oxygen isotope record of benthic foraminifera (Fig. 1; Savin, 1977; Zachos *et al.*, 1994). Deep water temperatures as interpreted from the latter should be indicative of surface water temperatures at high latitudes where dense, cold water sinks to form deep water, i.e. they should be representative of the most extreme T-S conditions globally. Regardless of the assumption used for ice sheet volumes in the calculation of temperature, there is ~16°C temperature deterioration from the Eocene to the present (Miller *et al.*, 1987).

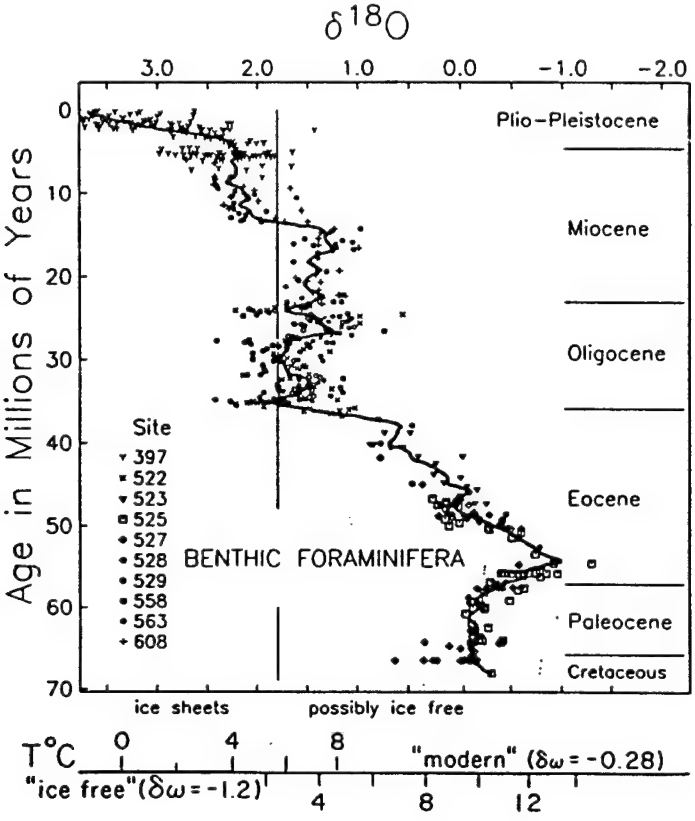

Figure 1. Composite benthic foraminiferal oxygen isotope record for Atlantic DSDP sites corrected to Cibicidoides and reported to PDB standard. From Miller *et al.*, 1987.

Since this long-term decline, unlike the Quaternary climatic fluctuations, cannot be caused by changes in orbital forcing, changes in the atmospheric thermal budget must be the cause. Variation in P_{CO_2} is the most plausible candidate as it gives rise to a strong greenhouse effect and as it has the potential to vary considerably on long timescales (Mitchell, 1989; Kasting, 1987). The processes that control the levels of P_{CO_2} over time are less well understood.

On multimillion year timescales, the reservoirs in the inorganic carbon cycle reduce down to the combined atmosphere-ocean-biosphere and rocks. The primary sources of atmospheric CO_2 are from the mantle, i.e. oceanic hotsprings, volcanoes, and the recycled component from deep-burial metamorphism, a simplified reaction of which is:

$$CaCO_3 + SiO_2 \leftrightarrow CaSiO_3 + CO_2$$

The major sinks are the weathering of aluminosilicates and carbonates. Atmospheric CO_2 reacts with water to give carbonic acid which, as a weak acid, dissociates to generate the protons necessary for weathering resulting in non-exchangeable bicarbonate in the dissolved load.

$$CO_2 + H_2O \leftrightarrow H_2CO_3 \leftrightarrow H^+ + HCO_3^-$$

The CO_2 consumed by weathering of carbonates is subsequently returned by deposition of calcium carbonate in the ocean:

$$Ca^{2+} + 2HCO_3^- \leftrightarrow CaCO_3 + CO_2$$

Therefore, aluminosilicate weathering is the only important sink on timescales of millions of years. The input and output fluxes of atmospheric CO_2 (~8×10^{18} moles per million

years) are very large compared to the mass of carbon in the atmosphere (~3 x 10^{18} moles) (Goddéris and François, 1995). Thus the atmosphere does not have the capacity to sustain large imbalances in the input and output fluxes, and it has been commonly assumed that there is a negative feedback to keep things in balance (Walker *et al.*, 1981; Berner and Caldeira, 1997).

Walker originally proposed a negative feedback mechanism by aluminosilicate weathering to explain the relative stability of the Earth's climate early in its history in spite of the "cool" young sun (Walker *et al.*, 1981). The crux of the hypothesis is embodied in the Clausius-Clapeyron equation. It states that the saturation vapor pressure of a liquid, P, increases almost exponentially with increasing temperature:

$$P(T) = P(T_0)\exp\left[\frac{\Delta H_{vap}}{R}\left(\frac{1}{T_0} - \frac{1}{T}\right)\right]$$

where ΔH_{vap} is the enthalpy of vaporization, T is temperature in Kelvin, T_0 is temperature at reference state, and R is the gas constant. The water vapor pressures measured at different latitudes closely follow the Clausius-Clapeyron relationship at all temperatures (Fig. 2; Webster, 1994). Increase in temperature leads to increased water vapor pressure, increased precipitation and runoff, increased weathering rates and hence increased uptake of CO_2. This then leads to a decrease in temperature due to the greenhouse effect, thereby closing the negative feedback cycle.

Past Work on Chemical Weathering

Although there is ample evidence in laboratory mineral dissolution experiments that reaction rates are dependent on temperature, there is as yet no field confirmation of the

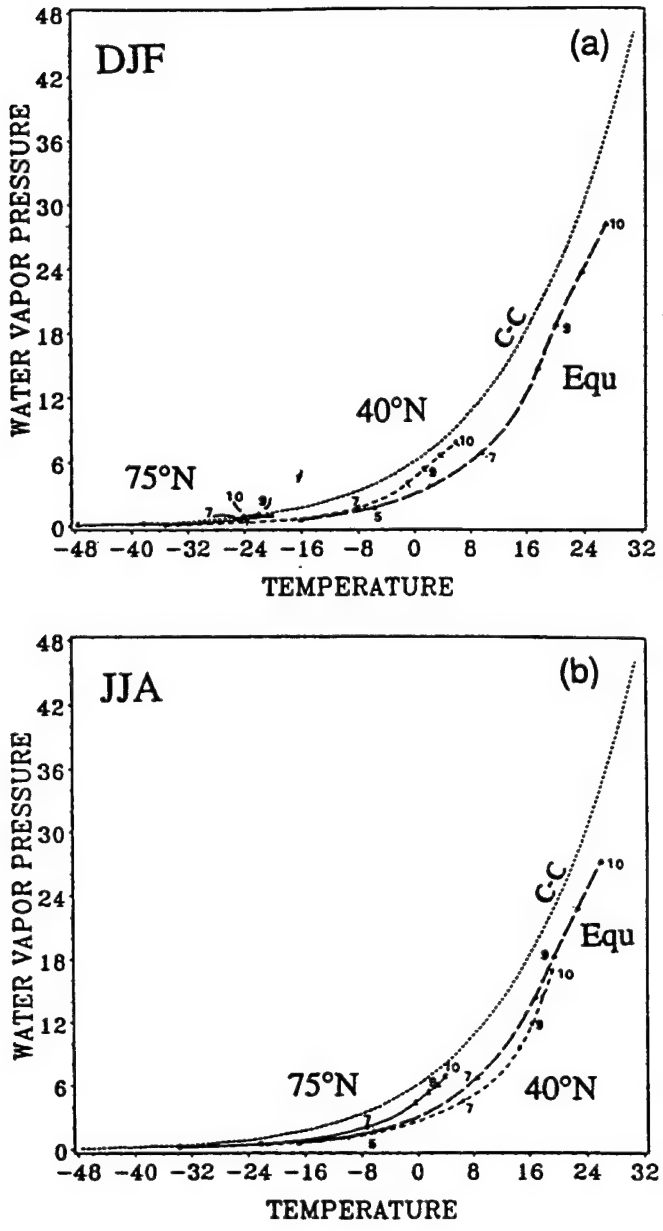

Figure 2. Atmospheric vapor pressure (mbar) as a function of temperature (°C) for mean atmospheres located at the equator (large dashes), 40°N (small dashes), and 75°N (solid curve) as a function of pressure levels in the vertical (marked in hundreds of mbars on curves) for (a) boreal winter (December-January-February) and (b) boreal summer (June-July-August). The dotted curve (C-C) is the Clausius-Clapeyron saturation vapor pressure. The environmental curves are consistently parallel to C-C at all temperatures. From Webster, 1994.

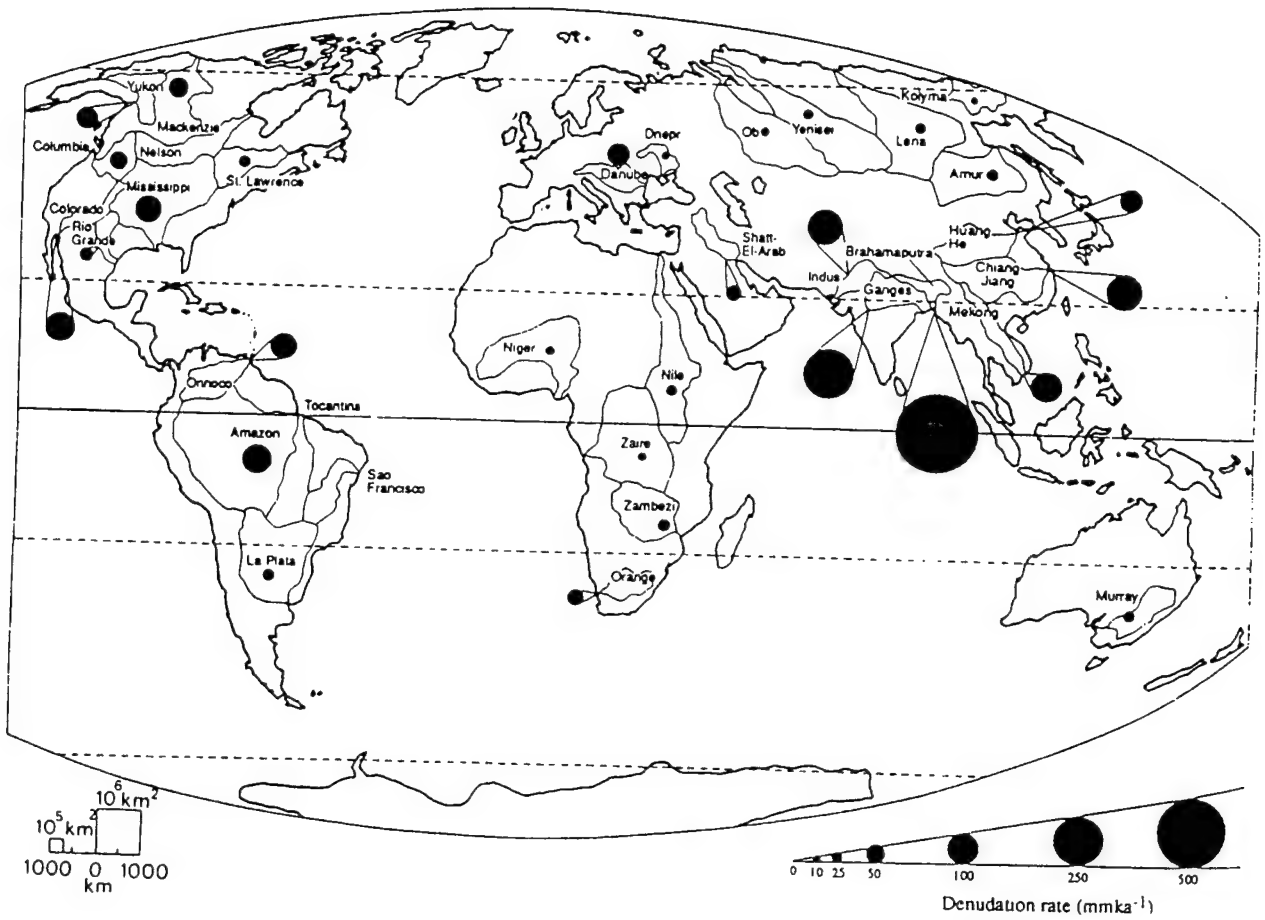

Figure 3. Locations and estimated total denudation rates for major externally drained basins. From Summerfield and Hulton, 1994.

negative feedback hypothesis. The only possible experiment in nature to test this idea is to exploit the present gradient of temperature with latitude (Fig. 3). Unfortunately, rivers in temperate latitudes are impacted by human activities, and the northern hemisphere landscapes are largely dominated by recent glaciations. Data from tropical rivers have been generated on the Amazon-Orinoco rivers draining the Andes mountains and the Guayana and Brazilian shields (Stallard and Edmond, 1983; Edmond *et al.*, 1995, 1996), on the Zaire (also called Congo) draining the Congo Shield (Négrel *et al.*, 1993), for the Ganges-Brahmaputra and Indus draining the Himalayas and its foreland basin (Sarin *et al.*, 1989; Krishnaswami *et al.*, 1992; Pande *et al.*, 1994; Trivedi *et al.*, 1995). The only comparable datasets in high latitudes are from the pioneering study of the Mackenzie by Reeder *et al.* (1972), though unfortunately they were not able to access the Canadian Shield due to logistical reasons, and from the Fraser and St. Lawrence (Cameron *et al.*, 1995; Yang *et al.*, 1995).

Ideal Features of the Siberian Rivers

To support this dearth of data at high latitudes, I have studied the large rivers of eastern Siberia, east of Lake Baikal. The area is comparable to the size of the contiguous United States and contains some of the last pristine basins. The rivers of Eastern Siberia account for about a third of the total discharge to the Arctic Ocean (Gordeev *et al.*, 1996) and offer an ideal opportunity to study weathering in pristine arctic/subarctic regions.

The climate is extreme; dominated by frost action, it bears a nice contrast with the tropics. Under about a meter of active seasonally melted layer the ground is perennially frozen to depths ranging from about 200-400 m. In some places the thickness of this permafrost layer can reach 1,600 m. In the southern discontinuous permafrost zone, there are pockets of unfrozen ground called taliks and the permafrost is ~30 m thick. The climate is continental with warm summers and very cold winters. Summer average temperature is

18-19°C and the winter average is -34~-50°C. The coldest inhabited settlement other than scientific bases on the ice caps is Verkhoyansk village on the Yana River, where the coldest recorded temperature is -69.8°C. Most of the study area is semi-arid with precipitation of ~200 mm/yr. For comparison, in the Amazon-Orinoco basin temperatures are ~28°C with little seasonal variation, and precipitation is ~2500 mm/yr.

Eastern Siberia, though it is dominated by frost action, was free from extensive ice sheets during the Last Glacial Maximum unlike much of North America and Europe (Velichko and Faustova, 1991). This is mainly due to the semi-arid climate and the fact that most of the precipitation occurs in summer. Figure 4 shows precipitable water in January going from 6 mm in the North Atlantic to 2-3 mm over Siberia. The meridional fluxes are also high (38 kg/m/s) over the North Atlantic but diminish rapidly to only 2-6 kg/m/s over Siberia (Serreze *et al.*, 1994). Most of the water vapor originates in the North Atlantic and is lost by the time it reaches Siberia. The absence of glaciers precludes weathering of glacial overburden that originated outside the basin.

The Russian Far East is diverse in topography and geology, making it feasible to draw comparisons to existing data from physical counterparts in the tropics. In order to make comparisons with lower latitude rivers, I have divided my dataset into three groups based on geology: 1) the Platform, 2) the Collisional/Accretionary zone, and 3) the Shield. A vast platform with classical marine sedimentary sequences and continental sediments cover most of the Siberian craton, and there are collisional mountain belts to the east. Aluminosilicate basement is exposed as the Aldan and Anabar shields on the craton. The Platform is 200-500 m in elevation. The Verkhoyansk and Cherskiy ranges of the Collision zone are 2,000 - 3,000 m. The elevation on the shield, >1,000 m, is comparable to that of the tropical shields. The Arctic coastal lowlands, with scattered lakes and bogs, lie to the north. The left bank tributaries of the Lena drain the carbonates and evaporites extending to the Precambrian and continental detrital sediments together reaching

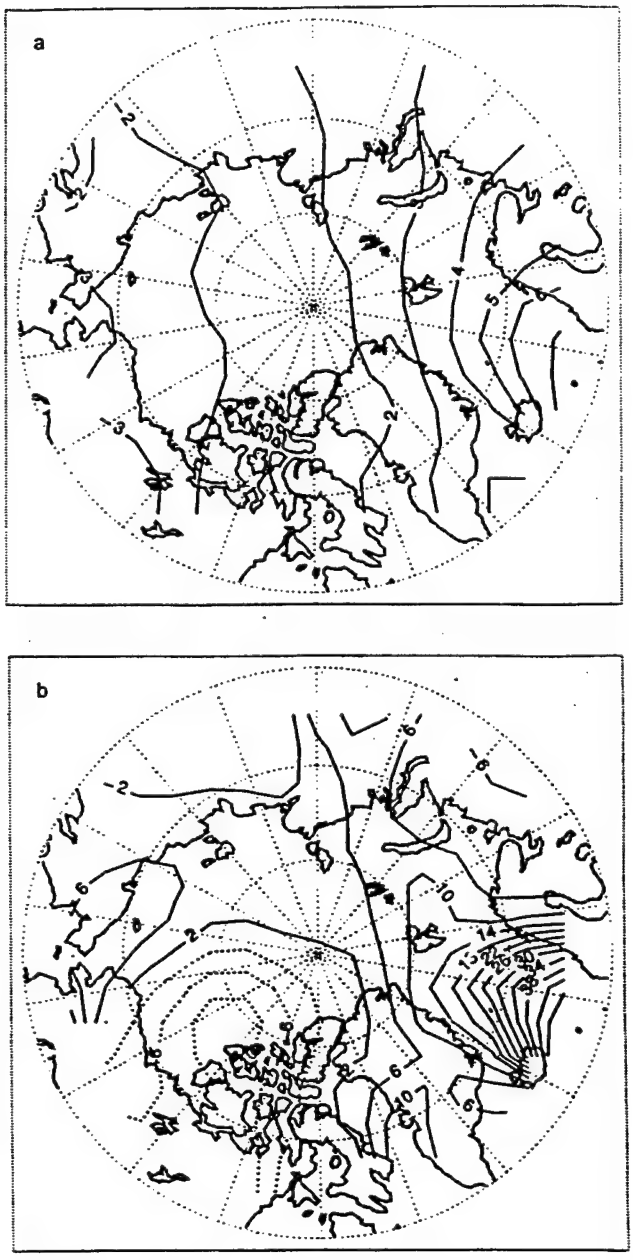

Figure 4. Fields in January of (a) precipitable water (mm) and (b) the vertically integrated meridional flux (kg/m/s) for the surface to 300 mbar layer. Positive values are northward fluxes and negative (dashed contours) are southward. From Serreze *et al.*, 1994.

thicknesses of 12 km in some areas. A similar terrain in the tropics is the platform in China drained by the Yangtze. The right bank tributaries of the lower Lena drain the Verkhoyansk foldbelt which is composed of detrital sediments of the slope and rise sequence of the pre-collisional Siberian craton. The Yana, Indigirka and Kolyma rivers drain a geologically complex region of arc basalts and acid intrusions formed by the collision and accretion of the Kolyma plate with the Siberian craton in the Mesozoic and of sedimentary accumulations on the cratonic fragments. These regions have geologic similarities to the eastern slope of the Northern Andes drained by the Amazon-Orinoco. The right bank tributaries of the Upper Lena and the Anabar drain the ancient igneous and metamorphic rocks of the Trans-Baikal Highlands and the Aldan Shield. Comparable terrain in the tropics are the Brazilian, Guayana and Congo shields drained by the Amazon, Orinoco and Congo. The sampling timetable is shown in Table 1.

Methods of Studying Weathering Rates

The two classical ways of studying weathering as a function of different parameters are by carrying out dissolution experiments in the laboratory under controlled settings and by examining clay weathering products and sedimentary records. Lab experiments are useful in deducing fundamental physico-chemical relationships, however they do not correctly simulate natural conditions (Anbeek *et al.*, 1994). Studying clay weathering products is attractive in that only aluminosilicate rocks form clays and therefore the complicating effect of carbonates and evaporites is absent. However Nd isotope studies show that the mean model age of clays is 2 billion years (Miller *et al.*, 1986). Very little clay is forming in the present weathering environment; most are relict from recycled shale. Denudation rates are dominated by mechanical weathering, but chemical weathering, which is the CO_2 sink and the parameter of importance in the geochemical carbon cycle, does not necessarily follow mechanical weathering (Fig. 5; Summerfield and Hulton, 1994).

Therefore the accumulation rates of deep sea detrital fans cannot be regarded as an index of chemical weathering.

Table 1. A chronological description of the expeditions to the rivers of eastern Siberia. Number of stations with the sample series names are given in brackets.

Date	River
Jul-Aug, 1991	Aldan (UL100; n=33)[1]
Aug, 1992	Kolyma (KY100; n=22)
Sep, 1992	Lena (UL200; n=7)[1]
Aug-Sep, 1993	Lake Baikal (LB100; n=11)[2]
Sep, 1993	Olenek (UL300; n=22)[2]
Jul-Aug, 1994	Upper Lena (UL400; n=46)[1]
Jul, 1994	Anabar and Olekma (UL500; n=16)[2]
Jul, 1995	Lower Lena (UL600; n=21)[1]
Aug, 1995	Yana (YN100; n=20), Omoloy (OM100; n=4)
Jul, 1996	Indigirka (IG100; n=21)
Aug, 1996	Upper Lena (UL700; n=16)[1]
Aug, 1997	Upper Aldan (UL800; n=11)[1]
Aug, 1997	Anadyr (AY100; n=9)
Sep, 1997	Magadan (MD100; n=3)

[1] Lena above Aldan and Aldan @ mouth samples were collected on these expeditions to monitor interannual variations. [2] "Grab" samples collected by other people are not filtered in the field. Previous experience in the Amazon showed these are good for major elements and $^{87}Sr/^{86}Sr$ ratios.

Measurement of the cation and anion composition of the dissolved load in rivers permits one to backtrack to the types of minerals being weathered. For example, high Na and high Cl concentrations can only be explained by dissolution of halites; high Ca and high alkalinity can derive from either carbonates or Ca-aluminosilicates, but high Si in addition to Ca and alkalinity, or high Na with low Cl definitely indicate aluminosilicate weathering. High SO_4, low alkalinity, and high Si can only come from weathering of

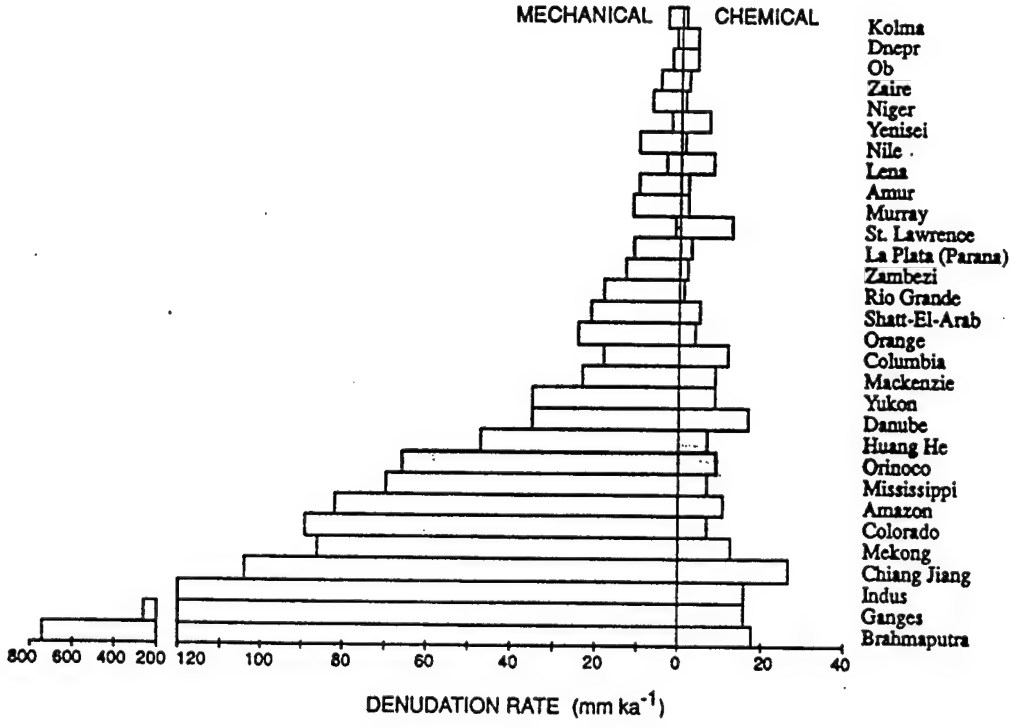

Figure 5. Histograms comparing mechanical and chemical denudation rates for major externally drained basins. From Summerfield and Hulton, 1994.

sulfides, as the sulfuric acid released can further dissolve proximal silicate rocks. In the case of aluminosilicate weathering, silica to cation ratios show the extent of reaction. For example, weathering of albite to Na-montmorillonite results in release of Si and Na into solution in the ratio 1.7. If the reaction progresses from albite to montmorillonite and further to kaolinite, the Si:Na release ratio is 2.0. If the reaction proceeds all the way to gibbsite, the ratio is 2.5. The cations are lost earlier in the reaction sequence and therefore as the weathering becomes more intense, the silica fraction increases.

Figure 6 shows a compilation of the major river basins of the Western Cordillera of the Americas (Edmond and Huh, 1997). Rivers draining the Orinoco Andes show carbonates (high Ca and alkalinity), evaporites (high $Cl+SO_4$ and Na), aluminosilicate (high Ca, alkalinity and Si), sulfide (low alkalinity, high Si and SO_4), and very intense

weathering (Si dominance). In the Amazon basin there is a range from high evaporites to carbonates to aluminosilicates to intensive weathering. In the Mackenzie carbonates and evaporites are dominant. The characteristically low Si values in that system may be due to biogenic removal of Si by diatom growth in thermokarst lakes and bogs that are prevalent in high latitude lowland regions. The Fraser shows carbonate and aluminosilicate weathering with a more basaltic composition as shown by relatively high Mg and Si. It is very important to distinguish the weathering of the aluminosilicate fraction from carbonate-evaporite dissolution, because the former is the major CO_2 sink as mentioned previously, but the latter can overwhelm the fluxes because of the lability of carbonates and evaporites to dissolution reactions. Strontium isotopes can be used to resolve this effect. The $^{87}Sr/^{86}Sr$ ratio of seawater for the past 500 Ma. as recorded in marine carbonates shows that limestones or evaporites that originally precipitated from seawater must fall between ~0.7065 and 0.7091.

A compilation of the available strontium isotope data in the river dissolved load is shown in Fig. 7. The present seawater value is 0.7091. The average river value is 0.712 and much less concentrated (0.89 µmol/kg) than seawater (90 µmol/kg) (Palmer and Edmond, 1989). Weathering of aluminosilicate rocks gives radiogenic but highly variable isotope ratios depending on the age and content of the parent Rb. Riverine concentrations are low because the aluminosilicates weather slowly relative to $CaCO_3$ and evaporites. Rivers draining the Guayana Shield have very radiogenic values (> 0.9) but with low concentrations. Basalts have very unradiogenic values, as low as 0.704. Weathering of carbonates produces ratios between 0.7065 and 0.7091 depending on age, and much higher concentrations because carbonate weathering is orders of magnitude faster than aluminosilicate weathering; this is the field where most of the data cluster in the $^{87}Sr/^{86}Sr$ vs. 1/Sr diagram (Fig. 7). Overall the pattern of distributions reflect a mixture of these three endmembers: carbonate/evaporite, silicic shields, and basalt. The only exception are

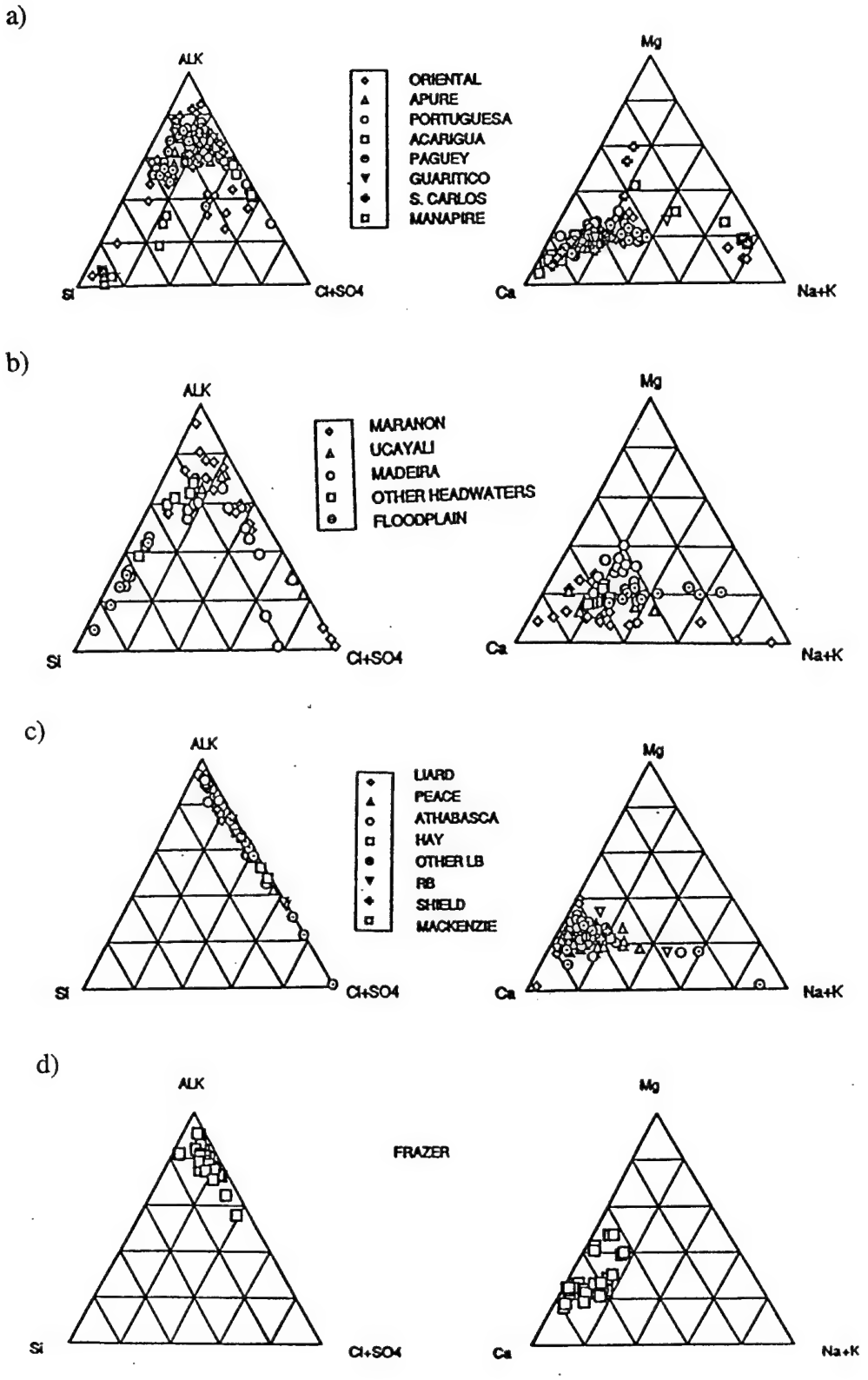

Figure 6. Ternary plots for the streams draining the Andes, (a) Orinoco and (b) Amazon, and Rockies, (c) Mackenzie and (d) Fraser. From Edmond and Huh, 1997.

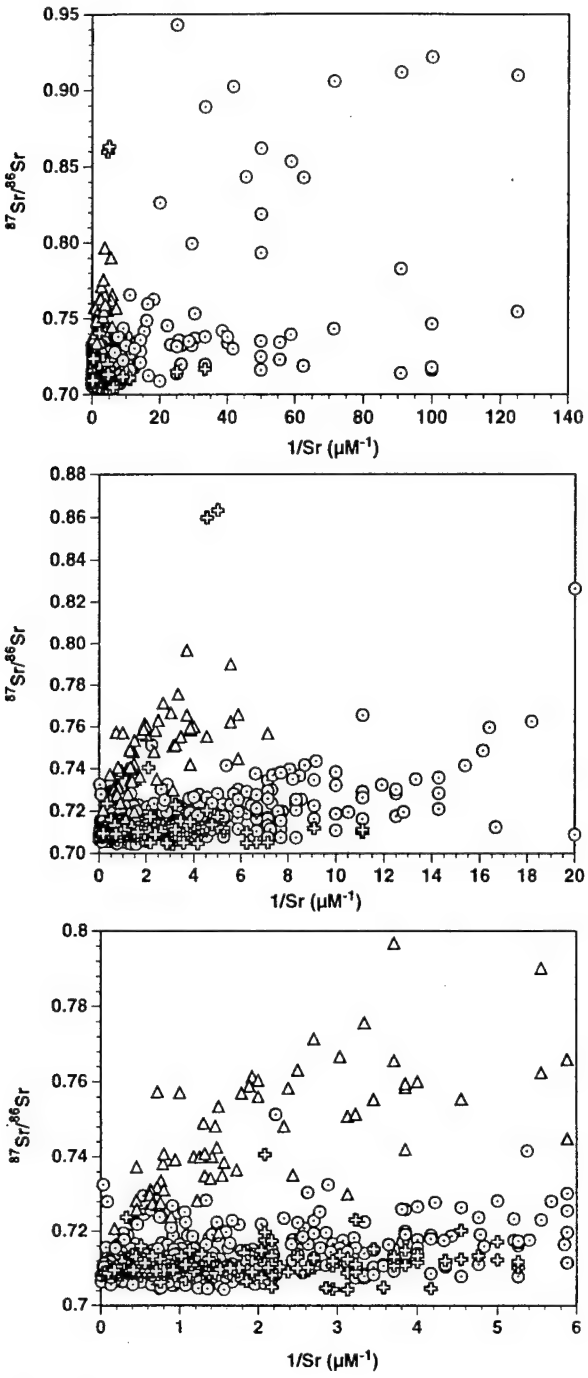

Figure 7. Available $^{87}Sr/^{86}Sr$ ratios for world rivers. Triangles—Himalayan rivers; Open Crosses—Siberian rivers; Dotted Circle—Other rivers. Data from Brass, 1976; Fisher and Stueber, 1976; Wadleigh *et al.*, 1985; Albarède and Michard, 1987; Goldstein and Jacobsen, 1987; Palmer and Edmond, 1989, 1992; Ingram and Sloan, 1992; Krishnaswami *et al.*, 1992; Négrel *et al.*, 1993; Blum *et al.*, 1994; Pande *et al.*, 1994; Cameron *et al.*, 1995; Trivedi *et al.*, 1995; Zhang *et al.*, 1995; Yang *et al.*, 1996; Huh *et al.*, 1998a,b; Huh and Edmond, ms.

the Himalayan rivers which are very radiogenic and have high Sr concentrations (Edmond, 1992; Krishnaswami *et al.*, 1992).

When carbonates are present even in minor quantities, because of their fast dissolution kinetics, their isotopic signal will dominate. From this general trend, we can assume the following. When strontium ratios are above 0.71 aluminosilicate weathering is dominant. When ratios are between 0.7065 and 0.7095 carbonate weathering dominates. When Sr ratios are below 0.706 basalts are being weathered.

Layout of the Thesis

The thesis will consist of 5 parts. Chapters 2, 3, and 4 will deal with the fluvial datasets for each of the three geologic terrains, the Platform, the Collision zone, and the Shield. As a preliminary attempt at obtaining an index for weathering intensity, the lithium isotopic system in continental fluvial systems is explored in chapter 5.

References

Albarède F. and Michard A. (1987) Evidence for slowly changing $^{87}Sr/^{86}Sr$ in runoff from freshwater limestones of southern France. *Chem. Geol.* **64**, 55-65.

Anbeek C., van Breemen N., Meijer E. L., and van der Plas L. (1994) The dissolution of naturally weathered feldspar and quartz. *Geochim. Cosmochim. Acta* **58**, 4601-4613.

Berner R. A. and Caldeira K. (1997) The need for mass balance and feedback in the geochemical carbon cycle. *Geology* **25**, 955-956.

Blum J. D., Erel Y., and Brown K. (1994) $^{87}Sr/^{86}Sr$ ratios of Sierra Nevada stream waters: Implications for relative mineral weathering rates. *Geochim. Cosmochim. Acta* **58**, 5019-5025.

Brass G. W. (1976) The variation of marine $^{87}Sr/^{86}Sr$ ratio during Phanerozoic time: interpretation using a flux model. *Geochim. Cosmochim. Acta* **40**, 721-730.

Cameron E. M., Hall G. E. M., Veizer J., and Krouse H. R. (1995) Isotopic and elemental hydrogeochemistry of a major river system: Fraser River, British Columbia, Canada. *Chem. Geol.* **122**, 149-169.

Edmond J. M. (1992) Himalayan tectonics, weathering processes, and the strontium isotope record in marine limestones. *Science* **258**, 1594-1597.

Edmond J. M. and Huh Y. (1997) Chemical weathering yields from basement and orogenic terrains in hot and cold climates. In *Tectonic Uplift and Climate Change*. (ed. W. F. Ruddiman), Plenum Press, pp. 329-351.

Edmond J. M., Palmer M. R., Measures C. I., Grant B., and Stallard R. F. (1995) The fluvial geochemistry and denudation rate of the Guayana Shield in Venezuela, Colombia and Brazil. *Geochim. Cosmochim. Acta* **59**, 3301-3325.

Edmond J. M., Palmer M. R., Measures C. I., Brown E. T., and Huh Y. (1996) Fluvial geochemistry of the eastern slope of the northeastern Andes and its foredeep in the drainage of the Orinoco in Colombia and Venezuela. *Geochim. Cosmochim. Acta* **60**, 2949-2976.

Fisher R. and Stueber A. M. (1976) Strontium isotopes in selected streams within the Susquehanna River basin. *Water Resources Res.* **12**, 1061-1068.

Goddéris Y. and François L. M. (1995) The Cenozoic evolution of the strontium and carbon cycles: relative importance of continental erosion and mantle exchanges. *Chem. Geol.* **126**, 169-190.

Goldstein S. J. and Jacobsen S. B. (1987) The Nd and Sr isotopic systematics of river-water dissolved material: Implications for the sources of Nd and Sr in seawater. *Chem. Geol. (Isotope Geosciences Section)* **66**, 245-272.

Gordeev V. V., Martin J. M., Sidorov I. S., and Sidorova M. V. (1996) A reassessment of the Eurasian river input of water, sediment, major elements and nutrients to the Arctic Ocean. *Am. J. Sci.* **296**, 664-691.

Huh Y. and Edmond J. M. (ms) The fluvial geochemistry of the rivers of eastern Siberia III: Tributaries of the Lena and Anabar draining the basement terrain of the Siberian Craton and the Trans-Baikal Highlands. *Geochim. Cosmochim. Acta* submitted, March 1998.

Huh Y., Tsoi M.-Y., Zaitsev A., and Edmond J. M. (1998a) The fluvial geochemistry of the rivers of Eastern Siberia I: Tributaries of the Lena River draining the sedimentary platform of the Siberian Craton. *Geochim. Cosmochim. Acta* in press.

Huh Y., Panteleyev G., Babich D., Zaitsev A., and Edmond J. M. (1998b) The fluvial geochemistry of the rivers of Eastern Siberia II: Tributaries of the Lena, Omoloy, Yana, Indigirka, Kolyma, and Anadyr draining the collisional/accretionary zone. *Geochim. Cosmochim. Acta* in press.

Ingram B. L. and Sloan D. (1992) Strontium isotopic composition of estuarine sediments as paleosalinity-paleoclimate indicator. *Science* **255**, 68-72.

Kasting J. F. (1987) Theoretical constraints on oxygen and carbon dioxide concentrations in the Precambrian atmosphere. *Precam. Res.* **34**, 205-229.

Krishnaswami S., Trivedi J. R., Sarin M. M., Ramesh R., and Sharma K. K. (1992) Strontium isotopes and rubidium in the Ganga-Brahmaputra river system: Weathering in

the Himalaya, fluxes to the Bay of Bengal and contributions to the evolution of oceanic $^{87}Sr/^{86}Sr$. *Earth Planet. Sci. Lett.* **109**, 243-253.

Miller K. G., Fairbanks R. G., and Mountain G. S. (1987) Tertiary oxygen isotope synthesis, sea level history, and continental margin erosion. *Paleoceanography* **2**, 1-19.

Mitchell J. F. B. (1989) The "greenhouse" effect and climate change. *Rev. Geophys* **27**, 115-139.

Négrel P., Allègre C. J., Dupré B., and Lewin E. (1993) Erosion sources determined by inversion of major and trace element ratios and strontium isotopic ratios in river water: The Congo Basin case. *Earth Planet. Sci. Lett.* **120**, 59-76.

Palmer M. R. and Edmond J. M. (1989) The strontium isotope budget of the modern ocean. *Earth Planet. Sci. Lett.* **92**, 11-26.

Palmer M. R. and Edmond J. M. (1992) Controls over the strontium isotope composition of river water. *Geochim. Cosmochim. Acta* **56**, 2099-2111.

Pande K., Sarin M. M., Trivedi J. R., Krishnaswami S., and Sharma K. K. (1994) The Indus river system (India-Pakistan): Major-ion chemistry, uranium and strontium isotopes. *Chem. Geol.* **116**, 245-259.

Potter P. E. (1994) Modern sands of South America: composition, provenance and global significance. *Geol. Rundsch.* **83**, 212-232.

Rayner R. J. (1995) The palaeoclimate of the Karoo: evidence from plant fossils. *Palaeogeography, Palaeoclimatology, Palaeoecology* **119**, 385-394.

Reeder S. W., Hitchon B., and Levinson A. A. (1972) Hydrogeochemistry of the surface waters of the Mackenzie River drainage basin, Canada—I. Factors controlling inorganic composition. *Geochim. Cosmochim. Acta* **36**, 825-865.

Sarin M. M., Krishnaswami S., Dilli K., Somayajulu B. L. K., and Moore W. S. (1989) Major ion chemistry of the Ganga-Brahmaputra river system: Weathering processes and fluxes to the Bay of Bengal. *Geochim. Cosmochim. Acta* **53**, 997-1009.

Savin S. M. (1977) The history of the Earth's surface temperature during the past 100 million years. *Annu. Rev. Earth Planet. Sci.* **5**, 319-355.

Serreze M. C., Rehder M. C., Barry R. G., and Kahl J. D. (1994) A climatological data base of arctic water vapor characteristics. *Polar Geography and Geology* **18**, 63-75.

Stallard R. F. and Edmond J. M. (1983) Geochemistry of the Amazon 2. The influence of geology and weathering environment on the dissolved load. *J. Geophys. Res.* **88**, 9671-9688.

Summerfield M. A. and Hulton N. H. (1994) Natural controls of fluvial denudation rates in major world drainage basins. *J. Geophys. Res.* **99**, 13,871-13,883.

Trivedi J. R., Pande K., Krishnaswami S., and Sarin M. M. (1995) Sr isotopes in rivers of India and Pakistan: A reconnaissance study. *Current Science* **69**, 171-178.

Velichko A. A. and Faustova M. A. (1991) Reconstruction of the last post-Pleistocene glaciation of the northern hemisphere (18-20 thousand years ago). *Doklady Akademy Nauk USSR* 223-225.

Wadleigh M. A., Veizer J., and Brooks C. (1985) Strontium and its isotopes in Canadian rivers: Fluxes and global implications. *Geochim. Cosmochim. Acta* **49**, 1727-1736.

Walker J. C. G., Hays P. B., and Kasting J. F. (1981) A negative feedback mechanism for the long-term stabilization of Earth's surface temperature. *J. Geophys. Res.* **86**, 9776-9782.

Webster P. J. (1994) The role of hydrological processes in ocean-atmosphere interactions. *Rev. Geophys* **32**, 427-476.

Yang C., Telmer K., and Veizer J. (1995) Chemical dynamics of the St. Lawrence riverine system: ∂D_{H2O}, $\partial^{18}O_{H2O}$, $\partial^{13}C_{DIC}$, $\partial^{34}S_{Sulfate}$, and dissolved $^{87}Sr/^{86}Sr$. *Geochim. Cosmochim. Acta* **60**, 851-866.

Zachos J. C., Stott L. D., and Lohmann K. C. (1994) Evolution of Early Cenozoic marine temperatures. *Paleoceanography* **9**, 353-387.

Zhang J., Takahashi K., Wushiki H., Yabuki S., Xiong J., and Masuda A. (1995) Water geochemistry of the rivers around the Taklimakan Desert (NW China): Crustal weathering and evaporation processes in arid land. *Chem. Geol.* **119**, 225-237.

Chapter 2

The Fluvial Geochemistry of the Rivers of Eastern Siberia I: Tributaries of the Lena River Draining the Sedimentary Platform of the Siberian Craton*

* Huh Y., Tsoi M.-Y., Zaitsev A., and Edmond J. M. (1998) The fluvial geochemistry of the rivers of Eastern Siberia I: Tributaries of the Lena River draining the sedimentary platform of the Siberian Craton. *Geochim. Cosmochim. Acta,* in press (February 12, 1998). Permission requested from Elsevier Science LTD.

Abstract

The response of continental weathering rates to changing climate and atmospheric P_{CO_2} is of considerable importance both to the interpretation of the geological sedimentary record and to predictions of the effects of future anthropogenic influences. While comprehensive work on the controlling mechanisms of contemporary chemical and mechanical weathering has been carried out in the tropics and, to a lesser extent, in the strongly perturbed northern temperate latitudes, very little is known about the peri-glacial environments in the sub-arctic and arctic. Thus, the effects of climate, essentially temperature and runoff, on the rates of atmospheric CO_2 consumption by weathering are not well quantified at this climatic extreme. To remedy this lack a comprehensive survey has been carried out of the geochemistry of the large rivers of Eastern Siberia, the Lena, Yana, Indigirka, Kolyma, Anadyr and numerous lesser streams which drain a pristine, high latitude region that has not experienced the pervasive effects of glaciation and subsequent anthropogenic impacts common to western Eurasia and North America.

The scale of the terrain sampled, in terms of area, is comparable to that of the continental United States or the Amazon/Orinoco and includes a similarly diverse range of geologic and climatic environments. In this paper the chemical fluxes from the western region, the very large, ancient and geologically stable sedimentary basin, Precambrian to Quaternary, of the Siberian Platform will be presented and compared to equivalent published results from analogous terrains in the tropical basins of China. While the range in the chemical signatures of the various tributaries included here (~60 sampled) is large, this mainly reflects lithology rather than the weathering environment. The areal chemical fluxes are comparable to those of the Chinese rivers being dominated by the dissolution of carbonates and evaporites. The net consumption of atmospheric CO_2 by aluminosilicate weathering is minor, as it is in the Chinese river basins. It is much smaller than in active orogenic belts in similar latitudes, e.g. the Fraser and Yukon, but comparable to those of

the Mackenzie tributaries that drain the eastern slope of the Rockies. Lithology exerts the dominant influence in determining the weathering yield from sedimentary terrains, and for a largely carbonate/evaporite terrain climate does not have a direct effect.

Introduction

The fluvial flux of dissolved material to the oceans is a reflection, by poorly understood mechanisms, of the environmental conditions prevailing over the continental surface. Given that chemical processes interior to the oceans, e.g. hydrothermal activity, diagenesis, etc., are either relatively stable or their variations amenable to interpretation, then the chemical signal imprinted on marine sediments during their accumulation records the general evolution and secondary changes of the surface environment of the Earth over geologic time. The inversion of the sedimentary record to give this information is the crux. However the fluvial fluxes from individual drainages are as diverse as the terrains themselves. Therefore it is not likely that a quantitative accounting is feasible. Rather, the problem is one of determining relative responses to change rather than absolutes. Interpretation is complicated by the fact that the weathering of exposed aluminosilicates is a sink for atmospheric CO_2 and hence is itself a potential determinant on climate change. Climate and weathering environment may therefore be closely coupled.

Observations show that the fluvial chemistry of world rivers in both stable and tectonically active regimes is dominated by the rapid weathering of biogenic and inorganic carbonates and evaporites and the slower dissolution of sedimentary aluminosilicate rocks—shales and sandstones—with relatively minor contributions from primary basement formations (Meybeck, 1986; Berner and Berner, 1987). Approximately 80% of the land surface is covered by sediments (Ronov, 1982) in the form of platform cover and uplifted margins in continental foldbelts. The concentration of total dissolved solids in waters draining sedimentary rocks is at least twice that in waters draining igneous and

metamorphic terrains (Holland, 1978). Extraction of the net CO_2 sink term is therefore difficult. Systematic work on the chemical manifestations of such geology in reasonably unperturbed river systems has been done mainly in tropical and temperate regions, on platforms e.g. China (Carbon Cycle Research Unit, 1982; Hu *et al.*, 1982; Gan *et al.*, 1983; Gan, 1985; Zhang *et al.*, 1990), southern India (Trivedi *et al.*, 1995), and central Africa (Négrel *et al.*, 1993) and in the continental foldbelts of the Americas (Edmond *et al.*, 1996). There is very little comparative data from high latitudes predominantly due to the difficulty of access (Reeder *et al.*, 171). Additionally, the pervasive influence of glaciation in North America and Baltica results in a cover of morainic debris of heterogeneous origin and composition which complicates the interpretation of the fluvial data (Newton *et al.*, 1987). Nevertheless the response of these weathering regimes to regional and global climate change at all time scales, in particular the effect on atmospheric P_{CO_2}, is currently a question of some importance since anthropogenic climatic impacts are expected to be strongly enhanced at high northern latitudes as compared to the global average (Hansen *et al.*, 1983; Cuffey *et al.*, 1995).

The rivers of Eastern Siberia (Fig. 1), east of Lake Baikal, are ideal for such studies in that the climate is extreme yet, due to their aridity, the basins have never been glaciated except in the highest alpine areas (Arkhipov *et al.*, 1986; Velichko and Faustova, 1991). The region contains a very wide range of geologic and tectonic environments and the complete spectrum of climatic and vegetational zones characteristic of continental interiors at middle and high latitudes (Lydolph, 1977; Zonenshain *et al.*, 1990). The river basins are pristine, with populations and economic activities at similar or much lesser scales as compared to those of the Yukon and the Mackenzie in North America. Previously reported data on the fluvial geochemistry have been restricted to samples from the Lena delta outlet and the estuarine plume (Gordeev and Sidorov, 1993; Gordeev *et al.*, 1996; French-Russian SPASIBA Program: See Marine Chemistry, Vol. 143, 1996 for major results; German Laptev Sea Program: see Reports of Polar Research, Vol. 176, 1996). As the

first in a series of studies of the major rivers that drain the sub-arctic and arctic terrains of Eastern Siberia—the Lena, Yana, Indigirka, Kolyma, Anadyr—presented here are the results of geochemical analyses of the streams of the Siberian Platform within the catchment basins of the Lena and the Olenek (Fig. 1). Through a comparison with an equivalent tropical terrain, the Chinese Platform, the influence of climate on weathering processes and fluxes in large sedimentary basins will be examined. The rivers in sedimentary platforms in turn will be compared to those in active orogenic zones—the Fraser and Mackenzie draining the Rockies.

Information of all types concerning the remote areas of Siberia discussed here is largely contained in the Russian literature and is therefore inaccessible and unfamiliar to the Western reader. An attempt will be made below to summarize what is available in order to establish the context of the chemical data.

Location

The Lena is the major river draining the Siberian Platform (Fig. 1,2). Its channel is ~4,260 km in length, discharge is 525 x 10^6 km^3/yr, and its basin occupies an area of ~2.5 x 10^6 km^2 between 52°N at the western edge of Lake Baikal and 73°N on the delta in the Laptev Sea and between 106°E (L. Baikal) and 138°E (slightly east of the Sea of Okhotsk). The basin occupies the eastern half of the Siberian craton, the central structure of the northeastern Eurasian continent. It is bordered in the east by the Verkhoyansk foldbelt and the associated Jurassic-Cretaceous collision zone between the Omolon-Kolyma massif and the Siberian Craton and in the south by the Proterozoic Trans-Baikal Highlands (TBH) and the Archean Aldan Shield (Fig. 2). The Triassic Tungussian flood basalt province occupies the broad area to the west of the Lena River drainage. The main channel of the river drains to the Laptev Sea (Arctic Ocean) to the north. Whereas the borders of the basin are composed of exposed igneous and metamorphic rocks and uplifted detrital sediments, the

interior is a stable craton with a sedimentary cover several kilometers thick, Precambrian to Quaternary in age, composed of marine carbonates and evaporites and continental deposits—sandstone, shale, red beds, and coal. This catchment geology, mountains in the headwaters and massive, long-lived sedimentary basins in the interior, is similar to that of the other Siberian rivers to the west and to major world rivers such as the Mississippi and the Yangtze.

The Lena rises on the northern slope of the uplifted mountains of the Baikal Rift at an altitude of ~1,450 m. In its upper course, the river runs west to east parallel to the right-bank basement outcrops of the TBH and the Aldan Shield (Fig. 2). The channel is deeply incised with bounding cliffs between ~25 and 150 m high and transports gravel and coarse sand. Karst formation is pronounced in the limestones particularly on the right bank ~280 km above Yakutsk, the "Lena Pillars". The channel then broadens considerably with numerous distributaries, islands and large sand bars; active dune fields occur on the banks fed by these exposed bars at falling stage. At the confluence with its largest tributary, the Aldan, below Yakutsk the river is several kilometers wide with bed material composed exclusively of sand. The Aldan is a high energy stream transporting coarse gravel. The bed and bank materials are strongly asymmetrical across the Lena main channel for several hundred kilometers below the confluence. Below the Aldan confluence the course of the river makes a sharp northwards turn and continues north against the flanks of the Verkhoyansk Range in a broad swampy valley dotted with numerous thermokarst lakes and ponds. The Lena is an ancient antecedent stream that has supplied detrital sediment from the Aldan Shield to the eastern Siberian margin since the Early Precambrian (Zonenshain *et al.*, 1990). The diachronous collision with the Kolyma terrain that produced the Verkhoyansk progressively diverted its course to the north. This is seen clearly at the Lena "chute", the deep, narrow defile north of Kusur above the delta, where the Lena cuts through the northwestern limb of the Verkhoyansk range in a single, narrow, very swift

channel. Here the river is funneled into a narrow gorge between bald, arid mountains before debouching into the enormous delta.

The Olenek is a minor river (219 x 10^3 km^2; 35.8 km^3/yr) to the west of the Lena also partly draining the platform. It heads on the southern slope of the Anabar Shield, a domal uplift of the Early Precambrian basement to the northwest of the Lena basin. It then flows around this cratonic block to drain into the Laptev Sea. The Nizhnyaya Tunguska, also outside of the Lena basin, has its major course in the Tungussian Traps and feeds the Yenisey to the west; however, the headwater sample is in the Platform. Appropriate data from both streams are included in this discussion.

Climate and Vegetation

The region experiences the most severe of continental climates with cool, wet summers and very cold, dry winters. Precipitation occurs mostly in summer with the result that the region is free from glaciers except in the highest alpine elevations, despite the cold winter temperatures. In the Pleistocene when western Siberia, Baltica, and North America all supported large ice caps (Denton and Hughes, 1981; Arkhipov *et al.*, 1986; Velichko and Faustova, 1991) this region was free from glacial cover although underlain by a thick layer of permafrost.

In winter the Asiatic high develops just south of Lake Baikal with its extension and secondary node in the Yana-Indigirka-Kolyma region to the east of the Lena basin. This high does not extend very far above the surface but the trough in the upper atmosphere is flooded by cold arctic air reinforcing its stability. The combination of a stable, dry airmass and long periods of darkness results in extreme cold and aridity. In summer, the trough between the two high nodes is a convenient passway for cyclones generated in the northwest over the Arctic Ocean. These supply the precipitation in summer and track above

the Vilyui-Yakutsk region in the central part of the basin keeping this area wetter than others in summer (Lydolph, 1977).

The vegetation patterns are broadly latitudinal and can be divided into three zones (Atlas of Yakutia). In the narrow strip near the Arctic coast, the mean temperature in July is 4-8°C and the mean January value is -32~-36°C. Annual precipitation is below 300 mm. This tundra zone supports only stunted shrubs, sparse grasses, moss, and lichen. In the sub-arctic the mean July temperature is 12-16°C though it can reach up to 35°C, and the January values are -36~-48°C. Annual precipitation is below 400 mm. Vegetation here is typical of the boreal taiga, open birch and larch forest. In this extremely continental climate larch forests survive because of the additional moisture available from summer melting of the uppermost layer of the permafrost. Small-needled species are dominant; they are light-demanding but lower in productivity and in biomass and therefore suited better to the drier climates. In the southern part of the basin mean July temperatures are around 16°C; in January -28~-32°C. Annual precipitation averages 500 mm. Here dense coniferous forest is the dominant vegetation type (Monserud *et al.*, 1993; Naidina, 1995). The total biomass of the boreal forests in the taiga that rings the arctic is comparable to that in the tropical rain forests, although consisting of only a few species (Adams *et al.*, 1990; Van Campo *et al.*, 1993).

The whole region is underlain by continuous permafrost except in the headwater areas (Piguzova, 1965). In the south the permafrost belt is discontinuous with thicknesses of ~25-100 m. Between ~60°N and the Arctic Circle the permafrost is continuous with a thickness is ~100-200 m but reaches 400-600 m in the Vilyui lowlands. Above the Arctic Circle, thickness is ~200 to >500 m with large-scale development of massive ice wedges in the surficial layers. Along the arctic coastal strip (several hundred kilometers wide), as much as 75% of the exposed terrain is composed of this ground ice.

Runoff

In terms of water discharge, the Lena (525 km^3/yr) ranks eighth in the world after the Mississippi (530 km^3/yr), and second after the Yenisey (620 km^3/yr) among those draining into the Arctic Ocean (Gordeev *et al.*, 1996; Meade, 1996).

The discharge hydrograph is shown as an inset in Fig. 2 for the Lena main channel above the delta (at Kusur) and in Fig. 3 for some of its tributaries. The spring thaw begins in early May in the south and several weeks later in the north. Because the Lena main channel runs south-north in the lower reaches, ice dams are frequent when spring thaw begins. Once a dam breaks, there is a flash flood containing large ice floes which can carry sizable boulders (drift rocks) plucked by the shore-fast ice. Scouring by ice and drift rocks on the rocky banks and the islands is a common feature leading to extensive undercutting and slope failure and to large inputs of driftwood. The maximum discharges occur in early June at the mouths of the Lena and Olenek rivers in the north. The spring peak discharge can reach 80,000 m^3/s at Kusur, greater than 100 times that during the low water period and comparable to the maximum discharge in the tropical Orinoco (Edmond *et al.*, 1995, 1996). There is a smaller but highly variable discharge peak in August-September (20,000-40,000 m^3/s) due to the summer monsoon bringing in precipitation from the northwest. In winter (November-April) the flow is almost nil for the headwater tributaries and <1,000 m^3/s for the lower Lena (Kusur). All of the streams in the basin are frozen under ~2 m of ice and are used as part of the "ice road" transportation network. Extremes in the mean annual discharge of water flowing into the delta are from 10,600 to 20,200 m^3/s. Individual tributaries by comparison show larger variations because of their smaller capacity of modulation. Despite the completely natural control of the Lena river runoff (the only significant impoundment is on the upper Vilyui), its long-term interannual variability is small, about 12% at the mouth (UNESCO, 1971), indicating the overall hydrological stability of the basin. The summer rain is more variable, and intermittent storm events can give rise to extreme discharges. Many of the other northern and arctic rivers have similar

magnitudes of variation, but tropical rivers with unstable precipitation conditions can show much greater instability (e.g. Godavari, 33%). The major tributaries to the Lena in terms of annual average water discharge are the Aldan (5,000 m^3/s) draining the Aldan Shield, the southern parts of the platform and the associated Verkhoyansk fold belt, and the Vitim (2,200 m^3/s) and Olekma (1,700 m^3/s) which drain the TBH (Fig. 2). For comparison, the Lena at Yakutsk above its confluence with the Aldan transports 7,200 m^3/s (Chalova *et al.*, 1995).

Geology

The basement of the Siberian Craton is an Archean continental nucleus exposed in the Aldan and Anabar shields. The platform has been stable at least since the Mid-Precambrian. It has been encroached upon by marine transgressions and regressions caused by sea-level fluctuations in turn driven by global and regional tectonics and eustasy; the major cycles are Archean-Early Cambrian, Early Cambrian-Late Silurian, Early Devonian-Late Permian and Mid Triassic-Quaternary (Zonenshain, 1990; Ronov, 1994). The inundation was most extensive in the Cambrian and has since never quite recovered that stage. The classic shelly fossil assemblages of the Late Precambrian-Early Cambrian (Riphean) limestones and shales fringe the northern margin of the Aldan Shield. Ordovician oceanic sequences are exposed from east of Lake Baikal to the Vilyui and also to the south of the Anabar Shield. In these Cambrian and Ordovician deposits there are lagoonal facies with abundant evaporites abutting the highs of the TBH and Aldan Shield. This region was farthest away from the ocean and was submerged only at the highest transgression in the Cambrian to Ordovician and not significantly affected by later inundations.

In addition to the sea-level fluctuations, there have been numerous rifting events giving rise to deep sedimentary basins around the margins of the craton (Lobkovsky *et al.*,

1996). In Early to Middle Riphean (1.6-1.0 Ga.), and especially during Middle Riphean (1.35-1.0 Ga.), there was rifting in the Trans-Baikal area related to ocean basin opening, followed by post-rifting subsidence in the Vendian (0.8-0.57 Ga.). In the Devonian to Permian (286-245 Ma), the main phase of this tectonic activity, there was an episode of multi-trough extension which formed the Vilyui basin. Over the continental sediments of Middle Devonian age (hundreds of meters) a further Late Devonian rifting event led to extrusion of plateau basalts and flank uplift and sediment accumulation of 2-7 km. Boreholes and seismic surveys in the western part of the Vilyui basin show sediment thicknesses of over 10 km in the Kempendyai depression. In Carboniferous-Middle Jurassic, there was less than one km of post-rift subsidence. A foreland basin containing a 4-5 km thickness of sediments formed in front of the Verkhoyansk orogen in Late Jurassic to Cretaceous. In the Mesozoic (241-65.0 Ma) the Baikal rift system developed and in the Cenozoic (56.5 Ma), 6-8 km of sediment were deposited in this 1500 km long trough. To the north, the complex Laptev Sea Rift (Cenozoic), a probable extension of the oceanic spreading system of the Eurasian Arctic Ocean, impinged on the region of the present Lena delta and is still active (Lobkovsky *et al.*, 1996).

The Verkhoyansk foldbelt is composed of a sedimentary complex deposited on the slope and rise of the Siberian passive margin by the proto-Lena during Late Paleozoic, Triassic, and Jurassic times. This underwent intense deformation in the collision between the Kolyma cratonic complex and the Siberian margin beginning in Middle and Late Jurassic and continuing through much of the Cretaceous. The clastics were derived solely from the Siberian Platform and overlie older Paleozoic and Upper Precambrian carbonate sequences. This passive margin probably existed for over half a billion years (Zonenshain *et al.*, 1990).

The platform sediments deposited during the marine transgressions of the Middle Ordovician, Middle Devonian and the Late Cretaceous are dominantly limestones and dolomites affected by diagenesis to varying degrees. At other times, tectonic events like the

Devonian uplift of the TBH and the Aldan Shield supplied abundant detrital sandstones and shales to the platform cover. The Siberian Platform is characterized by the remarkably widespread development of salt (marine halite and gypsum) and of coal-bearing sedimentary sequences (Ronov, 1982). Lower Cambrian salt extends from the west of Lake Baikal along the whole length of the Lena to Kempendyai in the Vilyui basin (Lefond, 1969). The most important exposed salt deposits are at Peleduy (UL429) on the Lena and Kempendyai on the Vilyui. Other salt occurrences are at Ust-Kut (UL413) and Ust-Biryuk (UL436) on the Lena.

Sampling and Analytical Methods

In this study sampling was conducted during river transits on a variety of vessels; to date the cumulative distances covered amount to ~8,000 km. A portable laboratory was installed on the ships so that filtration and sample preservation could be performed promptly under clean conditions. Given the constraints of time and logistics only pH was measured in the field.

Field investigations were made in the Lena basin in July-August of 1991, (Aldan, UL100 series), 1994 (Upper Lena, UL400), 1995 (Lower Lena, UL600), and 1997 (Upper Aldan, UL800) (Fig. 2). In addition, repeat samples were collected in 1992 and 1996 near Yakutsk. All significant tributaries draining the platform (~60 stations) were sampled from small boats a few kilometers above their confluences with the main navigable channel for the major and trace elements and the suspended and bed material. The major element, pH and $^{87}Sr/^{86}Sr$ data are reported in Table I along with an assignment of the geologic age of the rocks in the drainages. Aliquots for major ions were filtered through 0.45 μm Millipore (mixed cellulose esters) filters and those for trace elements through 0.4 μm Nuclepore polycarbonate filters. The latter were acidified with 3x-vycor-distilled, 6N HCl or 16N HNO_3 and stored in HDPE bottles within a few hours after collection. The

pH was measured immediately at the sampling sites to ensure against CO_2 loss. In addition, "grab" samples were collected on geologic expeditions by S. Pelechaty (MIT) in 1993 (Olenek, UL300) and 1994 (Chara-Olekma, UL500). These samples were unfiltered and pH was not measured. All the analyses of these samples occurred within 6 months of collection. Previous work showed that the sample integrity, in terms of major ions and strontium isotopes, is maintained during the time of storage (Edmond *et al.*, 1995). Upon return to the MIT laboratory, major cations (Na, K, Mg, Ca) were measured by flame atomic absorption spectroscopy, alkalinity by Gran titration, Cl and SO_4 by ion chromatography, and silica by colorimetry (on field-acidified aliquots, save for the grab samples). Strontium concentrations were determined by ICP-MS, the isotopic composition by TIMS.

Results and Discussion

As the river water inherits its chemical load from diverse sources, the dissolved composition is examined to isolate these. Comparisons are made to rivers with different lithologies—shield rivers, e.g. the Orinoco draining the Guayana Shield in the tropics and orogenic rivers, e.g. Mackenzie, Fraser and Yukon draining the Rockies and Amazon and Orinoco draining the Andes. Then the composition and concentration ranges are compared with those of Chinese rivers with similar lithology but warmer and wetter climate. Finally the dissolved solids and CO_2 uptake fluxes, which ultimately affect the global geochemical cycle, are computed. Following the geological distribution of the sedimentary deposits, as discussed above, samples are separated into four groups to facilitate interpretation (see Table 1). However, the headwaters of some tributaries lie in geologic zones outside their group; the dominant terrain in the drainage is used in the classification.

The only prospective atmospheric inputs to the fluvial dissolved load are seasalt and eolian dust. Since the region is pristine and very remote from heavily populated areas,

anthropogenic atmospheric contamination can safely be ignored. Given the size of the basin, the dust input must be overwhelmingly of local origin, i.e. redistribution of material rather than its importation. The element most seriously affected by seasalt aerosol is Cl. The Cl values in most of the rivers discussed here are high, ranging up to 30,000 μM in the evaporite-dominated tributaries of the Upper Lena left bank and to 50,000 in a spring (Fig. 8a,b). Some tributaries of the Upper Aldan and Olenek are very dilute and low in Cl (< 20 μM), but the high Na concentrations associated with them indicate that other ions are not severely influenced by marine aerosols. In this paper, the data are not corrected for atmospheric input because it is a negligible fraction of the total concentration for most of the rivers.

Data Presentation

Total cations, anions

A large number of tributaries were sampled making it difficult to include their often unfamiliar names in the location map (Fig. 2). Hence, samples will be referred to by number allowing reference to location and name to be made through Fig. 2 and Table 1.

The total cationic charge ($TZ^+ = Na^+ + K^+ + 2Mg^{2+} + 2Ca^{2+}$ in μEq = 10^{-6} equivalents per kg) and the total anionic charge ($TZ^- = Cl^- + 2SO_4^{2-} + HCO_3^-$ in μEq) balance to within experimental error (less than 6%, average 3%) (Fig. 4). The Normalized Inorganic Charge Balance, NICB, is defined as $(TZ^+ - TZ^-)/TZ^+$. This charge balance pertains to rivers in all the different vegetation zones (taiga, UL400; tundra, UL600) and geologic terrains (detrital to evaporitic). This is as expected for most rivers in the world except in tropical "black" streams, e.g. in the Amazon, Orinoco and Congo (Stallard and Edmond, 1983; Lewis *et al.*, 1987; Négrel *et al.*, 1993; Edmond *et al.*, 1995) and indicates that unanalyzed anions derived from organic acids are not significant in the Siberian rivers. On the Guayana Shield, by comparison, the NICB ranges up to ~1 in very dilute, acidic

(<100 μEq, pH<5.5) "black" tributaries with negative measured "alkalinities" (Edmond *et al.*, 1995).

The TZ^+ values (mostly < 6,000 μEq) range to over 2 orders of magnitude higher than those of the Guayana Shield (< 600 μEq); however, the levels are comparable to those of other platform rivers such as the Yangtze and Huanghe (<8,000 μEq; Fig. 11d; Hu *et al.*, 1982; Edmond *et al.*, 1995). Overall, the rivers of the Siberian Platform have a large range in TZ^+, from ~560 μEq (UL124) to 34,800 (UL420) to 55,200 for one of the springs (UL419) and bracket the "world average river water" (TZ^+ ~1,250 μEq; Meybeck, 1979).

Major Ion Compositions

Anion and cation ternary diagrams together provide a way to visualize the compositions and therefore the relative importance of the different weathering regimes (Fig. 5)(Hu *et al.*, 1982; Stallard and Edmond, 1983; Edmond *et al.*, 1995, 1996). On the anion diagram, purely carbonate weathering yields only alkalinity with no Si and the data therefore fall on the alkalinity apex. Na-feldspar weathering to kaolinite, as an example of silicate dissolution, produces both alkalinity and Si with a ratio of 0.5, placing the data on the alkalinity-Si tie. In general the ratio depends on the degree of cation depletion in the residual phase. Thus, extreme cases like kaolinite weathering to gibbsite yield silica but no alkalinity and data trend towards the Si apex. Evaporites yield ($Cl+SO_4$) in highly variable proportions; however, due to their high solubility they dominate the ternary distributions where present. Oxidative weathering of sulfidic black shales produces sulfuric acid, high silica from subsequent acid reaction with the shales, and low alkalinity; thus the water compositions fall in the center of the triangle. On the cation diagram, the evaporitic tributaries fall at the (Na+K) apex and limestones on the Ca-Mg axis, the exact location varying with the Mg enrichment of the limestones with dolomites in the middle (Ca:Mg=1:1). Silicate weathering is indicated by data extending from the Ca-Mg axis

towards the Na+K apex. This trend cannot be "contaminated" by the presence of evaporites given their much greater solubility and, hence, their overwhelming contribution where they exist to the absolute concentrations; evaporitic samples would plot close to the Na+K apex.

On the anion plot, most points fall near and on the alkalinity apex and the group of six highly evaporitic samples trend towards the ($Cl+SO_4$) apex; overall the distributions are indicative of weathering of platform carbonates and evaporites (Fig. 5a). This type of distribution can also be seen in the Mackenzie (data from Reeder *et al.*, 1972; plotted in Edmond *et al.*, 1996). The northern part of the eastern Andes (Cordillera Merida) of the Orinoco and the Peruvian Andes in Amazonia also show a similar pattern but with higher silica (90-250 μM). The Yukon at Eagle, Alaska has alkalinity:($Cl+SO_4$)≈3.5:1.5 and relatively high silica (100-190 μM). The low silica in these Siberian rivers and in the Mackenzie is unique and is discussed later.

The cation ternary diagram (Fig. 5b) is again much like that of the Mackenzie (data from Reeder *et al.*, 1972; plotted in Edmond *et al.*, 1996). A noticeable feature of Siberian rivers is the wide variation of the Mg/Ca ratio in streams draining the platform carbonates, from 0.1 to >1. This indicates that there are several sources of these elements. For comparison, reported Mg/Ca ratios for the Yangtze (~0.25), Huanghe (~1) Mackenzie (0.14 - 0.67), Yukon (~0.35), carbonate karst streams in Germany (0.2-.03) (Kempe, 1982), Orinoco Andes (0.25 and 0.5; corrected for contribution from gypsum) span a similarly wide range.

The Carbonate System

That Ca and bicarbonate are the dominant ions is demonstrated by the Ca vs. alkalinity plot (Fig. 6a). Below ~2,000 μEq Ca balances ~80% of the alkalinity; the rest is balanced by Mg. At higher concentrations, the points fall off the 1:1 equivalent line. These are data from the evaporitic rivers mentioned above where gypsum and to a smaller extent

Mg sulfates (Eugster *et al.*, 1980) contribute to this balance (Fig. 6b). Na and K from silicate weathering are minor components of the bicarbonate and sulfate balance. The dominance of carbonate and evaporite weathering is as expected, since the former is the most prevalent component in platform terrains and both constituents weather rapidly relative to detrital sediments.

The calcite, aragonite, and dolomite saturation indices (CSI, ASI, DSI) were computed using a chemical equilibrium program, MINEQL$^+$ ver. 3.01 (Westall *et al.*, 1976) with the thermodynamic database provided by the program corrected to 10°C. Water temperature was not measured in the field, but 10°C is a reasonable assumption based on field measurements for other Siberian rivers (Huh, unpublished data). Samples have a large range in calcite saturation (Fig. 7a). Changing the temperature has the largest effect on the undersaturated samples: a decrease from 10°C (summer) to 0°C (winter) lowers CSI by about 0.5 units and an increase from 10°C to 20°C gives approximately a 0.1 unit increase. Outgassing of CO_2 inherited from soil CO_2 in groundwater and lack of nucleation for calcite precipitation is responsible for this general supersaturation. Undersaturated rivers drain the shield or continental sediments in significant proportion and are low in total cations and pH. For CmO rivers this undersaturation is seen in subsequent years when stations were resampled (UL400 and UL700). For JK rivers the tributaries that were undersaturated one year can be supersaturated in the next (UL400 and UL700). The evaporitic rivers are supersaturated perhaps because of additional dissolution of $CaSO_4$. The springs are supersaturated. The pattern is similar for aragonite with slightly less supersaturation. DSI ranges between -4 and 2 (Fig. 7b). The Mackenzie, in comparison, has a larger range of CSI (-2 to 3) with supersaturation at over ~75 μM Ca and increasing with Ca. Amazon tributaries with limestone-dominant lithology also show a large range in CSI (-2 to 1) and DSI (-4 to 1) (Stallard and Edmond, 1987). In contrast, Siberian rivers draining orogenic zones to the east are predominantly undersaturated (Huh *et al.*, in review).

With the increasing interest in CO_2 and the greenhouse effect, arctic rivers have been proposed to play a potentially major role in CO_2 emissions due to the very large amounts of organic carbon stored as peat in the tundra and the occurrence of methane clathrates in the associated ground ice (Kling *et al.*, 1991). The P_{CO_2} of the tributaries has been calculated using bicarbonate alkalinity and pH where measurements are available. Bicarbonate is the dominant inorganic carbon species (500 - 4,000 μM and up to 7,000 μM for springs; Fig. 6a) and dissolved CO_2 makes up less than ~10% (3-129 μM, except UL412 at 1,050 μM). Carbonate is negligible. The tributaries are up to ~10 times supersaturated or undersaturated relative to the atmosphere (330 μatm) (Fig. 7c). One exception is UL412 which starts from the CmO region and drains to the Yenisey River (~60 times supersaturated). Surprisingly the springs are not more supersaturated than the rivers. The ratio $P_{CO_{2,river}}/P_{CO_{2,atm}}$ does not show any correlation with Ca or TZ^+; however, there is an inverse relationship with pH and CSI (Fig. 7a,c). The rivers are undersaturated with respect to atmospheric CO_2 where they are calcite supersaturated and alkaline. This is consistent with degassing of CO_2 to the atmosphere or its fixation into organic carbon.

Previous work has shown that, regardless of latitude, rivers are in general supersaturated with P_{CO_2} relative to the atmosphere (Kempe, 1982). The sources for this excess CO_2 could be in-situ oxidation of organic matter in the rivers themselves or, as suggested by data from the Niger, from groundwater inputs. The swift Andean rivers of the Amazon show $P_{CO_{2,river}}/P_{CO_{2,atm}}$ ratios in the same range as the samples reported here (1 to 10 times atmospheric) (Stallard and Edmond, 1987; Richey *et al.*, 1990). The Niger is on average 7 times supersaturated with a maximum of about 20 (Martins and Probst, 1991). The Mackenzie has a similar range to the Siberian rivers, again negatively correlated with CSI and pH. The Yukon has high P_{CO_2} (up to 100 times supersaturation in winter; ~5 times in summer) (Kempe, 1982).

Kling *et al.* (1991) also report high, early-season outgassing of CO_2 from Toolik lake in arctic Alaska. This can be explained by metabolic buildup under ice, thus excluding

exchange with the atmosphere until the evasion of the CO_2 during breakup. Repeated freezing and exclusion of CO_2 from ice can also be responsible. On the other hand, ice has a very low CO_2 concentration; therefore, melting ice can have a dilution effect on the buildup of CO_2 under ice. The Lena was sampled in summer well after the ice-melt and high P_{CO_2} values were not observed. Because the range of CO_2 saturation is similar for rivers in different latitudes and since the exchange rate or piston velocity is only a factor of two greater at 25° than 0°C, there is no evidence from this data set of high latitude rivers degassing unusually large amounts of CO_2 into the atmosphere at present.

Evaporites

A plot of Na vs. Cl (Fig. 8a,b) is informative in that it shows the evaporite dominance where Na:Cl is 1:1 and the Na contribution from silicate weathering where the data fall below the 1:1 trend. For the six evaporative rivers and to a lesser extent the carbonate rivers, the Na and Cl are from halite in evaporites. There is an excess of Na at concentrationes below 100 μM, which can only come from Na-feldspars or Na-silicate clays in sandstone, shales and other detrital sedimentary rocks.

No relationship is found between SO_4 and Cl (Fig. 8c,d). Although $CaSO_4$ is related to NaCl in its source formation, these do not necessarily form in proportion, thus the high but variable concentrations of SO_4 that are observed. Oxidative weathering of FeS_2, as pyrite in reducing sediments, can be rejected as a source of sulfate because the accompanying low alkalinity and high silica are not seen (Fig. 5a). The data show both high SO_4 with low Cl and low SO_4 with high Cl as is also seen in the Orinoco draining the Eastern Andes. The Mackenzie also shows this with no correlation at low concentrations. In Chinese rivers the two species seem to co-evolve (Fig. 11g). In only a few rivers, mostly in the OL category, with SO_4 <0.5 μM, can SO_4 be assigned a seasalt origin (SO_4/Cl = ~0.052).

From these observations, some calculations can be made to determine the contribution from the weathering of various rock types (Mackenzie and Garrels, 1966). Chloride is attributed to halite dissolution, SO_4 to gypsum. Some rivers are clearly dissolving large amounts of gypsum (up to 63% of TZ^+; UL436) and/or halite (up to 90%; UL420). Some tributaries of the Mackenzie River draining marine Cretaceous deposits also show this spread, though with lesser magnitudes.

Silicate Weathering

On average, weathering of Na- and K-silicates (parameterized as Na*+K = [Na-Cl]+K) accounts for only a small fraction (<12%) of TZ^+. Quantifying weathering of Ca-silicates is more problematic due to the overwhelming Ca signal from carbonates. The Si data were not directly used in calculations of detrital component because they seem to be anomalously low and also erratic, suggesting diatom growth in the many thermokarst lakes.

The sources of silica are sandstones and shales. The silica values have a large range, from 5 (UL205) to 166 μM (UL704) (Fig. 9a). There are some very low silica values; approximately 10% of the samples have < 20 μM. This has also been reported in the Mackenzie (Reeder *et al.*, 1972) and attributed to the lack of soil cover on the shield and of soluble silica in the carbonates exposed in the Rockies. These low abundances cannot be attributed to the cold climate and its inhibiting effect on weathering, since the Yukon at Eagle has high values (>100 μM most of the year, up to 200 μM at high discharge) (Edmond *et al.*, 1996) and the Fraser, where it is not affected by dams and lakes, has levels up to ~400 μM (Cameron *et al.*, 1995). Siberian rivers draining terrains other than the platform have large ranges but on average are significantly higher in Si. Tributaries draining the TBH and the Aldan Shield have 10-125 μM and rivers in the collision zone to the east of the Lena have 20 - 130 μM with most centered around 100 μM (Huh *et al.*, in review). Lack of silica is more likely due to its absence or the refractory nature of the

materials being weathered or to its secondary sedimentation via diatom growth in lakes, as in summer the air temperatures are quite high and there is abundant light. There are numerous lakes and ponds in the region (thermokarst lakes, pingos, etc.) especially on the Lower Aldan and the Vilyui valley and Lower Lena. It is not possible to develop a quantitative relationship between the density of lakes in the drainage basin and the silica values due to the unavailability of maps at the appropriate scale.

With this caveat in mind, to examine the extent of aluminosilicate weathering, Si is plotted against Na*+K (Fig. 9a). This enables one to consider silicate weathering in the absence of evaporites and carbonates. During weathering of aluminosilicate minerals, soluble cations are preferentially leached. As the weathering becomes more intense, advancing to kaolinite and gibbsite stages, silica fraction increases. For example, Na-feldspar to beidellite gives Si/(Na*+K) of 1.7, to kaolinite gives 2, and to gibbsite gives 3. Therefore Si/(Na*+K) ratios are indicative of the extent of aluminosilicate weathering. This is complicated by the presence of several different kinds of aluminosilicates which release Si and Na+K in different fractions. For example, Na-feldspar weathering to beidellite gives 1.7, and K-feldspar to illite gives 3. There is no clear relationship between silica and Na*+K for Siberian rivers but generally the Si/(Na*+K) ratios are very low (Fig. 9a). Heterogeneity of lithologies and loss of Si to diatoms is suspected to be responsible for the scatter. For comparison, Si/(Na*+K) for the Guayana Shield streams are mostly between 1.7 and 3.5 and higher indicating complete removal of the soluble cations (Edmond *et al.*, 1995). In the Orinoco Andes Si is not correlated with (Na*+K), but the silica values are higher (~80 to >700, mean ~175 μM).

The Sr System

The relationships between Sr and its isotopes to the overall water compositions provide important constraints on the relative contributions of detrital and marine sediments to the weathering fluxes of dissolved material (Burke *et al.*, 1982).

Strontium has a large range in concentration (up to 33 μM, UL436; Fig. 10a,b). For comparison, the shield rivers of the Orinoco and the Congo have less than 1 μM and the Andean Orinoco streams have less than 10 μM (Edmond *et al.*, 1995, 1996; Négrel *et al.*, 1993). There are very few reported values above 10 μM—a tributary of the Susquehanna river (15 μM; 0.71560) (Fisher and Stueber, 1976), the Colorado (13 μM; 0.71075) and two Australian rivers (34, 12 μM; 0.73255, 0.72796) (Goldstein and Jacobsen, 1987), and an East African lake (148 μM; 0.70640) (Palmer and Edmond, 1989), all high in evaporitic components. On the Mackenzie a few very concentrated streams have Sr from 300 μM to 4.5 mM but the bulk of the samples have less than 11 μM. As for the Siberian Platform rivers, the high Sr is correlated with high SO_4 though not with Cl and their isotopic ratios are as expected for marine evaporites.

Strontium generally replaces Ca in minerals, so it is informative to plot Sr against Ca. However, it does not necessarily mean that Sr is enriched in carbonates. According to budgets based on yields from monolithologic basins in France, Sr comes mainly from non-carbonate sedimentary rocks (shales and sandstones; 39.3%) and from gypsum deposits (27.8%) (Meybeck, 1988). Data from the Siberian rivers show variable Sr/Ca ratios, suggesting diverse sources for the Sr in the rivers (Fig. 10a,b).

Sr does not correlate significantly with Mg. Judging from the fact that high Sr samples have high SO_4 (Sr/SO_4=0.01~0.06) and low $^{87}Sr/^{86}Sr$ ratios (~0.7088), high Sr (> ~10 μM) probably originates from gypsum/anhydrite in sedimentary rocks formed from lagoonal or more saline waters. As $CaCO_3$ precipitates inorganically it excludes Sr, and the later precipitates, namely gypsum/anhydrite, have higher Sr/Ca ratios. This is consistent with the fact that the locations of the samples with high Sr/Ca ratios are in the area dominated by evaporites. Celestite ($SrSO_4$) is common in modern sabkha deposits as aragonite recrystallizes in the evaporitic environment (Kinsman, 1969).

The Sr isotopic composition of seawater as recorded in marine limestones has varied considerably over the last ~750 m.y. for which data are available (Burke *et al.*,

1982). The ratios are well constrained with the Cambrian and Recent being highest at ~0.709 and with lower and oscillating values in the intervening epochs: Jurassic 0.7068-0.7078; Cretaceous 0.7071-0.7081; Ordovician 0.7078-0.7094 (Burke *et al.*, 1982). Hence, the rocks of the CmO carbonate platform are expected to have values of ~0.709 if the ratios have not been changed by diagenesis. Though with scatter, the $^{87}Sr/^{86}Sr$ of the CmO river waters is quite consistently 0.709 (Fig. 10c,d). The tributaries with headwaters in the Trans-Baikal mountains or the Aldan Shield have higher values (up to 0.712). The six evaporitic rivers of JK have marine ratios but other rivers are more radiogenic indicating aluminosilicate weathering at low fluxes. Some rivers from the OL have ratios >0.71 indicative of the contribution of detrital sediments.

Overall, the $^{87}Sr/^{86}Sr$ values show a consistent compositional trend that agrees with those of other published rivers of the world with the exception of the Himalayan streams (Fig. 10c; Edmond, 1992; Négrel *et al.*, 1993; Blum *et al.*, 1994; Pande *et al.*, 1994; Cameron *et al.*, 1995; Trivedi *et al.*, 1995; Yang *et al.*, 1995; Zhang *et al.*, 1995). To this extent these Siberian rivers are not remarkable. The principal use of the isotopic ratios in this context is in discerning the weathering contributions of different lithologies. A $^{87}Sr/^{86}Sr$ vs. Ca plot (Fig. 10d) shows that at high Ca concentrations, evaporites and carbonates give low isotopic ratios as expected of marine carbonates, and at low Ca concentrations, the ratios are higher indicating a component from silicates (Fig. 10d). Na and K likewise are dominated by evaporites at high concentrations and have low associated $^{87}Sr/^{86}Sr$. Thus, the strontium isotope systematics are consistent with the geology and the general fluvial chemistry and can be used to discern whether aluminosilicate weathering and therefore CO_2 uptake from the atmosphere is significant, even when silica data are low due to biogenic uptake.

Comparison with Chinese Rivers

The Huanghe (Yellow) and the Yangtze (Chiangjiang) are the two main rivers that drain the sedimentary basins of the Chinese Platform. These are comparable in scale to the Siberian terrain, have similarly active fluvial systems but in a very different climatic regime. Therefore a useful comparison can be made with a view to examining the effects of climate on weathering rates. Data published by Hu *et al.* (1982), Zhang *et al.* (1990) and a series of reports from the SCOPE/UNEP program (1982, 1983, 1985) were consulted for comparison with the Siberian data. For the SCOPE/UNEP reports, monthly data are available. Unfortunately, only data for the main channel and two major tributaries of the Yangtze were available in these compilations.

The Yangtze has headwaters in the Qinghai-Xizang Plateau in Tibet but flows mainly through the carbonate platform in its lower reaches and is similar to its Lena counterpart on the ternary diagrams (Fig. 11a,b). The Huanghe originates in the foothills of the Bayan Khara Mountains in Qinghai Province, flows through an arid mountainous region and drains a loess covered terrain containing abundant soil carbonate and evaporites, as reflected in the water chemistry (Fig. 11a,b). The Yangtze has a very narrow range of Mg/Ca ratios (~0.43), those of limestones. The Huanghe is more magnesian (Mg/Ca=0.75). Ca and Mg are almost perfectly balanced by HCO_3 without as significant a contribution from gypsum or anhydrite weathering as seen in some of the Siberian rivers; this is true even for the evaporitic Huanghe (Fig. 11b). The range of Ca, Mg and HCO_3 concentrations are within those of Siberian rivers. The pH of the water is high (8.0 ± 0.2) demonstrating the buffering action of the limestone terrain. The water temperature ranges from <10°C in winter to 27°C in summer. CSI ranges from 2 to 4, higher in the Huanghe than for the Yangtze (Fig. 11c). The calculated P_{CO_2} is between 960 and 1,900 µatm for the Yangtze and 900 - 1,650 µatm for the Huanghe, only slightly supersaturated with respect to the atmosphere (Fig. 11d). Na vs. Cl generally follows the 1:1 line; Na higher than Cl can be accounted for by Na-silicate weathering (Fig. 11e). The Huanghe is very much higher in (Na-Cl) than the Yangtze. Unlike in the Siberian rivers, Cl and SO_4 show

a good correlation (Fig. 11f) probably because data from diverse tributaries are not available for the Chinese rivers. The Si/(Na*+K) ratio is higher for the Chinese rivers (Fig. 11g), but no firm conclusions can be drawn from this because of lack of more comprehensive Si data for the Chinese rivers. There are only two Sr isotope values available and those are ~0.711, higher than the bulk of the Siberian Platform values but still within the expected range (Fig. 11h). Overall, the major ion geochemistry is similar to that of the Siberian rivers, both in property-property relationships and concentration magnitudes.

Flux calculations

Fluxes of the major dissolved species and the total dissolved load were calculated for each sampled tributary of the Siberian Platform. The sums of fluxes of individual watersheds over each of the three geological categories are also reported in Table 2. Discharge was estimated from the annual runoff (discharge per unit area) map of Asia (1:20,000,000 scale) (UNESCO, 1977) which is based on the interpolation and contouring of the available measurements taken over many years. The annual runoff is highest to the north of Lake Baikal (300-800 mm) and lowest near Yakutsk (20 mm); the global average is 30 cm. The drainage area of each tributary was determined gravimetrically by tracing out the catchments from a 1:2,500,000 scale map. Concentrations determined from one-point sampling at falling stage and sometimes at the secondary high stage of the summer rain combined with the mean annual discharges are the best estimates of flux possible at present. The calculated flux at the mouth of the Lena, based on monthly chemical and discharge data (Gordeev and Sidorov, 1993), agrees to within 20% with that estimated here. Though such agreement is not guaranteed at small tributary scales, flux calculations based on one point in time appears not to be too far from the truth especially as the data are

from falling stage and therefore less prone to be sampling extreme conditions as during snow melt or under-ice flow (Edmond *et al.*, 1995, 1996).

Fluxes for the Yangtze and Huanghe main channels were calculated using the monthly chemical and discharge data sets reported by the SCOPE program (Table 2). Fluxes calculated from one-point sampling and mean annual discharge by Hu *et al.* (1982) are also shown.

The total dissolved flux of the Chinese rivers and the Siberian rivers are both dominated by Ca and in some cases Na from carbonate/evaporite weathering; the Si flux from silicate weathering accounts for only a small fraction (~10%; Table 2). The area-weighted average of the dissolved flux over each geological category of the Siberian rivers range from 0.53 to 2.1 x 10^6 mol/km^2/yr. This is comparable to that of the Chinese rivers within the uncertainties even though they are in drastically different climatic regimes. There is more variability within each geological category of the Siberian rivers' watersheds than between the two climatically different basins. The flux from rivers draining sedimentary basins (0.53-2.1 x 10^6 mol/km^2/yr Siberia; 0.37-2.4 x 10^6 mol/km^2/yr China) (Table 2) are comparable to that from orogenic zones (0.45 - 2.9 x 10^6 mol/km^2/yr Rockies; 0.59-4.1 x 10^6 mol/km^2/yr Andes; 0.04-0.38 x 10^6 mol/km^2/yr Siberia)(Edmond and Huh, 1997). The fluxes are much higher than in the shield regions, (0.05-0.75 x 10^6 mol/km^2/yr in the tropical shields, 0.08-0.81 x 10^6 mol/km^2/yr in high latitude shields).

To explicitly calculate the uptake rate of CO_2 (ϕCO_2) by aluminosilicate weathering, the scheme of Edmond and Huh (1997) is adopted. $\phi CO_2 = \phi TZ^{+*}$ ($TZ^{+*} = TZ^+ - Cl^- - 2SO_4^{2-}$) when $^{87}Sr/^{86}Sr$ ratios are indicative of aluminosilicate weathering, i.e. >0.710. $\phi CO_2 = 2\phi Si$ when carbonate/evaporites are dominant. This is the estimated ratio for aluminosilicate weathering in general, based on the global fluvial dataset (Garrels, 1967; Berner *et al.*, 1983). Using the silica flux gives an underestimate of the true uptake rate of CO_2 because of the likely removal of Si by organisms. In Siberian rivers, the area-weighted average ϕCO_2 over the geological categories ranges from 16 to 112 x 10^3

mol/km^2/yr (Table 2). However, as with the dissolved flux, individual tributaries show a large variability, and overall the ϕCO_2 values are not very different from those of the Chinese rivers (7-106 x 10^3 mol/km^2/yr). Orogenic zones have higher uptake rates (143-1,000 x 10^3 mol/km^2/yr in the tropics; 19-1,750 x 10^3 mol/km^2/yr at higher latitudes).

There are two aspects to "climate"—temperature and runoff. Higher equilibrium solubility of carbonate minerals at lower temperatures have been suggested to lead to higher concentrations in colder streams. Results to the contrary have been found by Harmon *et al.* (1975) and attributed to the kinetic effects and difference in discharge. This is important in considering whether carbonate weathering is saturation limited or kinetically limited at cold temperatures. Our results suggest that the system is saturation limited. But the temperature effect on saturation is only a factor of two between 10 and 25°C and the concentrations of carbonate-generated Ca and alkalinity in the Siberian rivers are expected to be only slightly higher. It is widely accepted that the chemical denudation rate for a given lithology is roughly proportional to runoff (Amiotte-Suchet and Probst, 1993; Summerfield and Hulton, 1994). However, at a regional scale the present data set does not show any relationship between chemical fluxes and runoff (Table 2). As runoff is generally lower for the Siberian rivers this reinforces the argument that they have comparable fluxes to those of the Chinese streams even though the temperature *and* the runoff is lower.

In comparisons of different watersheds, the heterogeneity of intra-basin climate and lithology has to be borne in mind. Whereas some of the Siberian river waters have headwaters in the southern regions (52°N), the headwaters of the Yangtze are at the high altitudes of the Tibetan Plateau. Also the lithology of a watershed is rarely homogeneous. In this study, samples have been collected at tributary scales; therefore, within each tributary the climate and lithology are relatively homogeneous. Another reinforcing argument for lack of climatic effect on weathering is by comparing the OL samples, all of which lie above the Arctic Circle, to the CmO or JK samples which come from more

southern locations. The chemical composition or the fluxes are not very different between them.

The actual rate of denudation is dominated by mechanical weathering giving rise to suspended material in the rivers. Chemical weathering generating the dissolved load is responsible for only a small fraction of total denudation, but this is what is ultimately involved in the global geochemical cycle. Chemical weathering in general bears no clear relationship to mechanical weathering (Summerfield and Hulton, 1994). In this study, only the dissolved load was considered.

Conclusions

Weathering in two major sedimentary basins are compared using extensive new data from the Siberian Platform in the subarctic/arctic zone and the existing information from the Chinese Platform in tropical/temperate latitudes. The chemistries are largely similar in that the rivers are Ca-HCO_3 dominated. The few values of the strontium isotope ratios for the Yangtze that are available are comparable to those of the Lena. The concentration range and isotopic ratios are consistent with the geology and with observations from other reported world rivers. The Siberian rivers have been sampled in far more detail and so show more diverse compositions. Carbonate weathering is saturation limited and based on the temperature-saturation relationship, the dissolution rates do not differ much. At regional scales, no direct relationship was found between runoff and chemical fluxes. The fluxes are about the same for the dissolved loads even though the basins are in very different climatic zones. Thus, it can be concluded that the cold climate in Siberia does not have a direct inhibiting effect on the chemical yields when the reactions are kinetically fast as for carbonates and evaporites. Uptake of CO_2 by aluminosilicate weathering as indicated by the Si concentrations and $^{87}Sr/^{86}Sr$ ratios is similar for the two regimes but much smaller for the platforms as compared to orogenic

belts (Edmond and Huh, 1996). Overall, weathering of sedimentary platforms is not a direct function of temperature but rather a result of the complex interplay of regional climate and physical processes that determine the chemical yields.

Acknowledgment — We owe our deepest gratitude to the personnel of the River Navigation Authorities of Yakutia for immense help and exertion in what were sometimes very trying situations. We thank the captains and crew of the various vessels for their enthusiasm and support, even running hard aground to get us the samples we needed. S. Pelechaty collected the UL300 and UL500 samples. The $^{87}Sr/^{86}Sr$ ratios were measured in the lab of S. Bowring. H. Hemond provided access to an IC. The MIT component of this work was supported by the Earth Sciences Division of the NSF. We have benefited from the thoughtful comments of F. Albarède and two anonymous reviewers.

References

Adams J. M., Faure H., Faure-Denard L., McGlade J. M., and Woodward F. I. (1990) Increases in terrestrial carbon storage from the Last Glacial Maximum to the present. *Nature* **348**, 711-714.

Amiotte-Suchet P. and Probst J. L. (1993) Modeling of atmospheric CO_2 consumption by chemical weathering of rocks: Application to the Garonne, Congo and Amazon basins. *Chem. Geol.* **107**, 205-210.

Arkhipov S. A., Isayeva L. L., Bespaly V. G., and Glushkova O. (1986) Glaciation of Siberia and North-east USSR. *Quaternary Science Reviews* **5**, 463-474.

Atlas of Yakutia (1989) Atlas selskovo khozyaistva Yakutskoi ASSR (Agricultural Atlas of the Autonomous Soviet Socialist Republic of Yakuts). Moscow, Glavnoe upravlenie geodezyi i kartografyi pri sovete ministrov SSSR.

Berner E. K. and Berner R. A. (1987) *The Global Water Cycle: Geochemistry and Environment.* Prentice-Hall, Englewood Cliffs, N.J., 397 pp.

Blum J. D., Erel Y., and Brown K. (1994) $^{87}Sr/^{86}Sr$ ratios of Sierra Nevada stream waters: Implications for relative mineral weathering rates. *Geochim. Cosmochim. Acta* **58**, 5019-5025.

Budd D. A. (1997) Cenozoic dolomites of carbonate islands: their attributes and origin. *Earth-Science Reviews* **42**, 1-47.

Burke W. H., Denison R. E., Heatherington E. A., Koepnick R. B., Nelson H. F., and Otto J. B. (1982) Variation of seawater $^{87}Sr/^{86}Sr$ throughout Phanerozoic time. *Geology* **10**, 516-519.

Cameron E. M., Hall G. E. M., Veizer J., and Krouse H. R. (1995) Isotopic and elemental hydrogeochemistry of a major river system: Fraser River, British Columbia, Canada. *Chem. Geol.* **122**, 149-169.

Carbon Cycle Research Unit (1982) The amount of carbon transported to the sea by the Yangtze and Huanghe Rivers (People's Republic of China) during the half-year July-December, 1981. In *Transport of Carbon and Minerals in Major World Rivers Part 1.* (ed. E. T. Degens), SCOPE/UNEP Sonderband 52, Mitt. Geol.-Paläont. Inst. Univ. Hamburg, pp. 437-448.

Chalova P. C., Panchenko B. M., and Zernova C. Y., eds. (1995) *Water ways of the Lena Basin.* Moscow, 600pp (in Russian).

Cuffey K. M., Clow G. D., Alley R. B., Stuiver M., Waddington E. D., and Saltus R. W. (1995) Large arctic temperature change at the Wisconsin-Holocene glacial transition. *Science* **270**, 455-458.

Denton G. H. and Hughes T. J., eds. (1981) *The Last Great Icesheets.* Wiley Interscience.

Edmond J. M. (1992) Himalayan tectonics, weathering processes, and the strontium isotope record in marine limestones. *Science* **258**, 1594-1597.

Edmond J. M. and Huh Y. (1997) Chemical weathering yields from basement and orogenic terrains in hot and cold climates. In *Tectonic Uplift and Climate Change.* W. F. Ruddiman, ed. Plenum Press, pp. 329-351.

Edmond J. M., Palmer M. R., Measures C. I., Grant B., and Stallard R. F. (1995) The fluvial geochemistry and denudation rate of the Guayana Shield in Venezuela, Colombia and Brazil. *Geochim. Cosmochim. Acta* **59**(16), 3301-3325.

Edmond J. M., Palmer M. R., Measures C. I., Brown E. T., and Huh Y. (1996) Fluvial geochemistry of the eastern slope of the northeastern Andes and its foredeep in the drainage of the Orinoco in Colombia and Venezuela. *Geochim. Cosmochim. Acta* **60**(16), 2949-2976.

Eugster H. P., Harvie C. E., and Weare J. H. (1980) Mineral equilibria in a six-component seawater system. Na-K-Mg-Ca-SO_4-Cl-H_2O, at 25°C. *Geochim. Cosmochim. Acta* **44**, 1335-1347.

Fisher R. and Stueber A. M. (1976) Strontium isotopes in selected streams within the Susquehanna River basin. *Water Resources Res.* **12**, 1061-1068.

Gan W.-B. (1985) Hydrochemistry of the Yangtze River basin. In *Transport of Carbon and Minerals in Major World Rivers. Part 3.* SCOPE/UNEP Sonderband 58, (eds. E. T. Degens, S. Kempe and R. Herrera), Mitt. Geol.-Paläont. Inst. Univ. Hamburg, pp. 539-557.

Gan W.-B., Chen H.-M., and Han Y.-F. (1983) Carbon transport by the Yangtze (at Nanjing) and Huanghe (at Jinan) Rivers, People's Republic of China. In *Transport of Carbon and Minerals in Major World Rivers. Part 2.* SCOPE/UNEP Sonderband 55, (eds. E. T. Degens, S. Kempe and H. Soliman), Mitt. Geol. -Paläont. Inst. Univ. Hamburg, pp. 459-470.

Garrels R. M. (1967) Genesis of some groundwaters from igneous rocks. In *Researches in Geochemistry*. (ed. P. H. Ableson), pp. 405-420.

Goldstein S. J. and Jacobsen S. B. (1987) The Nd and Sr isotopic systematics of river-water dissolved material: Implications for the sources of Nd and Sr in seawater. *Chem. Geol. (Isotope Geosciences Section)* **66**, 245-272.

Gordeev V. V. and Sidorov I. S. (1993) Concentrations of major elements and their outflow into the Laptev Sea by the Lena River. *Mar. Chem.* **43**, 33-45.

Gordeev V. V., Martin J. M., Sidorov I. S., and Sidorova M. V. (1996) A reassessment of the Eurasian river input of water, sediment, major elements and nutrients to the Arctic Ocean. *Am. J. Sci.* **296**, 664-691.

Hansen J. D., Johnson D., Lacis A., Lebedeff S., Lee P., Rind D., and Russell G. (1983) Climatic effects of atmospheric carbon dioxide. *Science* **220**, 874-875.

Harmon R. S., White W. B., Drake J. J., and Hess J. W. (1975) Regional hydrochemistry of North American carbonate terrains. *Water Resources Res.* **11**(6), 963-967.

Holland H. D. (1978) *The Chemistry of the Atmosphere and Oceans*. Wiley Interscience, New York.

Hu M.-H., Stallard R. F., and Edmond J. M. (1982) Major ion chemistry of some large Chinese rivers. *Nature* **298**(5874), 550-553.

Huh Y., Babich D., Zaitsev A., and Edmond J. M. (1998) The fluvial geochemistry of the rivers of Eastern Siberia II: Tributaries of the Lena, Yana, Indigirka, and Kolyma draining the accretionary zone. *Geochim. Cosmochim. Acta* in press (March 5, 1998).

Kempe S. (1982) Long-term records of CO_2 pressure fluctuations in fresh waters. In *Transport of Carbon and Minerals in Major World Rivers Part 1*. (ed. E. T. Degens), SCOPE/UNEP Sonderband 52, Mitt. Geol.-Paläont. Inst. Univ., Hamburg, pp. 91-332.

Kinsman D. J. J. (1969) Interpretation of Sr^{2+} concentrations in carbonate minerals and rocks. *J. Sediment. Petrol.* **39**, 486-508.

Kling G. W., Kipphut G. W., and Miller M. C. (1991) Arctic lakes and streams as gas conduits to the atmosphere: Implications for tundra carbon budget. *Science* **251**, 298-301.

Kulp J. L., Turekian K., and Boyd D. W. (1952) Strontium content of limestones and fossils. *Bulletin of the Geological Society of America* **63**, 70-716.

Lefond S. J. (1969) *Handbook of World Salt Resources*. Monographs in Geoscience Plenum Press, New York, 384 pp.

Lewis W. M., Hamilton S. K., Jones S. L., and Runnels D. D. (1987) Major element chemistry, weathering and element yields for the Caura River drainage, Venezuela. *Biogeochem.* **4**, 159-181.

Lobkovsky L. I. *et al.* (1996) Extensional basins of the former Soviet Union—structure, basin formation mechanisms and subsidence history. *Tectonophysics* **266**, 251-285.

Lydolph P. E. (1977) *Climates of the Soviet Union*. World Survey of Climatology 7, Elsevier Scientific Publishing Company.

Mackenzie F. T. and Garrels R. M. (1966) Chemical mass balance between rivers and oceans. *Am. J. Sci.* **264**, 507-525.

Martins O. and Probst J.-L. (1991) Biogeochemistry of major African rivers: Carbon and mineral transport. In *Biogeochemistry of Major World Rivers*. (eds. E. T. Degens, S. Kempe and J. E. Richey), John Wiley & Sons Ltd.

Meade R. H. (1996) River-sediment inputs to major deltas. In *Sea-Level Rise and Coastal Subsidence: Causes, Consequences, and Strategies*. J. D. Milliman and B. U. Haq, eds., Kluwer Academic Publishers, pp. 63-85.

Meybeck M. (1979) Concentrations des eaux fluviales en éléments majeurs et apports en solution aux océans. *Rev. Géol. Dyn. Géogr. Phys.* **21**(3), 215-246.

Meybeck M. (1986) Composition chimique des ruisseaux non pollués de France. *Sci. Geol. Bull* **39**, 3-77.

Meybeck M. (1988) How to establish and use world budgets of riverine materials. In *Physical and Chemical Weathering in Geochemical Cycles*. A. Lerman and M. Meybeck, eds., Kluwer Academic Publishers, pp. 247-272.

Monserud R. A., Denissenko O. V., and Tchebakova N. M. (1993) Comparison of Siberian paleovegetation to current and future vegetation under climate change. *Clim. Res.* **3**, 143-159.

Naidina O. D. (1995) Holocene climatic, vegetation and pollen data of Siberia adjacent to the Laptev Sea. *Reports on Polar Research* **176**, 135-153.

Négrel P., Allègre C. J., Dupré B., and Lewin E. (1993) Erosion sources determined by inversion of major and trace element ratios and strontium isotopic ratios in river water: The Congo Basin case. *Earth Planet. Sci. Lett.* **120**, 59-76.

Newton R. M., Weintraub J., and April R. (1987) The relationship between surface water chemistry and geology in the North Branch of the Moose River. *Biogeochem.* **3**, 21-35.

Palmer M. R. and Edmond J. M. (1989) The strontium isotope budget of the modern ocean. *Earth Planet. Sci. Lett.* **92**, 11-26.

Pande K., Sarin M. M., Trivedi J. R., Krishnaswami S., and Sharma K. K. (1994) The Indus river system (India-Pakistan): Major-ion chemistry, uranium and strontium isotopes. *Chem. Geol.* **116**, 245-259.

Piguzova V. M. (1965) Estimating underground flow into the rivers of the permafrost zone. *Soviet Hydrology* 114-129.

Reeder S. W., Hitchon B., and Levinson A. A. (1972) Hydrogeochemistry of the surface waters of the Mackenzie River drainage basin, Canada—I. Factors controlling inorganic composition. *Geochim. Cosmochim. Acta* **36**, 825-865.

Richey J. E., Hedges J. I., Devol A. H., Quay P. D. and Victoria R. (1990) Biogeochemistry of carbon in the Amazon River. *Limnol. Oceanogr.* **35**(2), 352-371.

Ronov A. B. (1982) The Earth's sedimentary shell (quantitative patterns of its structure, composition, and evolution). *Internat. Geology Rev.* **24**(11), 1313-1363.

Ronov A. B. (1994) Phanerozoic transgressions and regressions on the continents: A quantitative approach based on areas flooded by the sea and areas of marine and continental deposition. *Am. J. Sci.* **294**, 777-801.

Ronov A. B. and Migdisov A. A. (1970) Evolution of the chemical composition of the rocks in the shields and sediment cover of the Russian and North American Platforms. *Geochem. Int.* 294-325.

Rundquist D. V. and Mitrofanov F. P., eds. (1993) *Precambrian Geology of the USSR.* Developments in Precambrian Geology. Amsterdam, Elsevier.

Stallard R. F. and Edmond J. M. (1983) Geochemistry of the Amazon 2. The influence of geology and weathering environment on the dissolved load. *J. Geophys. Res.* **88**(C14), 9671-9688.

Stallard R. F. and Edmond J. M. (1987) Geochemistry of the Amazon 3. Weathering chemistry and limits to dissolved inputs. *J. Geophys. Res.* **92**(C8), 8293-8302.

Summerfield M. A. and Hulton N. H. (1994) Natural controls of fluvial denudation rates in major world drainage basins. *J. Geophys. Res.* **99**(B7), 13,871-13,883.

Trivedi J. R., Pande K., Krishnaswami S., and Sarin M. M. (1995) Sr isotopes in rivers of India and Pakistan: A reconnaissance study. *Current Science* **69**(2), 171-178.

Turekian K. K. (1964) The marine geochemistry of strontium. *Geochim. Cosmochim. Acta* **28**, 1479-1496.

Turekian K. K. and J. L. Kulp (1956) The geochemistry of strontium. *Geochim. Cosmochim. Acta* **10**, 245-296.

UNESCO (1977) *Atlas of World Water Balance.* Gidrometeoizdat, USSR National Committee for the International Hydrological Decade, Leningrad & The UNESCO Press, Paris.

UNESCO (1979) *Discharge of Selected Rivers of the World.* Studies and Reports in Hydrology III, Imprimeries Louis-Jean, Gap, France, 104 pp.

Vahrenkamp V. C. and Swart P. K. (1990) New distribution coefficient for the incorporation of strontium to dolomite and its implications for the formation of ancient dolomites. *Geology* **18**, 387-391.

Van Campo E., Guiot J., and Peng C. (1993) A data-based re-appraisal of the terrestrial carbon budget. *Global and Planetary Change* **8**, 189-201.

Velichko A. A. and Faustova M. A. (1991) Reconstruction of the last post-Pleistocene glaciation of the northern hemisphere (18-20 thousand years ago). *Doklady Akademy Nauk USSR* 223-225.

Westall J. C., Zachary J. L., and Morel F. M. M. (1976) MINEQL, A Computer Program for the Calculation of Chemical Equilibrium Composition of Aqueous Systems. Tech Note 18 Dept. of Civil Eng., Mass. Inst. Technol., Cambridge, MA.

Yang C., Telmer K., and Veizer J. (1995) Chemical dynamics of the St. Lawrence riverine system: δD_{H_2O}, $\delta^{18}O_{H_2O}$, $\delta^{13}C_{DIC}$, $\delta^{34}S_{Sulfate}$, and dissolved $^{87}Sr/^{86}Sr$. *Geochim. Cosmochim. Acta* **60**, 851-866.

Zhang J., Huang W. W., Liu M. G., and Zhou Q. (1990) Drainage basin weathering and major element transport of two large Chinese rivers (Huanghe and Changjiang). *J. Geophys. Res.* **95**(C8), 13277-13288.

Zhang J., Takahashi K., Wushiki H., Yabuki S., Xiong J., and Masuda A. (1995) Water geochemistry of the rivers around the Taklimakan Desert (NW China): Crustal weathering and evaporation processes in arid land. *Chem. Geol.* **119**, 225-237.

Zonenshain L. P., Kuzmin M. I., and Natapov L. P. (1990) *Geology of the USSR: A Plate-Tectonic Synthesis.* Geodynamics Series 21, Am. Geophys. U., Washington, D.C., 242 pp.

Table 1. Chemical data for rivers draining the Siberian Platform sampled above confluence with main channels unless specified. The Cambrian and Ordovician (CmO) category covers the streams draining the sedimentary cover of that age to the northwest of Lake Baikal and along the Upper Lena main channel fringing the Aldan Shield. Rivers draining carbonates and evaporites associated with predominantly continental sediments in the mid-reaches of the Lena to the west of the Verkhoyansk fold belt belong to the Jurassic and Cretaceous (JK) category. The tributaries of the Olenek river that drain the carbonate terrain surrounding the Anabar Shield are designated OL independent of geology. They are assigned to a separate group because they occupy significantly higher latitude (above 70°N) than the previous 2 categories. The various types of groundwater discharges sampled are also separately designated as SP, regardless of age. Springs reported here are all "cold" with temperatures less than 5 °C. Hot springs have not been sampled but are also reported to exist in this region.

River Name	Age	Sample Number	date d/m/yr	Na µM	K µM	Mg µM	Ca µM	Cl µM	SO_4 µM	Alk µEq	Si µM	pH	Sr µM	$^{87}Sr/^{86}Sr$
Cambrian & Ordovician (CmO)														
Manzurka	Cm,Pr	UL401	24/07/94	183	19.5	944	1680	142	1050	3206	146	n.d.	17.4	0.70845
Lena above Manzurka	Cm,Pr	UL402	24/07/94	701	10.0	593	983	607	453	2295	101	n.d.	9.26	0.70893
Tutura	O	UL403	25/07/94	428	19.9	540	1260	350	147	3513	83	n.d.	5.14	0.70836
Orlinga	O	UL404	26/07/94	62.5	21.2	531	1200	46.1	109	3369	52	8.31	2.09	0.70907
Tayura	O	UL407	27/07/94	41.6	14.4	525	877	26.3	125	2642	8	8.83	1.96	0.70924
Ulkan	O	UL410	28/07/94	95.3	21.8	602	776	20.1	141	2570	12	8.49	2.78	0.70950
Kuta	O	UL408	27/07/94	624	24.7	885	1110	614	404	3216	17	8.73	6.74	0.70891
Bolshaya Tira	O	UL409	28/07/94	117	33.0	1070	831	61.9	326	3236	9	8.42	7.04	0.70924
Nizhnyaya Tunguska	O	UL412	29/07/94	147	44.0	1050	1060	136	363	3574	19	6.60	14.4	0.70908
Kirenga	Cm,Pr	UL413	30/07/94	1630	10.0	314	635	1460	331	1374	84	7.42	3.45	0.70975
Mogol	Cm,Pr	UL415	31/07/94	1440	10.2	581	1020	1420	309	2721	66	8.33	4.02	0.70903
Pulka	Cm,Pr	UL430	06/08/94	1920	52.7	647	1160	1940	700	2162	81	8.08	4.48	0.70908
Chara	Cm,Pr,Ar	UL437	08/08/94	231	13.1	147	421	199	132	938	75	7.84	1.50	0.71211
		UL710	06/08/96	480	17.0	186	441	330	204	991	79	7.98	1.68	n.d.
Torgo	Cm,Pr	UL505	11/07/94	23.0	32.9	636	983	3.9	85.7	3145	77	n.d.	2.75	0.70874
Torgo	Cm,Pr	UL506	14/07/94	39.9	15.1	304	409	8.7	67.1	1392	91	n.d.	1.90	0.70999
Olekma	Cm,Pr,Ar	UL438	08/08/94	110	8.1	94.5	224	104	89.8	469	103	7.33	1.24	0.70976
		UL711	06/08/94	441	16.5	129	282	350	194	519	114	7.60	2.13	n.d.
Tuolbachen	Cm	UL204	03/08/92	160	15.4	909	1890	155	1017	3704	51	8.30	20.0	0.70854
		UL441	11/08/94	169	13.1	784	1710	153	795	3465	45	8.26	16.4	0.70856
		UL709	05/08/96	147	15.4	886	1740	111	1070	3441	58	8.39	21.0	n.d.
Tuolba	Cm	UL444	12/08/94	84.7	13.1	794	1370	60.0	655	3058	59	7.94	6.16	0.70871
		UL707	05/08/96	184	22.7	1120	2110	198	1480	3396	65	8.33	11.6	n.d.
Buotama	Cm	UL705	04/08/96	73.1	11.6	752	1160	39.0	104	3647	55	8.37	2.62	0.70925

Table 1. continued.

River Name	Age	Sample Number	date d/m/yr	Na µM	K µM	Mg µM	Ca µM	Cl µM	SO_4 µM	Alk µEq	Si µM	pH	Sr µM	$^{87}Sr/^{86}Sr$
Sumnagin	Cm	UL117	07/08/91	24.0	14.1	977	936	11.3	29.0	3812	73	n.d.	0.96	0.70955
Ice Field	Cm	UL116	07/08/91	27.0	5.9	788	862	12.8	14.4	3384	65	n.d.	0.46	0.71110
Yungyuele	Cm	UL111	03/08/91	32.0	16.2	990	734	32.8	104	3269	66	n.d.	5.60	0.70883
Amga	J,Cm,Ar	UL106	30/07/91	53.0	8.7	620	811	41.7	83.2	2777	73	n.d.	2.20	0.70912
Amga @ Verkhnyaya Amga		UL801	29/08/97	35.8	7.5	853	1020	9.7	70.7	3620	66	n.d.	1.80	0.70926
Muna	Cm	UL603	24/07/95	36.4	11.8	226	1240	6.0	23.3	3060	35	8.11	2.08	0.70934
Maya	Cm,P	UL109	02/08/91	56.0	10.3	153	344	9.8	47.6	1001	88	n.d.	0.86	0.71127
Allakh-Yun	P,Cm,J	UL123	13/08/91	46.0	13.7	115	429	11.8	44.0	1057	70	n.d.	1.24	0.71194
Khanda	O,S,Cm	UL125	15/08/91	38.0	8.5	324	1085	15.2	110	2681	40	n.d.	1.79	0.71145
Jurassic & Cretaceous (JK)														
Ichera	Cm,O,	UL420	02/08/94	28400	147	1250	1890	27900	1560	3239	29	8.33	22.6	0.70883
Peleduy	Cm,J	UL429	05/08/94	11200	46.9	1390	1940	11200	1930	3256	42	8.18	11.8	0.70855
Khamra	Cm,O	UL431	06/08/94	5740	50.4	1105	1550	5740	926	3447	47	8.13	13.2	0.70889
Nyuya	O,S,J	UL432	07/08/94	9030	42.8	1320	2440	9060	2190	2676	27	8.39	25.2	0.70874
Ura	Pr,J	UL433	07/08/94	1410	21.5	550	1030	1400	381	2416	92	8.34	5.76	0.71021
Biryuk	S,J	UL436	08/08/94	2780	55.4	1420	4010	2380	4460	2443	40	8.22	32.8	0.70878
		UL713	07/08/96	2430	46.8	1400	3960	2200	4140	2144	42	8.27	33.0	n.d.
Namana	J,K	UL440	10/08/94	7400	27.5	607	1820	7400	1620	1595	113	7.88	9.80	0.70863
Markha	Cm,J,N-Q	UL442	11/08/94	65.5	10.4	395	858	3.1	107	2337	42	8.64	14.7	0.70863
		UL708	05/08/96	95.2	12.4	479	980	7.6	162	2829	16	8.92	20.8	n.d.
Markhachan	Cm,J	UL443	12/08/94	54.3	3.9	320	570	0.1	21.3	1737	45	7.80	2.37	0.70927
Malykhan	Cm,J	UL445	13/08/94	55.4	18.2	685	1140	40.5	17.8	3764	82	7.89	1.41	0.70981
		UL706	05/08/96	81.1	21.3	732	1370	8.8	22.6	4142	90	7.80	1.54	n.d.
Sinyaya	Cm,J,N-Q	UL205	03/08/92	164	23.8	306	791	35.1	78.9	2175	5	9.08	2.43	0.70954
Kenkeme	N,K	UL134	18/08/91	170	38.6	253	405	19.4	14.1	1405	18	n.d.	1.33	0.71253
Vilyuy @ mouth	K,J,P-Tr,Cm	UL201	01/09/92	419	16.2	194	414	407	41.8	1150	56	7.87	1.38	0.70820
Vilyui @ Kysyl Syr	K,J,P-Tr,Cm	UL301	27/05/93	114	30.8	148	282	104	33.8	786	65	n.d.	0.85	0.70921
Notora	J	UL124	14/08/91	45.0	6.5	99.0	155	7.0	23.0	522	90	n.d.	0.55	0.71172
Tatta	J,N	UL129	16/08/91	193	26.2	580	866	14.0	7.0	3052	28	n.d.	1.52	0.71336
Olenek Plateau (OL)														
Eyekit	Pr,P,K	UL608	25/07/95	75.4	10.5	148	395	2.5	100	957	56	n.d.	0.93	0.71030
Erdilyakh-Yuryage	K	UL620	02/08/95	30.1	7.6	57.8	264	10.9	5.4	651	34	n.d.	0.82	n.d.
Kuogastakh-Yuryage	K	UL619	02/08/95	24.4	10.3	126	258	6.7	12.5	726	51	n.d.	0.61	0.71036
Ulakhen-Yuryage	K	UL617	02/08/95	41.0	10.1	109	296	36.2	116	565	38	n.d.	0.95	0.71036
Small river from a lake		UL613	31/07/95	35.9	8.5	168	519	28.6	35.9	1342	19	n.d.	0.87	0.71087

Table 1. continued.

River Name	Age	Sample Number	date d/m/yr	Na µM	K µM	Mg µM	Ca µM	Cl µM	SO_4 µM	Alk µEq	Si µM	pH	Sr µM	$^{87}Sr/^{86}Sr$
Oolahan-Ooehteh		UL302	21/06/93	8.7	10.4	151	413	5.0	0.1	1142	26	n.d.	0.11	0.71182
Kytyngeder		UL303	24/06/93	7.9	12.2	137	444	5.0	0.1	1177	22	n.d.	0.20	0.71227
Kytyngeder		UL304	26/06/93	14.8	15.1	161	463	10.0	1.0	1277	34	n.d.	0.26	0.71486
Xolomoloh		UL305	28/06/93	29.4	9.0	600	770	11.0	4.0	2706	45	n.d.	0.32	0.71254
Olenek	Cm,O,Ar	UL312	12/07/93	24.7	2.8	188	1120	17.0	8.0	2560	25	n.d.	0.55	n.d.
Olenek		UL313	12/07/93	39.9	7.5	211	783	39.0	3.0	1974	51	n.d.	1.39	n.d.
Olenek		UL314	14/07/93	46.1	7.4	252	804	45.0	3.0	2017	50	n.d.	1.24	0.70944
Erkeketsky	Cm	UL315	15/07/93	83.2	23.8	212	1310	64.6	77.0	2969	35	n.d.	0.93	0.71098
Olenek		UL316	19/07/93	52.1	7.0	255	857	53.0	3.0	2147	50	n.d.	1.32	0.70943
Khorbosunka	Cm,Pr	UL317	20/07/93	24.1	9.0	203	781	7.0	4.0	1898	25	n.d.	0.40	0.71003
Khorbosunka		UL311	09/07/93	12.0	1.1	178	615	7.0	3.0	1567	20	n.d.	0.57	0.71021
Anibil		UL310	06/07/93	7.9	7.8	140	641	6.0	2.0	1576	22	n.d.	0.38	0.71026
Khorbosunka		UL309	04/07/93	9.6	8.8	152	492	7.0	2.0	1331	20	n.d.	0.47	0.71016
Khorbosunka		UL308	01/07/93	7.1	8.7	136	368	4.0	0.1	1037	20	n.d.	0.31	0.71114
Khorbosunka		UL307	01/07/93	4.7	5.2	98.1	366	5.0	0.1	969	16	n.d.	0.42	0.70902
Khorbosunka		UL306	30/06/93	8.2	9.4	123	289	3.0	0.1	865	22	n.d.	0.21	0.71341
Olenek		UL318	20/07/93	52.3	8.5	280	826	55.0	3.0	2138	49	n.d.	1.25	0.70940
Bur	P,J	UL319	21/07/93	34.0	8.4	139	292	6.0	31.6	827	37	n.d.	0.61	0.71005
Olenek @ Town Tymatee		UL320	24/07/93	64.7	8.1	241	683	55.0	3.0	1772	43	n.d.	1.09	0.70953
Olenek @ mouth		UL621	01/08/95	155	9.1	245	833	72.7	21.9	2129	53	n.d.	1.42	0.70925
Groundwater Springs (SP)														
R.B. Spring bl Orlinga	O	UL406	26/07/94	81.3	37.6	1250	1520	81.0	862	3987	90	8.16	15.8	0.70886
Well @ Kirensk	O	UL411	29/07/94	2430	235	2260	2220	2430	1250	6945	111	8.17	5.06	0.71043
Melnichnui Creek	O,Cm	UL418	02/08/94	103	27.0	1250	1090	100	499	3503	85	8.27	18.0	0.70893
Spring	O,Cm	UL419	02/08/94	48000	116	1440	2100	48000	1550	4277	126	7.61	10.8	0.70871
R.B.Spring bl.Buotama	J,Cm	UL704	03/08/96	475	19.8	380	778	79.4	55.8	2784	166	8.00	5.90	0.70950

Codes for Age are crude estimates from 1:2 500 000 geologic map. Ar: Archean, Pr: Proterozoic, Cm: Cambrian, O: Ordovician, S: Silurian, P:Permian, Tr: Triassic, J: Jurassic, K: Cretaceous, N: Neogene, Q: Quaternary.
n.d.= not determined.

Table 2. Flux calculations for the Siberian and Chinese rivers draining sedimentary platforms.

River Name	Area	Discharge	Na	K	Mg	Ca	Cl	SO_4	HCO_3	Si	$^{87}Sr/^{86}Sr$ [c]	Dissolved Flux [d]	Dissolved Flux	Net CO_2 Flux [e]
	10^3 km^2	km^3/yr	<			10^9 mol/yr				>		10^9 mol/yr	10^6 mol/km^2/yr	10^3 mol/km^2/yr
SIBERIAN RIVERS														
Cambrian & Ordovician (CmO)														
Manzurka	4.40	0.661	0.121	0.013	0.624	1.11	0.093	0.694	2.12	0.096	0.7085	4.87	1.11	44
Lena ab Manzurka	9.59	1.92	1.34	0.019	1.14	1.89	1.16	0.868	4.40	0.194	0.7089	11.0	1.15	40
Tutura	19.5	3.51	1.50	0.070	1.89	4.42	1.23	0.515	12.3	0.291	0.7084	22.2	1.14	30
Orlinga	3.99	0.719	0.045	0.015	0.382	0.862	0.033	0.078	2.42	0.037	0.7091	3.87	0.97	19
Tayura	6.65	1.66	0.069	0.024	0.872	1.46	0.044	0.207	4.39	0.013	0.7092	7.08	1.06	4
Ulkan	1.48	0.371	0.035	0.008	0.223	0.288	0.007	0.052	0.953	0.004	0.7095	1.57	1.06	6
Kuta	13.6	2.04	1.27	0.050	1.80	2.26	1.25	0.822	6.55	0.035	0.7089	14.0	1.03	5
Bolshaya Tira	7.06	1.06	0.124	0.035	1.13	0.880	0.066	0.345	3.43	0.010	0.7092	6.02	0.85	3
Kirenga	39.1	13.7	22.3	0.137	4.29	8.68	19.959	4.52	18.8	1.15	0.7098	79.8	2.04	59
Mogol	2.00	0.699	1.01	0.007	0.406	0.713	0.992	0.216	1.90	0.046	0.7090	5.29	2.65	46
Pulka	2.16	0.649	1.25	0.034	0.420	0.752	1.26	0.454	1.40	0.053	0.7091	5.62	2.60	49
Chara	87.6	26.3	6.07	0.344	3.86	11.1	5.24	3.47	24.7	1.97	0.7121	56.7	0.65	275
Olekma	138	27.6	3.03	0.222	2.61	6.18	2.87	2.48	12.9	2.84	0.7098	33.2	0.24	41
Tuolbachen	4.29	0.214	0.034	0.003	0.195	0.405	0.033	0.218	0.794	0.011	0.7085	1.69	0.40	5
Tuolba	14.9	0.743	0.063	0.010	0.590	1.02	0.045	0.486	2.27	0.044	0.7087	4.53	0.30	6
Buotama	13.6	0.678	0.050	0.008	0.510	0.786	0.026	0.070	2.47	0.037	0.7093	3.96	0.29	5
Sumnagin	1.03	0.072	0.002	0.001	0.071	0.068	0.001	0.002	0.276	0.005	0.7096	0.42	0.41	10
Yungyuele	14.6	1.02	0.033	0.017	1.01	0.751	0.034	0.106	3.34	0.068	0.7088	5.36	0.37	9
Amga	67.5	3.38	0.179	0.029	2.09	2.74	0.141	0.281	9.37	0.246	0.7091	15.1	0.22	7
Muna	29.7	4.45	0.162	0.053	1.01	5.52	0.027	0.104	13.6	0.156	0.7093	20.7	0.70	10
Maya	172	34.4	1.93	0.354	5.26	11.8	0.337	1.64	34.4	3.03	0.7113	58.8	0.34	191
Allakh-Yun	24.8	4.95	0.228	0.068	0.570	2.12	0.058	0.218	5.24	0.347	0.7119	8.85	0.36	210
Khanda	8.18	1.64	0.062	0.014	0.530	1.78	0.025	0.180	4.39	0.065	0.7115	7.04	0.86	526
Total [f]	*685*	*132*	*40.9*	*1.54*	*31.5*	*67.6*	*34.9*	*18.0*	*172*	*10.7*		*378*	*0.55*	*112*
Jurassic & Cretaceous (JK)														
Ichera	5.55	0.8329	23.7	0.1224	1.04	1.57	23.2	1.30	2.70	0.024	0.70883	53.7	9.66	9
Peleduy	16.9	2.53	28.4	0.1189	3.52	4.92	28.4	4.89	8.25	0.106	0.70855	78.6	4.65	13
Khamra	2.56	0.384	2.20	0.0194	0.424	0.595	2.20	0.356	1.32	0.018	0.70889	7.14	2.79	14
Nyuya	39.9	5.99	54.1	0.2563	7.90	14.6	54.2	13.1	16.0	0.162	0.70874	160	4.02	8
Ura	7.38	0.7383	1.04	0.0159	0.406	0.760	1.03	0.281	1.78	0.068	0.71021	5.39	0.73	243
Biryuk	9.56	0.9556	2.66	0.0529	1.36	3.83	2.27	4.26	2.33	0.038	0.70878	16.8	1.76	8
Namana	15.6	1.09	8.08	0.030	0.663	1.99	8.08	1.77	1.74	0.123	0.70863	22.5	1.44	16
Markha	9.47	0.4737	0.031	0.0049	0.187	0.406	0.0015	0.051	1.11	0.020	0.70863	1.81	0.19	4
Markhachan	4.57	0.2284	0.012	0.001	0.073	0.130	0.000	0.005	0.397	0.010	0.70927	0.63	0.14	5

Table 2. continued.

River Name	Area	Discharge	Na	K	Mg	Ca	Cl	SO_4	HCO_3	Si	$^{87}Sr/^{86}Sr$ [c]	Dissolved Flux [d]	Dissolved Flux	Net CO_2 Flux [e]
	10^3 km^2	km^3/yr	<			10^9 mol/yr				>		10^9 mol/yr	10^6 mol/km^2/yr	10^3 mol/km^2/yr
Malykhan	2.26	0.1132	0.006	0.0021	0.078	0.129	0.0046	0.002	0.426	0.009	0.70981	0.66	0.29	8
Sinaya	30.6	0.9171	0.151	0.0218	0.281	0.725	0.0322	0.072	1.99	0.005	0.70954	3.28	0.11	0
Kenkeme	7.75	1.55	0.264	0.060	0.392	0.628	0.030	0.022	2.18	0.028	0.71253	3.60	0.46	295
Notora	6.50	0.260	0.012	0.0017	0.026	0.040	0.0018	0.006	0.136	0.023	0.71172	0.25	0.04	20
Tatta	10.0	0.3011	0.058	0.0079	0.175	0.261	0.0042	0.002	0.919	0.008	0.71336	1.44	0.14	92
Total[f]	*169*	*16.4*	*121*	*0.715*	*16.5*	*30.6*	*120*	*26.1*	*41.3*	*0.644*		*356*	*2.11*	*37*
Olenek Plateau (OL)														
Eyekit	7.05	1.06	0.080	0.0111	0.156	0.418	0.0026	0.106	1.012	0.059	0.7103	1.84	0.26	145
Erdilyakh-Yuryage	1.35	0.2019	0.006	0.0015	0.012	0.053	0.0022	0.001	0.131	0.007	n.d.	0.21	0.16	10
Kuogastakh-Yuryage	1.60	0.240	0.006	0.0025	0.030	0.062	0.0016	0.003	0.174	0.012	0.71036	0.29	0.18	116
Ulakhen-Yuryage	2.93	0.439	0.018	0.0044	0.048	0.130	0.0159	0.051	0.248	0.017	0.71036	0.53	0.18	89
Khorbosunka	5.27	0.7909	0.019	0.0071	0.161	0.618	0.0055	0.003	1.501	0.020	0.71003	2.33	0.44	298
Bur	14.1	2.12	0.072	0.0177	0.295	0.618	0.0127	0.067	1.752	0.078	0.71005	2.91	0.21	125
Total[f]	*32.3*	*4.85*	*0.201*	*0.044*	*0.701*	*1.90*	*0.041*	*0.231*	*4.82*	*0.193*		*8.13*	*0.25*	*149*
Olenek @ mouth	237	35.5	5.50	0.3239	8.684	29.55	2.5793	0.777	75.52	1.863	0.70925	125	0.53	16
CHINESE RIVERS														
Yangtze [a]	1950	953	169	46.7	284	656	116	131	1681	103	0.7108	3187	1.63	106
[b]	1960	1063	190	33.8	286	1190	123	198	2570	102		4693	2.39	104
Huanghe [a]	750	32.6	59.9	2.3	27.7	31.4	38.9	21.5	94.4	2.7	0.7111	279	0.37	7
[b]	745	48	102	3.0	43	60.0	54	37	178	4.5		482	0.65	12

a. Discharge weighted flux estimates based on monthly chemical and discharge data of Yangtze at Datong and Huanghe at Loukou (Gan et al., 1982).

b. Flux estimates for Yangtze at Wuhan and Huanghe at Gorges Dam from Hu et al., 1982 Table 3.

c. $^{87}Sr/^{86}Sr$ of Chinese rivers were taken from Palmer and Edmond, 1989.

d. Dissolved Flux = Flux of (Na + K + Mg + Ca + Cl + SO_4 + HCO_3 + Si).

e. $\phi CO_2 = 2\phi Si$ when $^{87}Sr/^{86}Sr < 0.710$, $\phi CO_2 = \phi TZ^{+*}$ when $^{87}Sr/^{86}Sr > 0.710$. For Chinese rivers Si fluxes are used due to lack of Sr isotope data at tributary scale.

f. Area-weighted averages are reported for Dissolved Flux (10^6 mol/km^2/yr) and Net CO_2 Flux (10^3 mol/km^2/yr).

Figure 1. Schematic map of the rivers of eastern Siberia that have been sampled in this project. Lake Baikal occupies the southwestern corner.

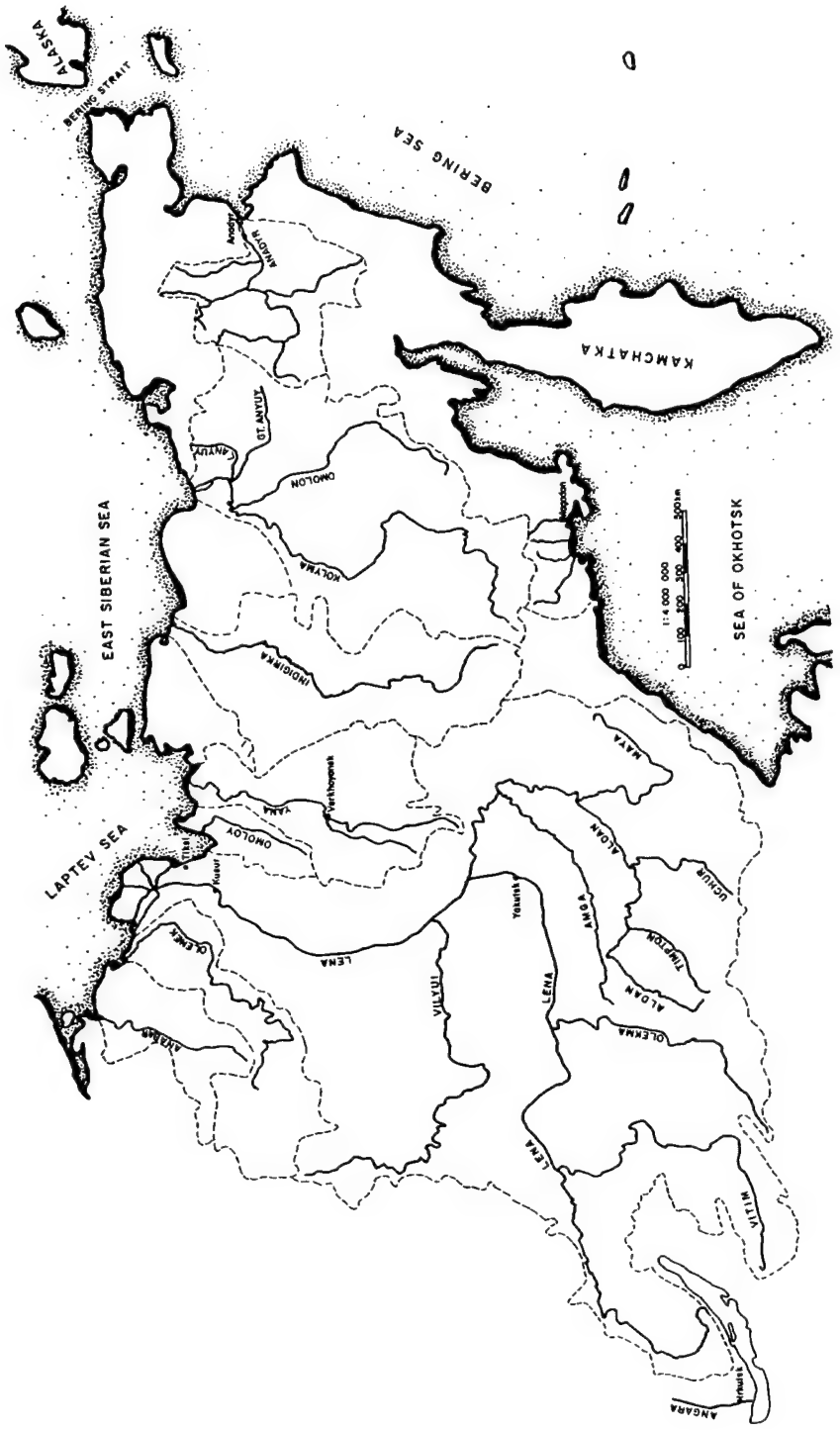
ALASKA
BERING STRAIT
BERING SEA
KAMCHATKA
EAST SIBERIAN SEA
LAPTEV SEA
SEA OF OKHOTSK
ANADYR
GT. ANYUY
ANYUY
OMOLON
KOLYMA
INDIGIRKA
YANA
Verkhoyansk
OMOLOY
Yakutsk
LENA
VILYUI
Yakutsk
LENA
AMGA
ALDAN
MAYA
ALDAN
TIMPTON
OLEKMA
UCHUR
VITIM
ANGARA
Irkutsk
0
100
200
300
400
500km
1:4 000 000

Figure 2. Location of stations on the Lena, Olenek, and Anabar rivers. UL100, 200, 300, 400, 500, 600, 700, and 800 series represent expeditions in 1991 (Aldan), 1992 (Lena), 1993 (Olenek), 1994 (Upper Lena), 1994 (Olenek-Chara, Anabar), 1995 (Lower Lena), 1996 (Upper Lena Reoccupation), and 1997 (Upper Aldan), respectively. Only rivers draining the Siberian Platform are discussed in this paper (Table 1). The stippled area denotes the continuous basement outcrop of the Trans-Baikal Highlands and Aldan Shield; the rest of the basin contains a sedimentary cover. Discharge measurements at Kusur above the delta shown in the inset is from the Global Hydrological Archive and Analysis System. The locations of the gauging stations are marked with filled squares and their discharge hydrographs are shown in Fig. 3.

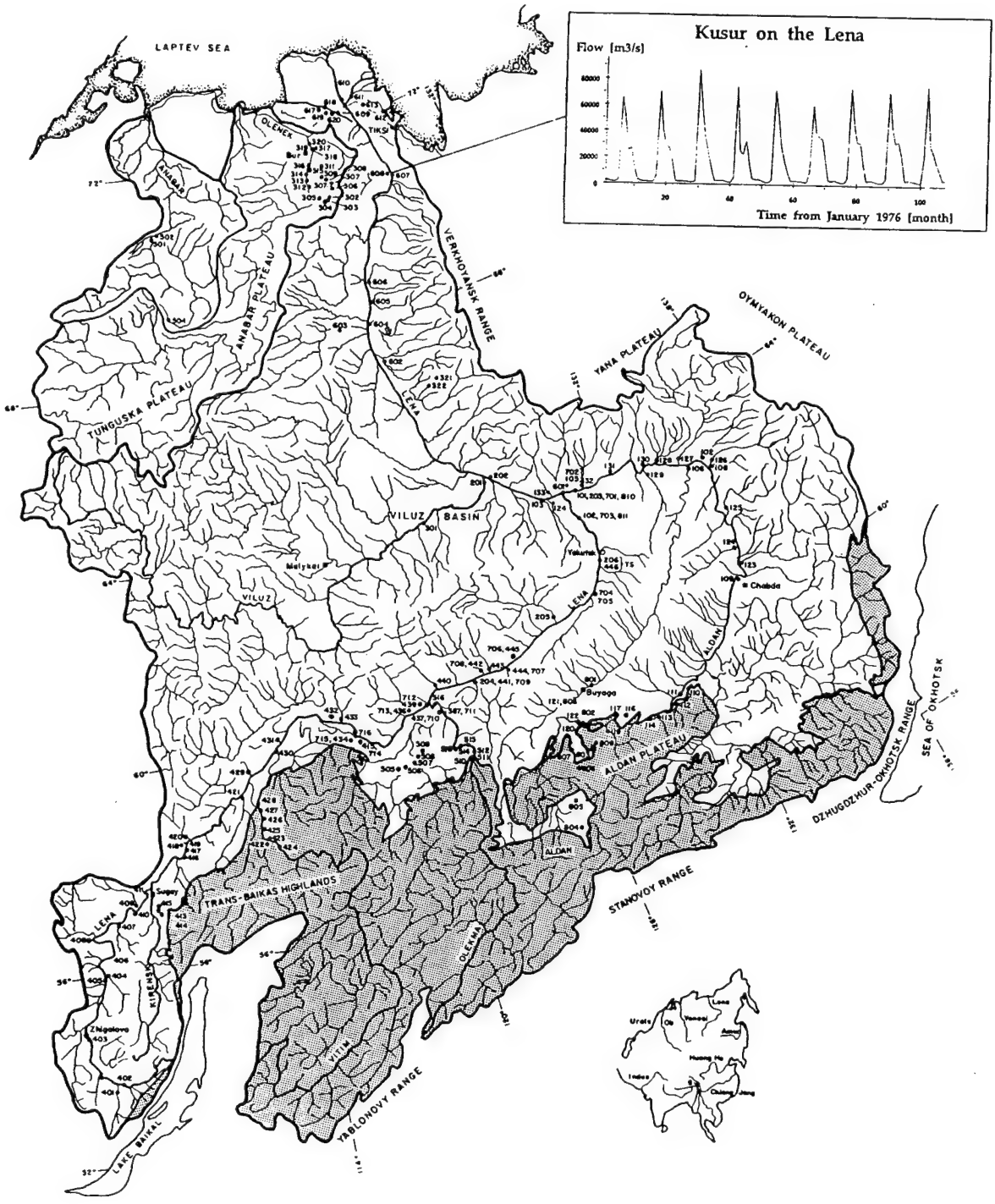
Kusur on the Lena
Flow [m3/s]
Time from January 1976 [month]
LAPTEV SEA
TUNGUSKA PLATEAU
ANABAR PLATEAU
VERKHOYANSK RANGE
YANA PLATEAU
OYMYAKON PLATEAU
VILUY BASIN
VILUY
LENA
ALDAN
ALDAN PLATEAU
DZHUGDZHUR-OKHOTSK RANGE
SEA OF OKHOTSK
STANOVOY RANGE
TRANS-BAIKAL HIGHLANDS
OLEKMA
YABLONOVY RANGE
LAKE BAIKAL
KIRENGA
Chabda
Buyoga
Yakutsk
Melyker
Suppy
Zhigalovo

Figure 3. The discharge hydrographs of the tributaries of the Lena from 1965-1975 (UNESCO, 1979). They are arranged geographically in order to facilitate comparison of the timing of the spring-melt and the summer monsoon. The sampling times are shown with the arrows. The locations of the gauging stations are shown in Fig. 2.

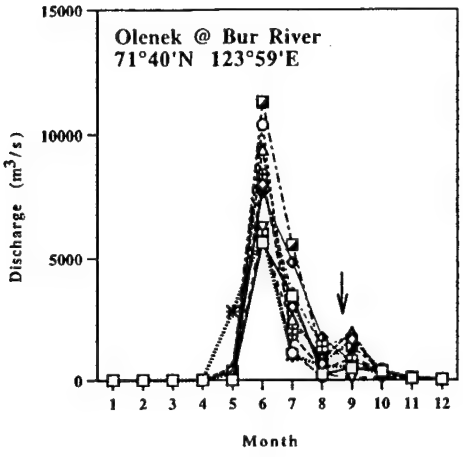
Olenek @ Bur River
71°40'N 123°59'E
Discharge (m3/s)
Month

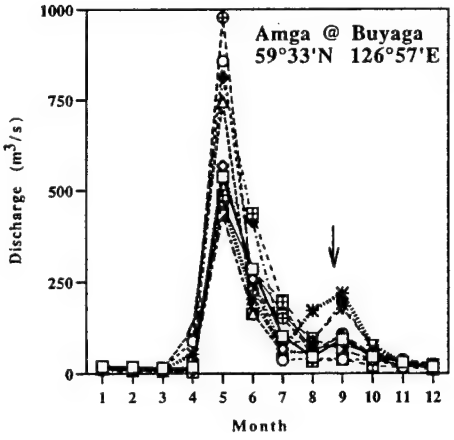
Amga @ Buyaga
59°33'N 126°57'E
Discharge (m3/s)
Month

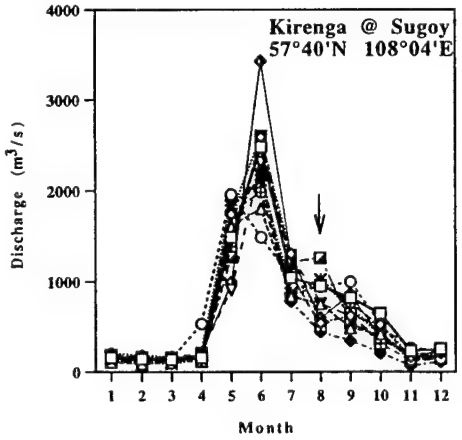
Kirenga @ Sugoy
57°40'N 108°04'E
Discharge (m3/s)
Month

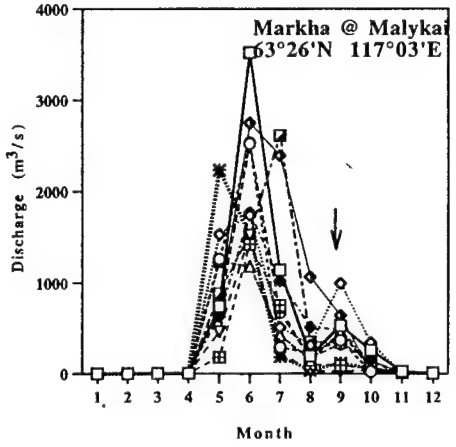
Markha @ Malykai
63°26'N 117°03'E
Discharge (m3/s)
Month

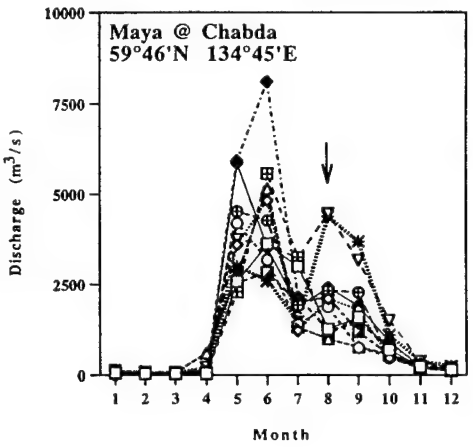
Maya @ Chabda
59°46'N 134°45'E
Discharge (m3/s)
Month

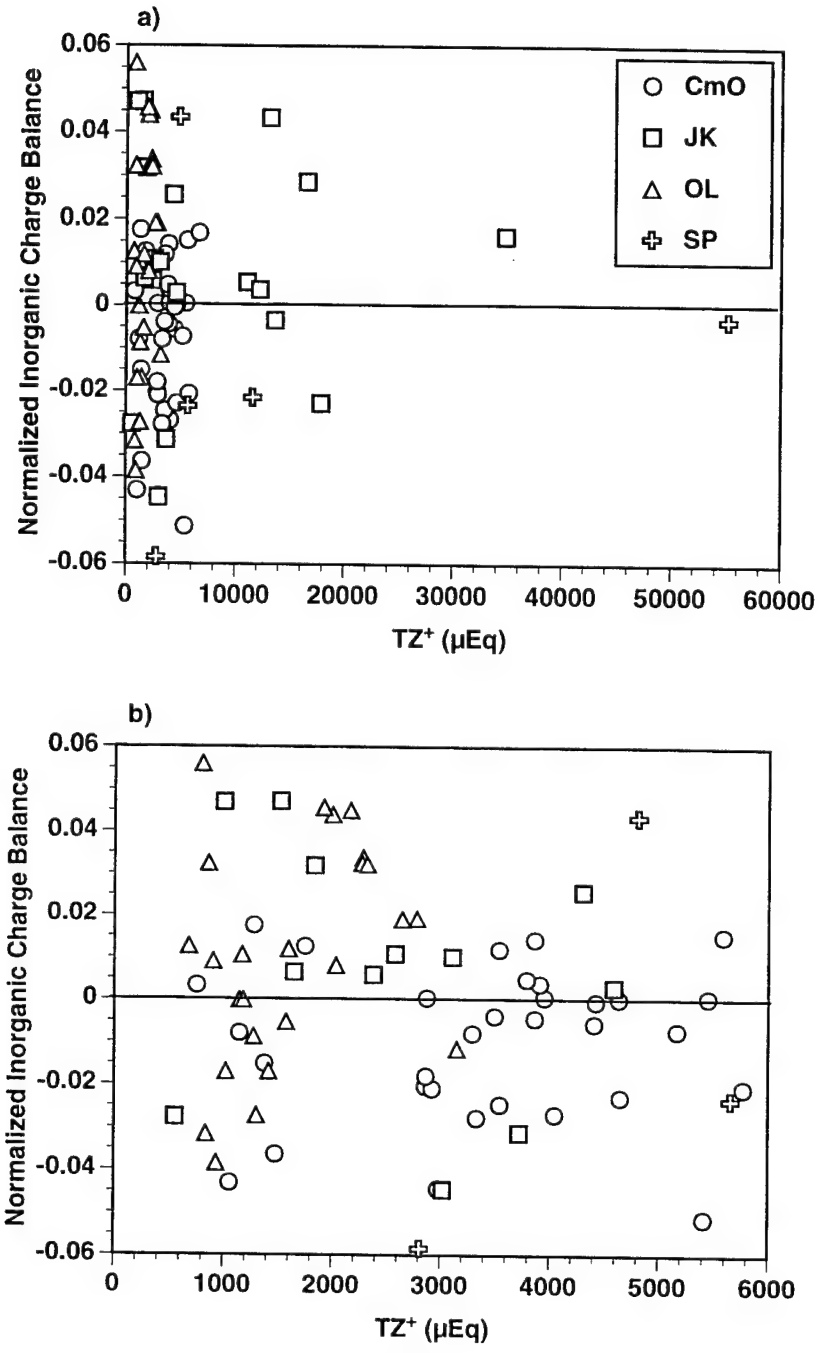

Figure 4. Normalized Inorganic Charge Balance (NICB) vs. TZ^+ at (a) full scale and at (b) expanded scale. NICB is defined as the fractional difference between the total cations and total anions. The measured major ions (Na^+, K^+, Mg^{2+}, Ca^{2+}, Cl^-, SO_4^{2-}, HCO_3^-) are enough to give a charge balance. A set of six tributaries (UL420, 429, 432, 430, 436, 431) in the JK category have >10,000 µEq. These rivers drain the distal evaporitic formations in the southern part of the basin as mentioned in the description of the geology. The tributaries in the OL category have lower TZ^+ values with a smaller range (~700 - 3,200 µEq), than those of CmO and JK (600 - 35,000 µEq) and SP (~3,000 - 55,200 µEq).

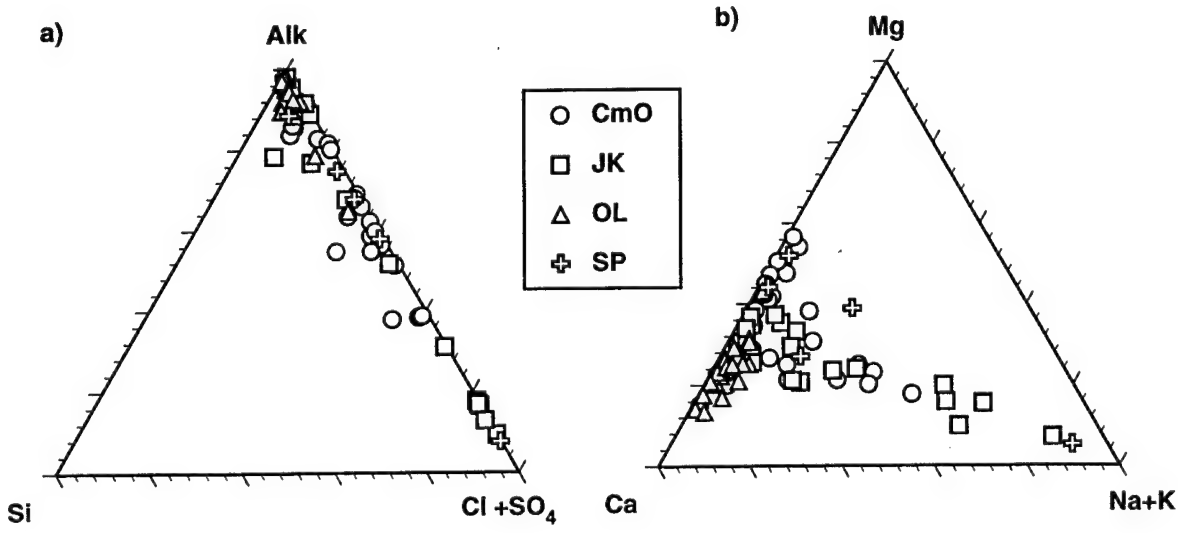

Figure 5. (a) Anion ternary diagram in units of μEq. Alkalinity dominance is readily visible with ($Cl+SO_4$) dominance in some evaporitic streams. The CmO samples fall on the alkalinity apex and extend to the ($Cl+SO_4$) apex with a $Si:TZ^+$ ratio <0.1. A few with headwaters in the TBH and the Aldan Shield have higher Si. The JK samples, especially the six evaporitic samples, fall on a line extending to ($Cl+SO_4$).

(b) Cation ternary diagram. Ca is dominant with increasing contribution of Na in evaporitic streams. The CmO streams have a variable Mg/Ca ratio (0.2-1.3). The CmO evaporitic platform carbonates in the south of the basin have abundant dolomite (Rundquist and Mitrofanov, 1993). Assuming complete dissolution of carbonates, a simple mixing calculation between pure limestone and pure dolomite end-members to give the observed Mg/Ca ratio in these river waters suggests that the most magnesian sample has 100% dolomite and the most calcic 20% dolomite. Generally the samples fall around Mg/Ca = 0.67 with <10% of TZ^+ accounted by (Na+K). A few samples trend to the (Na+K) apex, probably from the contribution of alkali feldspars. JK continental sediments have Mg/Ca ratios ~0.5 at low concentrations and at high concentrations ~1. Most fall near Mg/Ca = 0.6 (average carbonate) with the six evaporitic samples trending toward the (Na+K) apex maintaining the same Mg/Ca ratio. OL samples have Mg/Ca=0.25 and extend to (Na+K). One extreme sample (UL305) has Mg/Ca ~0.67. The SP samples have nearly equal proportions of Ca and Mg and trend toward (Na+K) maintaining this ratio. UL406 and 408 are more influenced by gypsum dissolution and UL419 is enriched in Na and Cl from halite.

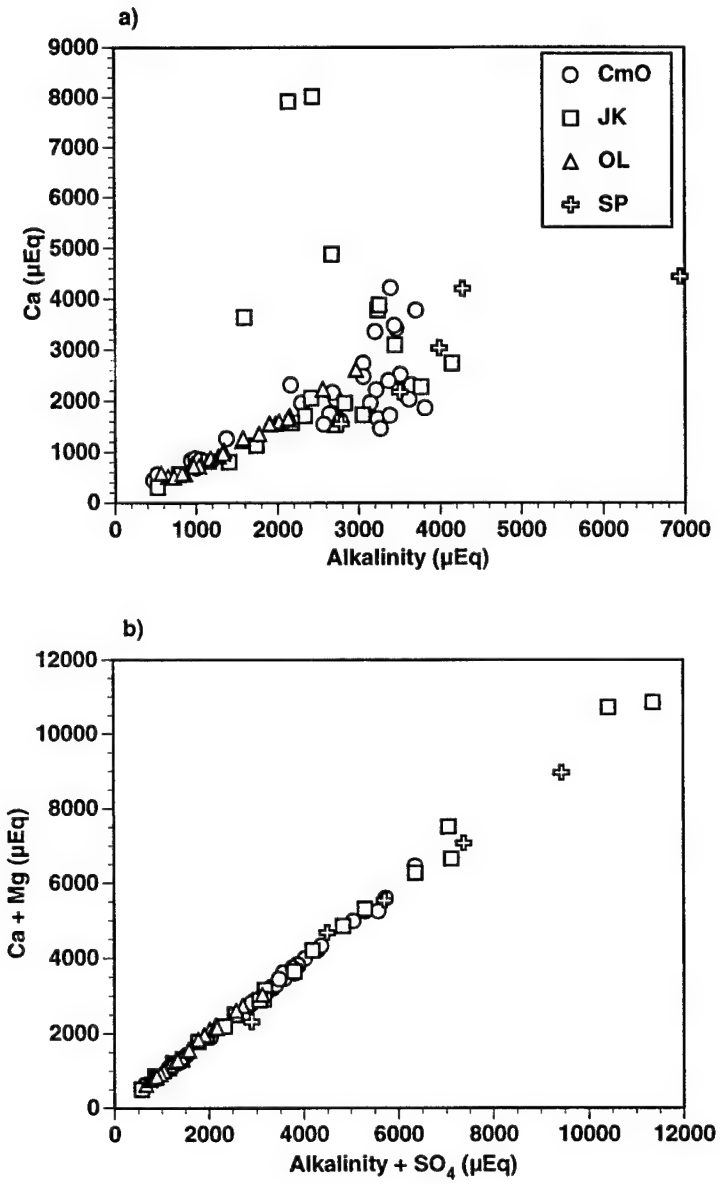

Figure 6. (a) Ca vs. alkalinity. (b) (Ca+Mg) vs. (alkalinity+SO_4). The rivers are Ca-HCO_3 dominated, and at high concentrations gypsum/anhydrite dissolution becomes important. The CmO samples have Ca values of ~200 - 1,900 µM and Mg ~100 - 1,100 µM. The JK continental sediments have much higher concentrations reaching 3,700 µM Ca and 1,500 Mg in the evaporitic rivers mentioned in the text. The OL samples have low Ca (<1,400 µM) and Mg (<300).

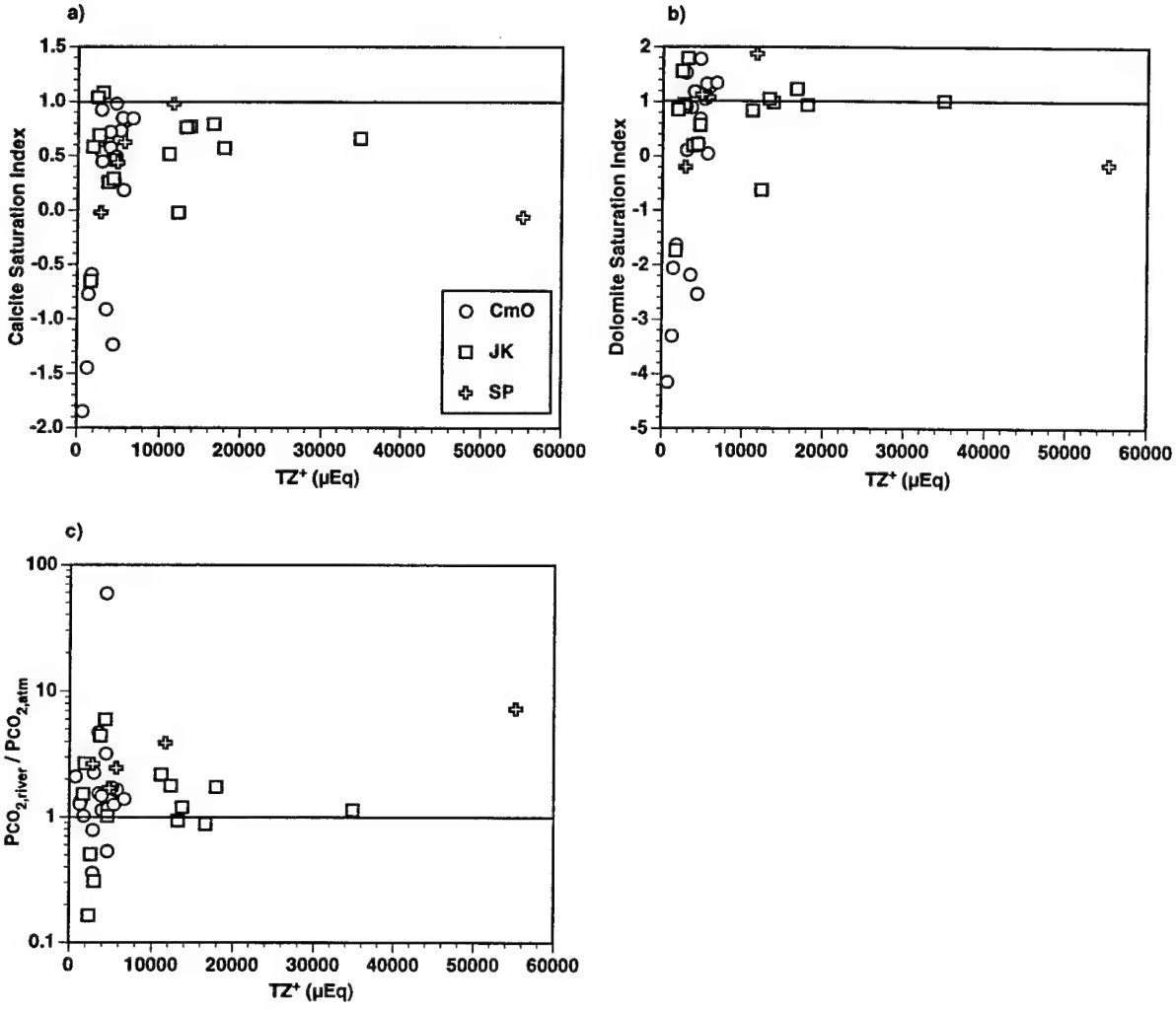

Figure 7. (a) Calcite Saturation Index (CSI) plotted against total cationic charge (TZ^+). CSI is defined as $\log(\{Ca^{2+}\}\{CO_3^{2-}\} / K_{calcite})$ where { } denotes activity. (b) Dolomite Saturation Index (DSI) against TZ^+. $DSI = \log(\{Ca^{2+}\}\{Mg^{2+}\}\{CO_3^{2-}\}^2 / K_{dolomite})$. (c) $PCO_{2,river}/PCO_{2,atm}$ vs. TZ^+ shows that the Siberian rivers do not have particularly high PCO_2 values and therefore are not a substantial source of CO_2 emissions. $PCO_{2,atm}$ is taken as 330 µatm.

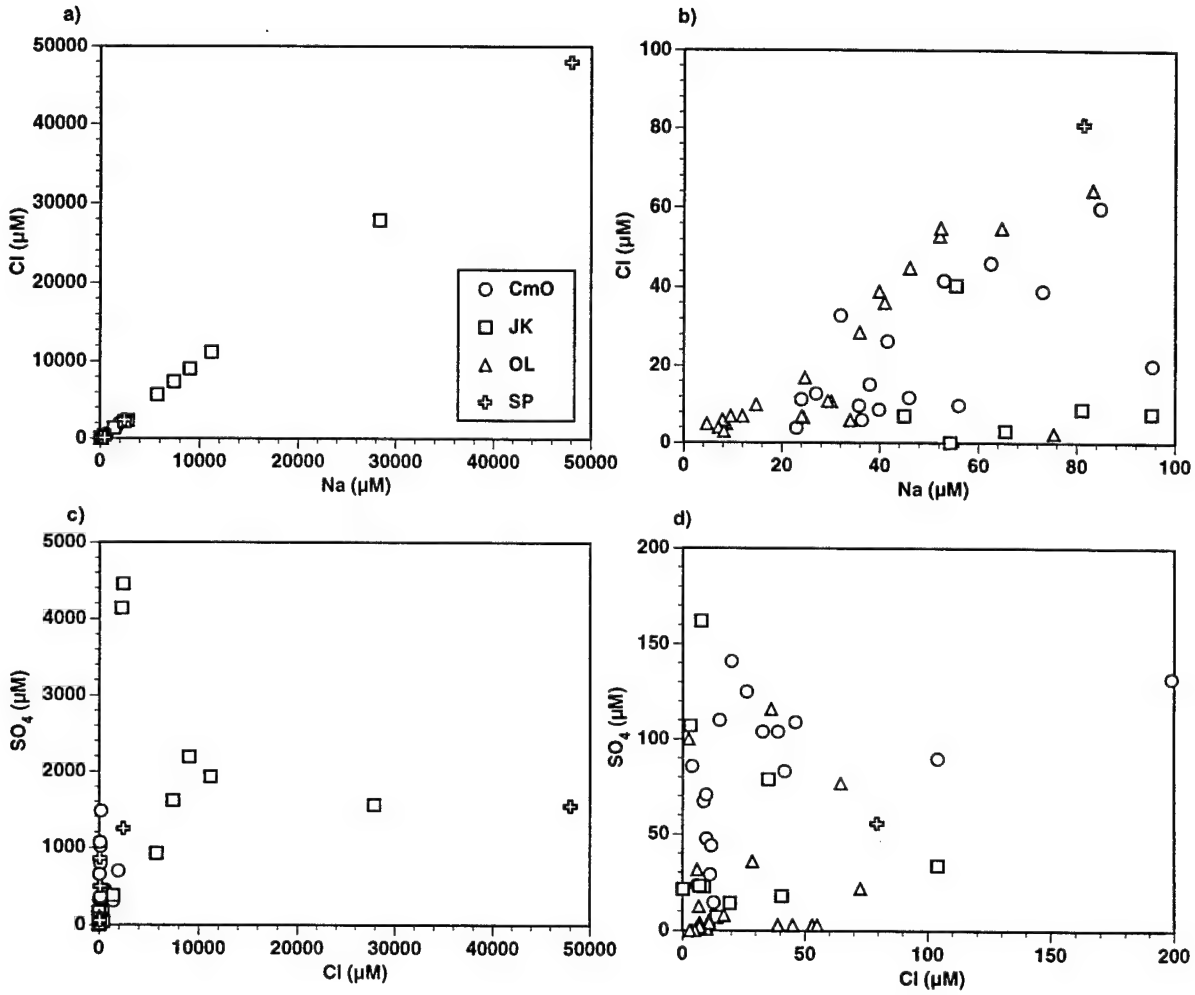

Figure 8. (a) Na vs. Cl at full scale highlights the evaporitic rivers at high concentrations. (b) Na vs. Cl at expanded scale shows that some of the rivers have higher Na than Cl, supplied by weathering of Na-silicates. (c, d) SO_4 vs. Cl. No relationship exists between SO_4 and Cl even for evaporitic rivers. The full range shows the most evaporitic samples of JK and SP to have both high SO_4 with low Cl and high Cl with low SO_4 trends. The proportions of SO_4 from gypsum/anhydrite to total cationic charge for CmO are 0 - 37% with UL401 having the highest and UL117 and 603 being purely Ca-Mg-HCO_3; for JK, 0 - 63 %;. OL has $CaSO_4$ in the range 1 - 28% but usually <5%, and SP has 5 - 27%.

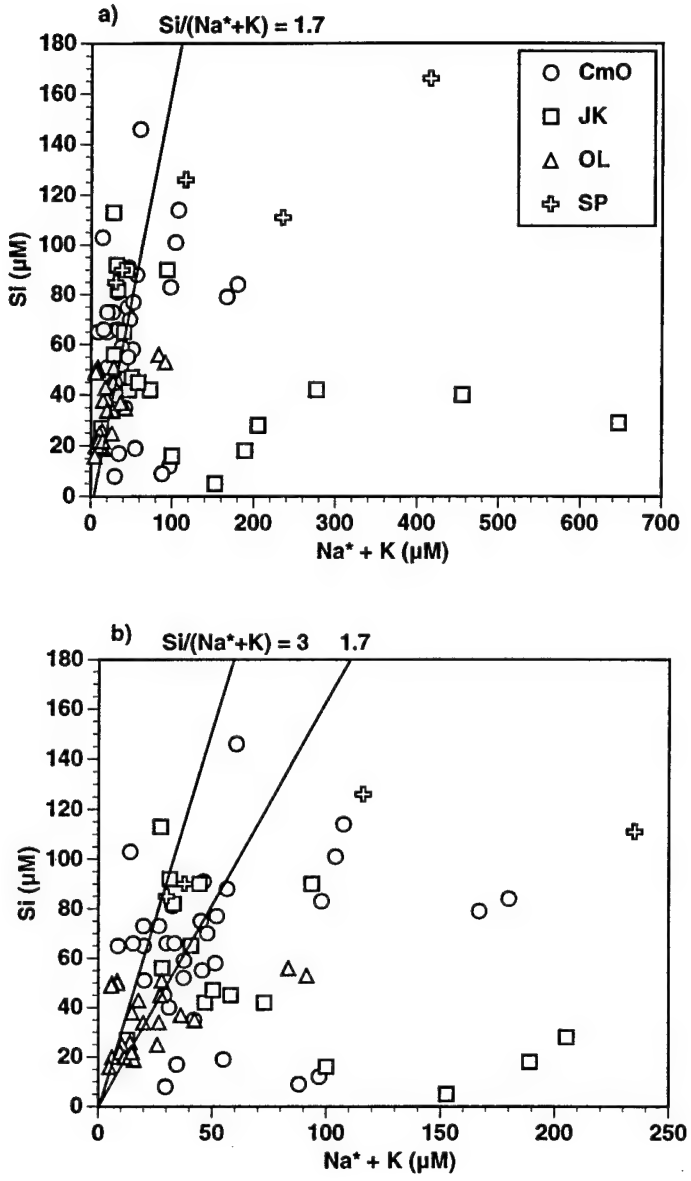

Figure 9. Si vs. Na*+K (= [Na-Cl]+K) at (a) full and (b) expanded scales show the large range in Si concentrations. Si values in the CmO category range from 8 to 146 µM, with higher values, >100 µM, in rivers near the TBH and Aldan Shield areas. JK silica values range from 5 to 113 µM. OL silica values are generally low (16-56 µM). SP has relatively high silica (85-166 µM). There is a lack of any tight correlation between Si and (Na*+K). Si/(Na+K) values reported for the Russian Platform range from 0.01 (salts) to 38 (siliceous rocks) (Ronov and Migdisov, 1970). As Cl values are not reported, correction was not made for evaporites. Si/(Na+K) ratios released during weathering of representative silicate minerals are:
Na-feldspar → beidellite (1.67); Na-feldspar → kaolinite (2); K-feldspar → kaolinite (2); K-feldspar → illite (3); Na-feldspar → gibbsite (3); 8: illite → gibbsite (3); beidellite → kaolinite (4); gibbsite → kaolinite (∞).

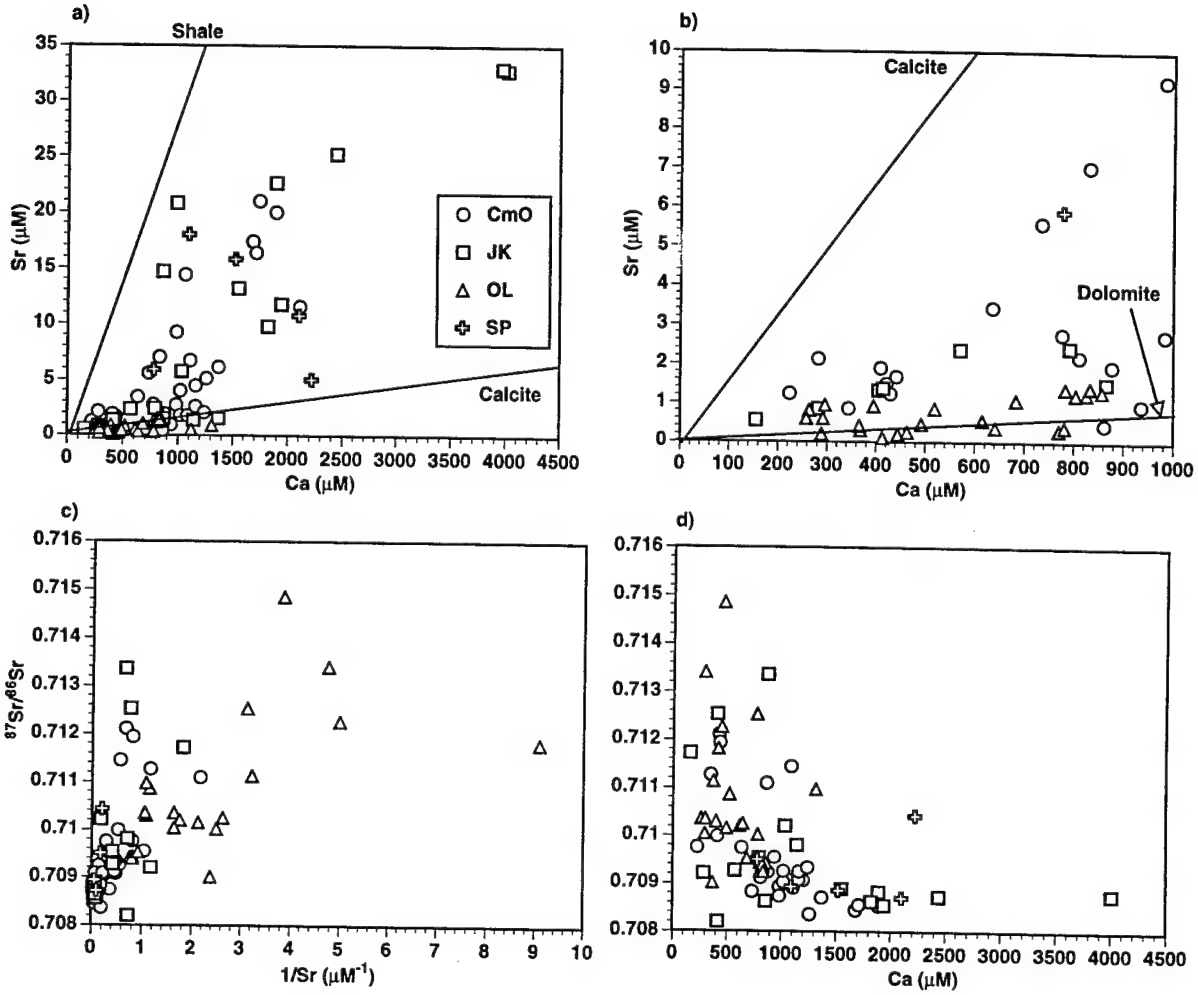

Figure 10. Sr vs. Ca plot at (a) full and (b) expanded scales. At high concentrations the Sr/Ca ratios are approach the values for average shale (0.028; Turekian and Kulp, 1956). At low concentrations the Sr/Ca ratios decrease to those of dolomites (0.00013; Vahrenkamp and Swart, 1990; Budd, 1997). Based on a review of the older data on Sr/Ca ratios in rivers, Meybeck (1986) reports molar Sr/Ca = 0.005 for shale and sandstone weathering, 0.0007 for carbonate, marble and carbonate cemented sandstone and 0.01 for evaporites. These representative Sr/Ca lines are shown for reference: shale (0.028), calcite (0.0026) and dolomite (0.00013). (c) $^{87}Sr/^{86}Sr$ vs. 1/Sr shows that all rivers fall in the range normally occupied by world rivers excepting the Himalayas. (d) $^{87}Sr/^{86}Sr$ vs. Ca highlights the Vendian carbonates at ~0.709.

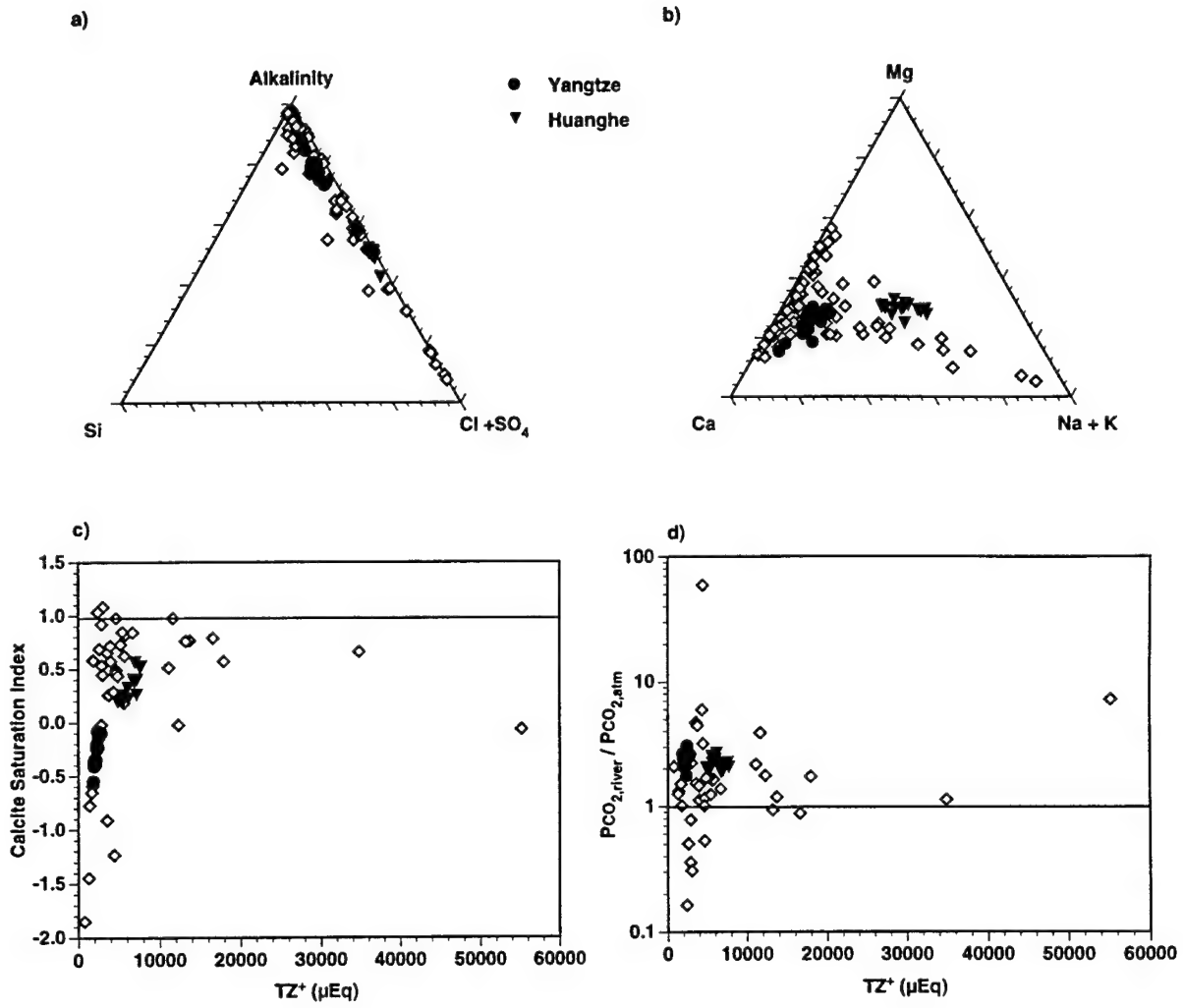

Figure 11. Dissolved chemical composition of Chinese rivers (filled symbols). Siberian rivers draining the platform (open symbols) are plotted in the background for comparison.

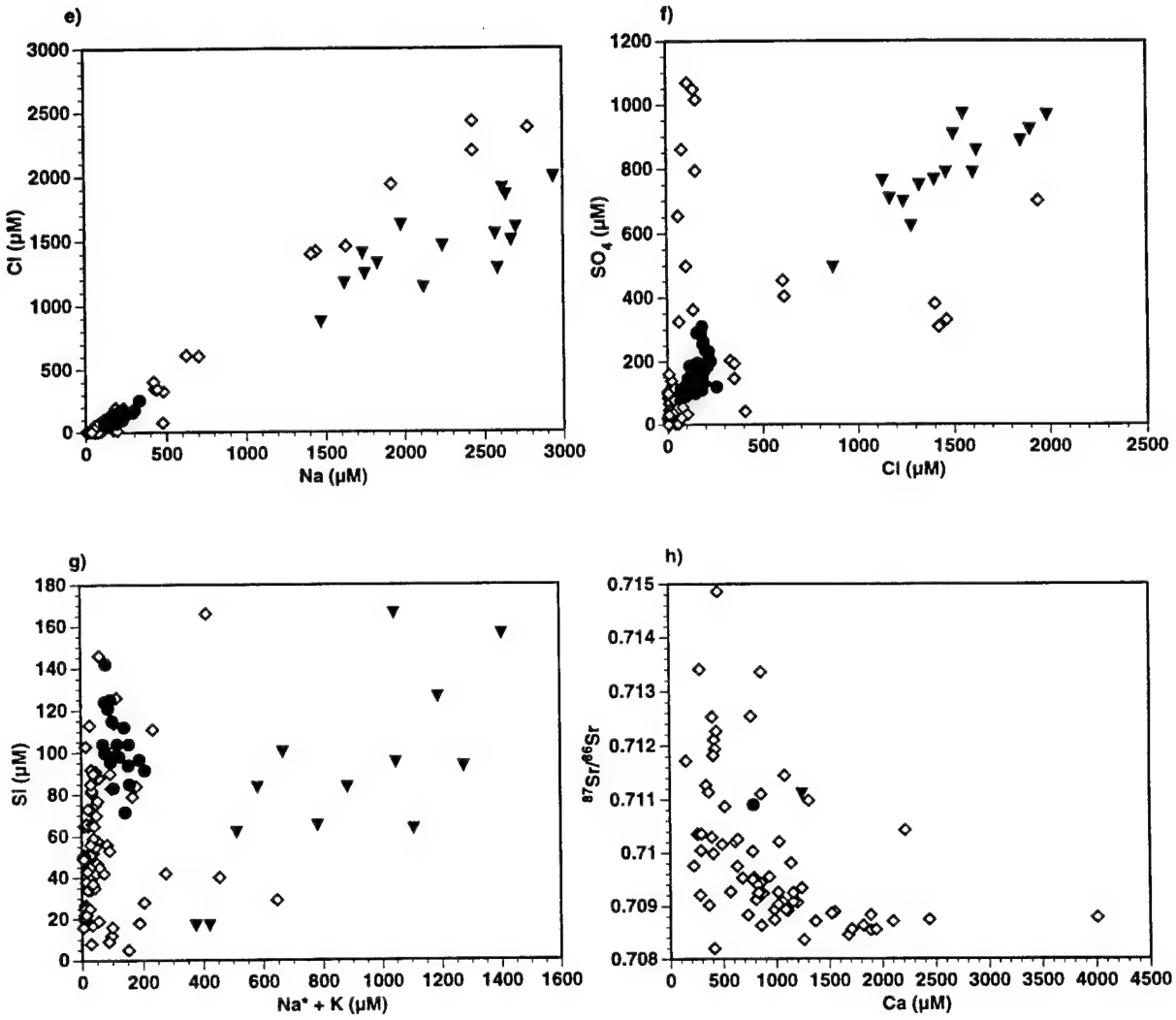

Figure 11 continued.

Chapter 3

The Fluvial Geochemistry of the Rivers of Eastern Siberia II: Tributaries of the Lena, Omoloy,Yana, Indigirka, Kolyma, and Anadyr Draining the Collisional/Accretionary Zone of the Verkhoyansk and Cherskiy Ranges*

* Huh Y., Panteleyev G., Babich D., Zaitsev A., and Edmond J. M. (1998) The fluvial geochemistry of the rivers of Eastern Siberia II: Tributaries of the Lena, Omoloy, Yana, Indigirka, Kolyma, and Anadyr draining the collisional/accretionary zone of the Verkhoyansk and Cherskiy ranges. *Geochim. Cosmochim. Acta* , in press (March 5, 1998). Permission requested from Elsevier Science LTD.

Abstract

Fundamental to the global carbon cycle over geologic time scales is the control of atmospheric CO_2 by aluminosilicate weathering. Much of the information on the rates of this process comes from rivers in the tropics and subtropics. To understand the possible climatic influences systematic studies are needed for the arctic/subarctic regions. This is the second in a series of papers addressing this problem by systematic studies of the pristine rivers of the Russian Far East.

The region to the east of the Siberian Platform (Huh *et al.*, in review) is a geologically complex terrain formed by the Mesozoic collision and accretion of the Siberian and Kolyma plates. Because of the arid continental climate, it has not been glaciated in the recent past. Thus, it is possible to study weathering processes in an arctic environment dominated solely by cryogenic interactions without contamination by heterogeneous components derived from scouring glaciers. All the major rivers and their tributaries in this area have been sampled on expeditions to individual basins (~100 samples) on a reconnaissance basis at falling stage, usually in July and August. The total dissolved cation levels (TZ^+) are moderate (up to ~3,100 μEq), and the major ion chemistry is indicative of Ca-aluminosilicate and carbonate weathering with significant contributions from black shales in some tributaries. The Si/TZ^{+*}, $Si/(Na^*+K)$ and $^{87}Sr/^{86}Sr$ ratios indicate that the weathering is superficial, i.e. only to cation-rich secondary minerals. The areal total dissolved solid fluxes range from 0.04 to 0.39 x 10^6 mol/km^2/yr, up to an order of magnitude lower than for the Amazon-Orinoco draining the Andes in the tropics (0.6 to 4.1 x 10^6 mol/km^2/yr). The CO_2 consumption by aluminosilicate weathering (18 to 230 x 10^3 mol/km^2/yr) is also at the lower end of the range observed in the Amazon-Orinoco headwaters (143 to 1,000 x 10^3 mol/km^2/yr). However, as the North American counterparts in similar latitudes and with comparable relief, the Mackenzie, Yukon and Fraser draining the Rockies, also have high dissolved solids (0.2 to 2.9 x 10^6 mol/km^2/yr)

and CO_2 (19 to 1,750 x 10^3 mol/km^2/yr) fluxes, these low values seem to be more a function of lithology than simply climate. Ice action in cold environments appears to overcome the inhibiting effects of the decreased temperatures and lack of precipitation in producing a high chemical yield but results in superficial weathering in the case of aluminosilicates.

Introduction

The possible responses of the continental weathering regime to climatic and tectonic variation on a variety of time scales is drawing much interest (Froelich *et al.*, 1992; Raymo and Ruddiman, 1992; Blum and Erel, 1995). While global deep-sea hydrothermal and subduction-related fluid inputs to the ocean are probably smoothly varying over time (Gaffin, 1987; Kastner *et al.*, 1991) and not directly influenced by climatic changes, the fluvial fluxes could be quite variable. In order to understand the link between these and climate, it is useful to study the current weathering patterns in high latitudes relative to those in the tropics as a surrogate for climatic deterioration. The very low temperatures and the cryogenic processes resulting from them make the arctic/subarctic a unique environment. The weathering fluxes and patterns might be expected to be quite distinct from those in the relatively well studied hot and humid tropics. Unusual magnitudes in the fluxes of certain elements or elemental and isotopic ratios associated with arctic fluvial weathering potentially could be used in interpreting the sedimentary record in terms of environmental change.

The arctic is a climatically sensitive region (Hansen *et al.*, 1983; Cuffey *et al.*, 1995). General Circulation Models predict that the global warming effects of carbon dioxide and other greenhouse gases will be amplified two to four times in the arctic relative to lower latitudes. How fast and how far the weathering regime will respond are important questions. The fluvial output to the shelf seas also affects the density stratification of the

Arctic Ocean, which can have effects extending to the whole ocean through the deep-water formation mechanisms (Aagaard and Carmack, 1989). Possible changes in the fluxes of nutrients like silica, nitrogen and phosphorus could affect the productivity and therefore the ecosystem in the shelf seas.

At present major signals are being imposed on the geochemical cycle by the active orogenies in the continental arc of the western Americas and the Tethyan collision zone (Sarin *et al.*, 1989; Edmond, 1992; Krishnaswami *et al.*, 1992; Edmond *et al.*, 1996). The effect of climate *per se* is more problematic. In global carbon cycle models, Arrhenius-type temperature-dependent weathering kinetics are central to the negative feedback mechanism of CO_2 over geologic time scales, presumed to be mediated by increased water vapor transport and precipitation (Berner *et al.*, 1983; Berner, 1994). The temperature feedback function of Berner (1994) is doubled if the temperature is 6°C higher than present and halved if the temperature is 6°C lower. This very large predicted variation can be tested with contemporary data on fluvial chemistry and fluxes as a function of climate.

In order to constrain the magnitude of the changes in weathering rates, and hence CO_2 consumption over time, and to study the effects of climatic and tectonic changes on the weathering yields from various geological settings, studies of pristine systems from a range of geologic, topographic, and climatological environments are needed. Various studies using the mass balance of major ions and the strontium isotope systematics have shown the close link between the geology of the drainage basins and the dissolved load and chemical composition of the rivers draining them —the Amazon (Gibbs, 1972; Stallard and Edmond, 1983, 1987), the Orinoco (Lewis and Weibezahn, 1981; Edmond *et al.*, 1995, 1996), the Yangtze and the Huanghe (Hu *et al.*, 1982; Zhang *et al.*, 1990), the Indus (Pande *et al.*, 1994), the Ganga-Brahmaputra (Sarin *et al.*, 1989; Palmer and Edmond, 1992), the Mekong (Carbonnel and Meybeck, 1975), and the Congo (Négrel *et al.*, 1993). However, these studies have been concentrated in the tropical/temperate zones. The only comparable work reported for high latitudes is on the Mackenzie (Reeder *et al.*, 1972), the

Fraser (Cameron *et al.*, 1995), the Lena delta outlets (Gordeev and Sidorov, 1993), the tributaries of the Siberian Platform (Huh *et al.*, in review), and the rivers of Iceland and Sweden (Gíslason *et al.*, 1996; Andersson *et al.*, 1994). For basins that have been glaciated in the recent past, like the Mackenzie, it is difficult to distinguish between the weathering of *in situ* basement rocks from that of the transported and disaggregated glacial overburden (Reeder *et al.*, 1972; Wadleigh *et al.*, 1985; Newton *et al.*, 1987). The data reported for the Lena delta gives a monitor of the flux of the major elements from the entire basin to the Arctic Ocean using information based on monthly samples.

The effect of climate on riverine dissolved loads has been addressed previously in some reconnaissance and budget studies. Peters (1984) surveyed the available data for U.S. rivers but did not find any conclusive evidence for an effect of temperature on weathering. He attributed this to enhanced physical and chemical weathering due to frost cracking and wedging in cold environments outweighing the effects of warm, humid processes in the tropics. Bluth and Kump (1994) looked at small rivers draining the basaltic terrains of Iceland, the Colombia Plateau and Hawaii and found comparable weathering rates, as represented by silica and bicarbonate fluxes. On the other hand, Meybeck (1986) examined French streams draining monolithologic watersheds and found a positive relationship with temperature. Drever and Zobrist (1992) showed that the concentrations of the major cations, silica and alkalinity decreased with elevation (decreasing temperature) within a single alpine watershed but that the weathering stoichiometry remained constant. In a comparison of two drainages at two different elevations and temperatures (11.7 vs. 10.6°C), Velbel (1993) observed higher dissolution rates of feldspars at higher temperatures and calculated the activation energy to be higher than previous estimates suggesting higher weathering-mediated negative feedback between global temperature and atmospheric CO_2. However the database remains very small.

New data from large basins are needed in other lithologic terrains at high latitudes in order to establish directly the influence of climate on weathering yields and the effects of

climate change on this sink for atmospheric CO_2. The study presented here of the rivers of the Russian Far East (east of Lake Baikal) provides a systematic look at drainage basins in a vast and relatively unstudied area (Fig. 1) in an effort to constrain the magnitude, composition and causes of the fluvial flux from high latitudes and to provide some "ground truth" for further modeling. This is the second part of a series, concentrating here on the tectonic collision zone of northeastern Russia; the Siberian Platform was explored in an earlier paper (Huh *et al.*, in review). The results will be compared to the published data from the orogenic belts in the tropical/temperate regions (Andes, Amazon and Orinoco) and also those of North American arctic/subarctic (Rockies, Mackenzie and Yukon). Reference is also made to studies of sedimentary platforms and basement terrains at both low and high latitudes to examine the general effect of tectonics.

Tectonic History and Lithology

Eastern Siberia has a mountainous topography. The salient features in the physiography of the Far East are the NW-SE trending Cherskiy Range with 3,000 m peaks and the Verkhoyansk Range with highs at 2,000 m. Pobeda Peak on the Cherskiy Range is the highest elevation (3,147 m). The Lena, Yana, Indigirka, Kolyma, and Anadyr are the major rivers of the Russian Far East and drain a Mesozoic continental collisional/accretionary zone of very complex geology, east of the Siberian Platform and stretching to the Pacific Ocean and the Bering Strait (Figs. 1, 2, 3).

During the Devonian rifting event on the Siberian Platform, terrains were split away from the eastern edge of the platform, amalgamated offshore in the Early Jurassic, and reaccreted in the Late Jurassic (Fujita *et al.*, 1997). The Omolon massif is a Precambrian structural unit which was separated from the platform and later formed the nucleus of the compound Kolyma-Omolon Superterrane (KOS) (Fig. 3; Rundquist and Mitrofanov, 1993). Its metamorphic basement consists of typical Precambrian rocks of the granulite or,

rarely, amphibolite facies, charnockites, granite-gneissic domes, and greenstone belts. The sedimentary cover of the massif commences with Vendian tillites which are followed by dominantly carbonate deposits of Cambrian age. Early and Middle Ordovician conglomerates with red beds crop out sporadically. The total thickness of the sediment cover is 900-1000 m (Rundquist and Mitrofanov, 1993).

Through the Late Paleozoic and Mesozoic period the Omolon massif underwent collision and associated folding and metamorphism on all sides (Fujita, 1978; Zonenshain *et al.*, 1990). To the southwest, subduction of oceanic crust during the Permian and Cretaceous gave rise to the Cherskiy Range and a deformed mosaic of tectonostratigraphic terrains that include a number of ancient exotic blocks in the Kolyma Structural Loop (KSL) (Fig. 2, 3; Zonenshain *et al.*, 1990). These blocks can be up to 10 km thick. They have similar composition and fauna to the Siberian Platform. The Alazeya-Oloy volcanic arc of Carboniferous to Lower Jurassic age occupies the center of the KSL (Fig. 3). It is composed of basalts, andesites, their tuffs, flysch, and chert. Greenschist, metapelite, quartzite and quartzitic schist with marble lenses also crop out. Mafic and ultramafic rocks, interpreted as Early Paleozoic ophiolite fragments derived from back-arc or oceanic crust located to the east of the Cherskiy Range, are found in isolated complexes along the range (Oxman *et al.*, 1995). Conforming to the KSL to the southwest is the Inyali-Debin synclinorium (Fig. 3). It is composed of Middle to Late Jurassic fore-arc and back-arc basin turbidites, flysch and flysch-like deposits thrust over the Kular-Nera slate belt, an arcuate feature of Permian to Early Jurassic black shales also concordant with the KSL (Oxman *et al.*, 1995). To the north, the KOS collided in the Cretaceous with the North America-Chukotka plate forming the Anyuy foldbelt (Fig. 3). This zone contains the remnants of Late Jurassic (and more ancient) oceanic basins that were consumed beneath the two island arcs. Greywackes, arkoses, and shales are predominant.

The amalgamated KOS collided with the Siberian Platform to the west and formed the Verkhoyansk foldbelt in the Early Cretaceous. This is a major mountain range running

from the Lena river delta in the north to the Sea of Okhotsk in the south, comparable in scale to the Urals and the Appalachians. It is separated from the KOS by a 900 km long, 40 km wide fault zone of intensely and multiply deformed shales and siltstones. The upthrusted detrital sediments of the Verkhoyansk range constituted the eastern passive margin of the Siberian Platform since pre-Riphean time. It consists of continental shelf deposits backthrust over the platform, mainly hemipelagic and pelagic phyllitized mudstone, siltstone, and sandstone of Late Permian to Early Jurassic age supplied from the emergent Aldan Shield (Oxman *et al.*, 1995). The Cretaceous coal-bearing deposits of the Preverkhoyansk foredeep lie to the west of the Verkhoyansk foldbelt. To the south, shelf carbonate deposits of Vendian to Early Devonian age and rift formations of Middle Devonian to Early Carboniferous are exposed in the Sette-Daban uplift.

The Koryak zone is made up of numerous Paleozoic terrains that developed in the Cretaceous involving collisional and accretionary processes and is composed mostly of ophiolites and sediments of island arcs, oceanic ridges, and atolls (Filatova, 1995; Puchkov, 1996). The Okhotsk-Chukotka volcanic belt is a continental arc of Cretaceous to Paleogene age superposed on all of the Mesozoic accretionary terrains from the Sea of Okhotsk to Chukotka and into Alaska. The Pacific Cretaceous is characterized by the absence of carbonates; continental clastic sediments and marine tuffaceous sediments dominate along with lacustrine rocks and subaerial volcanic deposits (basic and acid) (Pergament, 1981).

In the Cenozoic the present-day North America-Eurasia plate boundary developed concomitant with the opening of the Eurasian basin of the Arctic as reflected by a zone of seismicity (Cherskiy Seismic Belt) superimposed on the former Mesozoic accretionary region (Cook *et al.*, 1986; Imaev *et al.*, 1994).

For ease of interpretation of the data, the rivers are divided into 7 geological categories described in Table 2 and identified by symbols in all the figures.

Climate

The climate in the arctic lowlands is very severe, of the cold and arid continental type. It is winter for seven months of the year and snow-covered (~30 cm) for 260 days on average. Mean July temperatures range from 12 to 16°C along the river valleys and <8°C on the highlands. Mean January temperatures are lowest in the Indigirka headwaters and on the Yana near the village of Verkhoyansk (< -48°C), highest on mountain tops of the Verkhoyansk, Cherskiy and Moma ranges (-32~-28°C) (Atlas of Yakutia, 1989), i.e. a shallow, intense high in the lower troposphere.

Annual precipitation is highest on the coasts of the Bering Sea and the Sea of Okhotsk (~600 mm) and lowest on the eastern slope of the Verkhoyansk mountains and on the Yana-Indigirka-Kolyma lowlands (~250 mm) (UNESCO, 1977). The Urals block the humid Atlantic air masses and make the region very dry. There is no evidence for vast ice sheets such as existed on the North American continent and western Siberia. Only small valley glaciers at the highest elevations exist due to the semi-arid, continental climate and predominantly summer precipitation pattern (Velichko and Faustova, 1991).

Along a thin strip of the coast (~300 km) the vegetation is arctic tundra, and the lowlands are largely tundra with forest tundra in small strips. The Cherskiy and Moma ranges have a primitive brushwood belt above the timberline at ~2,000 m, and the highest peaks are polar deserts. The middle reaches of the Indigirka and Kolyma are occupied by deciduous forest at low altitude (~1,000 m) with larch and moss and lichen in the underbrush. The soil is composed of sand and sandy clay. The basins are pristine, comparable to Alaska in anthropogenic impact.

Lack of extensive ice sheets in the Pleistocene has led to the development of deep permafrost. It is 100-200 m thick in the upper reaches of the rivers in the south with general development of taliks (unfrozen layers within the permafrost). On the Arctic coast it is 200 to >500 m in thickness with infrequent taliks and widespread occurrences of fossil

ice (Piguzova, 1965). The active layer is ~1.4-2.5 m deep for sandy and clayey soils and 0.6-0.8 m for peat bog soils, becoming thinner on the Arctic coast, 0.7-1.2 m and 0.2-0.4 m, respectively (Piguzova, 1965). Evidence of frost-action can be seen all along the rivers especially in their lower reaches in the tundra zone. On eroding bends of the rivers, large ice wedges several meters wide and around ten meters apart are commonly exposed. Thermokarst lakes or bogs are prevalent in the northern lowlands.

Discharge

The hydrologic characteristics of the Lena, Omoloy, Yana, Indigirka, Kolyma, and the Anadyr are summarized in Table 1. In terms of water discharge, the Lena ranks 8th and the Kolyma 37th in the world (Schumm and Winkley, 1994). Together the first five rivers account for ~23% of the total runoff into the Arctic Ocean (Anadyr flows into the Bering Sea) and ~2% of total global discharge. Significant flow is restricted to the period mid-May through September when the region is ice-free, with a June peak during ice and snow melt and a shoulder due to summer monsoonal rainfall in the form of intense storms (Fig. 4). The headwaters thaw in mid-April and the ice breaks up there several weeks earlier than in the lowlands leading to the formation of ice dams which can cause extensive flooding and channel migration. Extreme high flows in the lower rivers occur in late June; base flows are about 30 to 91 m^3/s in the main channels in March and April when the rivers are essentially frozen to the bed (Fig. 4). The flux of dissolved material during the winter months (Nov to April) is ~20% of that during the summer (May to Oct.; Gordeev and Sidorov, 1993).

Sampling and Analytical Methods

Sampling expeditions were made in July-August over the period 1991-1997 to the Aldan (UL100, 1991), Kolyma (KY100, 1992), Lower Lena (UL600), Yana (YN100, 1995), Indigirka (IG100, 1996), and Anadyr (AY100, 1997) (Fig. 4). All significant tributaries (~100 stations) were sampled a few kilometers above their confluence with the main channel for major and trace elements, suspended and bed material. The dissolved chemical data are reported in Table 2. Samples for major ions were filtered through 0.45 μm Millipore filters and those for trace elements through 0.4 μm Nuclepore filters in a portable laboratory in the field within 24 hours of collection. The trace element samples and small aliquots for nutrient analyses were acidified with 3x vycor-distilled HCl or HNO_3 and stored in HDPE bottles and plastic and glass vials. The pH was measured at the sampling sites to ensure against CO_2 loss. Upon returning to the MIT laboratory, the major cations (K, Na, Ca, Mg) were measured by flame atomic absorption spectrometry, alkalinity by Gran titration, Cl and SO_4 by ion chromatography, and silica (on acidified samples) by colorimetry. Strontium concentrations were determined by ICP-MS, the isotopic composition by TIMS.

Results and Discussion

The data are presented based on the geological categorization of Table 2. First, the charge balance will be examined to identify possible contributions from organic acids to the charge balance. Then the composition of the river dissolved load will be discussed with respect to the major lithologies—evaporites, carbonates, and silicates: both clays and igneous rocks. Equilibrium relationships regarding different carbonate minerals and also atmospheric CO_2 are then explored. Sr isotope systematics are reported as a diagnostic means to discern the relative contribution of silicate weathering. Finally, flux calculations and comparisons with other river systems draining orogenic zones are presented and the implications for the effect of climate on weathering are discussed. The Amazon and the

Orinoco draining the eastern Andes (Stallard and Edmond, 1983; Edmond *et al.*, 1996), the Fraser and the Yukon draining the western Rockies (Cameron *et al.*, 1995; Edmond *et al.*, 1996), and the Mackenzie draining the eastern Rockies (Reeder *et al.*, 1972) have been selected based on the reliability of the data sets and the level of detail in sampling. A comparison of the geology and environment of these other rivers have been discussed in Edmond and Huh (1997).

One caveat in comparing the concentration of chemical species in the tropical Amazon/Orinoco systems with those in the arctic/subarctic is the difference in precipitation and evapotranspiration rates in the two systems. While the annual precipitation is much higher in the Amazon/Orinoco (1,500 to 4,000 mm/yr depending on geography), evapotranspiration is also high (>1,000 mm/yr for the Amazon and >800 mm/yr for the Orinoco). Average precipitation and evapotranspiration in Fraser/Yukon/Mackenzie and Siberian river basins are 400-1,000 and 300-600 mm/yr, respectively (UNESCO, 1977). The lower precipitation is to some extent compensated by the lower evapotranspiration, but the runoff in the Amazon/Orinoco is still an order of magnitude higher (100-2,500 mm/yr) than in eastern Siberia (30-500 mm/yr). Therefore, relative concentrations are useful for deducing sources, but the fluxes are the fundamental variables to be compared.

Data Presentation

The charge balance between total dissolved cations ($TZ^+ = Na^+ + K^+ + 2Mg^{2+} + 2Ca^{2+}$ in μEq = 10^{-6} equivalents per kg) and total dissolved anions ($TZ^- = Cl^- + HCO_3^- + 2SO_4^{2-}$ in μEq) is a direct proof of the precision of the data in the absence of unanalyzed organic anions. The NICB (Normalized Inorganic Charge Balance = $[TZ^+ - TZ^-]/TZ^+$) shows that at low TZ^+ (<650 μEq) there is an excess of cations over analyzed anions, especially for the Yana and Indigirka (Fig. 5a). This is far in excess of the experimental error (± ~5%) and is attributed to the unanalyzed organic acid anions. Unlike the Lower

Lena where the river banks are sandstone and limestone cliffs, the lower Yana and Indigirka river banks are in unconsolidated sediment and peat layers which, in the rainy summer season when the samples were taken, were being actively eroded. Peatland waters are generally acidic when isolated from groundwater input and are enriched in dissolved organic matter from decomposition of mosses etc. (Shotyk, 1988). The charge imbalance is also significant for peat waters in Iceland (Gíslason *et al.*, 1996). For other samples the NICB is within ± 0.05. As a comparison, in tropical black rivers the NICB is up to 1 at $TZ^+ < 100$ μEq (Edmond *et al.*, 1995).

TZ^+ values range up to ~3,100 μEq but most fall under 1,300 μEq. This is comparable to other orogenic zones—e.g. Orinoco (mostly <3,000 μEq), Mackenzie and Yukon (less than ~6,000 μEq). For comparison, the Orinoco rivers draining the Guayana Shield are very dilute (<600 μEq); the sedimentary platform rivers in Siberia and China are higher in their dissolved load (usually <6,000, but can reach 30,000 μEq); the estimated world average is 1,250 μEq (Meybeck, 1979). Stallard and Edmond (1983) classified the rivers draining silicate rocks into transport-limited (<200 μEq) and weathering limited (200-450 μEq) based on TZ^+ values. Accordingly, most of the rivers in the present study would fall in the latter category.

The Cl concentrations range up to ~100 μM in the tributaries; the Lena main channel has significantly higher values (up to ~600 μM) derived from the input from evaporitic platform tributaries (Huh *et al.*, in review); however, the majority of the values in the tributaries examined here are below 30 μM (Fig. 5b). Although rain water samples have not been collected in these river basins, data collected from the Amazon, Caura, and the Orinoco indicate that Cl present in precipitation is ~20 μM or lower (Stallard and Edmond, 1981; Edmond *et al.*, 1995) and varies depending on the distance from the ocean, position relative to air mass movements, and the presence of orogenic obstructions, making seasalt corrections difficult. Thus, the data are uncorrected; the maximum effect would be for Na and Mg (at most 30%, usually less than 10%) and is negligible for other ions.

The lower boundary of the Na and Cl relationship has a 1:1 slope but offset to higher Na (Fig. 5b). At lower levels there is excess Na which can be attributed to the weathering of Na-feldspars; the associated Cl levels are consistent with atmospheric input. There is no relationship between SO_4 and Cl with some SO_4 abundances ranging to high values independent of Cl (Fig. 5c). The SO_4 in these tributaries comes from dissolution of gypsum/anhydrite and the oxidation of sulfides as seen in the following sections.

Ternary diagrams are diagnostic tools in the characterization of the relative contribution of various lithologies to the total dissolved composition (Hu *et al.*, 1982; Stallard and Edmond, 1983). On the anion ternary plot the data, especially from the SD and KSL, fall near the alkalinity apex. There is a distinctive occupation of the interior of the triangle by the OC, EV and WC samples (Fig. 6a), coinciding with the Kular-Nera slate belt and the intermediate volcanics of the Okhotsk-Chukotka volcanic range (Fig.3). Oxidative weathering of black shales causes the relatively high SO_4 and Si and low alkalinity of the interior samples. Another characteristic of this data set, compared to other orogenic rivers, is the absence of evaporites or intense weathering of silicates shown by a lack of points near the ($Cl+SO_4$) and the Si apices, respectively.

On the cation ternary plot, the data fall in a cluster around the (0.6Ca + 0.3Mg + 0.1(Na+K)) region (Fig. 6b). Some EV rivers draining the slate belt and small tributaries from the KSL occupy the interior. The prevalence of alkalinity and Ca suggests that limestone or calcium silicate weathering is dominant. This bears some similarity to the Mackenzie River (Reeder *et al.*, 1972). The Orinoco left bank tributaries draining the Andes have more extreme compositions, ranging from completely limestone to totally evaporite dominated dissolution (Edmond *et al.*, 1996). Several early studies of sub-glacial weathering found streams of high cationic concentrations with Ca-alkalinity dominated compositions from quartz diorite, migmatite, and greenstone terrain (Reynolds and Johnson, 1972). This suggests weathering of relatively reactive Ca-rich plagioclases in these ice-associated regimes.

Carbonate weathering

As seen above (Fig. 6) Ca, Mg and alkalinity are the major components in all these rivers. For most of the samples alkalinity is balanced by Ca and Mg from limestone or Ca-silicate. Some KSL samples require additional SO_4, probably from gypsum/anhydrite. Rivers with pyrite oxidation that occupy the interior of the anion ternary diagram are very dilute and do not show as large an imbalance between (Ca + Mg) and alkalinity. The portion of alkalinity and SO_4 balancing Na and K produced by the weathering of Na- or K-silicates is minor.

On the Ca vs. Mg plot, the data define a diffuse relationship corresponding to a molar Mg/Ca ratio between ~0.3 and 0.7 (Fig. 7a). Mg/Ca ratios of some representative rock types are indicated on the figure. The diversity of Mg/Ca ratios in rivers is compounded by preferential retention of Mg in secondary minerals. For reference, the Andes give a value of 0.7 and the mafic terrains of the Fraser ~1 (Edmond *et al.*, 1996; Cameron *et al.*, 1995).

The pH varies from 6.5 to 8.1, except for a few outliers. The Calcite Saturation Index (CSI, defined in the caption of Fig. 7b) is calculated where pH data are available. High TZ^+ samples show high pH, and saturation increases with TZ^+. This can be explained by the dominance of limestone dissolution. Except for two tributaries (KY109, KY113) all have negative CSI (Fig. 7b). Rivers with positive or only slightly negative CSI drain the carbonate blocks of KSL. The aragonite and dolomite saturation indices follow the same pattern as for the CSI. All rivers have negative DSI except for the two rivers supersaturated with calcite (DSI = 0.2 and 0.5).

The CO_2 partial pressure (P_{CO_2}) in surface waters reflects both productivity and the dynamic state of the river. Highly productive lakes or swift rivers are undersaturated (Stallard and Edmond, 1987). The Amazon, for example, is 5~100 times supersaturated in the floodplains and approaches P_{CO_2} values in the range of soils. Springs and some

spring-fed waters in Iceland show P_{CO_2} values up to 1000 times *lower* than the atmosphere because of lack of gas exchange (Gíslason *et al.*, 1996). Most direct runoff and many glacier-fed rivers in Iceland show up to 10 times supersaturation. Siberian rivers in the collision zone are all supersaturated with respect to atmospheric P_{CO_2} (1-10 times) but not to such an extent as the Amazon in the floodplain (Fig. 7c). A small river in the tundra (OM101) is supersaturated by up to 8 times the atmospheric value. There is an inverse relationship between P_{CO_2} and CSI (Fig. 7b,c). $CaCO_3$ dissolution and weathering of aluminosilicates consume CO_2 and lower the $P_{CO_{2,river}}$ resulting in high Ca concentrations and CSI. Thus, arctic rivers could act as a source of CO_2 in terrains that are not carbonate dominated, but the magnitudes are not remarkable compared to rivers at other latitudes. Rivers that lie in the tundra or that flow through swampy bogs have time to equilibrate with soil CO_2 and may be a net source of CO_2 (Kling *et al.*, 1991).

Silicate weathering

Two factors influence the silica concentrations in river water—lithology and biology. In transport-limited basement terrains like the Guayana Shield, the Si content is high (up to 200 μM) due to intensive weathering of the primary aluminosilicates and residual secondary silicate minerals. Sedimentary terrains generally have lower Si concentrations (<100 μM) supplied mainly by shales interbedded with carbonates. In the basins studied here, by contrast, the presence of static water masses like lakes and bogs complicates the lithologic signature due to biological uptake and sedimentation of Si by diatoms; Si values in lakes can be close to zero during the growing season. The bulk of the Si values of the rivers in the present study are low (50-90 μM) for aluminosilicate lithology (Fig. 8a) and are suspected to be the result of this biogenic uptake.

The ratio of Si to cations can be used as a proxy for the intensity of silicate weathering. Average shield weathering to kaolinite yields Si/TZ^{+*} ($TZ^{+*} = TZ^{+} - Cl - 2SO_4$; the evaporite correction) of 0.78 whereas if the final product is gibbsite the ratio is

1.6; shale weathering to kaolinite and gibbsite yield Si/TZ^{+*} ratios of 0.25 and 0.88, respectively (Stallard, 1980). At high TZ^{+*}, the Si values are roughly constant at ~60 μM (Fig. 8a). At low TZ^{+*}, Si/TZ^{+*} values are between the two shale ratios.

Because carbonates weather orders of magnitude faster than silicates, TZ^{+*} may be dominated by carbonates. By looking at a ratio not affected by carbonates and evaporites, Si vs. (Na*+K = Na-Cl+K) one can resolve the weathering of silicates. Si/(Na*+K) = 1.7 for weathering of average shield to kaolinite and 3.5 to gibbsite; 1.0 for average shale to kaolinite and 3.4 to gibbsite. The Si/(Na*+K) ratio is 1.7 or slightly less and well correlated for most of the rivers (Fig. 8b). The low ratios indicate that the weathering is superficial, i.e. to cation-rich secondary minerals but not to kaolinite and gibbsite. However, it is possible that the biologic removal of Si erases information about weathering intensity. Some small KSL rivers in the swamps have very low ratios (0.2-0.5). Si/(Na*+K) is ~0.3 for the Mackenzie except for those tributaries draining Paleozoic metamorphic and igneous rock which have ratios over 1.

Plotting Si vs. K is another index of aluminosilicate weathering, because there is very little K signal from other rock types or salts. The K concentrations are very low, not surprising since K-feldspars are more resistant to weathering than the Ca- or Na-phases. There is no distinct correlation between Si and K as different rock types give different Si/K ratios but observed ratios are within the range expected for average igneous rocks undergoing superficial weathering (Fig. 8c). In an extreme case, the shield rivers of the Orinoco basin weather completely to gibbsite (Si/K = 10) or kaolinite (Si/K = 5) and show a linear relationship between Si and K.

From the K vs. Na diagram, it can be seen that the Kolyma waters are very sodic (K/Na < 0.3; Fig. 8d). Weathering is not intense enough to dissolve the resistant K-feldspars to a great extent. Weathering of biotite to vermiculite, resulting in high weathering yield and high strontium isotopic compositions, has been observed in formerly glaciated areas (Drever and Hurcomb, 1986; Blum *et al.*, 1994). The low K/Na ratios

suggest that these processes can only be minor in the Siberian rivers and cannot dominate the Sr isotope signals.

Strontium Systematics

The $^{87}Sr/^{86}Sr$ of seawater as recorded in marine limestones has varied over geologic timescales. The steep rise in the Cambrian and in the Cenozoic have been ascribed to global tectonic events, the Pan-African and the Himalayan orogenies, respectively (Edmond, 1992), but the reasons for the smaller variations are more ambiguous.

The strontium isotope ratio is a diagnostic indicator of the weathering from limestone versus silicate rock terrains. Because carbonates release Ca and alkalinity in equal proportion as anorthoclase and because this depends on the composition of the plagioclase, it is difficult to discern the contribution of limestone-derived Ca from silicate-generated Ca using alkalinity values; in addition fluvial silica values can be affected by diatom growth. Strontium isotopes provide a more definitive constraint. The $^{87}Sr/^{86}Sr$ in marine carbonates varies from a low of 0.7065 in the Permian and Jurassic to a high of 0.709 in the Cambrian and the present (Burke *et al.*, 1982). Small amounts of rapidly soluble rocks like limestones and dolomites buffer the river water between these values depending on the age of the limestone if not significantly affected by diagenesis. Values above 0.710 or below 0.7065 must be from either Rb rich, old aluminosilicate rocks or Rb-poor arc volcanics and associated sediments, and TZ^{+*} can be used with confidence in calculating the uptake of CO_2 by primary aluminosilicate weathering.

The fluvial strontium concentrations reported here range up to ~2.9 μM; however, most of the values are below 1 μM (Fig. 9a). The global average is estimated at 0.89 μM (Turekian, 1971; Palmer and Edmond, 1989). The Sr concentrations show a general increase with Ca (Sr/Ca molar ratios generally between 2 and 5 x 10^{-3}), but there is significant scatter reflecting the diverse lithologies with different Sr/Ca ratios at different stages of weathering and also the possible incongruent weathering of trace Sr unlike major

elements, e.g. Ca (Bullen *et al.*, 1997). However the ratio is higher than in other watersheds. The Andean Orinoco and Amazon and the Fraser and Indus all show relatively constant Sr/Ca ratios of ~2.5 x 10^{-3} (Edmond *et al.*, 1996; Cameron *et al.*, 1995; Pande *et al.*, 1994), consistent with that of meta-andesite leachates (Short 1961). The Mackenzie, which drains highly fossiliferous limestones and dolomites, has some tributaries with higher Sr/Ca ratios, but most fall in the range 2-2.5 x 10^{-3}. There is a diffuse relationship between Sr and SO_4, indicating that Sr originating from gypsum or anhydrite could be important at higher concentrations (Fig. 9b). Celestite ($SrSO_4$), the principal mineral phase of Sr existing as a minor phase in fissures and cavities in dolomites and dolomitic limestones, is an improbable candidate due to its rarity.

The $^{87}Sr/^{86}Sr$ ratios vary from 0.704 to 0.718 (Fig. 9c) well within the reported range of world rivers (Edmond, 1992; Pande *et al.*, 1994; Cameron *et al.*, 1995; Yang *et al.*, 1996). Where the values are radiogenic, the Sr concentrations are too low to affect the seawater ratio. OC samples have characteristically nonradiogenic values indicative of arc regions as also seen in the basaltic terrains of the Fraser (Cameron *et al.*, 1995) and indicate the complete absence of a limestone/evaporite contribution. Compared to the high Andes and the Rockies, where $^{87}Sr/^{86}Sr$ values reach up to 0.73, Siberian rivers are less radiogenic. There are three possible explanations for these less radiogenic ratios. i) The parent rocks that undergo weathering are inherently less radiogenic (i.e. Rb poor or young) than those in other river basins. ii) The weathering is superficial in the Siberian rivers, leaching out only the easily weathered and non-radiogenic "initial" Sr in the plagioclase (~0.704). The physical weathering by ice action and the temperature inhibition on chemical weathering could be responsible for the superficial weathering. However this does not explain the radiogenic values reported for the Fraser which is also at high latitudes. iii) Mixing between a radiogenic silicate endmember and the non-radiogenic basalts lowers the observed $^{87}Sr/^{86}Sr$ in the river waters. Considering the detailed and extensive sampling, it is

remarkable that a very radiogenic endmember has not been identified. This suggests that the carbonate contribution is negligible.

The German Laptev Sea Program has produced some $^{87}Sr/^{86}Sr$ data on the carbonate-free suspended particulate material sampled at the Lena and Yana river mouths (Eisenhauer *et al.*, 1997). The average $^{87}Sr/^{86}Sr$ for the SPM of the Lena is 0.7162 and that for the Yana is 0.7148. These compare favorably with our values on the dissolved load; Lena (UL607, 0.71048) and Yana (YN104, 0.70991). The suspended load is more radiogenic, as expected, since the more resistant and small grain sized material contains more radiogenic components like biotite and muscovite. It is hard to infer the bedrock $^{87}Sr/^{86}Sr$ from the suspended load, as the solids are more apt to be affected by settling and storage along the river course.

Flux Estimates

Though there are a number of gauging stations in the region, it was not possible to obtain discharge data for individual tributaries for the year they were sampled. Continuous discharge data on the Kolyma are available for two stations, on the Sugoy (KY105) since 1941 and at Srednekolymsk (above KY118) since 1927, on the Indigirka at Vorontsovo (IG121) since 1936 and on the Nera (major headwater tributary of Indigirka) since 1944, on the Yana at Dzhangky (below YN122) since 1937, and on the Lena at Kusur (UL607) since 1934 (Fig.4). Averages of the annual mean discharges were taken for the above gauging stations. Where such data are absent, the annual runoff (mm) was estimated from the runoff map of Asia (1:20,000,000 scale) which is based on the interpolation and contouring of the available discharge measurements (UNESCO, 1977). The annual runoff is highest on the western slope of the Verkhoyansk (200-400 mm) and the southern headwaters near the Pacific (200-300 mm). The eastern slope of the Verkhoyansk has the lowest runoff (30-50 mm), an obvious rain shadow effect. On the Arctic coast the value is

about 100 mm. The drainage area of each tributary was measured gravimetrically by tracing out the drainages from a 1:2,500,000 scale map. River discharge values thus determined and the chemical data taken from the sampling in the summer falling stage (Fig. 4) are used to estimate the relative flux of dissolved ions of each tributary (Table 3). In the absence of time-series measurements of discharge and chemical content, this method provides a relatively good estimate (± 20%; Huh *et al.*, in review).

The alkalinity fluxes and runoff are in the range of rivers in different geological regions of the world (Fig. 10a; Bluth and Kump, 1994). At low discharge the flux increases with the measured flow but at higher values the fluxes show a large variation, depending on lithology. The composition of the exposed rocks seems to be the main determinant; runoff is an important variable only for monolithologic regions. SD samples fall between rivers draining shales and those draining carbonates. EV samples lie between granite and sandstone. Other categories cover the whole range of rock types (Fig. 10a).

The average fluxes summed over each geological category can be compared with other world rivers in orogenic zones. The areal transport of dissolved solids (= Na + K + Mg + Ca + Cl + SO_4 + Alk + Si in 10^6 mol/km^2/yr) is below 0.5 for the Siberian rivers examined here (Table 3). This is at the lower end of the range observed elsewhere (Fig. 10b; Edmond *et al.*, 1996), similar to the tropical shield rivers (Edmond and Huh, 1997) and about half of that from the platform rivers in Siberian and in China (Huh *et al.*, in review). However, there is an order of magnitude difference in areal dissolved flux within the Siberian rivers. EV, because it is in the rain shadow and has a low dissolved load, is ten times lower in areal dissolved flux than the SD which has higher discharge as well as easily weathered limestone outcrops. One caveat here is that part of the Yana (EV and WC) and the Indigirka (KSL) were sampled during a severe rainfall event. This, in conjunction with using the mean annual discharge, could result in an underestimation of the fluxes in these regions.

The areal TDS is not a good indicator of weathering of aluminosilicate rocks and therefore the draw down of atmospheric CO_2, because it includes ions from evaporites and carbonates which do not affect the CO_2 cycle over geologic time scales. Calculation of $ØCO_2$, the uptake rate of CO_2 from the atmosphere by weathering of aluminosilicate rocks, is described in detail elsewhere (Edmond and Huh, 1997). Briefly, when purely igneous terrain is being weathered, $ØCO_2 = ØTZ^+$. Corrections can be made for evaporites by using $ØTZ^{+*}$. In principle, Øalkalinity can also be used but will underestimate the flux when there are organic acids present. When a mixture of lithologies is being weathered Si fluxes have to be used, except for the case when lakes, bogs, dams and reservoirs are present and biogenic uptake of Si can be significant. Then, $ØTZ^{+*}$ is used, provided that the $^{87}Sr/^{86}Sr$ ratios are consistent with weathering of aluminosilicate rocks.

$ØCO_2$ for the tributaries varies between 8 and 520 $x10^3$ mol/km^2/yr (Table 3). The values are about twice those of shield rivers (~50 x 10^3 mol/km^2/yr; Edmond and Huh, 1997). As with the areal TDS, the values are very low in the EV and highest in the SD (Fig. 10c). The $ØCO_2$ values of other much younger active orogenic zones of the western Americas have been reviewed by Edmond and Huh (1997) to be compared with the results in this study. The higher $ØCO_2$ values for the Siberian rivers overlap with the lower ones in the Amazon and Orinoco and also with those from the Fraser and Yukon. $ØCO_2$ for the Mackenzie is calculated using Si data, due to the lack of $^{87}Sr/^{86}Sr$ measurements to constrain the relative proportion of limestones, and is thus a minimum estimate. The Fraser and Yukon, also in cold environments but with complete data sets, have $ØCO_2$ values calculated from alkalinity data comparable to the tropical rivers. The effect of discharge is not straight-forward. Although total chemical fluxes are in general proportional to discharge, there is no clear relationship between $ØCO_2$ and discharge either within the present data set for these Siberian rivers or those from globally distributed orogenic zones (Edmond and Huh, 1997). Thus, the low $ØCO_2$ values in the Siberian rivers cannot simply be attributed to the cold temperatures and their inhibiting effects on

reaction rates or on the associated arid climate. Rather, the relatively low fluxes from the Siberian rivers are more likely due to older and more resistant lithology as compared to the other regimes for which data are available.

Effect of climate on weathering

The characteristics of these arctic/subarctic watersheds that can affect weathering are: the extreme continental climate, permafrost and seasonally frozen ground, frost weathering—huge ice wedges in the lower courses, ice dams, mountainous topography, active tectonics past and present and associated lithology, and the tundra vegetation and thermokarst lakes.

Weathering of rocks in permafrost areas is a unique process producing a special kind of eluvium. Ice wedges are usually the most abundant type of massive ice occurring in areas of continuous permafrost. Wedge ice may constitute 50% or more of the upper several meters of the permafrost. Many lab experiments and much field work have established the immense forces of frost action and its effectiveness in generating fresh surfaces (Pewe, 1975; Walder and Hallet, 1985; Hallet *et al.*, 1991; Kaldova, 1992). When there is a temperature gradient, water migrates through the partially frozen rocks to the microfracture containing ice and freezes there, the driving force being the lowering of the free energy at the ice-water-mineral interface. The surface force at this interface generates pressures large enough to fracture any rock type (Walder and Hallet, 1985; Hallet *et al.*, 1991), and as a result, surface area is greatly increased. This process is especially effective during the spring thaw when water is supplied from the melting ice and a temperature gradient is developed over the permafrost. Frost action and related effects at all scales can increase the total erosion rate: frost cracking produces immature sands, repeated freezing and thawing can destabilize and disrupt the soil cover, gelifluction appears to be capable of moving this immature overburden laterally on slopes where fluvial transport is

not efficient; the river-fast ice carries large amounts of fine sediment and rock fragments (Danilov, 1990).

In the region under discussion, the winters are dry and lack significant snow cover; thus there is little moderation of the downward propagation of seasonal air temperature waves into the underlying frozen ground, and ice wedge cracking is vigorous. Both the active layer and the upper part of the permafrost show a year-round periodic movement—creep or stress relaxation (Mackay, 1993). With the ground permanently frozen below ~0.5 m depth, this combination of mechanical and chemical weathering is enough to overcome the kinetic inhibition on weathering reactions due to the drastically lower temperature. Lasaga *et al.* (1994) have shown that dissolution kinetics are nonlinearly dependent on the degree of saturation. Systems far from equilibrium, like those at high latitudes, have fast reaction kinetics. The weathering regime in the tropical watersheds, in contrast, do not have such an active mechanism of bedrock exposure except in high relief areas. In relatively flat basins, the weathering front is sealed from the weathering agents, atmospheric CO_2 and water, by the thick lateritic mantle generated by extensive weathering (Topp *et al.*, 1984).

Combined with the effect of lithology, tectonics, and climate are the actions of plants and organisms. Sampling was not suitable for the study of the effects of biology, since collections were at only one point in time. In the vast tundra areas above the Arctic Circle peat layers and swampy bogs abound. Because humification leads to lower hydraulic conductivity, flushing in the peat layers is poor and probably does not markedly affect the river chemistry, except when exposed along the river banks and affected by bank erosion in the spring melt.

Conclusions

1) The fluvial chemistry data set for large pristine rivers has been extended to the orogenic arctic/subarctic region of northeastern Siberia. The major element compositions are largely consistent with the lithology and the concentrations are in the range of those reported for similar well studied geotectonic regimes both in the tropics and at high latitudes in western North America.

2) The overall flux of dissolved material is comparable to that of the tropical and temperate rivers suggesting that physical weathering and the resulting exposure of fresh surfaces caused by frost action plays a large role in overcoming the simple large temperature effect on the reaction kinetics.

3) The silica data suggest that weathering is superficial. However, the silica values are lower than for most other rivers, with the exception of the Mackenzie. Diatoms and other organisms in the swamps and thermokarst lakes in the lower floodplain regions may take up and sediment silica to produce this anomaly. This requires further quantitative study.

4) The Sr isotope systematics are indicative of the weathering of volcanics, limestones and Ca-silicates. No especially radiogenic values were found indicative of severe tropical-style weathering.

5) Unlike in other orogenic zones where evaporites are common, there are no significant effects in the rivers studied here.

6) The rivers, sampled in the late summer, are up to 10 times supersaturated relative to atmospheric CO_2. For swampy basins or regions rich in thermokarst lakes these streams could be a net source of CO_2 to the atmosphere but not as large as previous estimates.

Acknowledgments — This paper is dedicated to Gera Panteleyev who participated in the expeditions to the Kolyma and Upper Aldan and was instrumental in initiating this project. We deeply regret his loss in an accident on a separate field expedition to the Ob River in Western Siberia. We thank S. Bowring, D. Coleman and M. Kurz for the use of their facilities at MIT and WHOI for strontium isotope measurements. The help of B. Grant in the lab and of UROP students, M.-Y. Tsoi and K. Taylor, are also greatly appreciated. We depended on the personnel of the River Navigation Authority of Yakutia for providing the logistics and making the sampling safe and rewarding and for their extreme generosity and crucial local knowledge. This work has been supported in the MIT laboratory by Earth Surface Processes, NSF and in the field by the River Navigation Authority of Yakutia. We have benefited from the thoughtful comments of P. Froelich and an anonymous reviewer.

References

Aagaard K. and Carmack E. C. (1989) The role of sea ice and other fresh water in the Arctic circulation. *J. Geophys. Res.* **94**, 14485-14498.

Andersson P. S., Wasserburg G. J., Ingri J., and Stordal M. C. (1994) Strontium, dissolved and particulate loads in fresh and brackish waters: the Baltic Sea and Mississippi Delta. *Earth Planet. Sci. Lett.* **124**, 195-210.

Atlas of Yakutia (1989) *Agricultural Atlas of the Autonomous Soviet Socialist Republic of Yakutsk*. State Agro-industrial Committee of ASR Yakutsk, State Committee of RSFSR People's Education and Yakutsk State University, Moscow (in Russian).

Berner R. A. (1994) GEOCARB II: A revised model of atmospheric CO_2 over Phanerozoic time. *Am. J. Sci.* **294**, 56-91.

Berner R. A., Lasaga A. C., and Garrels R. M. (1983) The carbonate-silicate geochemical cycle and its effect on atmospheric carbon dioxide over the past 100 million years. *Am. J. Sci.* **283**, 641-683.

Blum J. D. and Erel Y. (1995) A silicate weathering mechanism linking increases in marine $^{87}Sr/^{86}Sr$ with global glaciation. *Nature* **373**, 415-418.

Blum J. D., Erel Y., and Brown K. (1994) $^{87}Sr/^{86}Sr$ ratios of Sierra Nevada stream waters: Implications for relative mineral weathering rates. *Geochim. Cosmochim. Acta* **58**, 5019-5025.

Bluth G. J. S. and Kump L. R. (1994) Lithologic and climatologic controls of river chemistry. *Geochim. Cosmochim. Acta* **58**, 2341-2359.

Bullen T., White A., Blum A., Harden J., and Schulz M. (1997) Chemical weathering of a soil chronosequence on granitoid alluvium: II. Mineralogic and isotopic constraints on the behavior of strontium. *Geochim. Cosmochim. Acta* **61**, 291-306.

Burke W. H., Denison R. E., Heatherington E. A., Koepnick R. B., Nelson H. F., and Otto J. B. (1982) Variation of seawater $^{87}Sr/^{86}Sr$ throughout Phanerozoic time. *Geology* **10**, 516-519.

Cameron E. M., Hall G. E. M., Veizer J., and Krouse H. R. (1995) Isotopic and elemental hydrogeochemistry of a major river system: Fraser River, British Columbia, Canada. *Chem. Geol.* **122**, 149-169.

Carbonnel J. P. and Meybeck M. (1975) Quality variations of the Mekong River at Pnom Penh, Cambodia and chemical transport in the Mekong Basin. *J. Hydrol.* **27**, 249-265.

Cook D. B., Fujita K., and McMullen C. A. (1986) Present-day plate interactions in northeast Asia: North American, Eurasian, and Okhotsk plates. *J. Geodyn.* **6**, 33-51.

Cuffey K. M., Clow G. D., Alley R. B., Stuiver M., Waddington E. D., and Saltus R. W. (1995) Large arctic temperature change at the Wisconsin-Holocene glacial transition. *Science* **270**, 455-458.

Danilov I. D. (1990) Cryolithogenesis and its characteristics. *Lithology and Mineral Resources (USSR)* **25**, 1-8.

Drever J. I. and Hurcomb D. R. (1986) Neutralization of atmospheric acidity by chemical weathering in an alpine drainage basin in the North Cascade Mountains. *Geology* **14**, 221-224.

Drever J. I. and Zobrist J. (1992) Chemical weathering of silicate rocks as a function of elevation in the southern Swiss Alps. *Geochim. Cosmochim. Acta* **56**, 3209-3216.

Edmond J. M. (1992) Himalayan tectonics, weathering processes, and the strontium isotope record in marine limestones. *Science* **258**, 1594-1597.

Edmond J. M. and Huh Y. (1997) Chemical weathering yields from basement and orogenic terrains in hot and cold climates. In *Tectonic Uplift and Climate Change*. (ed. W. F. Ruddiman), Plenum Press, pp. 329-351.

Edmond J. M., Palmer M. R., Measures C. I., Grant B., and Stallard R. F. (1995) The fluvial geochemistry and denudation rate of the Guayana Shield in Venezuela, Colombia and Brazil. *Geochim. Cosmochim. Acta* **59**, 3301-3325.

Edmond J. M., Palmer M. R., Measures C. I., Brown E. T., and Huh Y. (1996) Fluvial geochemistry of the eastern slope of the northeastern Andes and its foredeep in the drainage of the Orinoco in Colombia and Venezuela. *Geochim. Cosmochim. Acta* **60**, 2949-2976.

Eisenhauer A., Rachold V., Meyer H., Kassens H., Lindemann F., Spielhagen F. F., and Wiegand B. (1997) Strontium-isotope geochemistry of Laptev Sea-surface sediments, ice-rafted detritus, and suspended particulate material of East Siberian Rivers: Implications for sediment distribution patterns in the Arctic Ocean. In *Seventh Annual V. M. Goldschmidt Conference*. Tucson, Arizona, pp. 66.

Filatova N. I. (1995) The history of the Cretaceous environments of the northeastern Asian continental margin, Russia. *The Island Arc* **4**, 128-139.

Froelich P. N., Blanc V., Mortlock R. A., Dunstan W., Udomkit A., and Peng T. (1992) River fluxes of dissolved silica to the ocean were higher during glacials: Ge/Si in diatoms, rivers, and oceans. *Paleoceanography* **7**, 739-767.

Fujita K. (1978) Pre-Cenozoic tectonic evolution of northern Siberia. *J. Geol.* **86**, 159-171.

Fujita K., Stone D. B., Layer P. W., Parfenov L. M., and Koz'min B. M. (1997) Cooperative program helps decipher tectonics of northeastern Russia. *EOS, Trans. Am. Geophys. U.* **78**(24), 245.

Gaffin S. (1987) Ridge volume dependence of seafloor generation rate and inversion using long term sealevel change. *Am. J. Sci.* **287**, 596-611.

Gibbs R. J. (1972) Water chemistry of the Amazon River. *Geochim. Cosmochim. Acta* **36**, 1061-1066.

Gíslason S. R., Arnórsson S., and Armannsson H. (1996) Chemical weathering of basalt in southwest Iceland: Effects of runoff, age of rocks and vegetative/glacial cover. *Am. J. Sci.* **296**, 837-907.

Gordeev V. V. and Sidorov I. S. (1993) Concentrations of major elements and their outflow into the Laptev Sea by the Lena River. *Mar. Chem.* **43**, 33-45.

Gordeev V. V., Martin J. M., Sidorov I. S., and Sidorova M. V. (1996) A reassessment of the Eurasian river input of water, sediment, major elements and nutrients to the Arctic Ocean. *Am. J. Sci.* **296**, 664-691.

Hallet B., Walder J. S., and Stubbs C. W. (1991) Weathering by segregation ice growth in microcracks at sustained subzero temperatures: Verification from an experimental study using acoustic emissions. *Permafrost and Periglacial Processes* **2**, 283-300.

Hansen J. D., Johnson D., Lacis A., Lebedeff S., Lee P., Rind D., and Russell G. (1983) Climatic effects of atmospheric carbon dioxide. *Science* **220**, 874-875.

Hardie L. A. and Eugster H. P. (1970) The evolution of closed-basin brines. *Mineral. Soc. Am. Spec. Publ.* **3**, 273-290.

Hu M.-H., Stallard R. F., and Edmond J. M. (1982) Major ion chemistry of some large Chinese rivers. *Nature* **298**, 550-553.

Huh Y., Tsoi M.-Y., Zaitsev A., and Edmond J. M. (1998) The fluvial geochemistry of the rivers of Eastern Siberia I: Tributaries of the Lena River draining the sedimentary platform of the Siberian Craton. *Geochim. Cosmochim. Acta* in press (February 12, 1998).

Imaev V. S., Imaeva L. P., and Kozmin B. M. (1995) Active faults and recent geodynamics of Yakutian seismic belts. *Geotectonics* **28**, 146-158.

Kaldova J. (1992) *Geomorphological Record of the Quaternary Orogeny in the Himalaya and Karakoram.* Developments in Earth Surface Processes 3, Elsevier, New York, 315 pp.

Kastner M., Elderfield H., and Martin J. B. (1991) Fluids in convergent margins: what do we know about their composition, origin, role in diagenesis and importance for oceanic chemical fluxes? *Phil. Trans. Roy. Soc. Lond. A* **335**, 243-259.

Kling G. W., Kipphut G. W., and Miller M. C. (1991) Arctic lakes and streams as gas conduits to the atmosphere: Implications for tundra carbon budget. *Science* **251**, 298-301.

Krishnaswami S., Trivedi J. R., Sarin M. M., Ramesh R., and Sharma K. K. (1992) Strontium isotopes and rubidium in the Ganga-Brahmaputra river system: Weathering in the Himalaya, fluxes to the Bay of Bengal and contributions to the evolution of oceanic $^{87}Sr/^{86}Sr$. *Earth Planet. Sci. Lett.* **109**, 243-253.

Lasaga A. C., Soler J. M., Ganor J., Burch T. E., and Nagy K. L. (1994) Chemical weathering rate laws and global geochemical cycles. *Geochim. Cosmochim. Acta* **58**, 2361-2386.

Lewis W. M., Jr. and Weibezahn F. (1981) The chemistry and phytoplankton of the Orinoco and Caroni Rivers, Venezuela. *Arch. Hydrobiol.* **91**, 521-528.

Mackay J. R. (1993) Air temperature, snow cover, creep of frozen ground, and the time of ice-wedge cracking, western Arctic coast. *Can. J. Earth Sci.* **30**, 1720-1729.

Meybeck M. (1979) Concentrations des eaux fluviales en éléments majeurs et apports en solution aux océans. *Rev. Géol. Dyn. Géogr. Phys.* **21**, 215-246.

Meybeck M. (1986) Composition chimique des ruisseaux non pollués de France. *Sci. Geol. Bull* **39**, 3-77.

Négrel P., Allègre C. J., Dupré B. and Lewin E. (1993) Erosion sources determined by inversion of major and trace element ratios and strontium isotopic ratios in river water: The Congo Basin case. *Earth Planet. Sci. Lett.* **120**, 59-76.

Newton R. M., Weintraub J., and April R. (1987) The relationship between surface water chemistry and geology in the North Branch of the Moose River. *Biogeochem.* **3**, 21-35.

Norton D. (1974) Chemical mass transfer in the Rio Tanama system, west-central Puerto Rico. *Geochim. Cosmochim. Acta* **38**, 267-277.

Oxman V. S., Parfenov L. M., Prokopiev A. V., Timofeev V. F., Tretyakov F. F., Nedosekin Y. D., Layer P. W., and Fujita K. (1995) The Chersky Range Ophiolite Belt, Northeast Russia. *J. Geol.* **103**, 539-559.

Palmer M. R., and Edmond J. M. (1992) Controls over the strontium isotope composition of river water. *Geochim. Cosmochim. Acta* **56**, 2099-2111.

Pande K., Sarin M. M., Trivedi J. R., Krishnaswami S., and Sharma K. K. (1994) The Indus river system (India-Pakistan): Major-ion chemistry, uranium and strontium isotopes. *Chem. Geol.* **116**, 245-259.

Parfenov L. M. (1991) Tectonics of the Verkhoyansk-Kolyma Mesozoids in the context of plate tectonics. *Tectonophysics* **199**(2-4), 319-342.

Pergament M. A. (1981) Pacific Regions of the USSR. In *Aspects of Mid-Cretaceous Regional Geology*. (ed. R. A. Reyment and P. Bengtson), Academic Press, New York, pp. 69-102.

Peters N. E. (1984) Evaluation of environmental factors affecting yields of major dissolved ions of streams in the United States. *USGS Water-Supply Paper* **2228**, 39pp.

Pewe T. L. (1975) Quaternary Geology of Alaska. U. S. Geol. Surv. Prof. Paper. **835,** 145pp.

Piguzova V. M. (1965) Estimating underground flow into the rivers of the permafrost zone. *Soviet Hydrology* 114-129.

Puchkov V. N. (1996) Eastern Regions of Russia. In *The Palaeozoic, B.* (ed. M. Moullade and A. E. M. Nairn), The Phanerozoic Geology of the World, Elsevier, pp. 68-88.

Raymo M. E. and Ruddiman W. F. (1992) Tectonic forcing of late Cenozoic climate. *Nature* **359**, 117-122.

Reeder S. W., Hitchon B., and Levinson A. A. (1972) Hydrogeochemistry of the surface waters of the Mackenzie River drainage basin, Canada—I. Factors controlling inorganic composition. *Geochim. Cosmochim. Acta* **36**, 825-865.

Reynolds R. C., Jr. and Johnson N. M. (1972) Chemical weathering in the temperate glacial environment of the Northern Cascade Mountains. *Geochim. Cosmochim. Acta* **36**, 537-554.

Rundquist D. V. and Mitrofanov F. P., eds. (1993) *Precambrian Geology of the USSR.* Developments in Precambrian Geology. Amsterdam, Elsevier.

Sarin M. M., Krishnaswami S., Dilli K., Somayajulu B. L. K., and Moore W. S. (1989) Major ion chemistry of the Ganga-Brahmaputra river system: Weathering processes and fluxes to the Bay of Bengal. *Geochim. Cosmochim. Acta* **53**, 997-1009.

Schumm S. A. and Winkley B. R., eds. (1994) *The Variability of Large Alluvial Rivers.* New York, ASCE Press.

Short N. M. (1961) Geochemical variations in four residual soils. *J. Geol.* **69**, 534-571.

Shotyk W. (1988) Review of the inorganic geochemistry of peats and peatland waters *Earth-Science Reviews* **25**, 95-176.

Stallard R. F. (1980) Major element geochemistry of the Amazon River system. Ph.D. dissertation, MIT-WHOI Joint Program in Oceanography.

Stallard R. F. and Edmond J. M. (1981) Geochemistry of the Amazon 1. Precipitation chemistry and the marine contribution to the dissolved load at the time of peak discharge *J. Geophys. Res.* **86**, 9844-9858.

Stallard R. F. and Edmond J. M. (1983) Geochemistry of the Amazon 2. The influence of geology and weathering environment on the dissolved load. *J. Geophys. Res.* **88**, 9671-9688.

Stallard R. F. and Edmond J. M. (1987) Geochemistry of the Amazon 3. Weathering chemistry and limits to dissolved inputs. *J. Geophys. Res.* **92**, 8293-8302.

Stumm W. and Morgan J. J. (1995) *Aquatic Chemistry: Chemical Equilibria and Rates in Natural Waters.* Wiley-Interscience, New York, 1022 pp.

Topp S. E., Salbu B., Roaldset E., and Jorgensen P. (1984) Vertical distribution of trace elements in lateritic soil. *Chem. Geol.* **47**, 159-174.

Turekian K. K. (1971) Rivers, tributaries and estuaries. In *Impingement of Man on the Oceans.* (ed. D. W. Hood), John Wiley and Sons, New York, N.Y., pp. 9-73.

UNESCO (1969) *Discharge of Selected Rivers of the World.* Studies and Reports in Hydrology I, Imprimeries Louis-Jean, Gap, France, 104 pp.

UNESCO (1977) *Atlas of World Water Balance.* USSR National Committee for the International Hydrological Decade, Paris.

Velbel M. A. (1993) Temperature dependence of silicate weathering in nature: How strong a negative feedback on long-term accumulation of atmospheric CO_2 and global greenhouse warming? *Geology* **21**, 1059-1062.

Velichko A. A. and Faustova M. A. (1991) Reconstruction of the last post-Pleistocene glaciation of the northern hemisphere (18-20 thousand years ago). *Doklady Akademy Nauk USSR* 223-225.

Wadleigh M. A., Veizer J., and Brooks C. (1985) Strontium and its isotopes in Canadian rivers: Fluxes and global implications. *Geochim. Cosmochim. Acta* **49**, 1727-1736.

Walder J. and Hallet B. (1985) A theoretical model of the fracture of rock during freezing. *Geol. Soc. Amer. Bull.* **96**, 336-346.

Westall J. C., Zachary J. L., and Morel F. M. M. (1976) *MINEQL, A Computer Program for the Calculation of Chemical Equilibrium Composition of Aqueous Systems.* Tech. Note 18, Dept. of Civil Eng., Mass. Inst. Technol., Cambridge, MA.

Yang C., Telmer K., and Veizer J. (1995) Chemical dynamics of the St. Lawrence riverine system: δD_{H_2O}, $\delta^{18}O_{H_2O}$, $\delta^{13}C_{DIC}$, $\delta^{34}S_{Sulfate}$, and dissolved $^{87}Sr/^{86}Sr$. *Geochim. Cosmochim. Acta* **60**, 851-866.

Zhang J., Huang W. W., Liu M. G., and Zhou Q. (1990) Drainage basin weathering and major element transport of two large Chinese rivers (Huanghe and Changjiang). *J. Geophys. Res.* **95**, 13277-13288.

Zonenshain L. P., Kuzmin M. I., and Natapov L. P. (1990) *Geology of the USSR: A Plate-Tectonic Synthesis.* Geodynamics Series 21, Am. Geophys. U., Washington, D.C., 242 pp.

Table1. Basic hydrologic information on the rivers of Eastern Siberia (Gordeev et al, 1996; Schumm and Winkley, 1994).

River Name	Length km	Area 10^3 km^2	Discharge km^3/yr
Lena	4828	2486	525
Kolyma	2129	660	132
Indigirka	1820	362	61
Anadyr	1117	191	60
Yana	1073	238	34
Omoloy	400	39	7

Table 2. Dissolved chemical data for the rivers of northeastern Siberia. The data are not corrected for seasalt. The rivers are divided into 7 geological categories: 1) WV: the right bank tributaries of the Lower Lena and Lower Aldan draining the western slope of the Verkhoyansk Range of Permian age with Jurassic and Cretaceous fans (Figs. 2, 3,4a). 2) SD: the right bank tributaries of the Mid-Aldan draining the Sette-Daban Range, a southern extension of the Verkhoyansk (Fig. 4a). 3) EV: the Omoloy and the left bank tributaries of the Yana draining the Triassic eastern slope of the Verkhoyansk Range and the Kular Mountains (Fig. 4b). 4) WC: the Yana right bank tributaries whose headwaters are in the western slope of the Cherskiy range and which drain the surrounding structures (Fig. 4b). 5) KSL: the Upper Indigirka and Kolyma left bank tributaries draining the complex Kolyma Structural Loop (Figs. 4c,d). 6) OC: the right bank tributaries of Upper Kolyma, the Anadyr, and small coastal streams draining the Okhotsk-Chukotka Volcanic Belt (Figs. 4d,e). 7) the two Lower Kolyma right bank tributaries draining the South Anyuy Suture (Fig. 4d). Main channel values are reported independently (UL, OM, YN, IN, KY). n.d.=not determined

River Name	Sample Number	Date dd/mm/yy	Na	K	Mg	Ca	Cl	SO_4	Alkalinity	Si	pH	Sr	$^{87}Sr/^{86}Sr$
			<		µM			>	µEq	µM		µM	
Western Slope of Verkhoyansk (WV)													
Khandyga	UL128	16/08/91	49	8.5	71.6	217	5.2	32.1	564	84	n.d.	1.24	0.71307
Barayy	UL130	16/08/91	46	8.1	88.0	315	3.3	59.1	756	70	n.d.	2.43	0.71299
Tukulan	UL131	16/08/91	52	7.6	74.0	406	17.0	70.0	895	60	n.d.	2.57	0.71354
Kelly	UL132	17/08/91	67	11.6	101	332	23.4	73.9	769	72	n.d.	2.26	0.71214
Tamara	UL105	28/07/91	104	12.9	108	326	57.4	59.0	848	60	n.d.	2.14	0.71062
	UL702	31/07/96	103	13.9	122	371	55.9	94.6	883	65	7.78	1.78	n.d.
Belyanka	UL133	18/08/91	73	11.4	49.0	237	17.6	35.5	578	67	n.d.	1.50	0.70984
Dyolabyn	UL321	04/08/93	65.8	10.4	43.6	120	15.2	33.0	313	78	n.d.	0.76	0.71059
Terekhtyakh	UL322	09/08/93	71.4	9.9	40.0	116	16.5	28.7	318	86	n.d.	0.61	0.71024
Sobolokh	UL602	23/07/95	155	10.7	175	520	86.6	162	1132	50	7.83	2.47	0.71370
Menkere	UL604	24/07/95	90.4	8.5	317	467	47.1	198	1242	55	8.03	2.26	0.71314
Natara	UL605	24/07/95	150	11.9	147	343	97.8	75.6	850	54	7.80	1.26	0.71144
Dzhardzhan	UL606	24/07/95	93.2	6.0	219	351	38.5	130	932	55	7.77	1.73	0.71064
Sette-Daban Range (SD)													
Maya	UL109	02/08/91	56	10.3	153	344	9.8	47.6	1001	88	n.d.	0.86	0.71127
Allakh-Yun	UL123	13/08/91	46	13.7	115	429	11.8	44.0	1057	70	n.d.	1.24	0.71194
Khanda	UL125	15/08/91	38	8.5	324	1080	15.2	110	2681	40	n.d.	1.79	0.71145
Small stream	UL108	01/08/91	44	13.9	372	894	29.5	39.8	2547	80	n.d.	0.48	0.71765

Table 2. continued.

River Name	Sample Number	Date dd/mm/yy	Na	K	Mg	Ca	Cl	SO_4	Alkalinity	Si	pH	Sr	$^{87}Sr/^{86}Sr$
			<		µM			>	µEq	µM		µM	
Tyry	UL126	15/08/91	101	14.3	234	685	62.8	141	1646	68	n.d.	2.90	0.71069
East Chandyga	UL107	31/07/91	31	9.3	233	894	21.6	111	2109	53	n.d.	2.17	0.71030
Tompo	UL127	15/08/91	39	9.4	135	414	4.4	55.8	1032	64	n.d.	1.12	0.71087
Eastern Slope of Verkhoyansk (EV)													
Turka creek	OM101	21/08/95	54.8	8.8	50.9	54.7	4.8	31.6	176	98	5.69	0.27	0.71160
Ekyes	OM102	21/08/95	89.0	18.9	166	177	35.4	151	397	102	7.23	0.52	0.71183
Kyugyulyur	OM103	21/08/95	69.0	5.1	67.8	68.4	3.3	73.9	167	70	6.66	0.25	0.71162
Omoloy ab. Kyugyulyur	OM104	21/08/95	49.2	8.0	74.4	150	3.5	83.4	351	60	7.49	0.65	0.70912
Baki	YN120	19/08/95	51.9	7.1	65.8	77.0	7.0	12.1	274	71	7.25	0.26	0.71078
Batantay	YN119	18/08/95	63.4	14.3	82.5	197	21.5	71.7	404	81	7.33	0.62	0.71015
Black River	YN118	18/08/95	66.6	11.7	86.8	159	38.2	7.2	405	108	7.16	0.37	0.71015
Kytalyktakh	YN113	16/08/95	61.9	14.4	64.8	102	21.2	10.7	295	87	6.61	0.27	0.71069
Yana @head	YN109	13/08/95	76.7	19.3	98.5	180	17.6	66.4	467	79	7.16	0.95	0.71077
Arga-Bullyakh	YN110	13/08/95	63.3	28.6	101	144	25.1	59.0	296	97	6.68	0.33	0.71236
Sartang	YN111	13/08/95	48.7	15.4	100	179	7.5	42.6	456	88	7.23	0.83	0.71023
Dulgalakh	YN112	13/08/95	80.3	13.6	76.4	162	45.9	55.0	384	79	7.21	0.78	0.71094
Western Slope of Cherskiy (WC)													
Adycha above Tuostakh	YN114	17/08/95	58.0	12.7	66.3	132	2.0	51.4	293	79	7.01	0.46	0.70967
Tuostakh	YN115	17/08/95	42.7	15.1	138	447	4.6	169	915	75	7.67	0.89	0.70939
Adycha @ mouth	YN116	17/08/95	44.6	15.4	72.7	165	6.1	56.7	353	78	7.20	0.47	0.70961
Oldzan	YN117	18/08/95	58.6	10.0	52.8	105	6.2	76.3	176	82	6.89	0.37	0.71001
Abyrabit	YN121	19/08/95	64.4	7.3	47.5	111	1.2	38.8	229	96	6.85	0.55	0.70980
Dzhangky	YN122	19/08/95	52.3	6.8	36.3	86.8	6.4	54.5	170	76	6.76	0.38	0.70936
Kolyma Structural Loop (KSL)													
Bolshaya Ercha	IG120	26/07/96	58.4	13.8	90.6	215	30.8	38.2	553	48	7.46	0.54	0.71024
Shanguina	IG119	26/07/96	62.9	14.0	101	250	6.6	62.8	660	61	7.49	0.70	0.71024
Tirekhtyakh	IG117	25/07/96	47.5	13.5	101	293	6.7	71.2	691	65	7.64	0.76	0.71022
Suturuokha	IG116	25/07/96	38.2	15.3	77.2	130	20.4	3.2	397	16	7.22	0.19	0.71024
Uyandina	IG115	23/07/96	27.7	15.2	110	354	8.1	73.5	865	49	7.68	0.64	0.71023
Badyarikha	IG114	23/07/96	59.0	12.6	113	196	7.4	67.1	531	65	7.49	0.78	0.71024
Bor-Uryakh	IG113	23/07/96	59.2	13.5	103	205	12.8	30.0	580	49	7.48	0.75	0.71025
Selennyakh	IG112	22/07/96	27.4	10.7	107	427	6.7	51.7	945	48	8.01	0.67	0.71025

Table 2. continued.

River Name	Sample Number	Date dd/mm/yy	Na	K	Mg	Ca	Cl	SO_4	Alkalinity	Si	pH	Sr	$^{87}Sr/^{86}Sr$
			<		µM			>	µEq	µM		µM	
Kebergene	IG111	21/07/96	28.8	4.2	37.3	68.2	8.7	3.2	164	36	6.94	0.19	0.71024
No Name	IG101	13/07/96	5.4	3.4	29.8	46.3	5.4	3.2	126	35	n.d.	0.16	0.70992
Red River	IG102	14/07/96	25.4	6.2	140	373	6.1	5.9	1074	54	8.01	0.77	0.70846
Talbykchan	IG104	14/07/96	47.9	9.0	136	303	6.2	11.3	891	50	7.60	1.09	0.70858
Kolyadin	IG105	15/07/96	114	14.3	84.1	157	4.8	47.4	451	53	7.23	1.50	0.71023
Jyekhatyekha	IG106	16/07/96	276	13.8	148	127	4.8	66.8	629	56	7.56	1.16	0.71025
Syuryuktyakh	IG107	17/07/96	70.5	9.0	271	575	5.4	85.3	1680	85	8.12	1.50	0.71025
Ilin-Eselyakh	IG108	18/07/96	143	9.8	193	156	4.0	98.3	618	55	7.77	0.90	0.71025
Moma	IG109	19/07/96	83.7	9.5	134	269	15.0	77.7	720	68	7.78	1.04	0.71023
Indigirka ab Moma	IG110	20/07/96	75.5	12.1	66.0	160	6.7	93.2	311	78	7.62	0.68	0.71024
Sedjodima	KY117	19/08/92	82.0	18.3	112	170	12.3	6.8	589	61	7.43	0.44	0.70921
Kamenka	KY116	19/08/92	68.8	6.6	187	552	19.3	64.5	1400	55	7.92	0.64	0.71025
Sepyakine	KY115	19/08/92	56.1	9.7	146	419	17.5	26.9	1183	60	7.88	0.45	0.71127
Ozhogina	KY114	18/08/92	171	15.8	197	340	11.7	321	585	64	7.64	1.74	0.70945
Zyryanka	KY112	17/08/92	178	11.4	213	558	16.1	260	1227	60	8.09	1.65	0.70871
Yasachnaya	KY113	18/08/92	69.5	10.2	296	1044	51.7	180	2425	75	8.39	2.14	0.70884
Popovka	KY111	16/08/92	85.0	12.4	187	399	16.2	80.7	1068	79	7.82	0.70	0.71070
Shamanikha	KY110	16/08/92	93.4	10.7	130	295	25.5	33.8	892	100	7.46	0.48	0.71114
Stolbovaya	KY109	15/08/92	79.4	8.8	436	1084	36.4	45.7	3000	69	8.08	0.78	0.71385
Burgali	KY107	15/08/92	134	13.2	265	723	11.2	266	1527	85	7.47	1.46	0.70892
Seymchan	KY101	13/08/92	87.8	7.0	117	372	19.3	114	813	92	n.d.	0.68	0.70848
Okhotsk-Chukotka Volcanic Belt (OC)													
Kolyma ab. Buyunda	KY103	13/08/92	78	9.4	82.2	203	5.5	136	356	108	7.40	0.71	0.70862
Buyunda	KY102	13/08/92	70	7.2	43.5	107	3.3	57.6	247	117	7.11	0.46	0.70818
Balygychan	KY104	14/08/92	81	8.2	47.2	125	13.0	75.1	256	123	6.73	0.49	0.70771
Sugoy	KY105	15/08/92	85	8.2	35.0	111	10.9	79.4	204	119	6.86	0.49	0.70744
Korkodon	KY108	15/08/92	77	11.4	50.1	188	8.4	62.3	411	110	7.46	0.56	0.70705
Berezovka	KY118	20/08/92	82.9	13.1	96.4	346	13.6	82.7	750	74	7.58	0.67	0.70814
Omolon	KY119	21/08/92	102	9.6	52.9	181	16.8	50.3	452	105	7.64	0.54	0.70642
Anadyr @ Markhovo	AY109	04/09/97	98.4	5.7	55.6	109	8.4	48.8	340	139	n.d.	0.32	0.704223
Anadyr ab. Mayn	AY108	01/09/97	110	9.7	58.5	108	12.1	40.1	381	143	n.d.	0.32	0.70428
Mayn	AY107	01/09/97	125	11.6	86.8	109	10.3	46.9	392	193	n.d.	0.28	0.704875
Anadyr ab. Belaya	AY106	28/08/97	112	9.7	66.2	118	12.2	49.3	406	147	n.d.	0.34	0.704383
Belaya	AY105	28/08/97	90.8	7.3	29.1	64.6	12.2	35.8	204	123	n.d.	0.15	0.705059

Table 2. continued.

River Name	Sample Number	Date dd/mm/yy	Na	K	Mg	Ca	Cl	SO_4	Alkalinity	Si	pH	Sr	$^{87}Sr/^{86}Sr$
			<		µM			>	µEq	µM		µM	
	AY104	25/08/97	87.9	12.0	27.0	64.1	6.6	42.4	202	124	n.d.	0.14	0.705066
Anadyr ab. Tanyurer	AY103	24/08/97	100	7.8	51.8	91.2	13.8	35.6	315	135	n.d.	0.24	0.704579
Tanyurer	AY102	24/08/97	77.0	4.7	38.1	73.3	10.1	33.1	240	90	n.d.	0.16	0.704874
Anadyr @ mouth	AY101	24/08/97	125	8.8	52.3	80.1	32.9	39.2	302	127	n.d.	0.35	0.704725
Kava	MD101	09/09/97	77.5	14.8	36.9	96.3	13.7	83.9	178	143	n.d.	0.34	n.d.
Yana	MD102	09/09/97	92.1	19.8	45.6	132	15.6	95.2	257	149	n.d.	0.44	n.d.
Arman	MD103	09/09/97	96.3	12.2	55.6	183	n.d.	n.d.	n.d.	130	n.d.	0.47	n.d.
Ola	UL207	09/09/92	155	7.5	34.0	123	35.1	21.4	384	135	7.16	0.21	n.d.
South Anyui Suture (SA)													
Malyy Anyuy	KY121	22/08/92	45.0	8.3	55.7	103	6.0	70.8	205	79	7.08	0.32	0.70873
Bolshoy Anyuy	KY122	22/08/92	66.9	8.2	64.2	129	5.3	32.3	370	126	7.57	0.46	0.70494
Main Channels (KY, IG, YN, UL)													
Kolyma ab. Sugoy	KY106	15/08/92	73.0	9.1	63.3	161	6.0	108	310	112	7.32	0.61	0.70849
Kolyma @ mouth	KY120	22/08/92	94.3	10.7	99.2	298	16.0	115	616	89	7.82	0.75	0.70895
Indigirka ab.Moma	IG110	20/07/96	75.5	12.1	66.0	160	6.7	93.2	311	78	7.62	0.68	0.71024
Indigirka @ Red River	IG103	14/07/96	81.2	10.7	92.5	215	9.9	71.8	544	64	7.59	0.88	0.70964
IG ab. Tirekhtyakh	IG118	25/07/96	64.8	13.0	99.2	268	9.4	83.5	636	65	7.54	0.81	0.71025
Indigirka bl. B. Ercha	IG121	26/07/96	48.1	14.3	99.9	265	10.0	74.4	672	65	7.50	0.82	0.70966
Yana @ head	YN109	13/08/95	62.1	19.3	98.5	180	17.6	66.4	467	79	7.16	0.95	0.71236
Yana bl. Oldzan	YN108	12/08/95	58.3	17.9	79.6	184	4.8	78.7	418	74	7.47	0.59	0.70995
Yana bl. Dzhangky	YN106	10/08/95	50.1	13.0	65.8	60.5	28.6	53.1	173	68	6.58	0.09	0.70995
Yana ab. delta	YN105	09/08/95	64.3	18.7	105	271	5.9	109	621	68	7.92	0.93	0.70687
Yana, 154km from mouth	YN104	09/08/95	49.3	19.0	106	271	15.1	106	611	69	7.85	0.99	0.70991
Kochevaya channel	YN103	09/08/95	63.4	18.8	111	268	13.9	110	621	68	7.80	0.85	n.d.
Kamelyot channel	YN102	09/08/95	54.0	19.7	116	277	13.4	107	622	68	7.81	1.08	0.70995
Yana, 47km from mouth	YN101	08/08/95	54.9	19.6	103	258	17.2	106	587	66	7.69	0.84	0.70997
Lena bl. Aldan	UL103	28/07/91	626	15.3	152	337	592	119	780	75	n.d.	1.54	0.71079
Lena ab. Vilyui	UL202	01/09/92	563	13.0	164	370	556	192	773	81	7.87	1.57	0.71030
Lena @ Kusur	UL607	25/07/95	273	12.1	137	337	238	93.0	796	57	7.61	1.10	0.710479

Table 3. Flux calculations for the eastern Siberian rivers draining the collision/accretionary zone.
The fluxes for each element are calculated using the concentration values in Table 2 and the discharge shown here. TDS flux is the sum of the fluxes of the 8 elements. $\phi CO2 = TZ+^*$ when $^{87}Sr/^{86}Sr$ ratio is >0.710 or <0.7065; otherwise, $\phi CO_2 = 2\phi Si$. Fluxes for individual elements and TDS are summed up for each geological category; areal fluxes for TDS and CO_2 are averaged.

River	Area	Discharge	Na	K	Mg	Ca	Cl	SO_4	HCO_3	Si	$^{87}Sr/^{86}Sr$	TDS flux	Areal TDS Flux	Net CO_2 Flux
	10^3 km^2	km^3/yr	<			10^9 mol/yr				>		10^9 mol/yr	10^6 mol/yr/km^2	10^3 mol/yr/km^2
Western Slope of Verkhoyansk (WV)														
Khandyga	11.9	1.79	0.088	0.015	0.128	0.389	0.009	0.057	1.01	0.150	0.7131	1.85	0.15	84.8
Barayy	3.64	0.546	0.025	0.004	0.048	0.172	0.002	0.032	0.413	0.038	0.7130	0.73	0.20	111
Tukulan	2.80	0.420	0.022	0.003	0.031	0.170	0.007	0.029	0.376	0.025	0.7135	0.66	0.24	129
Kelly	10.7	2.13	0.143	0.025	0.215	0.707	0.050	0.157	1.64	0.153	0.7121	3.09	0.29	155
Tamara	10.8	2.16	0.225	0.028	0.234	0.705	0.124	0.128	1.83	0.130	0.7106	3.41	0.32	162
Belyanka	4.90	0.979	0.071	0.011	0.048	0.232	0.017	0.035	0.566	0.066	0.7098	1.05	0.21	26.8
Dyolabyn	0.60	0.181	0.012	0.002	0.008	0.022	0.003	0.006	0.056	0.014	0.7106	0.12	0.20	96.7
Terekhtyakh	2.13	0.639	0.046	0.006	0.026	0.074	0.011	0.018	0.203	0.055	0.7102	0.44	0.21	95.8
Sobolokh	12.6	2.52	0.389	0.027	0.440	1.31	0.218	0.408	2.85	0.126	0.7137	5.77	0.46	229
Menkere	16.2	3.56	0.321	0.030	1.13	1.66	0.167	0.703	4.42	0.194	0.7131	8.62	0.53	269
Natara	6.82	1.71	0.256	0.020	0.251	0.585	0.167	0.129	1.45	0.092	0.7114	2.95	0.43	223
Dzhardzhan	12.3	3.07	0.286	0.018	0.673	1.08	0.118	0.398	2.86	0.170	0.7106	5.61	0.46	235
Total	*95.3*	*19.7*	*1.88*	*0.191*	*3.23*	*7.10*	*0.893*	*2.10*	*17.7*	*1.21*	*0.7122*	*34.3*	*0.36*	*181*
Sette-Daban Range (SD)														
Maya	172	34.4	1.93	0.354	5.26	11.8	0.337	1.64	34.4	3.025	0.7113	58.8	0.34	191
Allakh-Yun	24.8	4.95	0.228	0.068	0.570	2.12	0.058	0.218	5.24	0.347	0.7119	8.85	0.36	210
Khanda	8.18	1.64	0.062	0.014	0.530	1.77	0.025	0.180	4.39	0.065	0.7115	7.03	0.86	524
Tyry	13.7	2.74	0.277	0.039	0.641	1.88	0.172	0.386	4.51	0.186	0.7107	8.09	0.59	322
East Chandyga	9.93	1.99	0.062	0.018	0.463	1.78	0.043	0.220	4.19	0.105	0.7103	6.88	0.69	410
Tompo	41.8	8.36	0.326	0.079	1.13	3.46	0.037	0.466	8.63	0.535	0.7109	14.7	0.35	206
Total	*270*	*54.0*	*2.88*	*0.572*	*8.59*	*22.8*	*0.672*	*3.11*	*61.4*	*4.26*	*0.7111*	*104*	*0.39*	*220*
Eastern Slope of Verkhoyansk (EV)														
Kyugyulyur	3.69	0.258	0.018	0.001	0.018	0.018	0.001	0.019	0.043	0.018	0.7116	0.14	0.04	13.7
Omoloy ab. Kyugyulyur	32.9	2.30	0.113	0.018	0.171	0.345	0.008	0.192	0.808	0.137	0.7091	1.79	0.05	8.3
Baki	2.69	0.188	0.010	0.001	0.012	0.015	0.001	0.002	0.052	0.013	0.7108	0.11	0.04	21.9
Batantay	43.2	2.16	0.137	0.031	0.178	0.426	0.046	0.155	0.873	0.17	0.7102	2.02	0.05	23.6
Kytalyktakh	5.00	0.200	0.012	0.003	0.013	0.020	0.004	0.0021	0.059	0.02	0.7107	0.13	0.03	14.7
Yana @head	43.4	1.30	0.100	0.025	0.128	0.235	0.023	0.0865	0.609	0.10	0.7108	1.31	0.03	15.1
Sartang	16.7	0.667	0.033	0.010	0.067	0.119	0.005	0.0284	0.304	0.06	0.7102	0.63	0.04	21.2
Dulgalakh	26.8	1.07	0.086	0.015	0.082	0.173	0.049	0.0589	0.411	0.08	0.7109	0.96	0.04	16.6
Total	*174*	*8.15*	*0.509*	*0.105*	*0.669*	*1.35*	*0.138*	*0.544*	*3.16*	*0.61*	*0.7102*	*7.08*	*0.04*	*16.8*
Western Slope of Cherskiy (WC)														
Adycha above Tuostakh	71.4	7.14	0.414	0.091	0.473	0.942	0.014	0.367	2.09	0.56	0.7097	4.96	0.07	15.8
Tuostakh	20.6	2.06	0.088	0.031	0.285	0.922	0.009	0.348	1.89	0.15	0.7094	3.72	0.18	15.0
Oldzan	14.8	1.48	0.087	0.015	0.078	0.156	0.009	0.113	0.261	0.12	0.7100	0.84	0.06	16.4
Abyrabit	2.26	0.340	0.022	0.002	0.016	0.038	0.000	0.013	0.078	0.03	0.7098	0.20	0.09	28.8
Dzhangky	2.25	0.338	0.018	0.002	0.012	0.029	0.002	0.018	0.057	0.03	0.7094	0.17	0.07	22.9
Total	*111*	*11.4*	*0.629*	*0.141*	*0.865*	*2.09*	*0.036*	*0.859*	*4.37*	*0.90*	*0.7096*	*9.89*	*0.09*	*16.1*

Table 3. continued.

River	Area	Discharge	Na	K	Mg	Ca	Cl	SO_4	HCO_3	Si	$^{87}Sr/^{86}Sr$	TDS flux	Areal TDS Flux	Net CO_2 Flux
	10^3 km^2	km^3/yr	<			10^9 mol/yr				>		10^9 mol/yr	10^6 mol/yr/km^2	10^3 mol/yr/km^2
Kolyma Structural Loop (KSL)														
Bolshaya Ercha	2.69	0.323	0.019	0.004	0.029	0.069	0.010	0.012	0.179	0.02	0.7102	0.34	0.13	69.1
Shanguina	4.24	0.509	0.032	0.007	0.051	0.127	0.003	0.032	0.336	0.03	0.7102	0.62	0.15	77.6
Tirekhtyakh	1.85	0.222	0.011	0.003	0.022	0.065	0.001	0.016	0.153	0.01	0.7102	0.29	0.15	84.0
Sutturuokha	3.50	0.350	0.013	0.005	0.027	0.045	0.007	0.001	0.139	0.01	0.7102	0.24	0.07	44.1
Uyandina	40.7	6.11	0.169	0.093	0.672	2.16	0.049	0.449	5.28	0.30	0.7102	9.17	0.23	122
Badyarikha	11.6	1.74	0.102	0.022	0.196	0.340	0.013	0.117	0.922	0.11	0.7102	1.83	0.16	82.2
Bor-Uryakh	8.61	1.29	0.076	0.017	0.133	0.265	0.017	0.039	0.749	0.06	0.7103	1.36	0.16	92.4
Selennyakh	34.6	5.18	0.142	0.055	0.555	2.21	0.035	0.268	4.90	0.25	0.7103	8.42	0.24	149
Kebergene	1.02	0.153	0.004	0.001	0.006	0.010	0.001	0.000	0.025	0.01	0.7102	0.05	0.05	34.3
Syuryuktyakh	8.38	1.26	0.089	0.011	0.341	0.723	0.007	0.107	2.11	0.11	0.7103	3.50	0.42	239
Ilin-Eselyakh	2.40	0.359	0.051	0.004	0.069	0.056	0.001	0.035	0.222	0.02	0.7103	0.46	0.19	97.5
Moma	35.0	7.00	0.586	0.066	0.937	1.88	0.105	0.544	5.04	0.48	0.7102	9.63	0.28	146
Indigirka ab Moma	141	28.1	2.12	0.340	1.85	4.50	0.188	2.62	8.74	2.20	0.7102	22.56	0.16	69.3
Sedjodima	18.3	2.39	0.196	0.044	0.266	0.405	0.029	0.016	1.40	0.15	0.7092	2.51	0.14	15.8
Kamenka	6.39	0.895	0.062	0.006	0.167	0.494	0.017	0.058	1.25	0.05	0.7103	2.11	0.33	197
Sepyakine	5.21	0.730	0.041	0.007	0.107	0.306	0.013	0.020	0.863	0.04	0.7113	1.40	0.27	158
Ozhogina	26.8	4.02	0.688	0.064	0.790	1.37	0.047	1.29	2.35	0.26	0.7095	6.86	0.26	19.2
Zyryanka	7.91	1.27	0.226	0.014	0.269	0.707	0.020	0.329	1.55	0.08	0.7087	3.19	0.40	19.1
Yasachnaya	35.9	6.10	0.424	0.062	1.80	6.36	0.315	1.10	14.8	0.45	0.7088	25.3	0.71	25.3
Popovka	8.66	1.73	0.147	0.021	0.324	0.691	0.028	0.140	1.85	0.14	0.7107	3.34	0.39	218
Shamanikha	3.98	0.795	0.074	0.009	0.104	0.235	0.020	0.027	0.710	0.08	0.7111	1.26	0.32	172
Stolbovaya	3.51	0.877	0.070	0.008	0.382	0.951	0.032	0.040	2.63	0.06	0.7139	4.17	1.19	750
Burgali	2.60	0.728	0.097	0.010	0.193	0.526	0.008	0.194	1.11	0.06	0.7089	2.20	0.85	47.7
Seymchan	5.09	1.58	0.139	0.011	0.185	0.587	0.030	0.180	1.28	0.15	0.7085	2.56	0.50	57.0
Total	*419*	*73.7*	*5.58*	*0.885*	*9.48*	*25.1*	*0.999*	*7.63*	*58.6*	*5.11*	*0.7098*	*113*	*0.27*	*93.9*
Okhotsk-Chukotka Volcanic Belt (OC)														
Kolyma ab. Buyunda	89.6	28.7	2.24	0.270	2.36	5.82	0.157	3.90	10.2	3.09	0.7086	28.0	0.31	68.9
Buyunda	21.1	6.53	0.457	0.047	0.284	0.699	0.022	0.376	1.61	0.76	0.7082	4.26	0.20	72.4
Balygychan	18.8	5.65	0.458	0.046	0.267	0.707	0.073	0.425	1.45	0.70	0.7077	4.12	0.22	73.9
Sugoy	24.3	6.81	0.579	0.056	0.238	0.756	0.074	0.541	1.39	0.81	0.7074	4.44	0.18	66.8
Korkodon	34.2	8.88	0.684	0.101	0.445	1.67	0.075	0.553	3.65	0.97	0.7071	8.15	0.24	57.0
Berezovka	31.4	3.14	0.261	0.041	0.303	1.09	0.043	0.260	2.36	0.23	0.7081	4.58	0.15	14.7
Omolon	120	10.8	1.11	0.104	0.573	1.96	0.182	0.545	4.90	1.13	0.7064	10.5	0.09	41.5
Anadyr @ Markhovo	52.7	18.5	1.82	0.105	1.03	2.01	0.155	0.901	6.28	2.57	0.7042	14.9	0.28	115
Mayn	33.9	12.9	1.61	0.150	1.12	1.41	0.133	0.605	5.05	2.49	0.7049	12.6	0.37	161
Belaya	39.2	12.5	1.14	0.091	0.365	0.810	0.153	0.449	2.55	1.54	0.7051	7.10	0.18	64.5
Tanyurer	22.9	7.55	0.581	0.035	0.288	0.553	0.076	0.250	1.81	0.68	0.7049	4.27	0.19	75.3
Total	*489*	*122*	*10.9*	*1.05*	*7.27*	*17.5*	*1.14*	*8.81*	*41.3*	*15.0*	*0.7072*	*103*	*0.21*	*69.4*
South Anyui Suture (SA)														
Malyy Anyuy	49.3	5.42	0.244	0.045	0.302	0.559	0.033	0.384	1.11	0.43	0.7087	3.11	0.06	17.5
Bolshoy Anyuy	68.3	7.51	0.503	0.062	0.482	0.966	0.040	0.243	2.78	0.95	0.7049	6.02	0.09	43.0
Total	*118*	*12.9*	*0.75*	*0.107*	*0.784*	*1.52*	*0.072*	*0.626*	*3.89*	*1.38*	*0.7062*	*9.13*	*0.08*	*32.3*

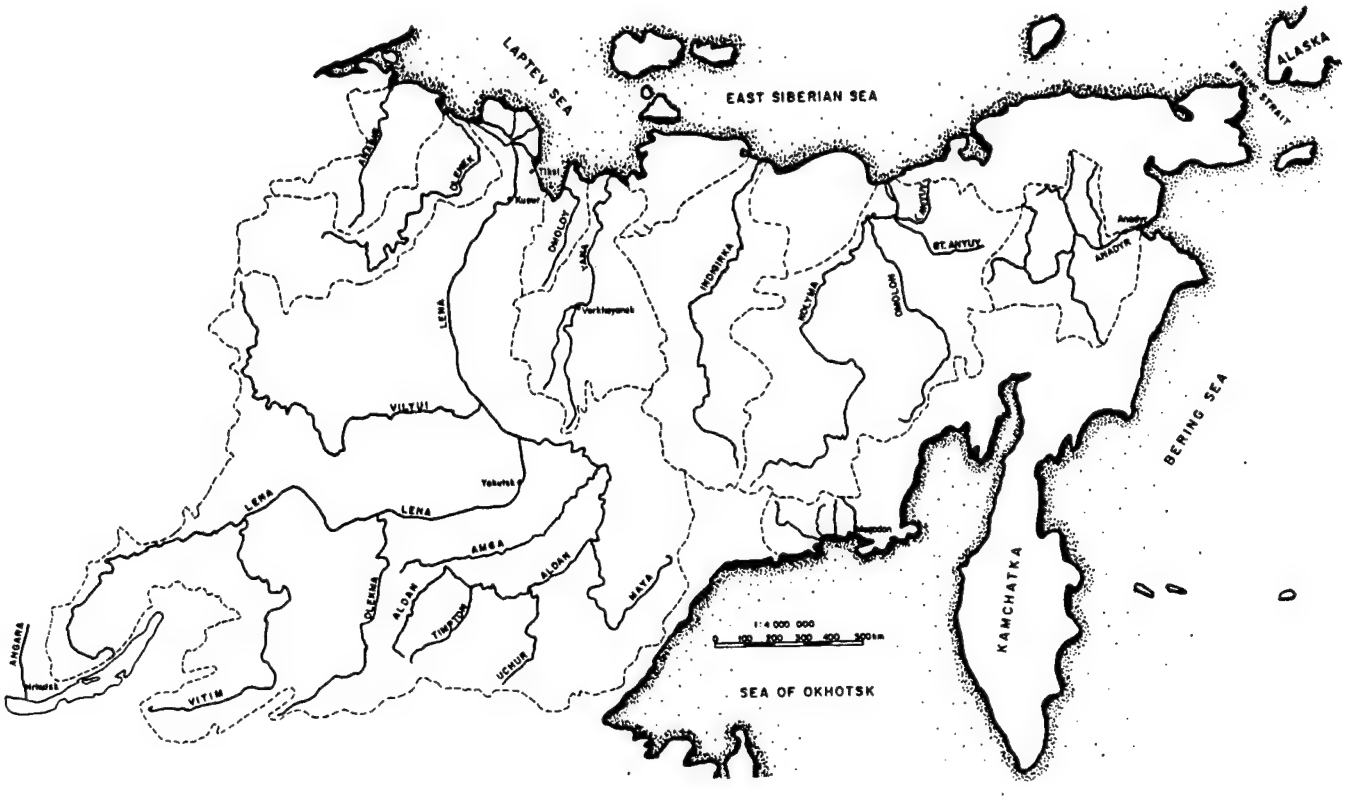

Figure 1. Schematic map of the rivers of Eastern Siberia which have been sampled as part of this project. Lake Baikal occupies the southwestern corner, Kamchatka and Alaska the east. Total drainage area investigated is ~4 x10^6 km^2, half the size of the U.S. (~9x10^6 km^2).

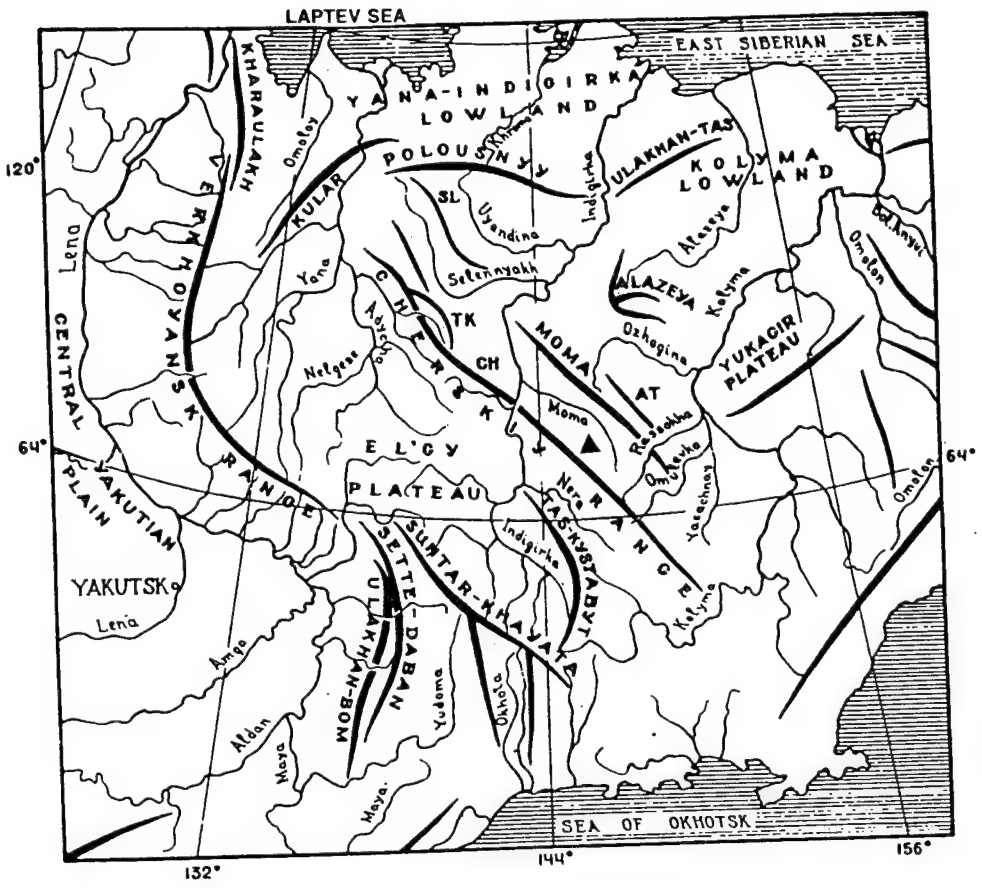

Figure 2. Physiographic elements and geographic index map of the Russian Far East. ▲ denotes Pobeda Peak, the highest point. AT = Arga-Tas Range, CH = Chemalginsky Range, TK = Tas-Khayakhtakh Range. From Parfenov (1991).

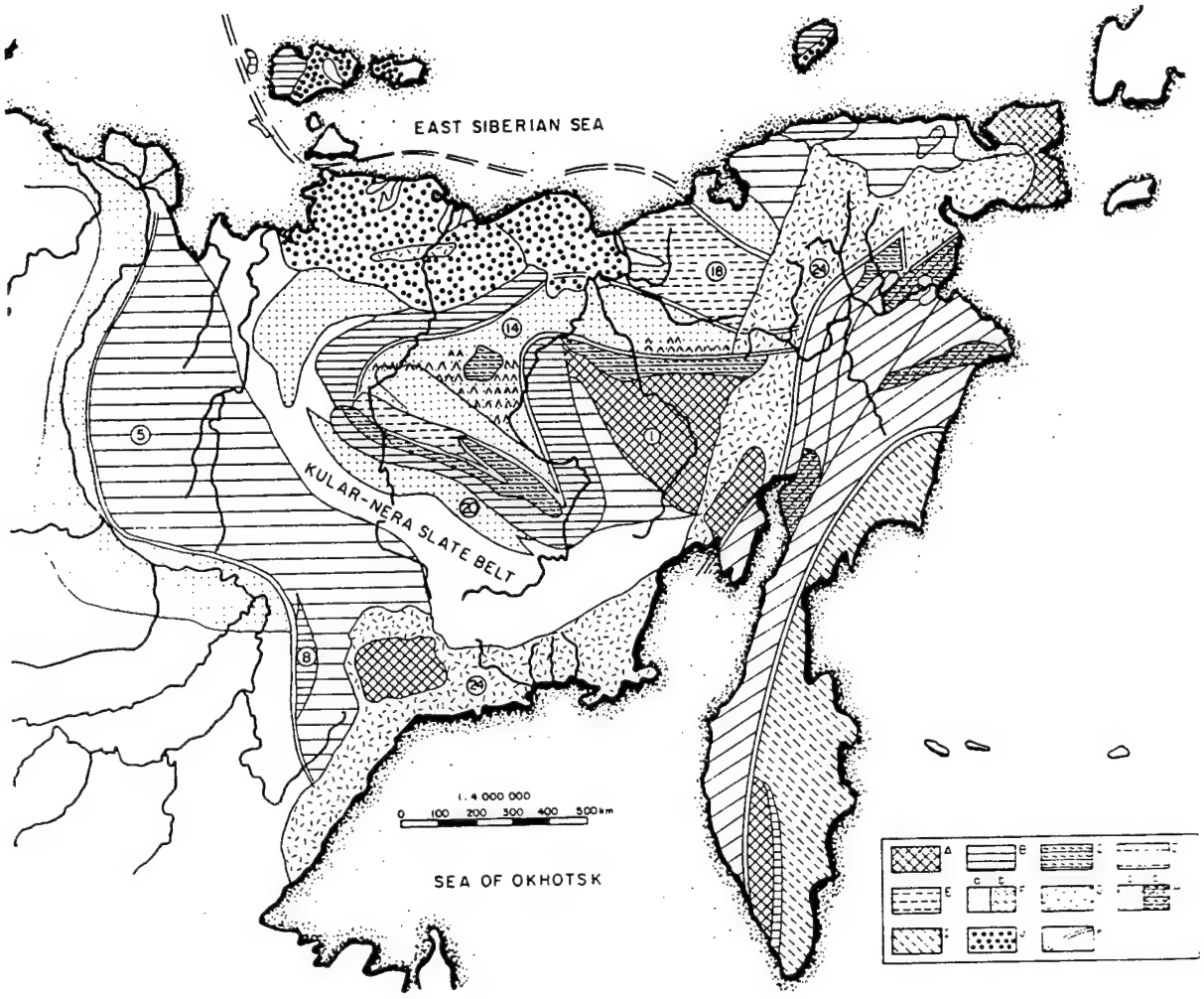

Figure 3. Main tectonic zones of the northeastern Siberia. Adapted from Parfenov (1991) and Puchkov (1996). The KSL is a series of uplifts that form a loop starting from the Lower Indigirka to Lower Kolyma. Legend: A= rigid uplifted massifs with outcrops of pre-Riphean basement; B,C = horst-like uplifts composed of folded Riphean—mid-Paleozoic sediments formed on continental crust (B) or on transitional and oceanic crust (C); D = folded zones composed of upper Paleozoic-lower Mesozoic Verkhoyansk complex, formed on subcontinental crust, partially destroyed by Devonian riftogenic processes; E = folded zones composed of Mesozoic complexes formed on transitional and oceanic crust; F = Middle Jurassic basins and Preverkhoyansk foredeep filled by a) terrigenous and b) volcanogenic-terrigenous sediments; G= volcano-plutonic complexes of Cretaceous age; H = Laramides a) Meso-Cenozoic complexes b) Paleozoic terranes formed mostly on oceanic and transitional crust; I = Cenozoic cover of young East Siberian Platform; J = Cenozoic cover of young East Siberian Platform; K = boundaries between Paleozoic structural-sedimentary megazones. Circled numbers: 1 = Omolon massif; 5 = Verkhoyansk foldbelt; 14 = Alazeya-Oloy volcanic arc; 18 = Anyuy foldbelt; 20 = Inyali-Debin synclinorium; 24 = Okhotsk-Chukotka volcanic belt.

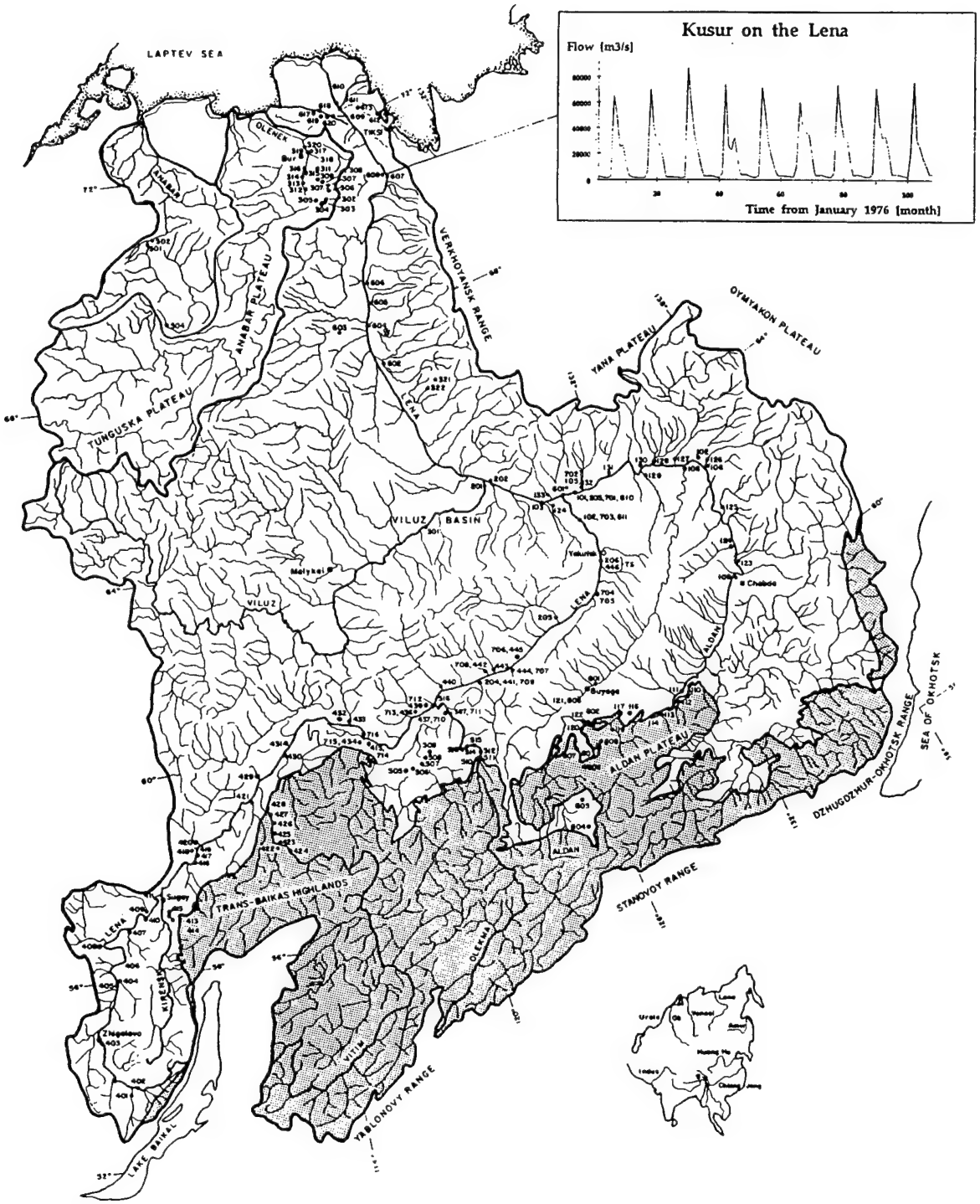

Figure 4. a) The location map of the Lena river drainage basin. The stippled areas denote exposed basement terrains. The Arctic Circle is at 66.5°N. Discharge measurements at Kusur above the delta, shown as an inset, are from the Global Hydrological Archive and Analysis System.

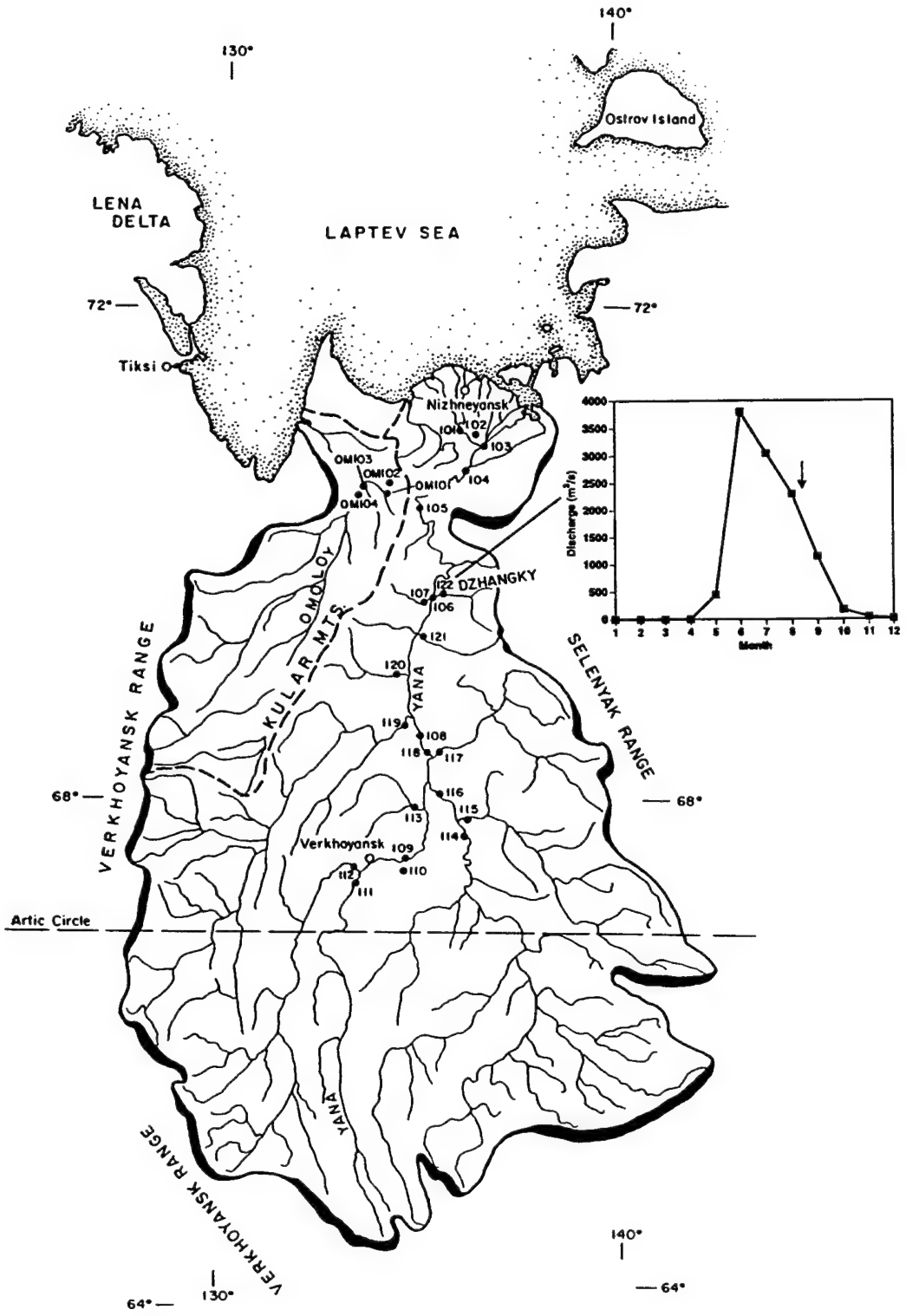

Figure 4. b) The location map of the Yana drainage basin. The "cold pole" (minimum recorded temperature of -69.8°C) is at Verkhoyansk village based on a meteorological record extending back continuously to 1883. Discharge shown as inset is at Dzhangky averaged over 1938-1964 (UNESCO, 1969). The arrow indicates when the sample was taken.

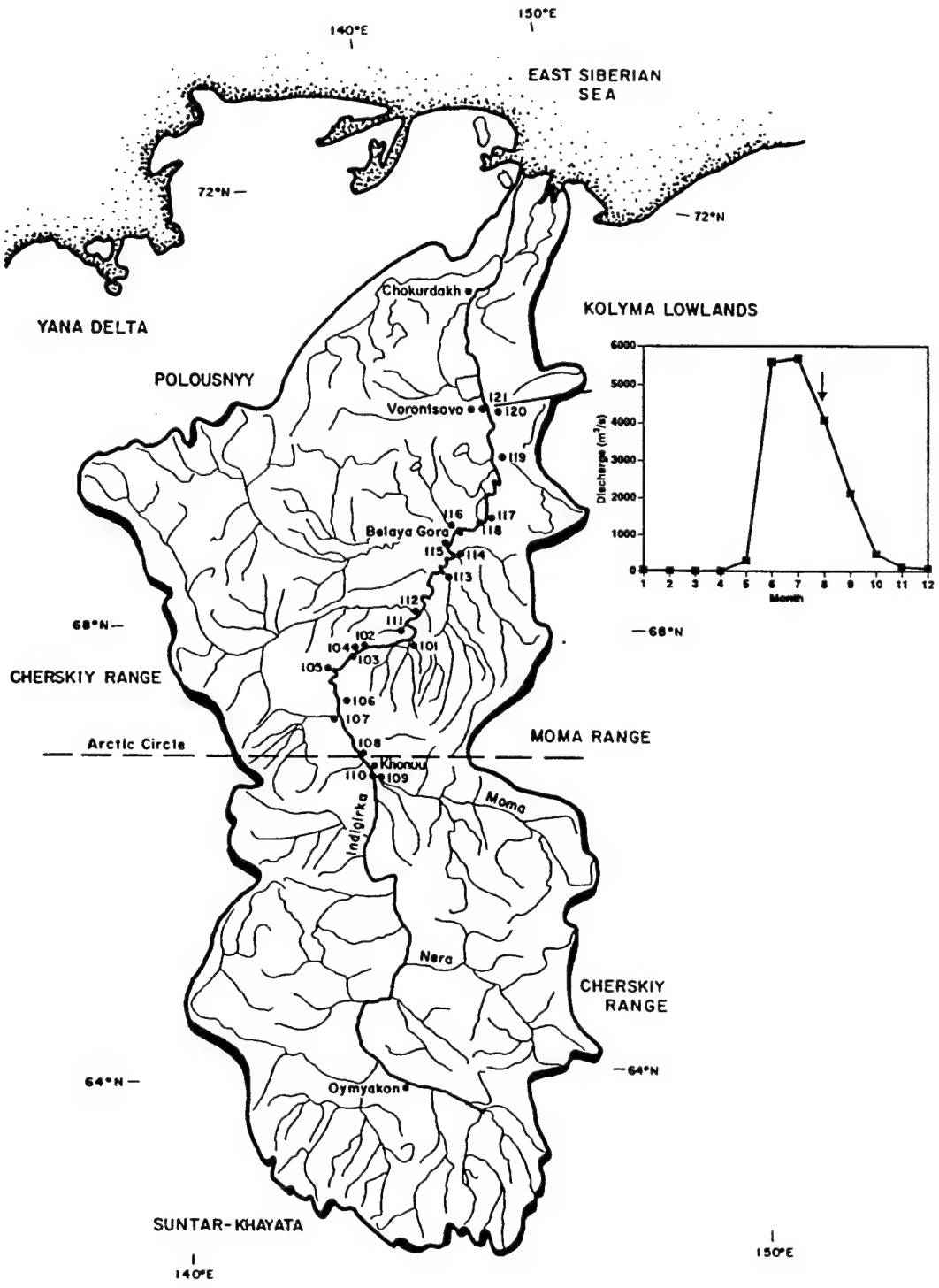

Figure 4. c) The location map of the Indigirka drainage basin. Except for the strip of mountain gorges in the Cherskiy Range the region is dominated by swamps and bogs. Discharge data are from Vorontsovo averaged over 1937-1964 (UNESCO, 1969).

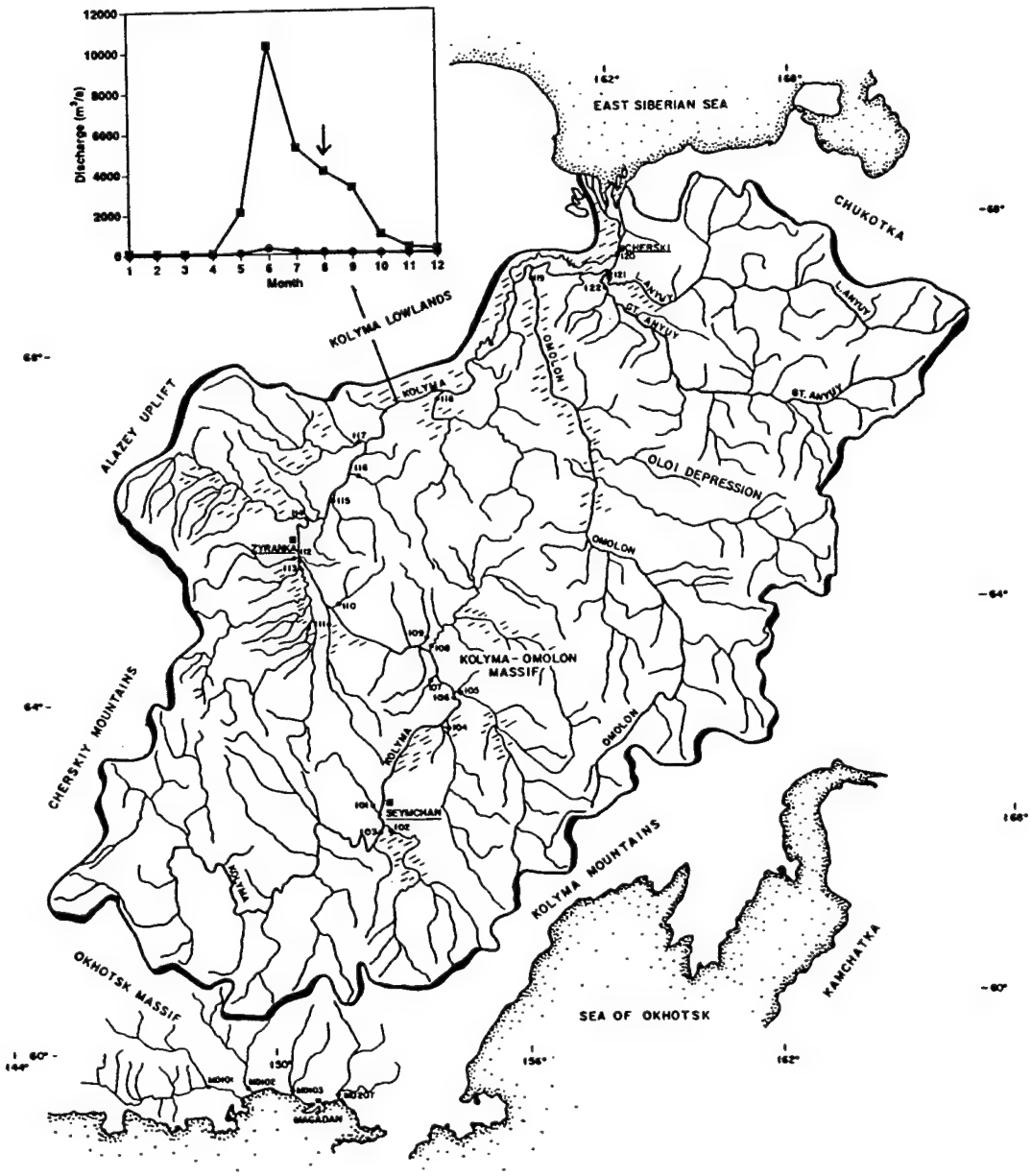

Figure 4. d). The location map of the Kolyma river drainage basin. The dashed lines indicate swampy areas. Discharge data are from Srednekolymsk averaged over 1927-1964.

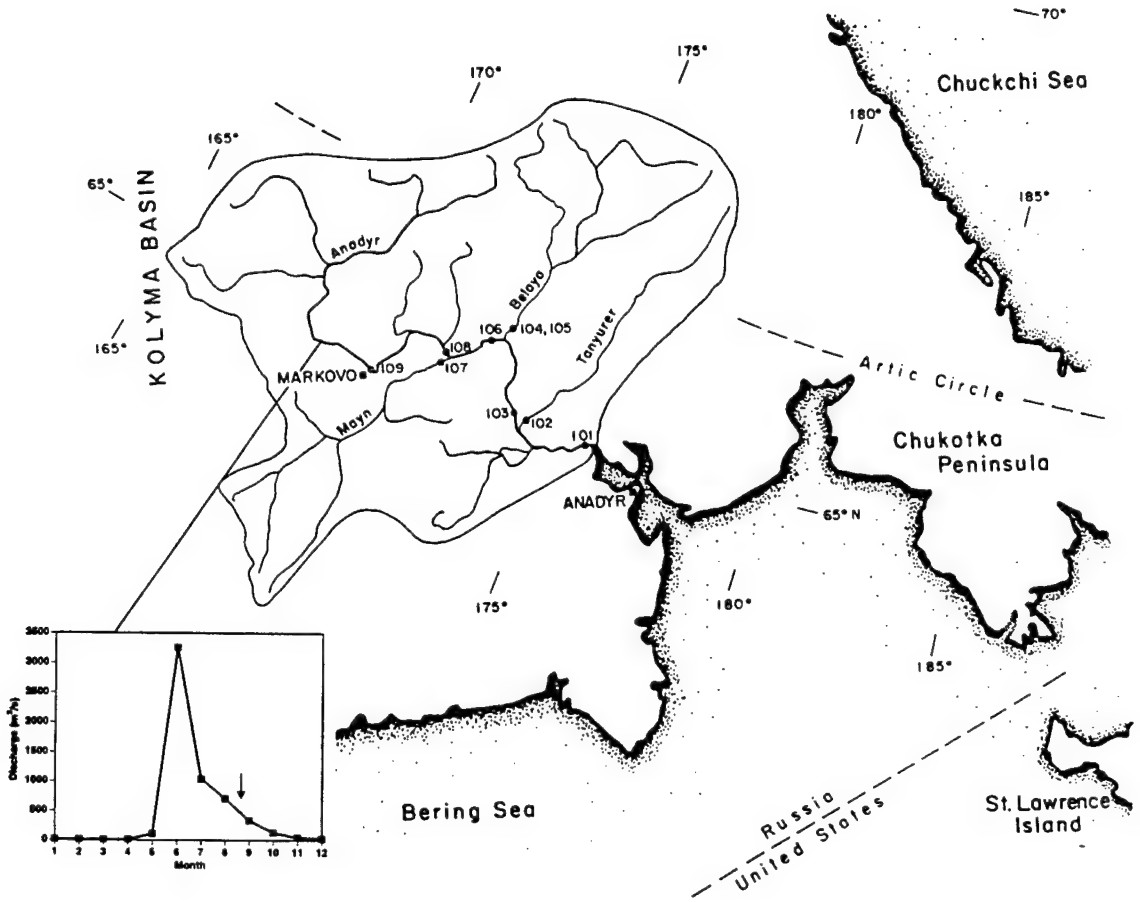

Figure 4. e) The location map of the Anadyr river drainage basin. Discharge data are from Novy Eropol averaged over 1958-1964.

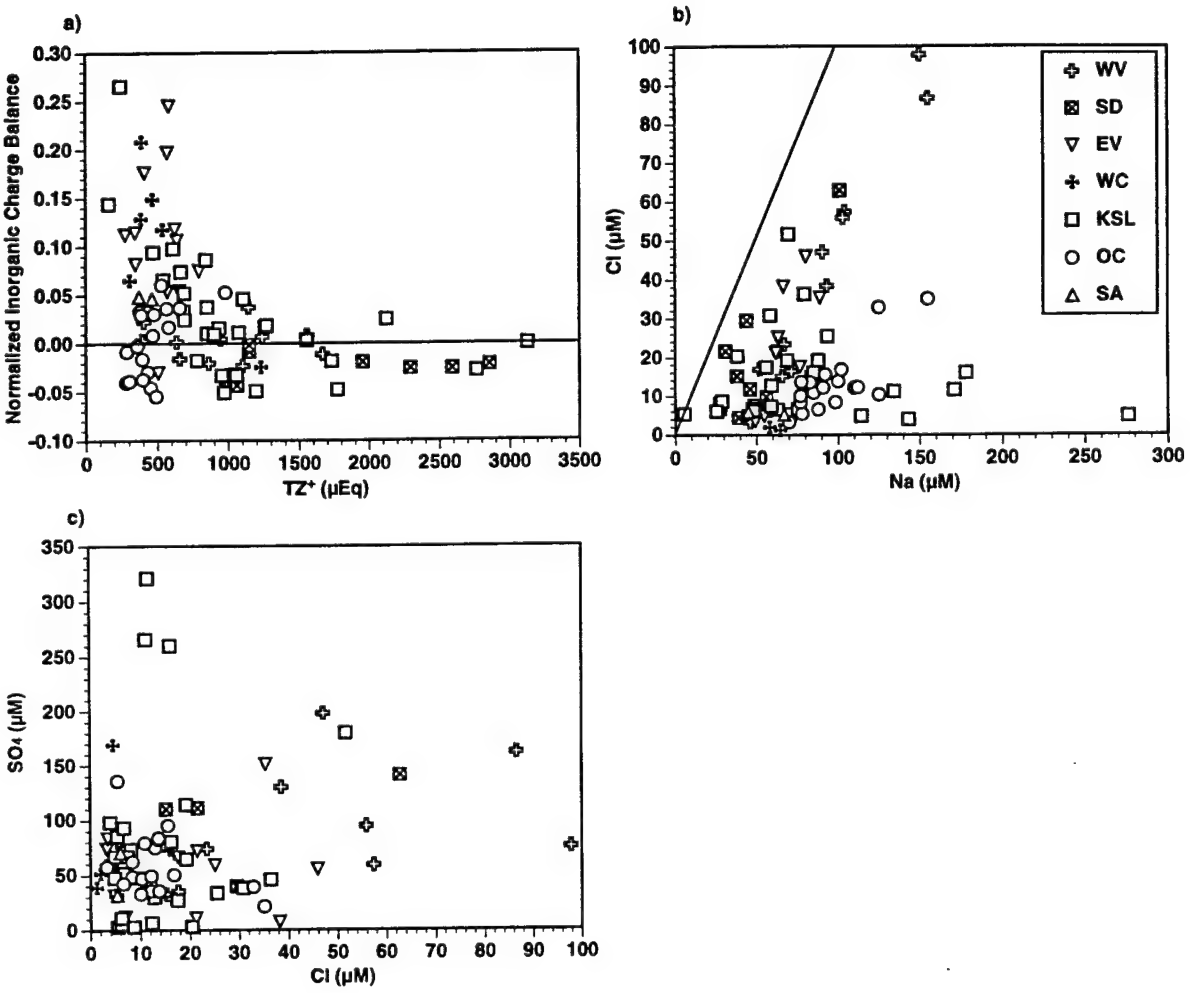

Figure 5. a) The Normalized Inorganic Charge Balance (NICB) vs. total dissolved cations (TZ^+). NICB is defined as $(TZ^+ - TZ^-)/TZ^+$. TZ^+ for the WV tributaries range from 400 to 1,700 µEq. SD have higher values (2,000-2,900 µEq) because of the exposed carbonates; tributaries which only partly drain the carbonates have lower values (~1,000 µEq). All the Yana tributaries have low values (EV: 300-800, WC 300-500 µEq) except YN115 (1,200 µEq) which drains isolated volcanics. KSL has a large range (160-3,100 µEq) as can be expected from the complex melange of lithological segments. OC tributaries have low TZ^+ (300-980 µEq), and SA is at the lower end (~400 µEq). TZ^+ increases from head to mouth in the main channels. b) There is minor halite as noted by the 1:1 Na:Cl relationship, and the excess Na can be attributed to weathering of Na-feldspars. c) SO_4 vs. Cl.

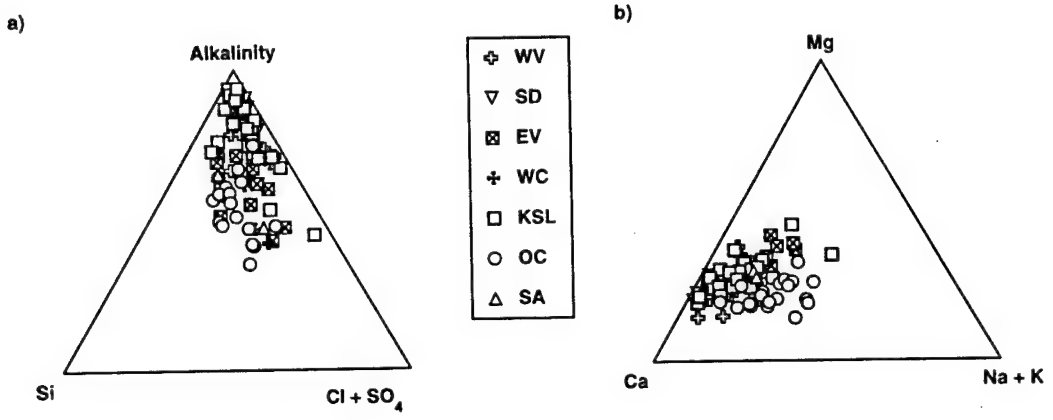

Figure 6. a) Anion ternary diagram. Alkalinity is from limestone and silicate weathering. SO_4 is from gypsum/anhydrite or pyrite weathering. Oxidative weathering of pyrite is unique in the occupation of the interior of the diagram. b) Cation ternary diagram. Ca and Mg are dominantly from carbonate weathering but also from Ca-feldspars and only to a small extent, pyroxenes. (Na+K) comes mainly from evaporites, Na-feldspars and to a lesser extent K-feldspars.

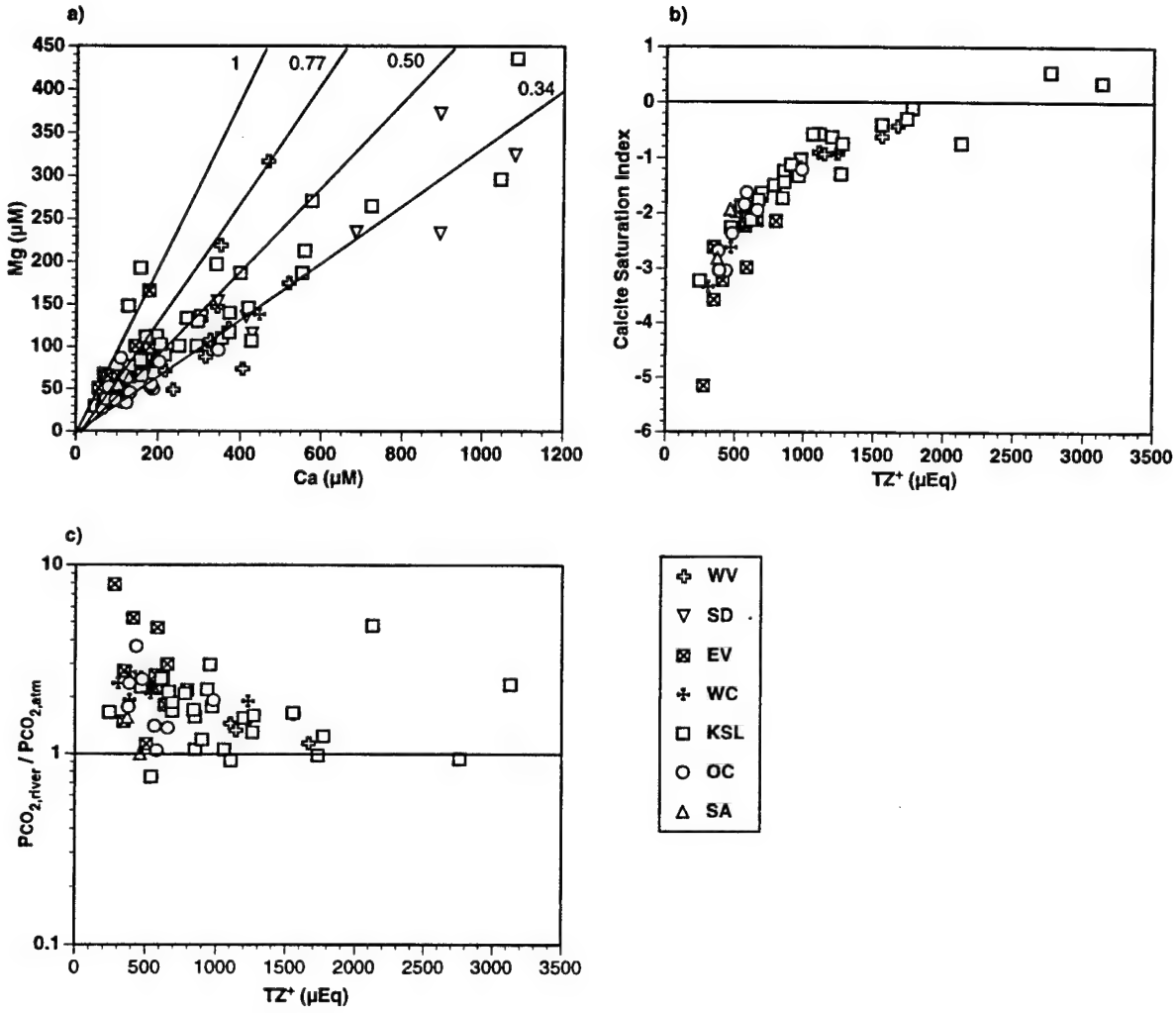

Figure 7. a) The Ca vs. Mg plot. The lines and numbers are Mg/Ca molar ratios. Weathering of average igneous rocks to kaolinite yields Mg/Ca ratios as follows: syenite 0.34; granite 0.50; diorite 0.51; tholeiite 0.77. b) Calcite Saturation Index is defined as $CSI = \log (\{Ca^{2+}\} \cdot \{CO_3^{2-}\} / K_{sp,calcite})$, where {} denotes activity. It is calculated using MINEQL+ ver. 3.01, a program for chemical equilibrium calculations (Westall *et al.*, 1976). CSI = 0 is saturation, CSI < 0 is undersaturation, and CSI > 0 is supersaturation. The temperature of the river water was assumed to be 10°C. Based on the field measurement of temperature on the Anadyr (8.7-16.9°C; avg=11.4°C), this is a reasonable assumption. SD samples are not shown due to lack of pH data. c) PCO_2(river) / PCO_2(atm) vs. TZ^+. $pK_H = -\log [H_2CO_3^* / PCO_2] = 1.27$ (Stumm and Morgan , 1995). PCO_2 (atm) is assumed to be 330 μatm.

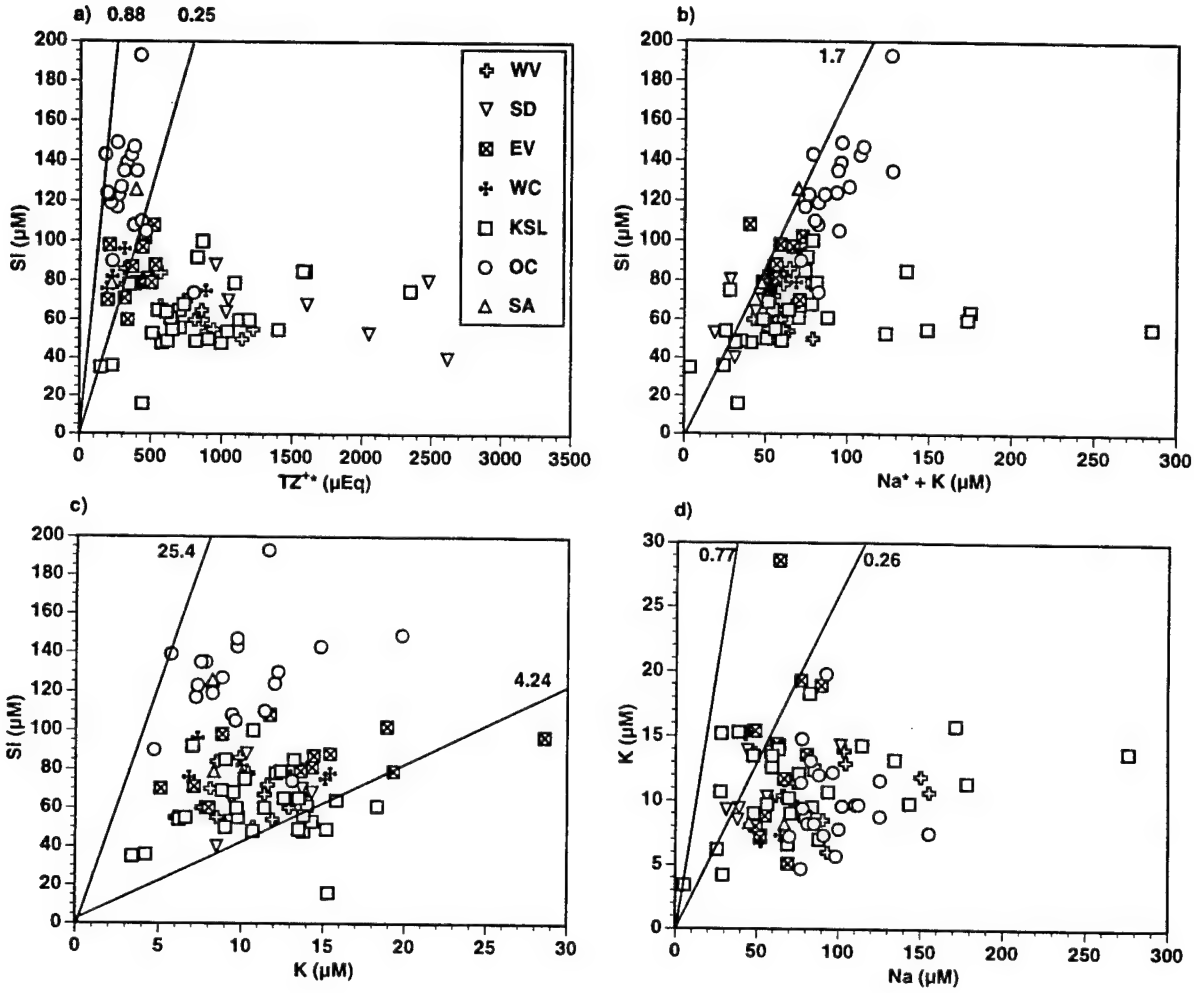

Figure 8. a) A plot of silica (µM) vs. TZ^{+*}(= TZ^{+} - Cl - $2SO_4$ in µEq). The lines and numbers indicate Si/TZ^{+*} ratios. Weathering of average igneous rocks to kaolinite yields Si/TZ^{+} ratios as follows: syenite 1.08, granite 2.32, diorite 1.15, and tholeiite 0.75. b) The relationship between Si and (Na*+K = Na - Cl + K). Weathering of average igneous rocks to kaolinite yields Si/(Na*+K) ratios as follows: syenite 3.41, granite 3.29, diorite 2.36, and tholeiite 5.17. c) The Si vs. K plot. Weathering of average igneous rocks to kaolinite yields Si/K ratios as follows: syenite 4.24, granite 7.72, diorite 7.28, and tholeiite 25.4. d) The K vs. Na plot. Weathering of average igneous rocks to kaolinite yields K/Na ratios as follows: syenite 0.45; granite 0.77; diorite 0.48; tholeiite 0.26.

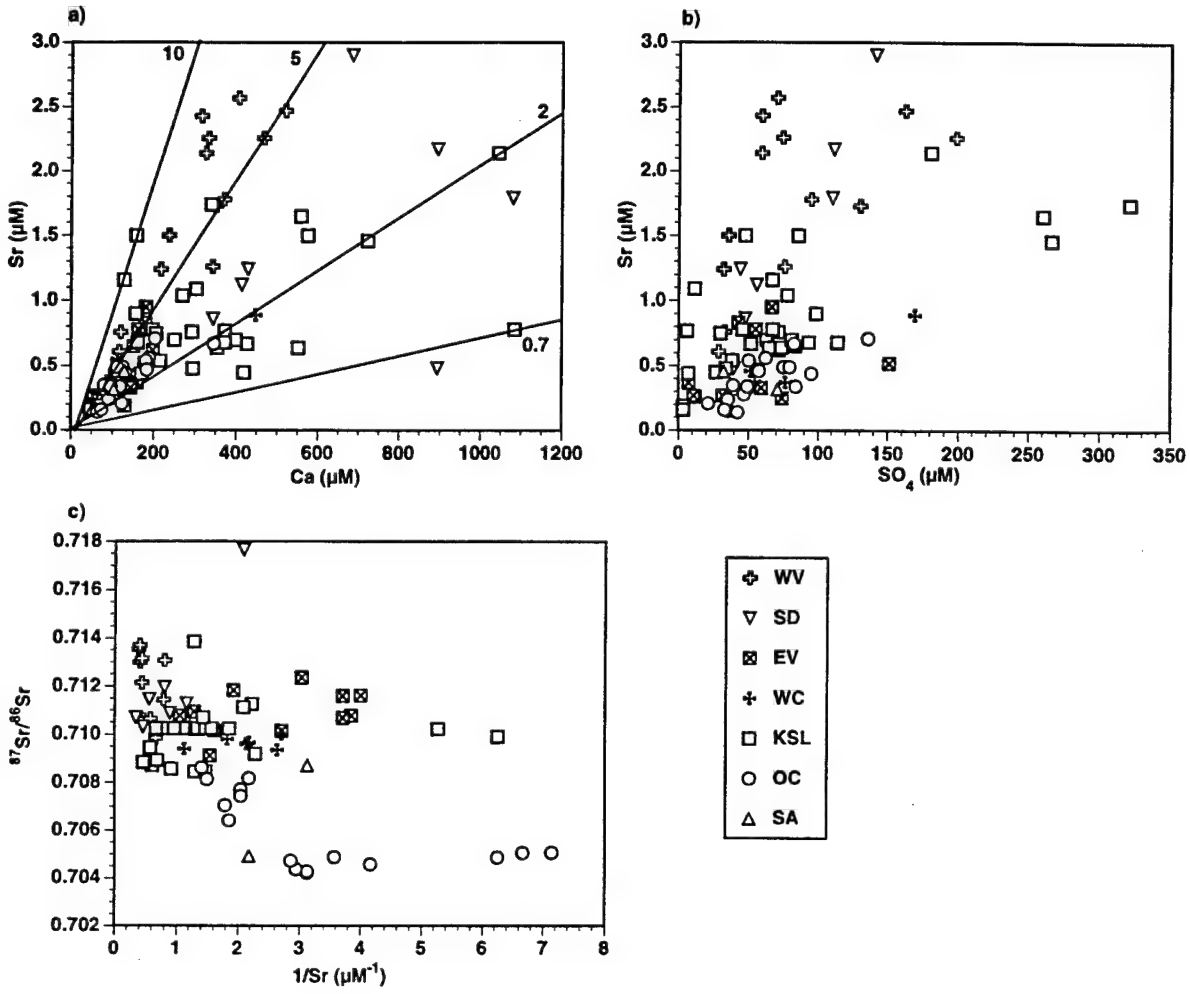

Figure 9. a) The relationship between Sr and Ca. Different lines and numbers indicate different Sr/Ca ratios in nmol/μmol in homogeneous watersheds draining single rock-type areas (Meybeck, 1986): carbonates including marble and carbonate sandstone = 0.7; plutonic rocks, gneiss and mica schist, shale and sandstone = 5; other metamorphics and volcanics = 6; evaporites (gypsum) = 10. b) Sr vs. SO_4. c) A plot of $^{87}Sr/^{86}Sr$ vs. 1/Sr. WV samples range between 0.710 and 0.714 with relatively high Sr concentrations (0.61-2.6 μM). SD varies between 0.710 and 0.712 except for the very radiogenic small stream (UL108; 0.7176). EV shows carbonate and silicate mixing in the range of 0.709 to 0.712. WC has a relatively constant ratio of ~0.7095 to high Ca concentrations (87-450 μM). In the KSL category, the Indigirka tributaries have constant ratios of ~0.710. The Kolyma samples have constant ratios at ~0.7085 with varying Sr concentrations (0.44-2.1 μM). OC and AZ samples are very unradiogenic (<0.7085) as is expected from the lithology.

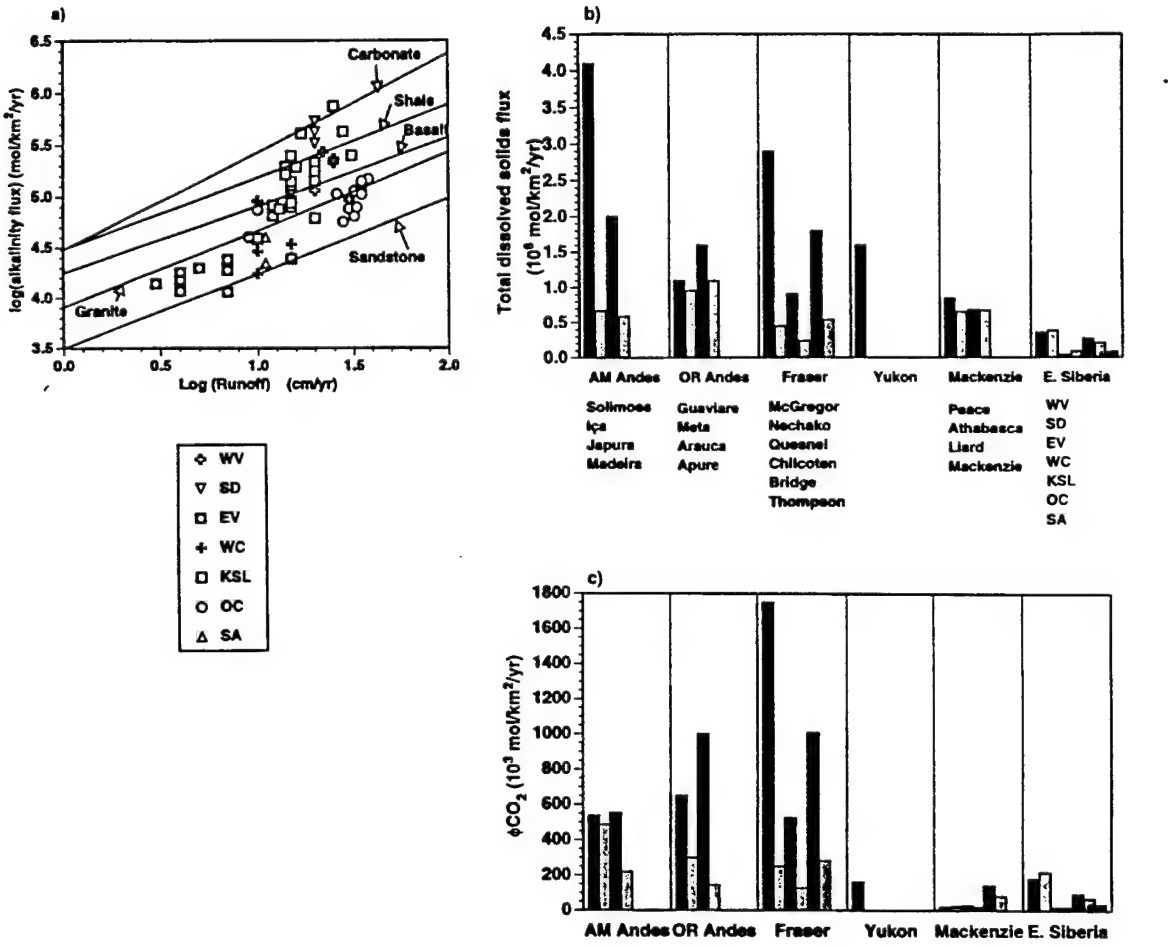

Fig. 10 a) The alkalinity flux vs. runoff. The guidelines for carbonate, shale, granite, basalt and sandstone are best fits to data from world rivers compiled for respective geological regions (Bluth and Kump, 1994). b) Areal total dissolved solids flux for rivers in orogenic zones. The data for other rivers are from Edmond *et al,* 1996. Each bar represents a sub-drainage of the river; the names are listed below. c) $\emptyset CO_2$ for world rivers in orogenic zones.

Chapter 4

The Fluvial Geochemistry of the Rivers of Eastern Siberia III: Tributaries of the Lena and Anabar Draining the Basement Terrain of the Siberian Craton and the Trans-Baikal Highlands*

* Huh Y. and Edmond J. M. (in review) The fluvial geochemistry of the rivers of eastern Siberia III: Tributaries of the Lena and Anabar draining the basement terrain of the Siberian Craton and the Trans-Baikal Highlands. *Geochim. Cosmochim. Acta* submitted, March 1998.

Abstract

The conventional view of the climatic influence on weathering is that the rates are strongly temperature-dependent due to the near-exponential relationship (Clausius-Clapeyron) between temperature and the saturation vapor pressure of water and hence precipitation and runoff. This is a central theme in the Earth thermostat model, i.e. weathering of aluminosilicate rocks on continents acts through accelerated reaction rates as a negative feedback on atmospheric CO_2. However, there is very little direct field evidence to support this hypothesis. To remedy the lack of systematic geochemical data for cold high latitude rivers as compared to the tropics, we have looked at the large, pristine drainages of eastern Siberia. Here, data from basement terrains of the Siberian Craton are reported. The chemical composition, low Si to total cation ratios and relatively unradiogenic Sr isotope values, suggests a superficially weathered system. The total dissolved solids (TDS) flux of 0.39×10^6 mol/km^2/yr and the CO_2 uptake flux of 149×10^3 mol/km^2/yr are similar to those of the tropical cratonic systems and the collisional/accretionary zone of northeastern Siberia, but about a factor of 3 lower than for the orogenic zones of the Western Americas at both low and high latitudes. The lack of systematic climatic effect on TDS and CO_2 fluxes can be ascribed to the unique non-glacial frost shattering processes which continuously expose fresh rock surfaces and thus overcome the effect of temperature inhibition on high-latitude shields and to the lateritic cover that seals in the weathering front away from the weathering agents on the tropical shields. There appear to be no primary climatic effects on weathering rates on the present Earth.

Introduction

Isotopic and paleontological evidence indicate that the Earth's climate has deteriorated from the Early Eocene to the Plio-Pleistocene, at times very rapidly (Savin, 1977; Zachos *et al.*, 1994). Deep water temperature recorded by the $\delta^{18}O$ of benthic foraminifera has dropped by about 12-15°C over that time interval (Miller *et al.*, 1987). The decrease of the atmospheric greenhouse gas CO_2 is almost certainly responsible for this cooling (Kasting, 1987); however, the governing mechanisms on the atmospheric CO_2 cycle over geologic timescales are not well understood. Sources of CO_2 to the atmosphere are primary volcanic outputs from the mantle, which are relatively constant over time, and continental metamorphism which occurs more randomly; the net sink is the continental weathering of aluminosilicate rocks which takes up CO_2 and fixes it as bicarbonate. The imbalance between these sources and sinks causes climate change at multi-million year timescales; however over its lifetime the Earth has maintained an approximate balance between the two such that the Earth's atmosphere was not lost like that of Mars or did not evolve like that of Venus. The "thermostat hypothesis" originally posed by Walker *et al.* (1981), that the temperature dependence of the weathering of aluminosilicate rocks act as a negative feedback on PCO_2, is intuitively elegant and has gained much consensus (Berner *et al.*, 1983; Berner, 1991, 1994). For valid model simulations of the evolution of atmospheric PCO_2, an understanding of the relationship between lithology, relief, greenhouse temperature and weathering rates is required. This can be achieved by exploiting the present gradient of environment with latitude.

Several factors complicate the endeavor to extract CO_2 uptake information from river data. Anthropogenic perturbations, e.g. farming and clear-cutting of forests, can greatly accelerate mechanical weathering (Gong and Xu, 1987; Meade, 1969); dams and reservoirs act as artificial storehouses for the suspended load (Trimble, 1975). The dissolved load can be affected by application of salts for agricultural or urban anthropogenic uses (Meade, 1969; Yang *et al.*, 1995). Small rivers have unstable hydrographs, so rare, undersampled storm events can dominate the sediment transport.

Glaciated areas have an overburden of easily erodible morainic debris which can be mistaken for high primary mechanical weathering rates. Sediment storage in floodplains adds complexity to data interpretation by increasing the reaction time, which can have quite significant consequences for igneous and metamorphic rocks transported by glacial erosion (Meade, 1988; Robinson and Johnsson, 1997). The geomorphology of many river basins take the form of exposed basement on the peripheries and sedimentary platform cover in the center along the main channel, hindering access to the headwaters draining the basement rocks in pristine areas. To date, the Brazilian and Guayana shields drained by the Amazon and Orinoco (Stallard and Edmond, 1983; Edmond *et al.*, 1995) and the northern Congo Shield drained by the Congo (Négrel *et al.*, 1993) have been studied in the tropics. In the high latitudes, the pioneering study of the Mackenzie lacked samples from the Canadian Shield due to logistical problems (Reeder *et al.*, 1972). The St. Lawrence, whose left bank tributaries drain the Canadian Shield, has been studied but is anthropogenically disturbed (Yang *et al.*, 1995). Some work has been done on the Baltic rivers, but they are impounded by dams and affected by the overburden from the Wischelian glaciation (Andersson *et al.*, 1994). In these respects, the large rivers of eastern Siberia (Fig. 1) are pristine, not glaciated in the recent past or at present except for some small alpine glaciers (Velichko and Faustova, 1991), and have a diversity of geological terrains that can be compared to the tropical counterparts. This is the third paper in a series reporting and discussing the fluvial chemistry of the rivers of eastern Siberia. Here, we address the chemical weathering of basement terrains in high latitudes. The previous two dealt with chemical weathering on the sedimentary platform in the Lena basin (Huh *et al.*, 1998a) and the collisional/accretionary zones to the east (Huh *et al.*, 1998b).

Geology

The Siberian craton occupies a vast area surrounded on all sides by Phanerozoic foldbelts. The Yenisey valley lies to the west, the Mesozoic Verkhoyansk and Mongol-Okhotsk orogenic belts to the east and southeast, the Taymyr foldbelt to the north and the Central Asia Paleozoic orogenic terrains to the south (Fig. 2; Rundqvist and Mitrofanov, 1993; Rosen *et al.*, 1994). The Precambrian basement of the craton crops out at the surface in the north (Anabar Shield), in the south-east (Aldan-Stanovoy Shield), and in the south-west (Yenisey, Sharyshalgay uplifts and Baikal-Patom foldbelt). In the rest of the territory the basement is hidden beneath a thick sedimentary cover.

The Aldan-Stanovoy Shield is divided into two provinces by the Kalar fault—the Aldan Shield proper and the Stanovoy province, and these are further partitioned into different blocks by deep faults as surmised from geophysical observations (gravity field gradients, magnetic anomalies, seismic data) and confirmed by geological field work (Fig. 2; Rosen *et al.*, 1994). The two main complexes on the shield are older granulitic granitic-gneissic basement and younger greenstone belts (Moralev, 1981; Windley and Bridgewater, 1971). The Olekma and Central Aldan blocks belong to the granite-greenstone terrain, the Uchur, Batomga, Sutam, Mogocha and Tynda blocks to the granulite-greenstone terrain (Fig. 2; Rundqvist and Mitrofanov, 1993). Archean gray gneisses which make up $\geq$ 95% of the granite-gneiss basement are quartz and sodic plagioclase-rich and K-feldspar poor and plot in the tonalitic field on the Quartz—Alkali-feldspar—Plagioclase modal diagram (Martin 1994; Streckeisen, 1976). The belts of supracrustal rocks are divided into two groups: 1) large volumes of mafic-ultramafic volcanic rocks that have been metamorphosed to intermediate, andalusite-sillimanite grade (T~560°C, P~4 kbar; Dook *et al.*, 1989) and 2) abundant clastic and carbonate rocks that have experienced higher-grade, kyanite-sillimanite facies metamorphism (T~600°C, P~5-6 kbar; Dook *et al.*, 1989). Anorthosites and gabbros are found in the Stanovoy province (Nutman *et al.*, 1992; Rosen *et al.*, 1994). Enderbites and metasediments of the Central Aldan block are 3.5-3.3 Ga.; enderbites and mafic granulites on Uchur and Tynda blocks

are dated 3.5-2.7 Ga.; and the TTG-greenstone complex of the Olekma, Batomga and Mogocha blocks are dated 3.3-2.8 Ga. (Morozova *et al.*, 1989; Nutman *et al.*, 1992). The crust-forming processes are thought to have ended over most of the shield by the Late Archean, i.e. by 2,500 ± 100 Ma., and Early Proterozoic effects are restricted locally to suture zones and did not alter the overall structure of the region, although they had a substantial effect on the closure time of isotopic systems. Isotopically dated thermotectonic reworking occurred in the interval 1.7-2.2 Ga., e.g. the intensely deformed enderbites and mafic granulites on the Sutam block dated at 1.9 Ga. (Gluchovsky *et al.*, 1993).

Three provinces are exposed on the Anabar Shield—enderbites and charnockites in the west and enderbites and mafic granulites in the middle, both of 3.1-3.0 Ga. age (Rosen *et al.*, 1994; Bibikova and Williams, 1990). The eastern side is chiefly metagraywackes and marbles of 2.4-2.0 Ga. Anorthosites of 2.1 Ga. are found in the shear zones between the three blocks. A Riphean rifting event resulted in deposition of continental platform sediments, clastics and carbonates with rare volcanic layers of basaltic composition and gabbro and diabase dikes. A new phase of magmatic activity resumed in the Mesozoic as seen in dolerite and kimberlite dikes (Rundqvist and Mitrofanov, 1993).

The Baikal-Patom foldbelt occupies the area from the west of Lake Baikal to the Vitim river basin (Fig. 2). It was formed by the accretion of arc systems to the southwestern margin of the Siberian craton beginning in the Late Riphean and continuing into the mid-Paleozoic. In the Devonian, the Barguzin terrain composed of Paleozoic and Late Proterozoic rocks was thrust onto the southern margin of the craton (Rosen *et al.*, 1994). The intense internal processes of the lower Proterozoic are expressed in the terrigenous and volcanic complexes of the Baikal-Patom foldbelt. In the region around the Mama, a tributary of the Vitim, there are significant deposits of pyrite-polymetallic ore (Rundqvist and Mitrofanov, 1993). We will call the area of Baikal-Patom foldbelt and the Barguzin terrain aggregately as the Trans-Baikal Highlands (TBH).

Riphean sediments occupy the periphery of the Baikal-Patom belt and the Anabar and Aldan Shields (Huh *et al.*, 1998a).

Location

The right bank tributaries of the Upper Lena drain the basement terrains on the southern rim (Fig. 3). The headwater tributaries of the Lena and the Vitim drain the TBH; the Olekma and the headwater and right bank tributaries of the Aldan drain the Aldan-Stanovoy Shield. The Anabar river in the north drains the Anabar Shield. The drainage areas and discharges of the more significant tributaries are given in Table 2. The Baikal mountains have the highest elevations in the region reaching up to ~3,000 m. On the Aldan-Stanovoy Shield the elevations are somewhat lower at ~2,000 m.

The Lena rises on the western slope of the Baikal rift mountains at an altitude of ~1,400 m. In the upper section the banks are high and the valley is very narrow. Below the confluence with the Vitim the volume of water in the channel increases noticeably and islands begin to appear scattered along its course. The valley opens up and the slopes are much lower by the time it joins with Olekma (Alabyan *et al.*, 1995). Once the river comes together with the Aldan, the valley is a broad plain, much of it swampy and filled with lakes. Finally the river course narrows once again when the Verkhoyansk range converges on the channel before branching out into a large delta. The Lena is navigable for 3,940 km of its 4,828 km length in June-October. The Aldan rises in the western portion of the Aldan Shield and runs north and east through a narrow valley on the margin of the shield; total length is 2,843 km. The chief tributaries, the Timpton and part of the Maya, drain the shield. As the valley broadens out, the river is utilized extensively for navigation in support of mining of gold, mica, and coal deposits. The river is frozen solid from mid-October to May but is navigable during the remainder of the year as far as 1,610 km from the mouth. The Vitim rises on the TBH and has a length of 1,821 km and is navigable for

250 km above the confluence. The Anabar is ~900 km long and flows north to the Laptev Sea in the Arctic Ocean; it is navigable for 150 km.

Climate, Soil and Vegetation

Overall the climate is extremely continental. The seasonal difference in air temperature is large; the average in January on the Aldan Shield is ~-29°C and ~-40°C on the Anabar Shield; the valleys are a few degrees colder. July air temperatures are 14°C and 12°C, respectively; high peaks are a few degrees colder. Diurnal variation is only ~2° in winter but ~10° in summer. Annual precipitation varies from ~400 mm on the lower reaches of the rivers to ~600 mm on the Aldan Shield to ~800 mm on the Baikal mountains. Less than 20% of the precipitation occurs in winter; the maximum occurs in the summer months of July and August, hence the lack of glaciation. Annual evapotranspiration is virtually zero in winter but up to ~60% of precipitation in summer (UNESCO, 1977a).

The river discharge is thus highly seasonal (Figs. 3, 4). Significant flow is restricted to the summer months with highest flow and turbidity during the snow and ice melt in May-June. Northern rivers like the Anabar freeze to the bottom in winter, whereas southern rivers have some flow under the ice. After a mid-summer low, there is a rainy season with a lesser amplitude runoff. Geographically, the discharge pattern follows closely the precipitation pattern with highest annual runoff north of Lake Baikal (up to 800 mm) and in the headwaters of the Aldan where the wet air masses from the Sea of Okhotsk slide in (~400 mm) (UNESCO, 1977a). The rest of the area averages ~250 mm.

The region is in the boreal forest zone. Spruce grow in river valleys, pines on sandy soils, and larch pine and light-needled species in the middle of the taiga. On the TBH and Aldan Shield, fir (*Abies sibirica*), pines (*Pinus sibirica*, *Pinus pumila*, and *Pinus sylvestris*), and aspens (*Populus tremula*) make up the dark taiga forest. Throughout the shield region, including the Anabar, are larch trees (*Larix gmelinii*) and spruce (*Picea*

obovata) (Nikolov and Helmisaari, 1992). Many of the species have good tolerance for peat bogs and permafrost. The soil in the region is lithic and mostly a combination of lithosols, gelic cambisols, and dystric podzoluvisols (UNESCO, 1977b).

During the Holocene optimum (4,600-6,000 BP) it was warmer (1-3°C) and moister (50-100 mm) in Siberia. Dark needled taiga expanded to northern and eastern Siberia, and the phytomass and net primary productivity were greater than at present (Monserud *et al.*, 1993, 1995). Future global warming is predicted to lead to wetter and milder climates with enhancement at high latitudes (Cuffey *et al.*, 1995; Thompson *et al.*, 1995).

Sampling and Analytical Methods

Sampling expeditions were made in July-August of 1991-1997 to the Aldan (UL100), Upper Lena (UL400), and Upper Aldan (UL800) (Fig. 3). All significant tributaries (~90 stations) were sampled for major and trace dissolved elements and for suspended and bed material. The dissolved chemical data are reported in Table 1. Sample collection, preservation and analyses methods are described in Huh *et al.* (1998 a,b). "Grab" samples were collected from streams draining into Lake Baikal (LB100) in 1993 and on the Olekma (UL300) and Anabar (UL500) rivers in 1994 and 1995. Field blanks which were processed with the other samples produced levels below detection limits for the major species reported here.

Results

The dataset is subdivided into 4 groups—rivers draining the TBH, the Aldan Shield, the Anabar Shield, and one warm spring (labeled "hot spring" in figures) from the right bank of Lake Baikal (Table 1, Fig.3). First, the chemical compositions (major

elements and $^{87}Sr/^{86}Sr$) will be examined to diagnose the weathering pattern; then the fluxes will be calculated. The format will be based on a comparison of each weathering parameter in different geologic terrains (sedimentary platform, collision/accretionary zone, craton basement) within the eastern Siberia river systems so as to explore the effect of geology on weathering at these latitudes. This analysis will then be extended to similar terrains in the tropics, i.e. the Guayana and the Congo shields, and in mid-latitudes, the Canadian Shield.

Overall chemical composition

The total cationic charge (TZ^+) ranges to 6,000 μEq for the hot spring sample; most values are below 1,000 μEq (Fig. 5a). The tributaries flowing partly through the Vendian carbonates and evaporites in the lower reaches have higher TZ^+, e.g. Chaya (UL416), M. Patom (UL435, 714), Olekma (UL510, 515), Jelinda (UL115), and Kuranakh (UL803, 807). They were included in the basement dataset because the greater part of their headwaters are in the shield (Fig. 3) as evidenced by the radiogenic $^{87}Sr/^{86}Sr$ (to be discussed later). The supracrustal carbonates on the shields are only local and have undergone extensive metamorphism (Dook *et al.*, 1989); the contribution from this source is limited. TZ^+ is significantly lower than in the rivers of the Siberian Platform (Huh *et al.*, 1998a), in the range of those draining the collisional/accretionary zone of the Russian Far East (Huh *et al.*, 1998b), but the most dilute streams (<200 μEq) are unique to the basement. The Orinoco has 40-600 μEq with the bulk less than 100 μEq (Edmond *et al.*, 1995), the Congo 200-600 μEq (Négrel *et al.*, 1993; Dupré *et al.*, 1996), St. Lawrence 265-1,025 μEq (Yang *et al.*, 1996), and the Baltic rivers 448-919 μEq (Andersson *et al.*, 1994); the world average is 1,200 μEq (Meybeck, 1979). Certainly the rivers of shield regions worldwide have some of the lowest dissolved loads but within a quite restricted range. For the streams studied here there is no significant charge imbalance among the measured inorganic ions that can be attributed to the presence of organic acids (Fig. 5a).

There is now quite a large database encompassing all latitudes indicating that rivers with considerable amounts of organic material show a deficit of anionic charge (up to NICB ~1; Lewis *et al.*, 1987; Négrel *et al.*, 1993; Edmond *et al.*, 1995; Gíslason *et al.*, 1996; Huh *et al.*, 1998b).

The portion of atmospheric input derived from outside the basin should be subtracted. Solutes derived from terrestrial dust or burning of vegetation are considered as true components of chemical denudation generated within the watershed. The rain and snow data (from 1960s) quoted in Gordeev and Sidorov (1993) give Cl concentrations of 39 μM in rain and 85 μM in snow in the upper reaches of the Lena and 37 μM and 65 μM in the middle reaches. Though these values are much higher than in the tropics (5-26 μM total fallout, Lewis *et al.*, 1987), if they are valid then most of the Cl in the rivers are from marine aerosols; however the correction for elements other than Na and Mg are minor (Fig. 5b; Edmond *et al.*, 1995). In this paper, the data in the tables and figures are not corrected for seasalt or other atmospheric inputs.

The lower limit of Na is defined by the Cl level in the rivers indicating marine aerosol or halite origin (Fig. 5b). Salt deposits of Lower Cambrian extend from the upper reaches of the Angara along the whole length of the Lena to the Vilyui river basin (Lefond, 1969), and the evaporite influence is more visible here, e.g. UL416, 421, 434. The Olekma and Chara (UL438, 711, 437, 710) also have an evaporitic contribution that they seem to acquire in the area adjacent to the shield/platform contact. The Na:Cl trend is slightly offset to higher Na; generally Na exhibits an excess over Cl, indicative of Na-silicate weathering.

Sulfate does not show any correlation with Cl (Fig. 5c) which is as anticipated in light of the recent finding that the NaCl in gypsum or anhydrite is in fluid inclusions and not in the lattice (Lu *et al.*, 1997). It is interesting to note that the bulk of the rivers have higher SO_4 than Cl. Only the Chaya (UL416), Kutima (UL414) and the Olekma and Chara mouth samples have higher Cl. However, compositions of the Olekma and Chara are

highly variable (e.g. UL515 is SO_4-dominant) and we do not have enough tributary samples to understand this. The Congo on the other hand has slightly higher Cl relative to SO_4 (Négrel *et al.*, 1993). Some St. Lawrence tributaries have very high Cl (200-300 μM) with low SO_4 (~40 μM) almost certainly from road salts (Yang *et al.*, 1996). The SO_4 can come from either gypsum/anhydrite dissolution or oxidative weathering of pyrite. In the first case, if halite and gypsum/anhydrite all dissolve rapidly at about the same rate, the dominance of SO_4 indicates that the platform fringing the Aldan Shield has more sulfate salts (Huh *et al.*, 1998a). As the Baikal Rift extends parallel to the Lena main channel north of Lake Baikal to the mid-Olekma river (Logatchev, 1993), the volcanic rocks and the riftogenic sediments could also be the source of high sulfide-derived sulfate concentrations. The sulfur concentrations in the volcanic rocks, though, rarely exceed 200 ppm due to loss during eruption and outgassing (Kuznetsova *et al.*, 1996). These two possibilities will be explored further below.

The overall compositional relationships observable in the anion ternary diagram are more siliceous than in the platform or orogenic rivers (Fig. 6a; Huh *et al.*, 1998a,b). The tributaries draining the vast carbonate and evaporite platform extend along the alkalinity-($Cl+SO_4$) axis; the collision zone rivers have values occupying the upper half of the diagram but with less Si. The St. Lawrence has a more evaporitic composition, along the lower right. Anion ternary diagrams for tropical shield rivers are not meaningful because of the presence of organic anions with negative "alkalinity" in extreme cases. On the cation ternary diagram, the TBH is distinctly more calcic, and the Aldan and Anabar are more magnesian (Fig. 6b). The St. Lawrence and the Baltic rivers are more calcic, similar to TBH; the Congo is slightly more magnesian. The Orinoco has a unique pattern plotting near the (Na+K) apex and follows the igneous rock trend to the middle of the triangle. Unlike the Siberian rivers, this trend is not due to evaporite dissolution but to complete weathering of basement rocks (Edmond *et al.*, 1995).

Several features of individual tributaries can be surmised from a comparison of the two ternary diagrams (Fig. 6a,b). The hot spring has a very distinct evaporitic composition, dominantly NaCl but also significant $NaHCO_3$. The two evaporitic rivers (UL414, 416) are also immediately visible. The issue of whether the SO_4 is inherited from evaporites or sulfides can be examined with the anion ternary diagram; sulfide oxidation occupies the middle as the SO_4 generated further weathers the neighboring silicate minerals and lowers the alkalinity. What emerges from Figs. 5c and 6a is that the many rivers have pyrite oxidation but the SO_4 released is small; the high (>~150 μM) SO_4 is mainly from evaporites, e.g. Chaya (UL416), Kutima (UL414), Patom (UL434, 715, 435, 714), Chuya (UL421), etc. The rest of the samples cluster in the upper center of the anion and lower left of the cation diagrams and drain exclusively aluminosilicate rocks. Depending on the degree of differentiation of the basement rocks, the rivers have varying proportions of Mg and Ca; overall they are enriched in Ca (Fig. 6b). The olivines and pyroxenes from the volcanic rocks of the Baikal rift and the greenstone belts of the Aldan Shield are expected to have higher proportions of Mg whereas differentiated rocks have higher Ca. This is perhaps most clear on the Guayana Shield where the Aro basin dominated by primitive greenstones has Mg/Ca ratios ~1 whereas the extremely fractionated Parguaza batholith has a value of ~0.25. The magnesian nature of the Aldan and Anabar samples are as expected from the prevalence of greenstone belts (Rundqvist and Mitrofanov, 1993). The TBH samples are calcic because the volcanic rocks are localized on the Vitim Plateau and the Udokan Ridge in between the Vitim and Olekma rivers.

For tributaries where pH data are available, the calcite saturation index (CSI) and PCO_2 levels can be calculated. The pH ranges from 6.61-8.27 (Table 1), slightly more acidic than the platform or orogenic zone rivers of Siberia but less so than the tropical rivers (pH 4.5-7) (Huh *et al.*, 1998a,b; Edmond *et al.*, 1995). The temperatures were measured only for UL100 series samples; the average is 15.4°C (n=11) and the mode is at 14.3°C. 15°C was used for all calculations. For CSI different temperature assumptions have little

effect, <0.1 unit more saturated at 20°C and <0.1 unit less saturated at 10°C (Fig. 7a). For PCO_2, there is more dependence on temperature especially for the highly saturated rivers (Fig. 7b). At 20°C there can be up to 3 times more supersaturation and up to 2.5 times less at 10°C. For our discussion this is not critical. Only the high TZ^+, sulfate-rich M. Patom (UL435, 714) and carbonate-rich Kuranakh (UL803, 807) have CSI>0 (Fig. 7a). Other high TZ^+ and gypsum/anhydrite rivers are close to saturation (CSI>-1; Chuya, UL421; B. Patom, UL434, 715; Chara UL437, 710). The CSI shows a general increase with TZ^+, indicating that Ca is the dominant cation. The rivers are all supersaturated with CO_2 relative to the atmosphere, up to ~20 times in low TZ^+ Vitim tributaries draining silicate rocks (Fig. 7b). These equilibria patterns and saturation magnitudes are similar to those of the platform and orogenic rivers of eastern Siberia. Only the floodplain rivers of the Amazon are reported to have high (up to 100 times PCO_2) supersaturation (Stallard and Edmond, 1987).

Perhaps the most direct evidence of silicate rock weathering are the levels of Si, though here too there are caveats. The silica concentrations range from 16 μM on the Anabar Shield to 300 in a small tributary draining into Lake Baikal (LB108) and 1,400 μM in the hot spring. The majority of samples have levels of ~100 μM (Fig. 8), higher than the platform rivers (most 20-90 μM). We attributed the low silica levels in the Siberian rivers studied previously to biogenic uptake in thermokarst lakes and bogs. This situation is not so conspicuous in the shield rivers. The estimated percentage of drainage basin occupied by lakes is 0.1 - 0.3% in the Upper Lena basin except for the Vitim where it is 0.6% and up to 1.1% for a tributary to Vitim. The average for the whole of the Lena is 0.7% (Chalova *et al.*, 1995) suggesting that the northern environments with their large flood plains have more lakes. The low Si values of the Anabar Shield may be due to this effect. The St. Lawrence and the Baltic rivers have similar ranges of Si concentrations (50-100 μM), but the Orinoco and the Congo have significantly higher values (over 200 μM).

Information on the intensity of weathering can be derived from the Si to cation ratios. The Si/TZ^+* ratios ($TZ^+* = TZ^+ - Cl^- - 2SO_4^{2-}$; the evaporite correction) are lower than for average shield weathering to kaolinite (0.78; Stallard, 1980), suggesting superficial weathering (Fig. 8a). $Si/(Na*+K)$ ($Na*+K = Na^+-Cl^-+K^+$; the halite correction) is between the ratios of average shale weathering to kaolinite and average shield weathering to gibbsite, and again indicates superficial weathering (Fig. 8b). The Orinoco shows a tight correlation between Si and TZ^+* or (Na*+K) and is between the kaolinite and gibbsite ratios indicative of complete removal of soluble cations. The few samples from the Congo follow a similar intensive weathering trend; the St. Lawrence and the Baltic rivers are more like those of Siberia.

The rivers are quite sodic (K/Na ~0.15; Fig. 8c) compared to the Orinoco where K/Na ratios range from 0.3 to 0.8 and up to ~1 for the highly differentiated rocks of the Parguaza batholith. Applying an evaporite correction to Na does not change the relationship significantly. Assuming that all the rivers are draining silicate rocks completely Mg/(Mg+Ca) vs. K/(Na*+K) plots should follow the igneous rock fractionation trend. The Mg-rich basic to K-rich alkaline trend is present but with large scatter (Fig. 8d). In contrast to the intense weathering regime of the Orinoco, there is no indication of further reaction of transported fluvial detritus, which would be evidenced by the development of a positive slope at higher K ratios.

Because the major objective of this study is to quantify the CO_2 uptake rate by weathering of basement rocks in different environments, it is important to distinguish between weathering of aluminosilicate rocks and carbonate dissolution. The latter returns CO_2 upon burial in the ocean as carbonates without significant time lag; only the former acts as a sink for CO_2. As the dissolution kinetics of limestones are orders of magnitude faster than even the most labile aluminosilicate rocks, the dissolved load is usually dominated by carbonates when they are present. Where biogenic removal (e.g. in lakes and bogs) is not substantial, Si is a good index of silicate weathering. The strontium

isotope ratios provide a clearer distinction. The present seawater ratio is 0.7091, average river 0.7111, and hydrothermal solutions 0.7028 (Palmer and Edmond, 1989). Limestones or evaporites have ratios corresponding to the seawater value at the age of deposition, if postdepositional diagenesis can be disregarded. As there is no fractionation in the weathering regime, limestones should have 0.7065-0.709 based on the seawater curve (Brass, 1976; Burke *et al.*, 1982). Aluminosilicate rocks vary in their radiogenic character depending on age and Rb content. They generate low dissolved concentrations of Sr due to their inert nature; recent studies suggest that there may be some fractionation during weathering with radiogenic Sr in biotite being released in the initial stages (Blum and Erel, 1997).

The $^{87}Sr/^{86}Sr$ values in rivers draining the basement range from 0.706 to 0.741 (Fig. 9a) with the exception of two small streams draining the eastern slope of Lake Baikal (0.86). The Sr concentrations are in general lower than in the platform rivers but similar to the collision zone streams (Huh *et al.*, 1998a,b). The $^{87}Sr/^{86}Sr$ ratio reaches up to 0.74 on the Congo; the Orinoco has some of the most radiogenic values reported (> 0.9); the St. Lawrence is ~0.71. The very high ratios of the Orinoco are peculiar to that river owing to the unique basement lithology and are not representative of tropical shields in general. The less radiogenic values of the Siberian rivers compared to the Orinoco, and to a lesser degree the Congo, are partly due to the low intensity of weathering. Unradiogenic, but labile, plagioclase weathering at the expense of radiogenic but inert K-feldspars leads to low ratios, since Rb follows K. It is also quite possible that the metamorphic overprint caused isotopic re-equilibration. The Rb/Sr ratios of Archean gray gneisses are low and highly dependent on metamorphic grade (Martin, 1994). Some granulitic rocks from Scotland and E. Greenland, which underwent similar grade metamorphism as the Siberian shields, are also strongly depleted in Rb, U and Th (Tarney, 1979). Isotopic re-equilibration of the clay-hosted Sr with metamorphic fluids is also possible (Schaltegger *et al.*, 1994). On the Aldan Shield, the measured $^{87}Sr/^{86}Sr$ ratios range from 0.702 in plagioclase to 2.5 in biotite

of the Olekma-Kalarskiy anorthosite massif, but the values are predominantly <0.74 (Vinogradov and Leytes, 1987). The ratios in the riftogenic depression in TBH are 0.705 for trachybasalts, 0.726 for trachydacite, 0.718-0.759 for trachyrhyodacite (Gordienko *et al.*, 1997). Thus, the bedrocks of the Siberian basement are much less radiogenic than those of the Guayana Shield. It is not clear why the two Lake Baikal streams are so radiogenic, but it seems to be a local effect.

Sr shows a general correlation with Ca and SO_4, especially at higher concentrations, indicating the association with gypsum/anhydrite (Fig. 9c,d). Nevertheless, judging from the radiogenic $^{87}Sr/^{86}Sr$ found even for high concentration samples (Fig. 9b), Sr is not totally or stoichiometrically from gypsum/anhydrite. In fact, the waters retain radiogenic $^{87}Sr/^{86}Sr$ characteristics from their basement headwaters. The Sr to Ca ratios are in the range expected from watersheds in plutonic and metamorphic rocks (Meybeck, 1986).

When compared to the values reported in Gordeev and Sidorov (1993), the total cationic charge is similar for the Vitim and about 3 times lower for the Olekma. The cationic ratios differ slightly; e.g. for the Vitim, K/Na = 0.10 (this work = 0.2) and Mg/ca = 0.50 (this work = 0.4); for the Olekma 0.10 (this work = 0.03-0.07) and 0.47 (this work = 0.42-0.46).

Fluxes

Fluxes of total dissolved solids (ϕTDS) were calculated using the chemical composition of one-point sampling in summer, the annual average discharge estimated from the runoff map (UNESCO, 1977a) and the drainage basin area (Table 2; Huh *et al.*, 1998a,b). CO_2 uptake fluxes (ϕCO_2) can be calculated using 2ϕSi when $^{87}Sr/^{86}Sr$ is below 0.71 and $\phi TZ^{+}*$ when $^{87}Sr/^{86}Sr$ is above 0.71 (Edmond and Huh, 1997). This is a minimal estimate as some silicates have low $^{87}Sr/^{86}Sr$, in the range of carbonates

(Vinogradov and Leytes, 1987), yet are net sinks of CO_2. The above strategy was necessary in order to take into account the potential effect of biogenic uptake of Si in lakes. ϕCO_2 values calculated from Si fluxes alone are on average one third lower (Table 2) but this does not affect the general conclusion, given the uncertainties in runoff and the temporal variation of dissolved flux.

The fluxes can be compared to those from other basins draining basement rocks (Fig. 10). The compilations for other rivers are from Edmond and Huh (1997) and are calculated on a tributary scale. As the Siberian rivers have been sampled in far more detail, we have averaged over each geological category, but fluxes for individual rivers are also reported in Table 2. The areal TDS flux ranges from 0.05 to 1.50 x 10^6 mol/km^2/yr, and the CO_2 uptake rates range from 26 to 456 x 10^3 mol/km^2/yr (Table 2). The fluxes are highest on the TBH and lowest on the Anabar shield. This variability is similar in magnitude to or larger than that between rivers in different latitudes (Fig. 10). It may be argued that while at similar latitudes the active margin of the TBH yields higher fluxes than the passive uplift zone of the Aldan Shield, if comparing the similar passive uplift zones of the Aldan and Anabar shields, a difference of 14° latitude there is a temperature dependence. However, the Anabar result is based on only 3 grab samples and, when taken with the uncertainties in runoff, is not drastically different from the Aldan. The ϕTDS and ϕCO_2 are in the same range as those of the collisional/accretionary zones of northeastern Siberia (Huh *et al.*, 1998b). The shield rivers of the world taken together have fluxes about a factor of 3 lower than the rivers of the American Arc (Edmond and Huh, 1997). The lack of such contrast in Siberia is because the collisional/accretionary zone is fundamentally not of the same nature as the American Arc, being older and not presently active except for the Cherskiy seismic belt (Cook *et al.*, 1986; Imaev *et al.*, 1995). Also, a large part of the northern basins are swampy, tundra lowlands. The TBH similarly is not a stable shield terrain but a fringing uplift zone and, although the magnitude can be argued, certainly has higher fluxes than the shields (Fig. 10).

In many denudation data compilations, the relationship that almost always emerges is the strong correlation between runoff and denudation rates, either mechanical or chemical (Dunne, 1978; Pinet and Souriau, 1988; Bluth and Kump, 1994; Summerfield and Hulton, 1994). In the existing river data set for all the shield rivers of the world there is no systematic relationship between fluxes and runoff (Fig. 11a,b). For the Siberian streams alone, there is a positive correlation with runoff (Fig. 11c,d). Thus, it is an important parameter within a watershed, but when comparing two different basins in different environments, is not the sole or the major variable.

The CO_2 uptake rates calculated from dissolved fluvial data are instantaneous weathering fluxes from catchment areas and cannot be directly compared with those from rock data integrated over tens of millions of years or the sediment data affected to varying degrees by the storage effect (Meade, 1988). The suspended sediment fluxes dominate the weathering fluxes but show no correlation with the chemical weathering (Summerfield and Hulton, 1994) . With these caveats in mind, a crude denudation estimate can be made by calculating the lowering of elevation from the fluvial dissolved and suspended sediment data sets assuming a rock density of 2.5 g/cm^3. The averaged suspended load over a multi-year period for the Kirenga and Olekma are below 25 mg/L; for other regions near Lake Baikal or near Yakutsk the values are 25-50 mg/L (Chalova *et al.*, 1995). The suspended material is greatest during spring flood (50-80 mg/L), diminishes during the summer-autumn low (~10mg/L), increases again during the rain flood (10-50 mg/L), and is <5 mg/L in winter. It is similar to or slightly lower than the dissolved flux on per weight basis (D/S = 1~5); in the Orinoco D/S = 0.2~1.1. The calculated denudation rates are 2-6 m/m.y. At one extreme the accumulation rate of oceanic detrital sediments in deep basins away from direct continental input is about 1 m/m.y. Denudation rates from glaciated terrains, on the other extreme, range from 10 m/m.y. on polar glaciers and temperate plateau glaciers on crystalline bedrock to 10,000-100,000 m/m.y. on large, fast-moving temperate valley glaciers in tectonically active areas like southeast Alaska (Hallet *et al.*,

1996). Thus, given the same tectonic regime of stable crystalline basement, the glacier- (Greenland) and ice- (Lena) dominated regimes seem to have similar denudation rates. On a smaller scale, inferred rates of postglacial bedrock lowering from measurements on the Swedish Lappland (68°N) are 1.2 m/m.y. in quartzite, 0.3 m/m.y. in amphibolite and less than 1.0 m/m.y. in phyllite (André and Clermont-Ferrand, 1996). Solution rates of dolomite are somewhat higher (5 m/m.y. on avg.) and depend on humidity and temperature. The surface lowering rate by fluvial weathering calculated similarly as here in the Orinoco river is ~5 m/m.y. for the lowland shield and 10-20 m/m.y. for the uplands (Edmond *et al.*, 1995; Lewis *et al.*, 1987). This is similar to the estimates from cosmogenic exposure ages for the quartzite erosion surface on Mount Roraima of the Guayana Shield (~1 m/m.y.; Brown *et al.*, 1992) and outcropping quartz veins in laterite on the West African Craton in Burkina Faso (3-8 m/m.y.; Brown *et al.*, 1994). Conclusively, there are no significant differences between denudation rates in the tropics and the subarctic. Regardless of whether it is a glaciated terrain, permafrost or a tropical rain forest, the denudation rates are similar in crystalline basement, though not through the same mechanisms. Only in tectonically active areas, and especially in those with active glaciers, are the rates significantly higher but show no climatic variation.

Discussion

Frost shattering as an agent of high chemical fluxes

Classical geology literature assigns chemical weathering to the tropics and mechanical weathering to high latitudes because of the necessity of water and high enough temperatures for chemical weathering and of the dominance of ice action in polar regions to produce sand (Ollier, 1969). Indeed frost action, even in the absence of glaciation, is a powerful agent capable of changing the landscape at every scale making the arctic/subarctic

a unique weathering regime (French, 1996). The 9% volumetric expansion of pore water as it crystallizes into ice, or the greater expansion resulting from migration of water to ice lenses can give rise to heaving of the bedrock or soil (Walder and Hallet, 1985; Hallet *et al.*, 1991); thermal contraction of the landscape at <-20°C leads to ice wedging in the overburden and mechanical disruption. In all these processes the lithologic properties of the rock, e.g. grain size, porosity and permeability, joints and bedding plains are important variables (Dredge, 1992). The presence of ice gives rise to other uniquely periglacial weathering environments. Perennially frozen ground, permafrost, acts as an impermeable layer towards groundwater flow and affects the hydrology. Collapse of ground ice or permafrost can give rise to thermokarst features, sunken ground and lakes. Together with the warmer summer temperatures and restricted flow during the 3 summer months, the ice action in effect gives rise not just to high physical weathering but also to comparable chemical weathering to tropical systems (Fig. 10).

In the tropics a completely different physical factor restrains the chemical weathering yield. On a flat terrain without relief, like the Guayana Shield, the residual oxides and terminal clays accumulate as a thick mantle above the weathering front. Even with the high temperatures and runoff the fresh bedrock is sealed underneath meters of completely weathered lateritic cover and chemical reaction occurs on the same scale as on the Aldan Shield where ice action continues to disrupt any mantle that forms and exposes new material.

Chemical denudation in alpine catchments with warm-based glaciers also shows accelerated rates relative to the world average (Reynolds and Johnson, 1972; Eyles *et al.*, 1982; Sharp *et al.*, 1995, Axtmann and Stallard, 1995). Thus, ice action in the periglacial shields of Siberia enables significant chemical weathering giving yields similar to tropical shields and also to basement rocks under glaciers. The efficiency and magnitude of frost weathering depends on climatic variables, e.g. the number of air and ground freeze/thaw cycles, intensity of freezing, and the rapidity of freezing. The number of freeze-thaw

cycles in Siberia are probably the annual ones in spring and fall; because diurnal fluctuations are small, the number is low. The rates of freezing do not appear to have been determined in this area.

Organic acids from peatlands, CO_2 released during the decay of organic matter in the tundra, and lichen have been proposed to be responsible for higher weathering rates at high latitudes (Shotyk, 1988; Anderson, 1995; Walton, 1985). These biotic and organic mechanisms are hard to prove with field data at present because of the geographical diversity of the biologic communities and the lack of organochemical studies of large watersheds.

Superficial weathering

To first order, the water chemistry is consistent with the bedrock composition. The Ca dominance of TZ^+ and low K/Na ratios indicate that plagioclase is the main primary aluminosilicate undergoing weathering. Plagioclase (oligoclase, andesine) accounts for 10-65% of feldspars in granites, 65-90% in granodiorites and 90-100% in tonalites (Streckeisen, 1976), the main rock types that constitute the granitic shields. The low $^{87}Sr/^{86}Sr$ and Si/TZ^+* ratios in the rivers studied here indicate superficial weathering, i.e. weathering of primary aluminosilicates to secondary clays. In the Orinoco the values are high indicative of complete weathering (Edmond *et al.*, 1995).

A puzzling fact is that superficial weathering should produce clays, but the headwater gravel streams are clear with low suspended loads (12-48 mg/L; Chalova *et al.*, 1995) and the middle reaches are sandy; only thin layers of clay are found on the banks. The soils in this boreal forest are podzols and are very thin. On the Guayana Shield where the weathering goes to completion beyond the secondary clay generation, the suspended load ranges from 3 to 60 mg/L (Edmond *et al.*, 1995), rivers are also very clear but rich in organic colloids. Either the clay generated by weathering is flushed out of the system

during ice break-up in spring and transported to the delta or the cations are leached out without authigenic clay formation. The suspended load increases in the lower reaches (to 100 mg/L and averaging ~60 mg/L; Rachold, 1994). There is a clear Lena river signal in the Laptev sea surface sediments. It is rich in illite with quartz (40-50%) and feldspar (~50%); the heavy mineral suite consists of epidote (15-20%), amphibole (30-40%) and feldspar (Stein and Korolev, 1994). The persistence of clays occurs on timescales of billions of years judging from the average crustal residence age calculated from Nd isotopes (Miller *et al.*, 1986). Soil distributions are very heterogeneous, even more so than the lithology, and it is difficult to estimate quantitatively the amount of soil currently generated in the present weathering environment. The soil profiles are generally relict and where there is a physical mechanism to strip this cover they can be very thin or absent. Therefore it is plausible that the transport capacity of the basin far exceeds the generation rates of clays. Concerning the possibility of lack of clay formation, the work of Dixon *et al.* (1984) on the grus and soil profiles of the Vantage Peak nunatak in Alaska using total chemical analysis and scanning electron microscopy is pertinent. They found evidence of extensive chemical alteration with the observation that vermiculite from biotite alteration is the principal secondary clay mineral, but that quartz and feldspars weather primarily by dissolution of soluble cations with no evidence of transformation to secondary clays. This is not homogeneous leaching of a thin surface layer of cations but through micropore and micropit generation. Bed material has been collected along with the water samples for the Siberian rivers. The sand grains observed under a petrological microscope are altered through weathering but not totally destroyed, whereas in the Amazon lowland almost everything is destroyed except quartz (Potter, personal communication). Many feldspars are cloudy or split open along fractures, and rock fragments are very hard to recognize due to their altered states.

The type of clay generated during weathering has also been thought to be intimately related to climate (temperature and precipitation) (Jenny, 1941). The distribution of clay

minerals in the ocean is commonly used in this sense, namely the kaolinite and gibbsite from weathering of silicate minerals in the tropics and detrital minerals, chlorite and illite in the higher latitudes (Biscaye, 1965). This distribution is however more a function of ocean currents and point sources than a continuous function of temperature. The chlorite dominance is a result of a glacial source; the gibbsite/kaolinite has large point sources in the tropical basins, e.g. Amazon/Orinoco, where prolonged weathering on the floodplains generates clean quartz and cation-depleted clays. Mineral variability, weathering environment, e.g. vegetation and microorganisms, soil development stage, etc., and microenvironment of the specific site affects clay mineralogy. The only clear link between climate and clay mineralogy is that montmorillonite is rarely found in areas that have not experienced arid or semi-arid climates (Gerrard, 1994). Although kaolinite and gibbsite would be expected to be the dominant clay mineral in lateritic deposits under humid tropical conditions, they can be produced under a variety of environments (Gerrard , 1994). Therefore, it can be argued that the weathering of the eastern Siberian basement terrains is superficial with any clay produced being transported down the river by ice and meltwater. Alternatively there may be only a leaching of the cations without formation of secondary clays. The fact that much feldspar is found in the Laptev Sea supports the latter scenario. That illite is the main clay found in the mouth does not affect our argument. The chemical fluxes from this superficial weathering are comparable to the tropical counterparts though the compositions are different. This weathering pattern of high Ca/Na and low dissolved Si seems to be common in cold environments, i.e. periglacial and glaciated terrains (Axtmann and Stallard, 1995).

Effect of Litho-tectonics on CO_2 uptake

Tectonics and lithology have been demonstrated to be the governing factors in determining CO_2 uptake. Chemical weathering rates in orogenic zones are a factor of ~3

higher than on stable basement shields (Fig. 10b; Huh *et al.*, 1998b); where there is easily eroded material such as volcanic rocks chemical fluxes and CO_2 uptake can be very high, as for the Fraser (Cameron *et al.*, 1995; Edmond and Huh, 1997). Strong correlations exist between denudation rates and relief, another measure of tectonics (Milliman and Syvitski, 1992; Summerfield and Hulton, 1994).

Tectonic reconstructions indicate that in mid-Paleozoic the Siberian Craton was in the tropics (Zonenshain *et al.*, 1990). In fact before the climatic deterioration beginning in the Eocene the whole earth experienced much warmer conditions judging from fossil evidence (Zachos *et al.*, 1994; Greenwood and Wing, 1995). The Aldan Shield, emergent since the Precambrian, would therefore have been covered with a thick lateritic mantle just like what is seen on the Guayana Shield today. Only the movement of the craton to the arctic region and the disruption of the mantle by ice action led to the chemical flux visible today. The Indian continent before its collision with Eurasia would similarly have been a flat terrain with a residual cover over fresh bedrock. Collision and subsequent uplift made it possible to shed the overburden and exposed the basement to the weathering agents, water and CO_2. Therefore, chemical weathering of silicate rocks and uptake of CO_2 over geologic time scales cannot be modeled as a continuous function of temperature/latitude. Exposure of the basement effected by tectonics or comparable physical mechanisms like ice action is the decisive factor.

The question then is given sufficient relief, doesn't climate also play an important role in weathering? Or put slightly differently, if the Guayana Shield were rid of its mantle would it have much higher weathering rates than the Aldan Shield? It should be pointed out that the mantle is an integral consequence of tropical weathering. All stable shields in the tropics are covered with a thick accumulation of laterite; the absence of it indicates the presence of tectonic action. Therefore, under all circumstances, the exposure mechanism is dominant and the climatic effect is only secondary. When trying to understand the first-

order controls on weathering and on the geochemical carbon cycle, climate is important but not in the form of a negative feedback.

On a multimillion year timescale the global input and output fluxes of CO_2 (~$8x10^{18}$ moles per million years) are very large compared to the mass of carbon in the atmosphere (~$0.06x10^{18}$ moles). Thus the atmosphere does not have the capacity to sustain large imbalances in the input and output fluxes. The lack of a stabilizing climate-weathering feedback implied by our data set poses serious problems on how the degassing and weathering were kept closely balanced since the origin of life. If tectonics and exposure mechanisms are the major drivers of continental weathering, as argued here, it implies that intermittent tectonic events have occurred at approximately the right rates to balance the increasing solar input and the relatively slowly varying volcanic degassing.

Conclusion

The global fluvial chemical dataset for basement terrains has been considerably enlarged to include the subarctic and arctic rivers of eastern Siberia. From these it is possible to extract information regarding CO_2 uptake rates by weathering of aluminosilicate rocks under cold climates. The magnitudes are not very different from those in tropical systems. Any significant temperature inhibition effect on weathering rates seems to be overridden by mechanical exposure of fresh surfaces by the frost shattering processes. The chemical compositions are different from that of the tropical shields in that they are representative of a superficially weathered system with high Ca and HCO_3 and relatively low silica, even when $^{87}Sr/^{86}Sr$ ratios are significantly radiogenic and indicate basement weathering. This has been observed in a number of glacial and high latitude streams and we ascribe these features to weathering limited superficial processes.

Acknowledgment —We appreciate the help of the captains and personnel of the River Navigation Authority of Yakutia and A. Zaitsev for the superb logistical support. S. Pelechaty, J. Boit and B. Bull kindly collected the "grab" samples. S. Bowring, D.

Coleman, and M. Kurz provided access to their TIMS facilities and D. B. Senn and H. Hemond to IC. We thank S. Bowring, K. Ruttenberg, K. Turekian, and K. Whipple for many very helpful discussions. A. Skorokhod helped with Russian translations and agonized over the hectic travel arrangements in this collaborative project. Work in the laboratory at MIT was supported by NSF EAR grants over the years.

References

Alabyan A. M., Chalov R. S., Korotaev V. N., Sidorchuk A. Y., and Zaitsev A. A. (1995) Natural and technogenic water and sediment supply to the Laptev Sea. In *Reports on Polar Research.* (eds. H. Kassens, D. Piepenburg, J. Thiede, L. Timokhov, H.-W. Hubberten, and S. M. Priamikov), Alfred-Wegener Institute for Polar and Marine Research, pp. 265-271.

Anderson L. G. (1995) Chemical Oceanography of the Arctic and its Shelf Seas. In *Arctic Oceanography: Marginal Ice Zones and Continental Shelves.* (ed. Smith W. O., Jr. and J. M. Grebmeier), Coastal and Estuarine Studies, American Geophysical Union, Washington, D.C., pp. 183-202.

Andersson P. S., Wasserburg G. J., Ingri J., and Stordal M. C. (1994) Strontium, dissolved and particulate loads in fresh and brackish waters: the Baltic Sea and Mississippi Delta. *Earth Planet. Sci. Lett.* **124**, 195-210.

André M.-F. (1996) Rock weathering rates in arctic and subarctic environments (Abisko Mts., Swedish Lappland). *Z. Geomorph. N. F.* **40**, 499-517.

Axtmann E. V. and Stallard R. F. (1995) Chemical weathering in the South Cascade Glacier basin, comparison of subglacial and extra-glacial weathering. In *Biogeochemistry of Seasonally Snow-Covered Catchments (Proceedings of a Boulder Symposium, July 1995)*, IAHS Publ. no. 228, pp. 431-439.

Berner R. A. (1991) Atmospheric carbon dioxide levels over Phanerozoic time. *Science* **249**, 1382-1386.

Berner R. A. (1994) GEOCARB II: A revised model of atmospheric CO_2 over Phanerozoic time. *Am. J. Sci.* **294**, 56-91.

Berner R. A., Lasaga A. C., and Garrels R. M. (1983) The carbonate-silicate geochemical cycle and its effect on atmospheric carbon dioxide over the past 100 million years. *Am. J. Sci.* **283**, 641-683.

Bibikova E. V. and Williams I. S. (1990) Ion microprobe U-Th-Pb isotopic studies of zircons from three Early Precambrian areas in the U.S.S.R. *Precam. Res.* **48**, 203-221.

Biscaye P. E. (1965) Mineralogy and sedimentation of recent deep-sea clay in the Atlantic Ocean and adjacent seas and oceans. *Geol. Soc. Amer. Bull.* **76**, 803-832.

Blum J. D. and Erel Y. (1997) Rb-Sr systematics of a granitic soil chronosequence: The importance of biotite weathering. *Geochim. Cosmochim. Acta* **61**, 3193-3204.

Bluth G. J. S. and Kump L. R. (1994) Lithologic and climatologic controls of river chemistry. *Geochim. Cosmochim. Acta* **58**, 2341-2359.

Brass G. W. (1976) The variation of marine $^{87}Sr/^{86}Sr$ ratio during Phanerozoic time: interpretation using a flux model. *Geochim. Cosmochim. Acta* **40**, 721-730.

Brown E. T., Edmond J. M., Raisbeck G. M., Bourlès D. L., Yiou F., and Measures C. I. (1992) Beryllium isotope geochemistry in tropical river basins. *Geochim. Cosmochim. Acta* **56**, 1607-1624.

Brown E. T., Bourlès D. L., Colin F., Sanfo Z., Raisbeck G. M., and Yiou F. (1994) The development of iron crust lateritic systems in Burkina Faso, West Africa examined with in-situ produced cosmogenic nuclides. *Earth Planet. Sci. Lett.* **124**, 19-33.

Burke W. H., Denison R. E., Heatherington E. A., Koepnick R. B., Nelson H. F., and Otto J. B. (1982) Variation of seawater $^{87}Sr/^{86}Sr$ throughout Phanerozoic time. *Geology* **10**, 516-519.

Cameron E. M., Hall G. E. M., Veizer J., and Krouse H. R. (1995) Isotopic and elemental hydrogeochemistry of a major river system: Fraser River, British Columbia, Canada. *Chem. Geol.* **122**, 149-169.

Chalova P. C., Panchenko B. M., and Zernova C. Y., eds. (1995) *Water Ways of the Lena Basin*. Moscow, 600pp. (in Russian)

Cook D. B., Fujita K., and McMullen C. A. (1986) Present-day plate interactions in northeast Asia: North American, Eurasian, and Okhotsk plates. *J. Geodyn.* **6**, 33-51.

Cuffey K. M., Clow G. D., Alley R. B., Stuiver M., Waddington E. D., and Saltus R. W. (1995) Large arctic temperature change at the Wisconsin-Holocene glacial transition. *Science* **270**, 455-458.

Dixon J. C., Thorn C. E., and Darmody R. G. (1984) Chemical weathering processes on the Vantage Peak Nunatak, Juneau Icefield, Southern Alaska. *Physical Geography* **5**, 111-131.

Dook V. L., Neymark L. A., Rudnik V. A., and Kröner A. (1989) *The Oldest Rocks of the Aldan-Stanovik Shield, Eastern Siberia, USSR. Excursion guide for geological field trip to the Aldan-Stanovik Shield.* IGCP Project 280, Leningrad-Mainz, 121 pp.

Dredge L. A. (1992) Breakup of limestone bedrock by frost shattering and chemical weathering, eastern Canadian Arctic. *Arctic and Alpine Research* **24**, 314-323.

Dunne T. (1978) Rates of chemical denudation of silicate rocks in tropical catchments. *Nature* **274**, 244-246.

Dupré B., Gaillardet J., Rousseau D., and Allègre C. J. (1996) Major and trace elements of river-borne material: The Congo Basin. *Geochim. Cosmochim. Acta* **60**, 1301-1321.

Edmond J. M. and Huh Y. (1997) Chemical weathering yields from basement and orogenic terrains in hot and cold climates. In *Tectonic Uplift and Climate Change*. (ed. W. F. Ruddiman), Plenum Press, pp. 329-351.

Edmond J. M., Palmer M. R., Measures C. I., Grant B., and Stallard R. F. (1995) The fluvial geochemistry and denudation rate of the Guayana Shield in Venezuela, Colombia and Brazil. *Geochim. Cosmochim. Acta* **59**, 3301-3325.

Eyles N., Sasseville D. R., Slatt R. M., and Rogerson R. J. (1982) Geochemical denudation rates and solute transport mechanisms in a maritime temperate glacier basin. *Can. J. Earth Sci.* **19**, 1570-1581.

Falkner K. K. *et al.* (1997) Minor and trace element chemistry of Lake Baikal, its tributaries and surrounding hot springs. *Limnol. Oceanogr.* **42**, 329-345.

French H. M. (1996) *The Periglacial Environment.* Longman, 341 pp.

Gerrard J. (1994) Weathering of granitic rocks: Environment and clay mineral formation. In *Rock Weathering and Landform Evolution.* (eds. D. A. Robinson and R. B. G. Williams), John Wiley & Sons Ltd., pp. 3-20.

Gíslason S. R., Arnórsson S., and Armannsson H. (1996) Chemical weathering of basalt in southwest Iceland: Effects of runoff, age of rocks and vegetative/glacial cover. *Am. J. Sci.* **296**, 837-907.

Gluchovsky M. Z., Moralev V. M., and Sukhanov M. K. (1993) Tectonic setting of the Early Proterozoic anorthosites and granites of the Aldan Shield and the zonation of thermotectonic processes. *Geotectonics* **27**, 227-237.

Gong G. and Xu J. (1987) Environmental effects of human activities on rivers in the Huanghe-Huaihe-Haihe Plain, China. *Geografiska Annaler* **69A**, 181-188.

Gordeev V. V. and Sidorov I. S. (1993) Concentrations of major elements and their outflow into the Laptev Sea by the Lena River. *Mar. Chem.* **43**, 33-45.

Gordienko I. V., Klimuk V. S., Ivanov V. G., and Posokhov V. F. (1997) New data on composition and age of bimodal volcanic series of the Tugnui riftogenic depression, Trans-Baikal region. *Transactions (Doklady) of the Russian Academy of Sciences/Earth Science Sections* **353**, 273-276.

Greenwood D. R. and Wing S. L. (1995) Eocene continental climates and latitudinal temperature gradients. *Geology* **23**, 1044-1048.

Hallet B., Walder J. S., and Stubbs C. W. (1991) Weathering by segregation ice growth in microcracks at sustained subzero temperatures: Verification from an experimental study using acoustic emissions. *Permafrost and Periglacial Processes* **2**, 283-300.

Hallet B., Hunter L., and Bogen J. (1996) Rates of erosion and sediment evacuation by glaciers: A review of field data and their implications. *Global and Planetary Change* **12**, 213-235.

Huh Y., Tsoi M.-Y., Zaitsev A., and Edmond J. M. (1998a) The fluvial geochemistry of the rivers of eastern Siberia I: Tributaries of the Lena River draining the sedimentary platform of the Siberian Craton. *Geochim. Cosmochim. Acta,* in press.

Huh Y., Panteleyev G., Babich D., Zaitsev A., and Edmond J. M. (1998b) The fluvial geochemistry of the rivers of eastern Siberia II: Tributaries of the Lena, Omoloy, Yana, Indigirka, Kolyma, and Anadyr draining the collisional/accretionary zone of the Verkhoyansk and Cherskiy ranges. *Geochim. Cosmochim. Acta,* in press.

Imaev V. S., Imaeva L. P., and Kozmin B. M. (1995) Active faults and recent geodynamics of Yakutian seismic belts. *Geotectonics* **28**, 146-158.

Jenny H. (1941) *Factors of Soil Formation*. McGraw-Hill, New York, pp.

Kuznetsov A. A. (1996) The Anabar Shield and geochemical features of the crystalline rocks in the early crust. *Geochem. Int.* **33**, 115-123.

Kuznetsova S. Y., Grinenko V. A., and Polyakov A. I. (1996) Sulfur in volcanic rocks of the Baykal rift zone. *Geochem. Int.* **33**, 1-10.

Lefond S. J. (1969) *Handbook of World Salt Resources*. Monographs in Geoscience, Plenum Press, New York, 384 pp.

Lewis W. M., Hamilton S. K., Jones S. L., and Runnels D. D. (1987) Major element chemistry, weathering and element yields for the Caura River drainage, Venezuela. *Biogeochem.* **4**, 159-181.

Logatchev N. A. (1993) History and geodynamics of the Lake Baikal rift in the context of the eastern Siberia rift system: A review. *BCREDP* **17**, 353-370.

Lu F. H., Meyers W. J., and Schoonen M. A. A. (1997) Minor and trace element analyses on gypsum: an experimental study. *Chem. Geol.* **142**, 1-10.

Martin H. (1994) The Archean grey gneisses and the genesis of continental crust. In *Archean Crustal Evolution*. (ed. K. C. Condie), Developments in Precambrian Geology 11, Elsevier, pp. 528.

Meade R. H. (1969) Errors in using modern stream-load data to estimate natural rates of denudation. *Geol. Soc. Amer. Bull.* **80**, 1265-1274.

Meade R. H. (1988) Movement and storage of sediment in river systems. In *Physical and Chemical Weathering in Geochemical Cycles*. (eds. A. Lerman and M. Meybeck), NATO Advanced Institute Series. Mathematical and Physical Sciences 251, pp. 165-180.

Meybeck M. (1979) Concentrations des eaux fluviales en éléments majeurs et apports en solution aux océans. *Rev. Géol. Dyn. Géogr. Phys.* **21**, 215-246.

Meybeck M. (1986) Composition chimique des ruisseaux non pollués de France. *Sci. Geol. Bull* **39**, 3-77.

Miller K. G., Fairbanks R. G., and Mountain G. S. (1987) Tertiary oxygen isotope synthesis, sea level history, and continental margin erosion. *Paleoceanography* **2**, 1-19.

Miller R. G., O'Nions R. K., Hamilton P. J., and Welin E. (1986) Crustal residence ages of clastic sediments, orogeny and continental evolution. *Chem. Geol.* **57**, 87-99.

Milliman J. D. and Syvitski J. P. M. (1992) Geomorphic/tectonic control of sediment discharge to the ocean: The importance of small mountainous rivers. *J. Geol.* **100**, 525-544.

Monserud R. A., Denissenko O. V., and Tchebakova N. M. (1993) Comparison of Siberian paleovegetation to current and future vegetation under climate change. *Clim. Res.* **3**, 143-159.

Monserud R. A., Denissenko O. V., Kolchugina t. P., and Tchebakova N. M. (1995) Change in phytomass and net primary productivity for Siberia from the mid-Holocene to the present. *Global Biogeochem. Cycles* **9**, 213-226.

Moralev V. M. (1981) Tectonics and petrogenesis of Early Precambrian complexes of the Aldan Shield. In *Precambrian Tectonics*. (ed. A. K. Kroner), Elsevier, pp. 237-260.

Morozova I. M., Bogomolov E. S., Jakovleva S. Z., Belyatsky B. V., and Berezhnaya N. G. (1989) U/Pb dating of granite-gneiss and tonalite-trondhjemite gneisses. In *The Oldest Rocks of the Aldan-Stanovik Shield, Eastern Siberia, USSR. Excursion Guide, IGCP 280.* (ed. V. A. Rudnik), Leningrad-Mainz, pp. 105-107.

Négrel P., Allègre C. J., Dupré B., and Lewin E. (1993) Erosion sources determined by inversion of major and trace element ratios and strontium isotopic ratios in river water: The Congo Basin case. *Earth Planet. Sci. Lett.* **120**, 59-76.

Nikolov N. and Helmisaari H. (1992) Silvics of the circumpolar boreal forest tree species. In *A Systems Analysis of the Global Boreal Forest.* (eds. H. H. Shugart, R. Leemans, and G. B. Bonan), Cambridge University Press, pp. 13-84.

Nutman A. P., Chernyshev I. V., Baadsgaard H., and Smelov A. P. (1992) The Aldan Shield of Siberia, USSR: the age of its Archean components and evidence for widespread reworking in the mid-Proterozoic. *Precam. Res.* **54**, 195-210.

Ollier C. (1969) *Weathering*. Elsevier, New York, 304 pp.

Palmer M. R. and Edmond J. M. (1989) The strontium isotope budget of the modern ocean. *Earth Planet. Sci. Lett.* **92**, 11-26.

Pinet P. and Souriau M. (1988) Continental erosion and large-scale relief. *Tectonics* **7**, 563-582.

Rachold V. (1995) Geochemistry of Lena River suspended load and sediments - preliminary results of the expedition in July/August 1994. *Reports on Polar Research* **176**, 272-279.

Reeder S. W., Hitchon B., and Levinson A. A. (1972) Hydrogeochemistry of the surface waters of the Mackenzie River drainage basin, Canada—I. Factors controlling inorganic composition. *Geochim. Cosmochim. Acta* **36**, 825-865.

Reynolds R. C., Jr. and Johnson N. M. (1972) Chemical weathering in the temperate glacial environment of the Northern Cascade Mountains. *Geochim. Cosmochim. Acta* **36**, 537-554.

Robinson R. S. and Johnsson M. J. (1997) Chemical and physical weathering of fluvial sands in an arctic environment: Sands of the Sagavanirktok River, North Slope, Alaska. *Journal of Sedimentary Research* **67**, 560-570.

Rosen O. M., Condie K. C., Natapov L. M., and Nozhkin A. D. (1994) Archean and Early Proterozoic evolution of the Siberian Craton: A preliminary assessment. In *Archean Crustal Evolution*. (ed. K. C. Condie), Developments in Precambrian Geology 11, Elsevier, 411-459.

Rundqvist D. V. and Mitrofanov F. P., eds. (1993) *Precambrian Geology of the USSR.* Developments in Precambrian Geology 9, Elsevier.

Savin S. M. (1977) The history of the Earth's surface temperature during the past 100 million years. *Annu. Rev. Earth Planet. Sci.* **5**, 319-355.

Schaltegger U., Stille P., Rais N., Piqué A., and Clauer N. (1994) Neodymium and strontium isotopic dating of diagenesis and low-grade metamorphism of argillaceous sediments. *Geochim. Cosmochim. Acta* **58**, 1471-1481.

Sharp M., Tranter M., Brown G. H., and Skidmore M. (1995) Rates of chemical denudation and CO_2 drawdown in a glacier-covered alpine catchment. *Geology* **23**, 61-64.

Shotyk W. (1988) Review of the inorganic geochemistry of peats and peatland waters. *Earth-Science Reviews* **25**, 95-176.

Stallard R. F. (1980) Major element geochemistry of the Amazon River system. Ph.D. dissertation, MIT-WHOI Joint Program in Oceanography.

Stallard R. F. and Edmond J. M. (1983) Geochemistry of the Amazon 2. The influence of geology and weathering environment on the dissolved load. *J. Geophys. Res.* **88**, 9671-9688.

Stallard R. F. and Edmond J. M. (1987) Geochemistry of the Amazon 3. Weathering chemistry and limits to dissolved inputs. *J. Geophys. Res.* **92**, 8293-8302.

Stein R. and Korolev S. (1994) Shelf-to-basin sediment transport in the eastern Arctic Ocean. *Reports on Polar Research* **144**, 87-100.

Streckeisen A. (1976) To each plutonic rock its proper name. *Earth-Science Reviews* **12**, 1-33.

Summerfield M. A. and Hulton N. H. (1994) Natural controls of fluvial denudation rates in major world drainage basins. *J. Geophys. Res.* **99**, 13,871-13,883.

Tarney J., Weaver B. L., and Drury S. A. (1979) Geochemistry of Archaean trondhjemitic and tonalitic gneisses from Scotland and E. Greenland. In *Trondhjemites, Dacites and Related Rocks*. (ed. F. Barker), Elsevier, Amsterdam, pp. 275-299.

Thompson L. G., Mosley-Thompson E., Davis M. E., Lin P.-N., Henderson K. A., Cole-Dai J., Bolzan J. F., and Liu K.-B. (1995) Late glacial stage and Holocene tropical ice core records from Huascaran, Peru. *Science* **269**, 46-50.

Trimble S. W. (1975) Denudation studies: Can we assume stream steady state? *Science* **188**, 1207-1208.

UNESCO (1977a) *Atlas of World Water Balance.* USSR National Committee for the International Hydrological Decade, Gidrometeoizdat, Leningrad & The UNESCO Press, Paris.

UNESCO (1977b) Soil Map of the World, VIII-2: North and Central Asia 1:5,000,000. Paris.

UNESCO (1979) *Discharge of Selected Rivers of the World.* Studies and Reports in Hydrology III, Imprimeries Louis-Jean, Gap, France, 104 pp.

Velichko A. A. and Faustova M. A. (1991) Reconstruction of the last post-Pleistocene glaciation of the northern hemisphere (18-20 thousand years ago). *Doklady Akademy Nauk USSR* 223-225.

Vinogradov V. I. and Leytes A. M. (1987) Rb-Sr dating of the stages of granitization of the South Aldan Shield. In *Isotope Dating of Metamorphic and Metasomatic Processes.* (ed. Y. A. Shukolyukov), Nauka, Moscow, pp. 103-115 (in Russian).

Walder J. and Hallet B. (1985) A theoretical model of the fracture of rock during freezing. *Geol. Soc. Amer. Bull.* **96**, 336-346.

Walker J. C. G., Hays P. B., and Kasting J. F. (1981) A negative feedback mechanism for the long-term stabilization of Earth's surface temperature. *J. Geophys. Res.* **86**, 9776-9782.

Walton D. W. H. (1985) A preliminary study of the action of crustose lichens on rock surfaces in Antarctica. In *Antarctic Nutrient Cycles and Food Webs.* (ed. W. R. Siegfried, P. R. Condy and R. M. Laws), Springer-Verlag, pp. 180-185.

Westall J. C., Zachary J. L., and Morel F. M. M. (1976) *MINEQL, A Computer Program for the Calculation of Chemical Equilibrium Composition of Aqueous Systems.* Tech Note 18, Dept. of Civil Eng., Mass. Inst. Technol., Cambridge, MA.

Windley B. F. and Bridgewater D. (1971) The evolution of Archaean low- and high-grade terrains. *Geol. Soc. Aust. Spec. Publ.* **3**, 33-46.

Yang C., Telmer K., and Veizer J. (1995) Chemical dynamics of the St. Lawrence riverine system: δD_{H_2O}, $\delta^{18}O_{H_2O}$, $\delta^{13}C_{DIC}$, $\delta^{34}S_{Sulfate}$, and dissolved $^{87}Sr/^{86}Sr$. *Geochim. Cosmochim. Acta* **60**, 851-866.

Zachos J. C., Stott L. D., and Lohmann K. C. (1994) Evolution of Early Cenozoic marine temperatures. *Paleoceanography* **9**, 353-387.

Zonenshain L. P., Kuzmin M. I., and Natapov L. P. (1990) *Geology of the USSR: A Plate-Tectonic Synthesis.* Geodynamics Series 21, Am. Geophys. U., Washington, D.C., 242 pp.

Table 1. Chemical data for the rivers draining the basement terrain of the Siberian Craton and the Trans-Baikal Highlands. The locations are shown in Fig. 3. n.d. = not determined; trib.=tributary; bl.=below.

River Name	Sample Number	Date d/m/yr	Na µM	K µM	Mg µM	Ca µM	Cl µM	SO_4 µM	HCO_3 µEq	Si µM	pH	Sr µM	$^{87}Sr/^{86}Sr$
Trans-Baikal Highlands (TBH)													
Kurkula	LB101	12/8/93	44.0	6.9	11.8	57.4	3.2	11.4	169	104	n.d.	0.22	0.85984
Kurkula	LB102	12/8/93	49.0	7.7	11.5	57.0	2.6	6.5	172	104	n.d.	0.20	0.86333
Frolikha	LB103	22/8/93	82.0	9.1	14	87.3	1.0	39.0	215	68	n.d.	0.70	0.71018
Tompuda	LB104	28/8/93	54.9	25.2	96	613	38.0	146	1218	77	n.d.	1.49	0.70832
Shegnanda	LB105	31/8/93	74.0	12.9	38	278	38.0	61.0	532	103	n.d.	0.86	0.70841
Oorbykan	LB106	31/8/93	71.0	17.9	76	294	62.0	45.0	676	127	n.d.	0.73	0.70861
Maksimikha	LB108	14/9/93	244	20.4	138	360	35.0	36.0	1182	294	n.d.	1.43	0.70695
Kika	LB109	16/9/93	74.9	11.4	52	155	15.4	18.2	460	182	n.d.	0.69	0.70869
Bolshaya Rechka	LB110	19/9/93	82.6	9.9	66	211	17.3	42.4	538	184	n.d.	0.89	0.70833
Pereyomnaya	LB112	22/9/93	79.0	17.6	46	243	6.0	71.0	529	141	n.d.	0.52	0.70908
Khara-Murin	LB111	21/9/93	44.9	16.4	28	83.8	13.6	63.7	156	87	n.d.	0.40	0.71297
Kutima, trib. of Kirenga	UL414	31/7/94	360	8.8	65.7	120	295	50.8	375	110	7.67	0.31	0.72305
Chaya	UL416	2/8/94	1570	11.8	202	430	1570	126	991	96	n.d.	1.32	0.71214
Chuya	UL421	2/8/94	185	18.0	201	490	126	160	1093	110	7.98	0.98	0.71334
Mama, trib. of Vitim	UL422	3/8/94	44.8	10.0	33.3	143	11.3	34.6	348	91	7.37	0.34	0.71057
Vitim bl. Mama	UL423	4/8/94	48.2	10.6	55.7	138	12.1	37.5	348	81	7.30	0.37	0.71282
B. Severnaya, trib. of Vitim	UL424	4/8/94	40.9	15.2	21.8	281	29.7	43.3	565	125	6.87	0.55	0.71423
Maximikha, trib. of Vitim	UL425	4/8/94	39.2	18.3	32.7	200	3.8	51.7	416	114	6.75	0.20	0.71718
Barchikha, trib. of Vitim	UL426	4/8/94	42.5	17.4	30.0	206	6.6	35.9	460	97	6.88	0.48	0.71974
V. Yzobaya, trib. of Vitim	UL427	4/8/94	32.5	13.7	38.1	147	19.0	0.5	377	73	6.61	0.48	0.74059
N. Yzobaya, trib. of Vitim	UL428	4/8/94	60.5	9.2	168	315	29.4	88.0	845	113	6.76	0.66	0.70973
B. Patom	UL434	7/8/94	116	17.4	173	506	92.9	252	918	86	7.97	1.83	0.71245
B. Patom	UL715	8/8/96	108	16.1	152	471	67.6	246	866	80	7.93	1.69	n.d.
M. Patom	UL435	7/8/94	76.4	11.1	130	1120	36.2	329	1917	57	8.07	3.79	0.71198
M. Patom	UL714	8/8/96	89.2	12.3	145	1270	40.2	387	2197	68	8.27	4.33	n.d.
Aldan Shield (Aldan)													
Chara	UL437	8/8/94	258	13.3	148	424	199	132	938	75	7.84	1.50	0.71211
Chara	UL710	6/8/96	423	17.0	184	441	330	214	934	78	7.98	1.68	n.d.
Tokko, trib. of Chara	UL507	18/7/94	124	10.2	106	186	54.8	62.8	578	94	n.d.	0.89	0.71483
Tokko, trib. of Chara	UL508	20/7/94	161	10.8	138	204	61.7	104	589	95	n.d.	1.20	0.71297
Tokko, trib. of Chara	UL509	21/7/94	164	10.8	167	266	91.7	166	660	94	n.d.	1.62	0.71167
Olekma @ mouth	UL438	8/8/94	123	8.3	94.7	225	104	89.8	469	103	7.33	1.24	0.70976

Table 1. continued.

River Name	Sample Number	Date d/m/yr	Na µM	K µM	Mg µM	Ca µM	Cl µM	SO_4 µM	HCO_3 µEq	Si µM	pH	Sr µM	$^{87}Sr/^{86}Sr$
Olekma @ mouth	UL711	6/8/96	384	12.5	129	282	350	200	519	114	7.60	2.13	n.d.
Stream into Olekma	UL510	25/7/94	82.1	20.1	1180	1200	84.7	160	4250	78	n.d.	3.08	0.72371
Olekma	UL511	26/7/94	88.0	11.2	54.6	110	43.2	40.2	316	99	n.d.	0.49	0.71482
Olekma	UL512	26/7/94	69.2	9.7	44.9	98.2	23.9	36.7	280	99	n.d.	0.25	0.71343
Olekma	UL513	30/7/94	41.4	7.3	80.8	133	26.0	18.0	403	87	n.d.	0.23	0.71210
Olekma	UL514	31/7/94	45.2	6.9	52.4	94.9	16.3	24.4	274	93	n.d.	0.22	0.71244
Olekma	UL515	31/7/94	53.7	9.0	570	1300	16.2	300	3049	64	n.d.	2.23	0.70876
Olekma-Chara	UL516	2/8/94	52.0	7.0	84.2	175	20.2	49.9	447	92	n.d.	0.44	0.71044
B. Nimnyr, trib. of Aldan	UL806	30/8/97	53.2	6.2	202	269	11.5	57.7	840	154	7.53	0.27	0.71312
B. Kuranakh, trib. of Aldan	UL803	29/8/97	97.7	17.1	732	957	9.9	182	3206	85	8.12	1.43	0.71172
M. Kuranakh, trib. of Aldan	UL807	30/8/97	97.4	28.2	464	732	38.8	132	2265	143	7.92	1.96	0.71602
Aldan @ Tommot	UL122	10/8/91	63.0	6.3	154	243	13.5	46.0	776	115	n.d.	1.34	0.71232
Aldan @ Tommot	UL802	29/8/97	61.9	11.3	394	469	n.d.	n.d.	1600	122	7.81	0.73	0.71260
Upper Elkon, trib. of Aldan	UL808	30/8/97	61.2	6.2	192	330	11.6	129	838	130	7.80	1.06	0.70792
Elkon @ mouth, trib. of Aldan	UL121	9/8/91	42	19.0	358	503	15.0	79.0	1670	95	n.d.	2.92	0.70855
Yakokut, trib. of Aldan	UL120	9/8/91	65	7.2	158	305	16.1	121	722	113	n.d.	1.97	0.70786
Yllymakh @ village, trib. of Aldan	UL809	30/8/97	38.6	7.0	207	292	11.7	47.0	933	124	7.60	0.31	0.70898
Yllymakh @ mouth, trib. of Aldan	UL118	8/8/91	37	4.3	150	237	4.7	49.6	753	102	n.d.	0.39	0.70888
Chulman, trib. of Timpton	UL804	30/8/97	129	13.2	104	343	28.6	74.4	840	141	7.31	2.87	0.71057
B. Khatymy, trib. of Timpton	UL805	30/8/97	81.2	6.7	161	252	9.8	32.1	834	172	7.54	0.33	0.71355
Timpton, trib. of Aldan	UL119	8/8/91	46.9	4.3	43.7	105	9.2	22.3	299	110	n.d.	0.34	0.71202
Jelinda	UL115	5/8/91	45	1.6	549	618	12.2	8.0	2412	127	n.d.	0.46	0.71338
Sumnayn	UL114	5/8/91	34	2.6	37	69.8	3.9	9.3	226	97	n.d.	0.46	0.71740
Junikan	UL113	4/8/91	31	2.2	54	85.2	3.8	8.0	300	88	n.d.	0.29	0.71521
Great Seligri	UL112	4/8/91	29	3.1	45	98.0	7.9	13.7	287	91	n.d.	0.22	0.72018
Uchur	UL110	3/8/91	31.5	5.8	104	138	6.3	14.9	502	82	n.d.	0.19	0.71186
Maya	UL109	2/8/91	56	10.3	153	344	9.8	47.6	1001	88	n.d.	0.86	0.71127
Anabar Shield (Anabar)													
B. Kuonamka	UL501	1/7/94	17.7	3.9	35.0	38.2	11.8	12.1	131	20	n.d.	0.03	0.71657
B. Kuonamka	UL502	1/7/94	8.0	5.4	41.3	61.0	13.0	13.0	190	16	n.d.	0.04	0.71482
M. Kuonamka	UL504	1/7/94	23.0	1.3	150	235	6.0	18.0	749	71	n.d.	0.09	0.71108
Hot Spring (HS)													
Kurbulik	LB107	9/9/93	5890	50.5	5.1	14.2	1060	1980	841	1400	n.d.	1.32	0.70621

Table 2. Flux calculations for the shield rivers. Column *a* of CO_2 flux is calculated based on the $^{87}Sr/^{86}Sr$ isotope criteria (see text) and column *b* is calculated using silica fluxes only.

River Name	Area	Dschrg	Na	K	Mg	Ca	Cl	SO_4	HCO_3	Si	Si/TZ+	$^{87}Sr/^{86}Sr$	TDS Flux	Areal TDS Flux	Net CO_2 Flux	
	10^3 km^2	km^3/yr	10^9 mol/yr										10^9 mol/yr	10^6 mol/yr/km^2	10^3 mol/yr/km^2	
															a	*b*
Trans-Baikal Highlands (TBH)																
Tompuda	2.52	0.756	0.042	0.019	0.073	0.463	0.029	0.110	0.921	0.058	0.066	0.70832	1.71	0.68	46	46
Kutima, trib of Kirenga	3.41	1.36	0.491	0.012	0.090	0.164	0.402	0.069	0.511	0.150	0.320	0.72305	1.89	0.55	138	88
Chaya	9.65	2.90	4.55	0.034	0.585	1.24	4.55	0.365	2.87	0.278	0.094	0.71214	14.5	1.50	307	58
Chuya	17.3	6.92	1.28	0.125	1.39	3.39	0.869	1.11	7.56	0.761	0.097	0.71334	16.5	0.95	456	88
Mama, trib of Vitim	18.9	13.2	0.593	0.132	0.441	1.892	0.149	0.458	4.60	1.20	0.278	0.71057	9.47	0.50	229	127
B. Severnaya, trib of Vitim	1.81	0.724	0.030	0.011	0.016	0.203	0.022	0.031	0.409	0.091	0.229	0.71423	0.81	0.45	218	100
B. Patom	28.4	7.10	0.824	0.124	1.23	3.59	0.660	1.79	6.51	0.611	0.096	0.71245	15.3	0.54	224	43
Total	*82.0*	*33.0*	*7.80*	*0.457*	*3.82*	*11.0*	*6.68*	*3.93*	*23.4*	*3.15*	*0.17*	*0.71215*	*60.2*	*0.74*	*231*	*79*
Aldan Shield (Aldan)																
Chara	87.6	21.9	5.65	0.291	3.24	9.29	4.36	2.89	20.5	1.64	0.079	0.71211	47.9	0.55	238	38
Tokko, trib of Chara	23.1	5.78	0.947	0.062	0.964	1.54	0.530	0.959	3.81	0.543	0.152	0.71167	9.35	0.40	154	47
Olekma @ mouth	210	42.0	5.17	0.349	3.98	9.45	4.37	3.77	19.7	4.33	0.211	0.70976	51.1	0.24	41	41
B. Nimnyr, trib of Aldan	1.35	0.270	0.014	0.002	0.055	0.073	0.003	0.016	0.23	0.04	0.176	0.71312	0.43	0.32	175	62
Aldan @ Tommot	50.1	7.52	0.473	0.047	1.16	1.83	0.101	0.346	5.83	0.864	0.152	0.71232	10.6	0.21	114	35
Yllymakh @ mouth, trib of Aldan	3.26	0.489	0.018	0.002	0.073	0.116	0.002	0.024	0.368	0.050	0.143	0.70888	0.65	0.20	31	31
Chulman, trib of Timpton	2.92	0.730	0.094	0.010	0.076	0.250	0.021	0.054	0.613	0.103	0.164	0.71057	1.22	0.42	215	71
B. Khatymy, trib of Timpton	0.54	0.108	0.009	0.001	0.017	0.027	0.001	0.003	0.090	0.019	0.205	0.71355	0.17	0.31	168	69
Timpton, trib of Aldan	44.4	8.88	0.416	0.038	0.388	0.932	0.082	0.198	2.66	0.977	0.373	0.71202	5.69	0.13	59	44
Great Seligri	1.79	0.269	0.008	0.001	0.012	0.026	0.002	0.004	0.077	0.024	0.322	0.72018	0.15	0.09	42	27
Uchur	113	28.3	0.890	0.164	2.94	3.90	0.178	0.421	14.2	2.32	0.169	0.71186	25.0	0.22	121	41
Maya	171	34.2	1.92	0.352	5.23	11.8	0.335	1.63	34.2	3.01	0.092	0.71127	58.5	0.34	191	35
Total	*709*	*150*	*15.6*	*1.32*	*18.1*	*39.2*	*10.0*	*10.3*	*102*	*13.9*	*0.187*	*0.71146*	*211*	*0.29*	*129*	*45*
Anabar Shield (Anabar)																
B. Kuonamka	21.9	4.38	0.078	0.017	0.153	0.167	0.052	0.053	0.572	0.088	0.152	0.71657	1.18	0.05	26	8
M. Kuonamka	1.74	0.348	0.008	0.000	0.052	0.082	0.002	0.006	0.260	0.025	0.094	0.71108	0.44	0.25	150	28
Total	*23.6*	*4.73*	*0.086*	*0.018*	*0.206*	*0.249*	*0.054*	*0.059*	*0.832*	*0.112*	*0.123*	*0.71261*	*1.62*	*0.15*	*88*	*18*

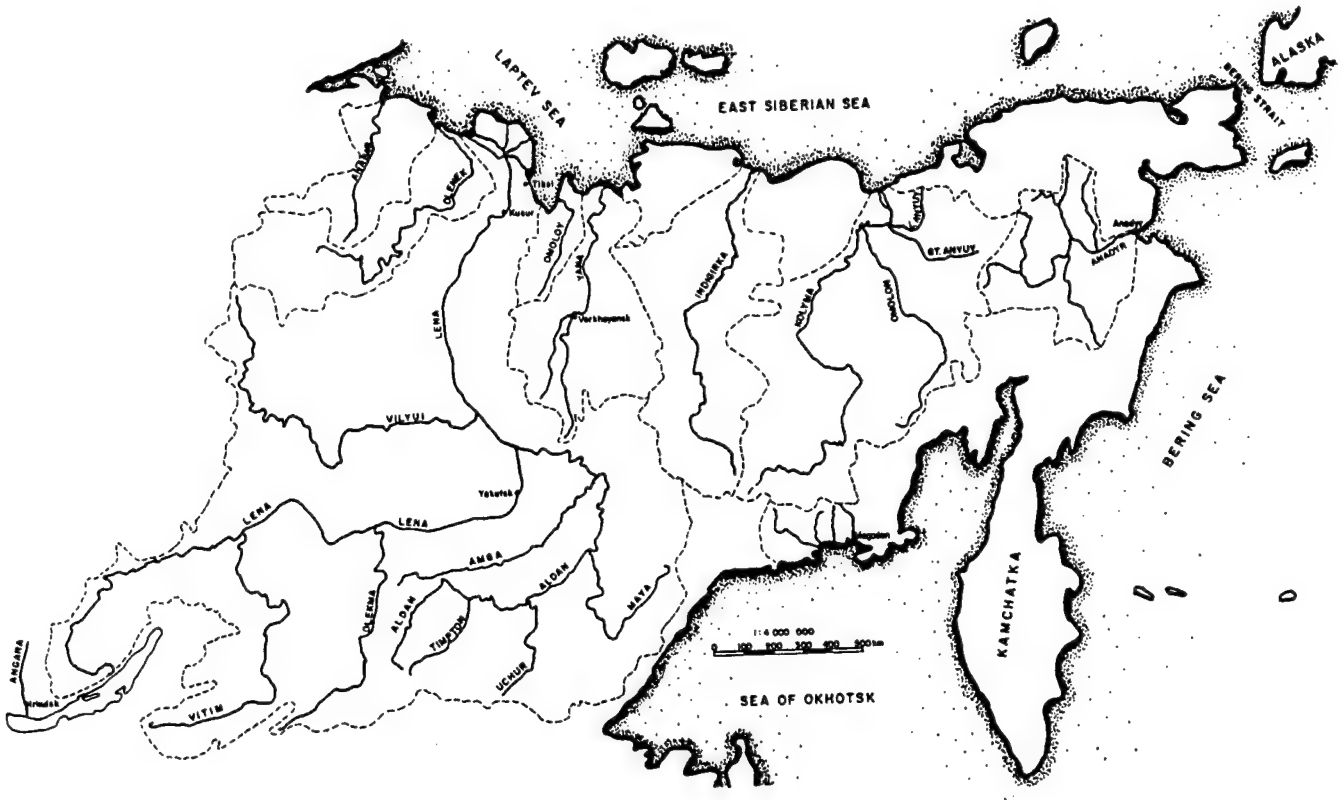

Figure 1. A schematic map of the rivers of eastern Siberia. The Anabar and the right bank tributaries of the Upper Lena are discussed here.

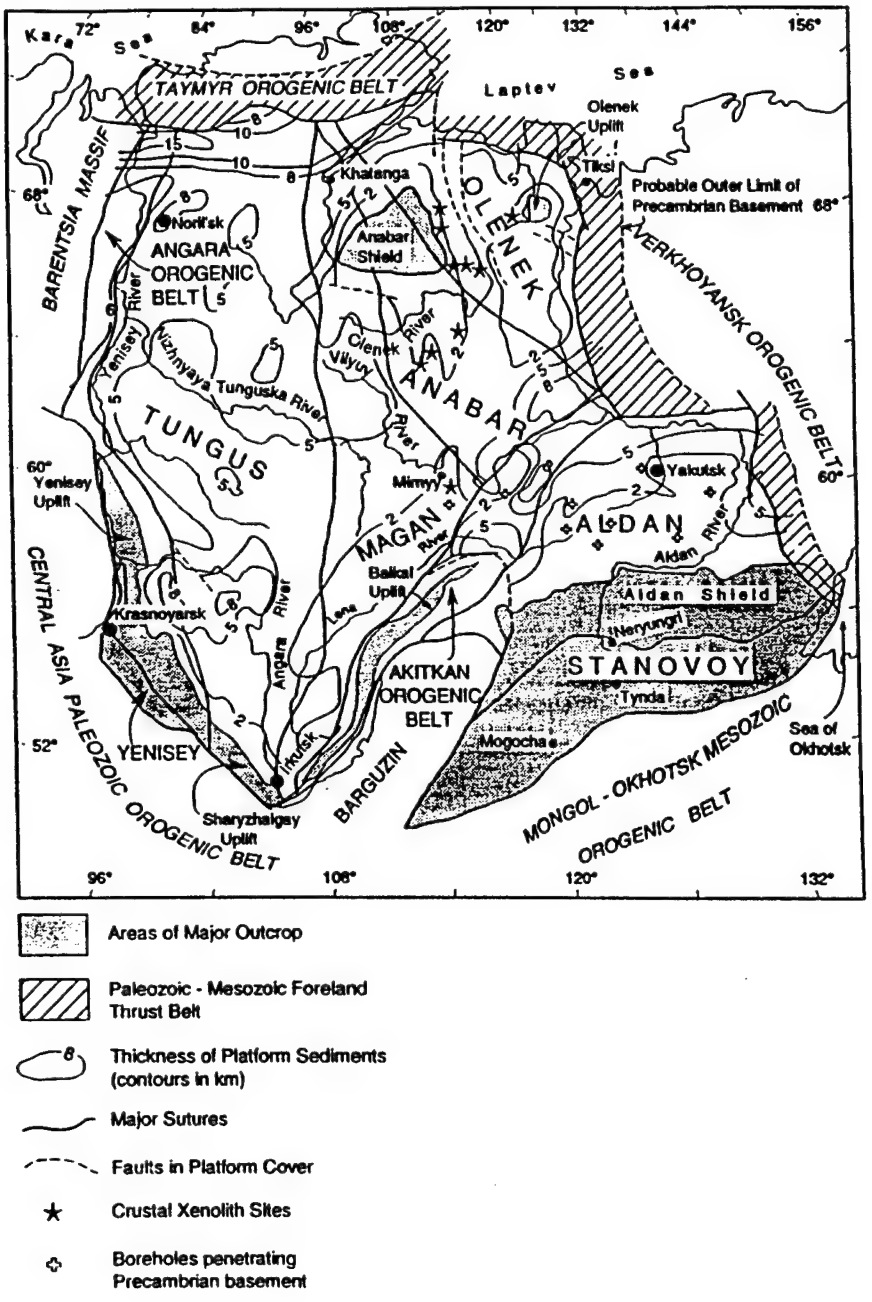

Figure 2. Geotectonic map of the Siberian craton showing the outcrops of the Precambrian basement (adapted from Rosen *et al.*, 1994).

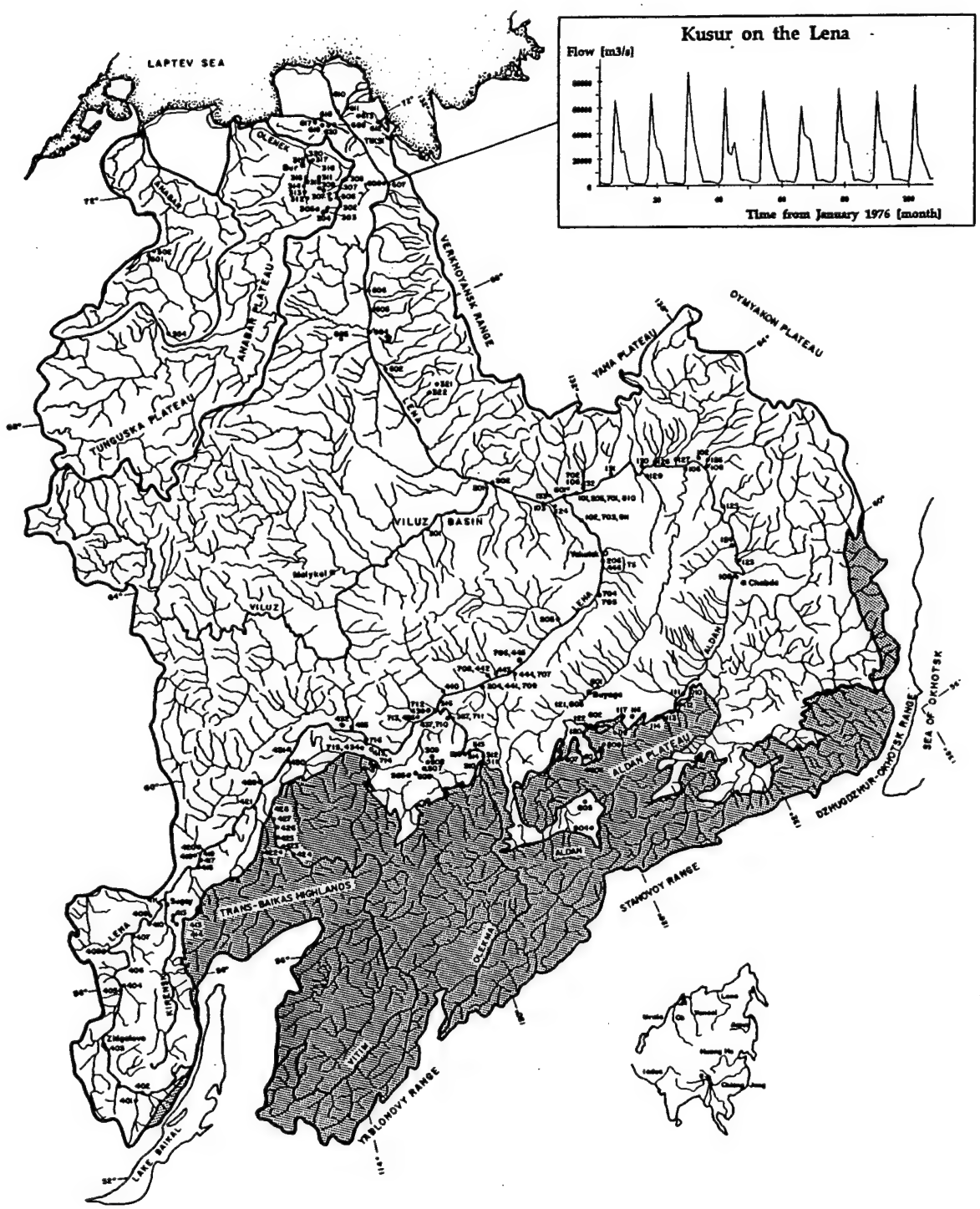

Figure 3. The drainage basin of the Lena and the Anabar. The stippled areas denote the exposed basement of the Siberian Craton, the Trans-Baikal Highlands and the Aldan-Stanovoy Shield. The Anabar Shield is not shown; it occupies the headwater region of the Anabar basin. The hydrograph at the mouth of the Lena is shown as an inset (from Global Hydrological Archive and Analysis System).

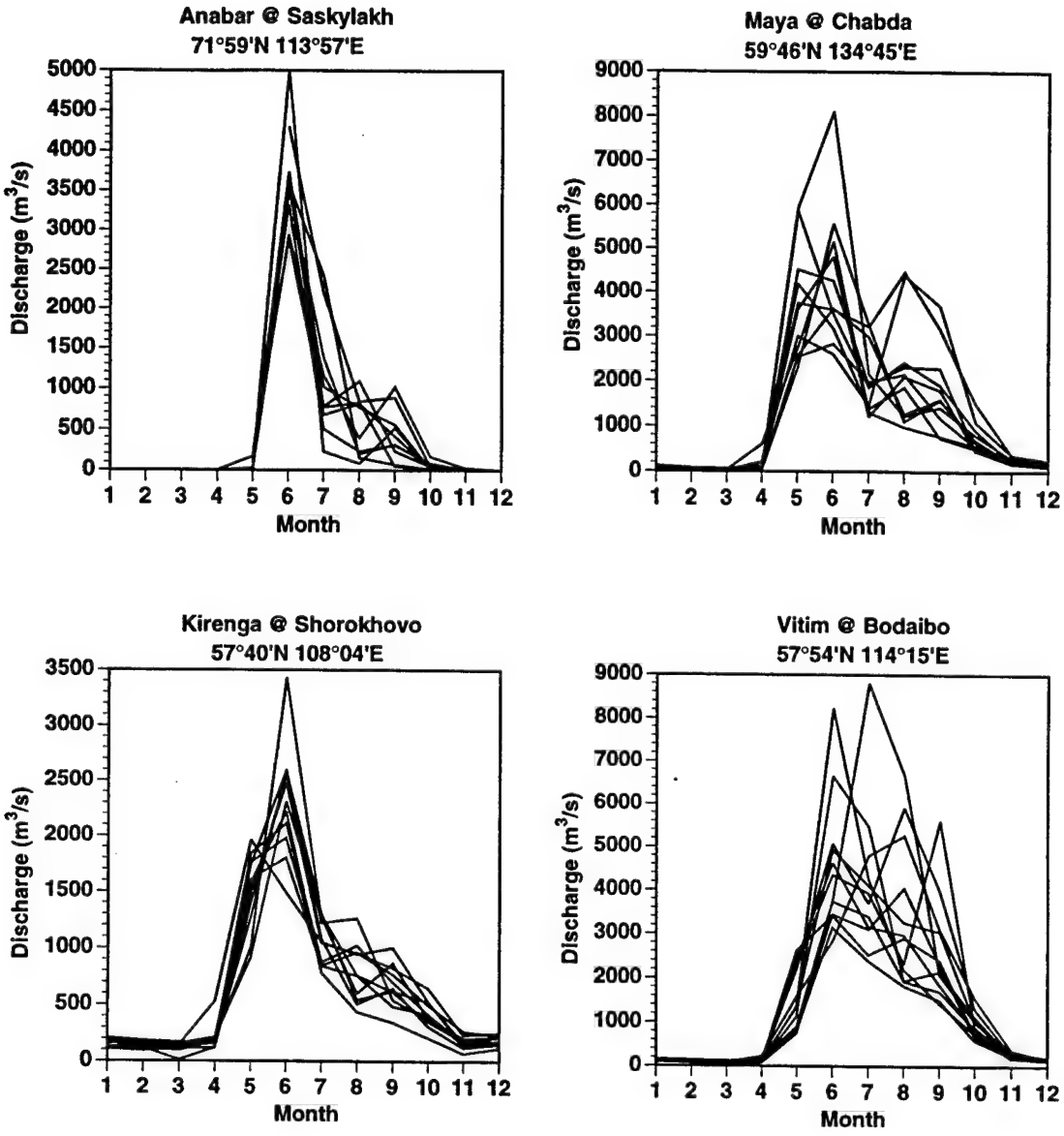

Figure 4. Multi-year hydrographs of some tributaries discussed in the text. Note the substantial inter-annual variability. Data are from UNESCO (1979).

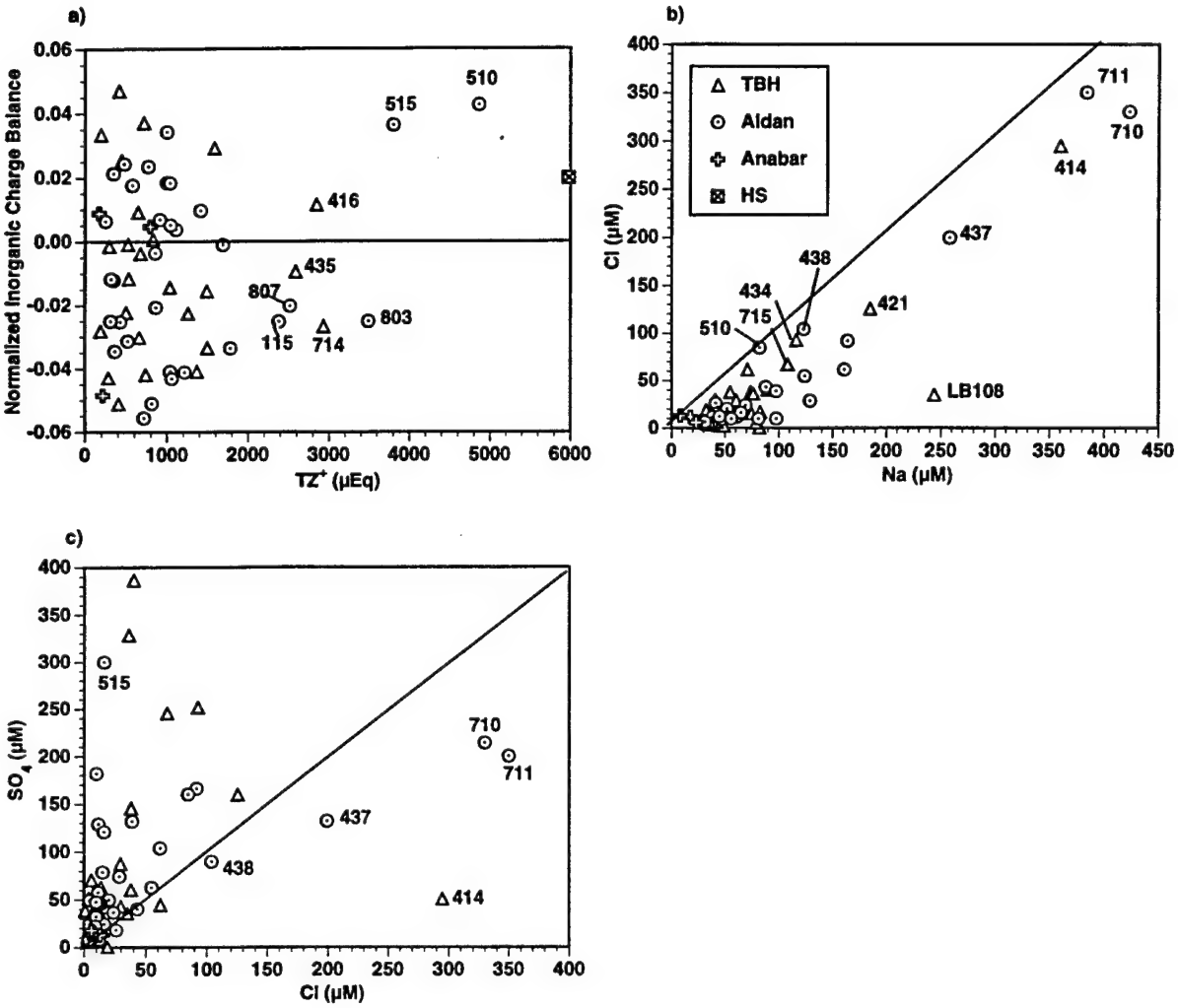

Figure 5. (a) The Normalized Inorganic Charge Balance (NICB = $[TZ^+ - TZ^-]/TZ^+$) vs. TZ^+. Well balanced NICB implies that organic anions are not substantial in these rivers, i.e. that the values are within analytical uncertainty. Two main channel samples of the Olekma have locally high TZ^+ (>3,500 μEq: UL510, 515), but at the mouth the values are lower (~800 μEq). The rivers in the Cambrian salt deposit zone have moderately high TZ^+ (2,500-3,000 μEq) and 1:1 Na:Cl ratios, e.g. UL416. Some tributaries have high TZ^+ presumably derived from the Cambrian carbonates in the lower reaches (2,500-3,000 μEq; UL115, 435, 714, 803, 807).

(b) Cl vs. Na with the 1:1 line shown for reference. Most of the samples have low concentrations of Cl and Na with an excess of Na indicating weathering of Na-silicates. The rivers that flow through the Cambrian evaporites in the lower reaches have high concentrations close to the equivalent line; the Chaya (UL416) is off the scale with very high Na and Cl (~1,600 μM). The hot spring sample is not plotted; although both Cl and Na are high, there is a great excess of Na over Cl suggesting input from continental $NaHCO_3$ (red beds) as in the Cojedes of the Orinoco basin.

(c) SO_4 vs. Cl shows no clear correlation between the two evaporitic (gypsum/anhydrite and halite) parameters. The line indicates the 1:1 molar ratio and shows that the bulk of the samples are skewed to higher SO_4. The hot spring sample is not plotted; it has almost 2:1 molar ratio. The Chaya (UL416) is dominated by Cl (1:10 molar ratio) and also is off scale.

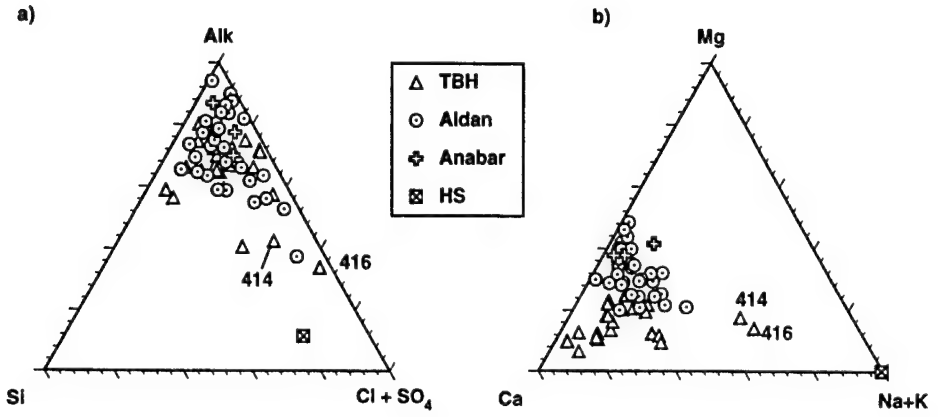

Figure 6. (a) The ternary anion diagram shows relatively high proportions of silicate weathering with oxidative weathering of sulfides occupying the middle.

(b) The ternary cation diagram shows that the Aldan and Anabar shield samples are magnesian compared to those of the TBH presumably due to the weathering of greenstone belts. The HS sample is extremely evaporitic.

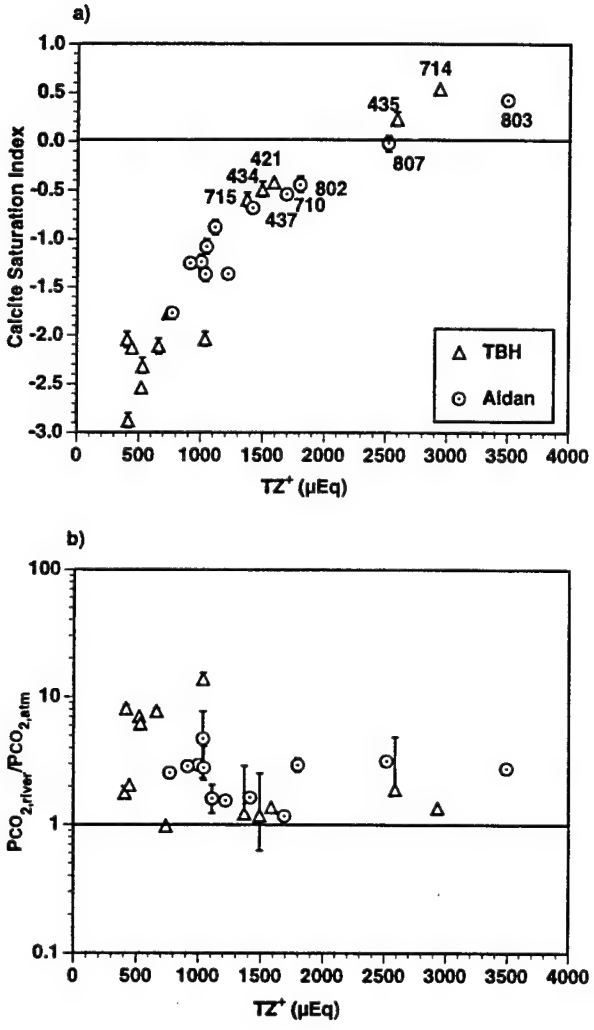

Figure 7. (a) The calcite saturation index (CSI) defined as $\log(\{Ca^{2+}\}\ \{HCO_3^-\}/ K_{calcite})$, where { } denotes activities; these were calculated using MINEQL+ ver. 3.01 (Westall *et al.*, 1976). The CSI increases with TZ^+ since Ca is the major cation, and only the highest TZ^+ rivers are supersaturated; the pH of the Chaya (UL416) was not available.

(b) $PCO_{2,river}$ / $PCO_{2,\ atm}$ shows that the rivers are all slightly supersaturated. $PCO_{2,\ atm}$ was taken to be 330 µatm.

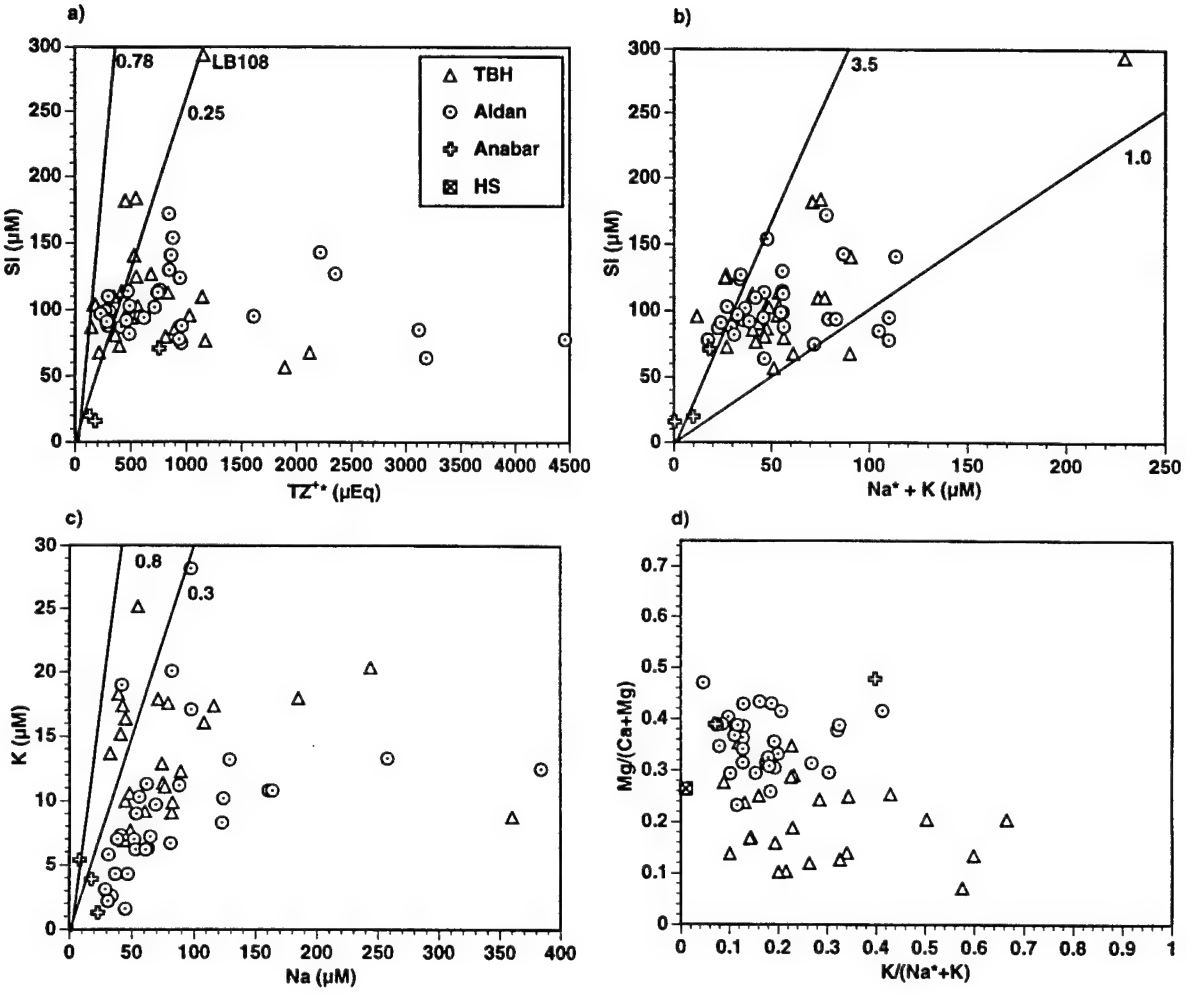

Figure 8. (a) Si vs. TZ^{+*} with lines indicating ratios expected for average shield weathering to kaolinite (0.78) and average shale weathering to kaolinite (0.25). The HS sample is not plotted; Si = 1,400 µM and TZ^{+*} =~985 µEq

(b) Si vs. (Na*+K) with lines indicating ratios expected for average shield weathering to gibbsite (3.5) and average shale weathering to kaolinite (1.0). The HS sample is not plotted; Na*+K = 4,906 µM.

(c) K vs. Na shows that the rivers are sodic. The lines bracket the ratios found in the Guayana Shield in the Orinoco.

(d) Mg/(Mg+Ca) vs. K/(Na*+K) shows large scatter around the igneous differentiation trend but no secondary weathering of fluvial detritus.

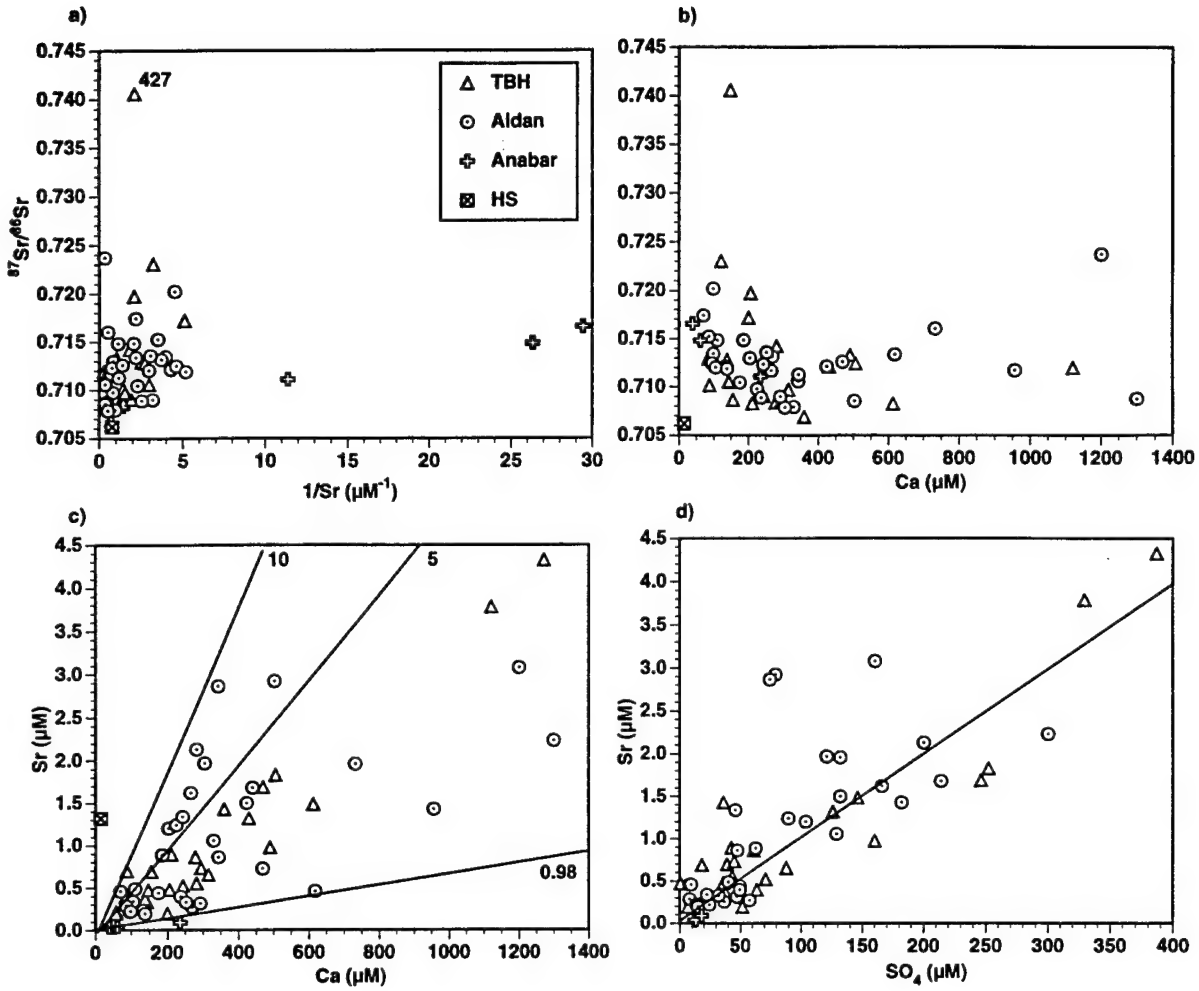

Figure 9. (a) $^{87}Sr/^{86}Sr$ vs. 1/Sr shows that many of the streams have radiogenic values (>0.71) and suggests aluminosilicate weathering. LB101 and 102 with ratios >0.86 are not plotted.

(b) $^{87}Sr/^{86}Sr$ vs. Ca shows that even high Ca rivers draining minor gypsum/anhydrite and carbonates have radiogenic values.

(c) Sr vs. Ca. Different lines and numbers indicate different Sr/Ca ratios in nmol/μmol in homogeneous watersheds draining single rock-type areas (Meybeck, 1986): carbonates including marble and carbonate sandstone = 0.7; plutonic rocks, gneiss and mica schist, sale and sandstone = 5; other metamorphics and volcanics =6; evaporites (gypsum) = 10.

(d) Sr vs. SO_4. The ratio for gypsum would be 10 nmol/μmol based on the above relationship between Sr and Ca. The data with a large scatter fall on either side of the line. The HS sample is not plotted; it has very high SO_4 (1,980 μM) with moderate Sr (1.32 μM).

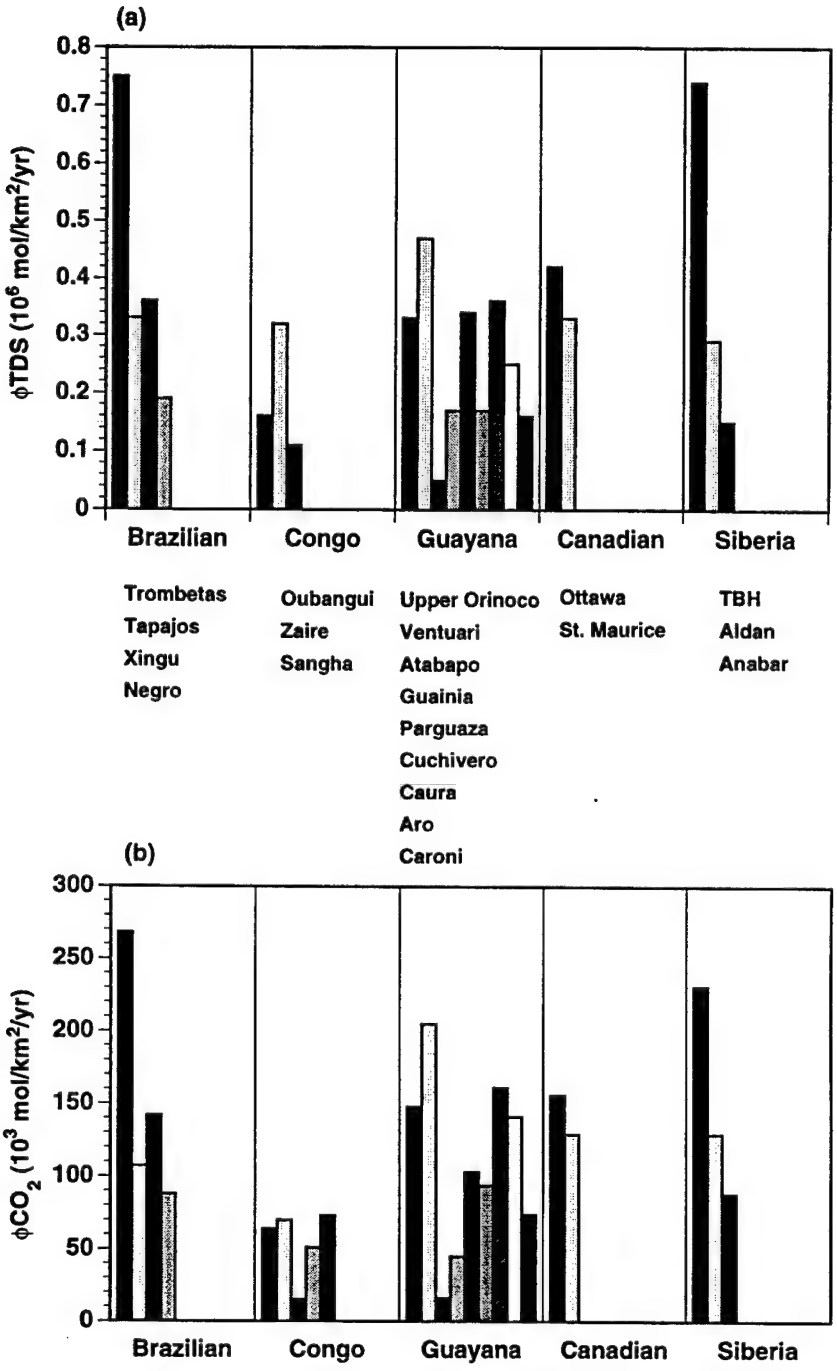

Figure 10. (a) The flux of total dissolved solids and (b) CO_2 uptake rate calculated as described in Huh *et al.* (1998a,b) and Edmond and Huh (1997). The individual bars indicate different tributary systems within a watershed except for Siberia where the bars indicate the three geological categories. On the left are the tropical rivers and on the right are the subarctic/arctic rivers. The river names for each bar are listed underneath.

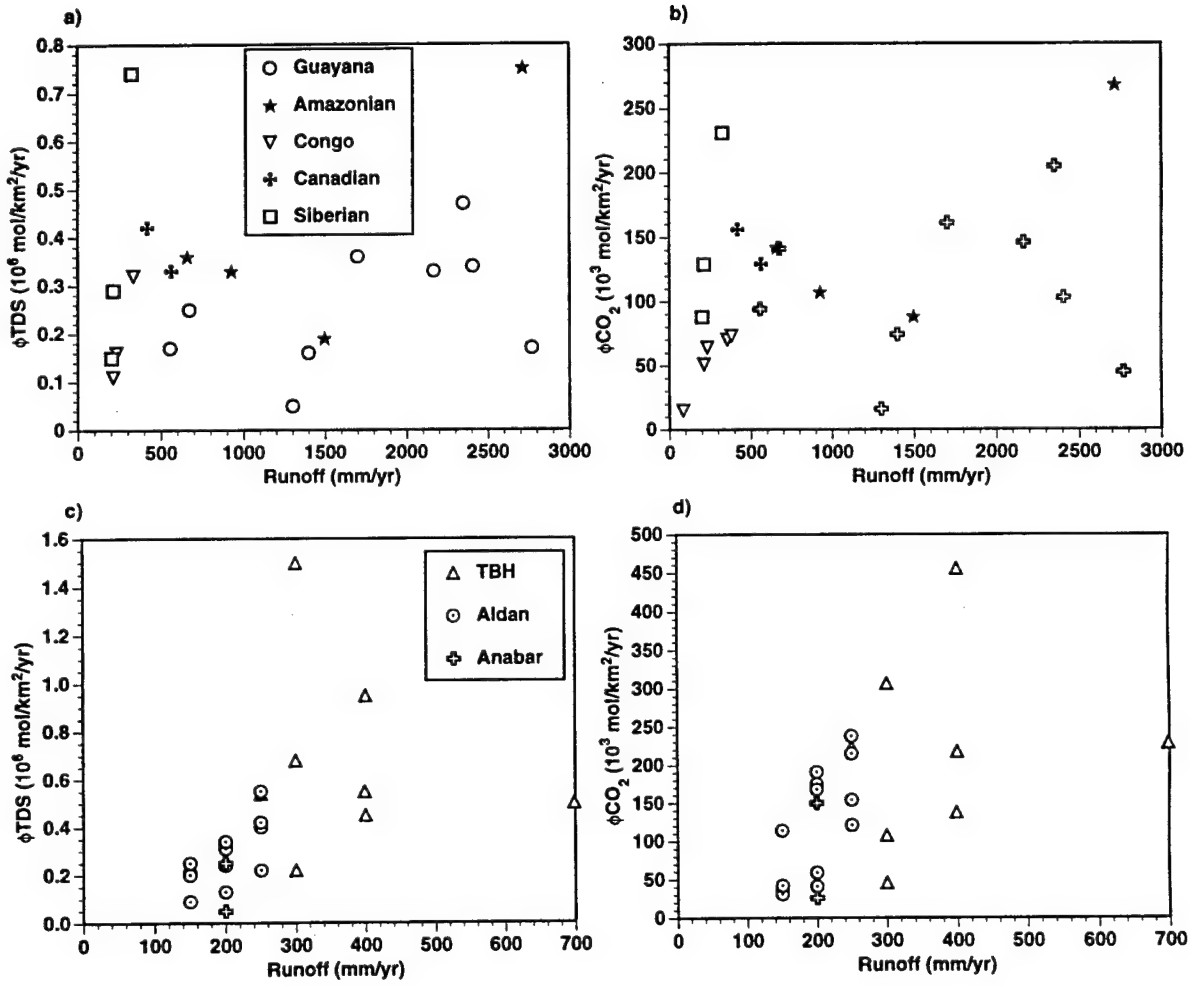

Figure 11. (a) TDS flux and (b) CO_2 uptake rates for major basement watersheds of the world show that there is no systematic relationship with runoff.

(c) TDS flux and (d) CO_2 uptake rates for tributary of the Siberian rivers studied here show that there is a positive correlation with runoff.

Chapter 5

Lithium and its Isotopes in Major World Rivers: Implications for Weathering and the Oceanic Budget*

* Huh Y., Chan L.-H., Zhang L., and Edmond J. M. (1998) Lithium and its isotopes in major world rivers: implications for weathering and the oceanic budget. *Geochim. Cosmochim. Acta,* in press (March 5, 1998).

Abstract

The outstanding problem in the lithium geochemical cycle is the lack of an isotopic mass balance in the ocean. The δ^6Li compositions of fresh basalts (-4‰), the hydrothermal fluids derived from them (average -9‰), and seawater (significantly heavier at -32‰) are well understood, but only very sparse river input data are available for lithium mass balance calculations. In an attempt to rectify the situation we have measured the lithium concentrations and isotopic compositions of major world rivers draining representative geological terrains. This helps both to constrain the river end-member and to understand the behavior of lithium isotopes in the continental weathering environment. Fluvial isotopic compositions display a very large range, -6.0 to -32.2‰. There is no definitive relationship between δ^6Li and lithology but, in general, rivers draining marine evaporites are -20 to -22‰, carbonates -26 to -32‰, black shales -26‰, shields -6.6 to -19‰, and mixed siliceous terrains -6 to -28‰. The flow-weighted mean concentration of the measured rivers is 215 nM at -23‰. This updated riverine δ^6Li value, responsible for ~30% of the global riverine discharge, does not solve the isotopic imbalance if the measured Li concentrations and isotopic compositions are representative of all rivers. The presence of a yet unidentified sink with a higher fractionation factor ($\alpha \approx 1.023$) than determined for low temperature basalt alteration ($\alpha = 1.019$) is required for an isotopic steady state of lithium in the ocean. Authigenic clays are a possible candidate as clays are known to be enriched in both lithium and in the light isotope preferentially. Alternatively, the hydrothermal flux must be much less than half of that estimated by the ^{3}He inventory and the oceanic budgets for $^{87}Sr/^{86}Sr$ and Mg. The relationship of δ^6Li to the major ions and $^{87}Sr/^{86}Sr$ suggests that the important processes affecting river dissolved Li isotopic compositions are fractionation between solution and secondary minerals and thus the intensity of weathering.

Introduction

There is an apparent lack of a Li mass balance in the ocean probably due to the poorly constrained hydrothermal fluxes and insufficient known sinks (Stoffyn-Egli and Mackenzie, 1984). The current river and hydrothermal flux estimates for water, based on the Sr isotope budget, are 3.74 x 10^{16} kg/yr and 1 x 10^{14} kg/yr, respectively but there are uncertainties in calculating the latter (Palmer and Edmond, 1989). The ^{3}He inventory (Edmond *et al.*, 1979) and the oceanic budgets for Mg and the Sr isotopes (Palmer and Edmond, 1989) agree with each other within the estimation error and yield much higher ridge-crest hydrothermal fluxes than the geophysical estimates based on heat flow (3~6 x 10^{13} kg/yr) (Morton and Sleep, 1985; Stein and Stein, 1994). The lithium isotope mass balance, using the known fractionation factor from low-temperature basalt alteration, yields hydrothermal water fluxes similar to geophysical values (1~4 x 10^{13} kg/yr) (Chan *et al.*, 1992). This calculation was based on only a few lithium isotope measurements from rivers, whereas the behavior during hydrothermal alteration has been thoroughly studied (Chan *et al.*, 1993, 1994), and the ocean is isotopically homogeneous at 26 μM and -32.3‰ (Chan and Edmond, 1988).

Lithium has two stable isotopes in approximate abundances of ^{6}Li 7.5% and ^{7}Li 92.5%. Because of the large relative mass difference, lithium isotopes have the potential to exhibit sizable fractionation in nature and thus to be an effective tracer of weathering processes. What few data exist show that there may be fractionations of up to 60‰ in the terrestrial environment. Lithium isotopic systematics have already been used as diagnostic tracers for processes associated with ocean crust alteration, submarine hydrothermal activity, and fluid expulsion at convergent margins (Chan *et al.*, 1992, 1993, 1994; You *et al.*, 1995).

The study of lithium isotopes in natural waters has been analytically hindered by 1) the large relative mass difference which can cause significant temperature-induced

fractionations in mass spectrometry and 2) the large amounts of material required especially for low concentration freshwater systems. The lithium tetraborate method (Chan, 1987) overcame the fractionation problem but still required large samples (3 μg Li). The average Li concentration in freshwater is ~200 nM, thus requiring a sample size of ~2 liters. The present study was made possible by the development of the phosphate method that achieves similar precision (± 1.3‰, n=21) with much smaller sample sizes (<100 ng Li thus requiring less than 100 ml of water; You and Chan, 1996).

Here we report δ^6Li and Li concentrations of some major world rivers and of tributaries that drain distinctive geologic environments in order to understand the behavior of Li isotopes during weathering and to estimate the fluvial isotopic flux to the ocean and thus constrain the marine Li budget.

The chemistry of lithium

Lithium is an alkali element but because of its small ionic radius as Li^+ (0.78Å) it behaves more like Mg^{2+} in nature. It substitutes for Al^{3+}, Fe^{2+} (0.77Å) and especially Mg^{2+} (0.72Å) in crystal structures rather than for Na^+ (0.98Å). It has a high solvation energy and a large degree of covalent character in its chemical bonds causing the low solubilities of its phosphate and carbonate salts (Cocco *et al.*, 1978). The oxygen coordination of Li^+ varies between 3 and 8 with preference for tetrahedral and to a lesser extent octahedral positions (Wenger and Armbruster, 1991). Li^+ forms stable complexes with water molecules in which the cation is complexed by four water molecules in tetrahedral geometry. A coordination number of six is common for lithium salts, but because Li^+ has a preference for anions with high charge/radius ratio, Li^+ mainly occurs in silicates in evaporitic environments while Na^+ forms chlorides (Olsher *et al.*, 1991). The high degree of covalent character in its chemical bonds and the presence of different atomic

environments that lithium is found in (e.g. tetrahedral vs. octahedral sites) make lithium prone to isotopic fractionation (O'Neil, 1986).

In the sedimentary environment, lithium is preferentially retained, in proportion with Al_2O_3, during the alteration of clay minerals relative to other soluble elements like Na^+ and Ca^{2+} (Ronov *et al.*, 1970). Li^+ has the weakest sorption chemistry of all the alkalis (Heier and Billings, 1978), and its affinity with clays is considered to be due to the isomorphic substitution of Mg^{2+} for Al^{3+} in the octahedral layer leaving a vacant position to accommodate Li^+. Indeed, examination of Li exchange in complex soil solution and pure clay mineral systems has shown that Li is selectively absorbed over other cations and apprently fixed in a non-exchangeable form (Anderson *et al.*, 1989). In laterites, where aluminosilicates have weathered completely to goethite and hydrargillites, the lithium content drops. Thus the lithium content of clay minerals is a function of the amount in the parent rocks and the extent of weathering (Ronov *et al.*, 1970). Although economic reserves of lithium exist in playa deposits, they are not in the salt minerals but rather in terminal silicates and phosphates (Vine, 1980).

Because Li is a moderately incompatible element in magmatic systems, it is generally expected to accumulate in residual melts during differentiation. Lithium is enriched in the continental crust over the mantle, especially in pegmatites where the content reaches a few % by weight (Heier and Billings, 1978). Initially Li tends to enter mafic silicates (e.g. pyroxene, amphibole) replacing Mg^{2+} and Fe^{2+} and later Al^{3+} sites in muscovite and plagioclase. The Li retained in residual melts forms lithium minerals like spodumene.

Experimental Methods

Samples used in this study were from archives ranging in age from 1977 for the Amazon to recently collected Siberian rivers. They were all filtered through 0.45 μm

Millipore filters in the field within 24 hours of collection and stored in Nalgene® polyethylene bottles, unacidified. Lithium isotope ratios were determined by thermal ionization mass spectrometry (TIMS) following the procedure of You and Chan (1996). Briefly, the sample solution is put through a cation exchange column with HCl to isolate Li from the matrix. For some organic-rich rivers, it was necessary to UV irradiate the samples overnight in order to break down the organics prior to the column procedure and prevent the columns from clogging. The eluate was then evaporated to dryness with H_3PO_4 to form Li_3PO_4 which was used as the ion source. The sample was loaded on double Re filaments, ionized, and detected as Li^+ using a Finnigan MAT 262 mass spectrometer at LSU. The precision was better than ~1‰ (1σ) based on repeated measurements of standards and samples. Following convention, δ^6Li is reported in ‰ units:

$$\delta^6Li = \{(^6Li/^7Li)_{sample}/(^6Li/^7Li)_{standard} - 1\} \times 1000$$

where $(^6Li/^7Li)_{standard} = 0.08274 \pm 0.00003$ (n=7) for a pure Li_2CO_3 standard, NBS L-SVEC. This is comparable with other reported values: 0.0832 ± 0.0002 (Flesch *et al.*, 1973), 0.08306 ± 0.00005 by the borate method (Chan *et al.*, 1992), and 0.08261 ± 0.00003 by the phosphate method (You and Chan, 1996). Unlike the case for other elements, the lighter isotope is less abundant and more negative δ values are therefore heavier. The isotopic fractionation factor (α) is defined as:

$$\alpha_{mineral\text{-}water} = (^6Li/^7Li)_{mineral}/(^6Li/^7Li)_{water}$$

Lithium concentrations were determined by ID-TIMS at LSU or by ICP-MS at MIT as noted in Tables 1 and 2. Concentrations determined by ICP-MS have precisions of 5% (1σ) and agree with the ID-TIMS data to within 6% (1σ).

Results and Discussion

Samples from the lower reaches of thirteen major rivers of the world were selected (Table 1). Together they represent about one third of the global river flow and cover diverse climatic regions from the Tropics to the Arctic. Most of the samples were obtained as a part of detailed surveys, and supporting chemical data are available (Table 1) (Hu *et al.*, 1982; Stallard and Edmond, 1983; Sarin *et al.*, 1989; Krishnaswami *et al.*, 1992; Palmer and Edmond, 1992; Edmond *et al.*, 1995, 1996). New data have also been obtained from the Siberian rivers (Huh *et al.*, in review a,b). Published data from the rivers entering Lake Baikal are also included for completeness (Falkner *et al.*, 1997). For the Mississippi, Mackenzie, Columbia, Fraser, and Jordan only lithium data and in some cases $^{87}Sr/^{86}Sr$ data are reported for "grab" samples from their mouths (Table 2). The fluvial chemistry of some of these basins has also been studied in detail elsewhere (Reeder *et al.*, 1972; Cameron *et al.*, 1995). The major lithologies of the basins are given in Table 1 and 2, and the locations of the samples are given by basin in Figures 1-5.

Controls on δ^6Li

The fluvial isotopic compositions display a large range, -6.0 to -32.2‰ (Fig. 6, Tables 1, 2). Rivers draining marine evaporites, e.g. the Amazon at Iquitos, the Cojedes of the Orinoco, and the Biryuk on the Siberian Platform, range from -20 to -22‰ (n=3). The Apure of the Orinoco and the Chinese rivers which drain carbonates have isotope ratios between -26 and -32‰ (n=3). The Madeira drains a black shale terrain in Bolivia and gives -26‰ (n=1). The Negro, Parguaza and Caroni of the Amazon-Orinoco, the Timpton in Siberia, and the Upper Mississippi drain shield terrains and vary from -6.6 to -19‰ (n=4). Other rivers of mixed siliceous terrains range from -6 to -28‰ (n=7). There is generally a direct relationship between lithology, the major elements, and the Sr isotope

ratios (Stallard and Edmond, 1983; Edmond *et al.*, 1995), however there is no obvious relationship with δ^6Li. Knowledge of the Li isotopic composition of continental rocks is limited. Data available from other ongoing studies are summarized in Fig. 6 for the purpose of comparison with river waters. There is a considerable overlap between different lithologies; δ^6Li is not an unambiguous tracer for basement geology. This in part explains the large spread of δ^6Li in river waters and the lack of clear correlation with lithology.

Added to this is isotopic fractionation accompanying the partitioning of Li between weathering products and solution. Clays are known to retain Li with preference for ^{6}Li, leaving the water enriched in the heavier isotope. The total digests of suspended sediments from the Madeira, Amazon @ Xingu and Mississippi have 71.6, 63.9 and 49.3 ppm Li, and δ^6Li values of -5, -1.1 and -3.8 ‰, 21, 20 and 14 ‰ lighter than the respective dissolved loads. There is thus a very large separation of the isotopes in the weathering regime. Alternatively, the suspended and dissolved material could be representative of different Li sources: the former from aluminosilicates, the latter predominantly from carbonates and evaporites.

For the main channels for which data from the major tributaries are available, e.g. the Amazon and the Orinoco, it is not possible to obtain a mass balance for the lithium isotopes based on the values of the few incoming tributaries measured. This is especially so for the Orinoco (Fig. 2).

The tropical shield rivers are relatively light in their Li isotopic compositions (-6.6 to -17‰). The Parguaza, draining the extremely evolved rapakivi granite terrain of the Guayana Shield, has the lightest value among the shields (-6.6‰). The few rock data that exist from Archean granitic rocks and tonalites of South Africa have a range of -8 to -10‰; Precambrian granodiorites and schists have δ^6Li of -20.8 and -16.8 ‰ respectively (Chan, unpublished data). The light isotopic composition of the tropical shield rivers, especially the Parguaza and Negro, may be related to the changing chemical and mineral

compositions of the weathering products with increasing intensity of reaction. These rivers are very dilute and their chemistries are consistent with complete transformation to kaolinite or gibbsite (Edmond *et al.*, 1995). Weathering profiles show relatively constant Li contents although major ions are progressively depleted with extent of weathering (Horstman, 1957; Ronov *et al.*, 1970). Therefore, initially the water will leach out the heavier isotope. Further weathering removes most of the alkalis from the solid substrate (Ronov *et al.*, 1970) and the residue becomes increasingly enriched in ^{6}Li. On the tropical shields where weathering is extreme the water values approach the values of the weathered residue and are very light.

Rivers of dominantly carbonate geology have extremely heavy isotopic compositions similar to seawater, especially the Yangtze and the Orinoco at their mouths. The few lakes and closed seas studied to date also have δ^6Li much like the ocean (Table 3) (Chan and Edmond, 1988; Falkner *et al.*, 1997). Unlike the relatively constant δ^6Li value of carbonate-dominated rivers, lakes, and the oceans, δ^6Li of limestones varies widely (Table 4). The isotopic composition of carbonates varies with the degree of diagenesis; δ^6Li of rivers from such terrains is consistent with values from uplifted and diagenetically altered marine deposits. The Li/Ca ratios in these rivers (0.15-0.71x10^{-3} mole ratio) are comparable with those in limestones (~0.11 x10^{-3} mole ratio; Heier and Billings, 1978). Carbonates precipitated from evaporated lake water can have high Li concentrations, as demonstrated by a Dead Sea aragonite with 19 ppm Li and a δ^6Li of -12.9‰ (Chan, unpublished). Some lithium in carbonate rivers, especially those that are not highly evaporitic, must come from associated shales, e.g. a calcareous shale from the Ellis Group of Yellowstone National Park has 18 ppm Li and δ^6Li of -21.6 ‰ (Chan *et al.*, 1997). Partial leaching of Li from such rocks would lead to a ^{7}Li-rich composition in the water.

Adsorption onto suspended sediments in rivers may also play a role, but preliminary experiments suggest that only about 1 ppm Li is adsorbed onto clays and river

sediments (i.e. <10%) with preferential uptake of the light isotope (Zhang, 1997). Therefore, the effect of adsorption may be important only in very dilute rivers.

Relation to major ions, $^{87}Sr/^{86}Sr$, and lithology

Lithium concentrations range from ~30 nM in the tropical shield rivers, Caroni and Negro, to 11,700 nM in the Jordan; the bulk of the samples are below 600 nM (Tables 1,2) (Fig. 7). The unusually high concentrations in the Jordan can be attributed to the arid climate and the evaporitic nature of the rocks and soils in its basin. Rivers with high lithium generally drain marine limestones and evaporites, e.g. Jordan, Mississippi, Biryuk, and Cojedes (450~11,700 nM). Rivers draining tectonically active zones like the Ganges-Brahmaputra (440~580 nM) and the Baikal rift streams (160~490 nM) have moderately high Li, and shield rivers have low values (27~70 nM). This is consistent with the known distribution of lithium in the terrestrial environment and the weatherability of various rock types.

Lithium concentrations are in general proportional to Mg ($r^2 = 0.96$; Fig. 7) but only poorly correlated to other major ions and even Si and K though these are almost exclusively from the weathering of aluminosilicates. This is consistent with the tendency of lithium to be retained in secondary clays, substituting for Mg^{2+} or occupying the vacancy generated by Mg^{2+} substitution of Al^{3+}. There is some relationship between Li and Cl, but the Li/Cl molar ratio (1.3×10^{-3}) is much higher than that expected in seasalt aerosols (4.7×10^{-5}), showing that the cyclic contribution is small.

δ^6Li has a large range, comparable to $\delta^{13}C$ and $\delta^{11}B$, from -6.0‰ in the headwaters of the Yana to -32.2‰ at the mouth of the Orinoco (Fig. 8); the latter is essentially the same as the seawater value (-32.3 ± 1 ‰). The mode is -21‰. The evaporite endmember stands out in plots of δ^6Li vs. the major ions and TZ^+ ($TZ^+ = \{Na^+ + K^+ + 2Mg^{2+} + 2Ca^{2+}\}$ in 10^{-6} equivalents per kg) (Fig. 8). δ^6Li is ~-20‰ for rivers with

evaporites in their drainages which have high TZ^+. This value is different from seawater indicating that lithium associated with evaporites has a distinctive δ^6Li. A less obvious relationship is the trend toward heavier values than -20‰ as the major ion concentrations increase. This could mean that in regions where, due to tectonics or lithology, the weathering is rapid and superficial, the heavier lithium is released preferentially whereas in transport-limited regions where reaction is slow but complete even the light fraction which is preferentially held in the clays is being solubilized.

There is no simple relationship between δ^6Li and 1/Li (Fig. 9a) or Si/TZ^+ (Fig. 9b) except that light δ^6Li correlates with the intense weathering in tropical shield rivers (Negro, Parguaza, Caroni). The isotopic systematics are complicated because of fractionation associated with reaction and retention in secondary clays as well as the different isotopic values in the various basement rocks. Samples with comparable Si/TZ^+ ratios have a wide range in δ^6Li, suggesting that δ^6Li carries unique information not available from the major ions. Plots of δ^6Li vs. $^{87}Sr/^{86}Sr$ have broadly similar trends as those of δ^6Li vs. Si/TZ^+ (Fig. 9b,c,d), Si/TZ^+ and $^{87}Sr/^{86}Sr$ both being indicators of silicate weathering. The fluvial values for the Negro (0.738, -10.5‰), Ganges headwaters (0.740, -11.3‰), and Caroni (0.732, -17.0‰) plot in the field of silicic rocks (Fig. 6); the Parguaza (0.85, -6.6‰) is very radiogenic and light because of the evolved composition of its bedrock. The Yangtze (0.711, -32‰) is much like seawater. The Verkhnyaya Yazobaya in Siberia, the Madeira, Ganges, Brahmaputra, and Mississippi (at Little Falls) fall in an intermediate region between the silicic rocks, carbonate rocks, and seawater fields. Samples from sedimentary basins, e.g. Biryuk, Cojedes and the Mississippi fall around -20 ‰ with $^{87}Sr/^{86}Sr$ ~0.709 in the carbonate rocks field. The upper Amazon gets most of its dissolved load from marine evaporites and carbonates in the Andes as is shown by the evaporite-like δ^6Li (-19.6‰) and $^{87}Sr/^{86}Sr$ (0.7086) (Chan *et al.*, 1992). The Yana headwaters (0.711, -6.0‰) have an unusual composition which cannot be explained in terms of its bedrock lithology, the Permian detrital rocks of the Verkhoyansk foldbelt.

Rivers with large drainage basins like the Amazon, Mississippi, and Yangtze, have relatively homogeneous $^{87}Sr/^{86}Sr$ ratios (~0.711), because they integrate the diverse geological terrains within their drainage basins and are dominated by limestones. In contrast, there is quite a large range of δ^6Li (-20 to -32 ‰) in these big rivers. The Li and Sr isotope systems seem to be decoupled in the continental weathering regime.

From the above observations, the important processes affecting river dissolved Li isotopic compositions are isotopic fractionation between solution and secondary minerals and the degree of weathering. Overlain on this is the effect of the bedrock type.

Flux Calculations and the oceanic budget

The flux and discharge weighted average concentration of lithium and δ^6Li are calculated using annual discharge values in Palmer and Edmond (1989) and Gordeev *et al.* (1996) (Table 5, Fig. 10). The rivers studied here account for about one third of the global runoff. The means are 215 nM and -22.9‰. This value, obtained on the measured samples, is extrapolated to represent the continental input. The seasonal and annual variability of rivers can give rise to significant uncertainty (~50%) in the estimation of elemental fluxes and, to an unknown degree, isotope ratios (Palmer and Edmond, 1989). Only one pair of lower Mississippi samples is available to compare low versus high stage values (Table 2) (Chan *et al.*, 1992). There is a 2.4‰ difference in isotopic composition, with the lighter value at low flow, and almost a factor of 4 difference in concentration. This is consistent with the "weathering-limited" argument.

Lithium is conservative in the ocean at 26 μM with a long residence time of about a million years. The isotopic composition is homogeneous with depth (-32.3‰) and does not show inter-ocean variation (Chan and Edmond, 1988). The two principal sources of lithium to the ocean are river runoff and ridge-crest hydrothermal solutions. The updated estimate of the river input of Li (concentrations in the range of 50-800 nM) gives a flux

calculated from mean concentration and runoff (37,400 km^3/yr; Palmer and Edmond, 1989) of 8.0 $x10^9$ mol/yr. This is lower than previous estimates of 14 x 10^9 mol/yr (Morozov, 1969; Stoffyn-Egli and Mackenzie, 1984; Von Damm *et al.*, 1985). Lithium behaves conservatively in estuaries (Stoffyn-Egli, 1982; Colten and Hanor, 1985) and the isotopic composition is probably not altered by processes in the freshwater-seawater mixing zone. Above 200°C, reaction between seawater and basalts extracts Li from basalts (Seyfried *et al.*, 1984), and hydrothermal solutions are therefore highly enriched in Li (411-1,322 μM; Edmond *et al.*, 1979; Von Damm *et al.*, 1985). Incomplete extraction of Li from igneous minerals or partial retention in secondary phases causes a small isotope fractionation from MORB (-3.4 to -4.7 ‰) and thus the solution compositions range from -6 to -10‰ ($\alpha \approx 1.005$ at ~350°C; Chan and Edmond, 1988; Chan *et al.*, 1993, 1994). Thus, conclusively, seawater Li is isotopically heavier than its principal sources.

Updated calculations can be made of the lithium isotope budget in the ocean following Chan *et al.* (1992). The only significant difference is that the riverine input term is much better constrained and shifted from -19‰ to -23‰. The steady state isotopic composition of Li in ocean water can be represented by the following mass balance equation, as for Sr (Brass, 1976):

$$(\delta^6Li)_i = f_r(\delta^6Li)_r + f_h(\delta^6Li)_h = f_r(\delta^6Li)_r + (1-f_r)(\delta^6Li)_h$$

where f's are fractions of the total flux due to river and hydrothermal inputs and subscripts i, r, h denote input, river, and hydrothermal, respectively. However this balance cannot be closed unless fractionation of Li, probably by preferential removal of the lighter isotope into authigenic clays, is accounted for by a fractionation factor α (Chan *et al.*, 1992),

$$1/\alpha = (^6Li/^7Li)_{ocean}/(^6Li/^7Li)_i = (^6Li/^7Li)_{ocean}/(^6Li/^7Li)_o$$

where the subscript o stands for output. The data we have at present are inadequate to address the question of whether dissolved lithium is at steady state in the ocean but this is assumed to gain an understanding of the oceanic budget. It is interesting to note that the Li/Ca ratio in planktonic forams over the past 40 m.y. remains relatively constant (Delaney and Boyle, 1986) and that the hydrothermal flux has not varied much over this period. Using the same values for the river and hydrothermal fluxes and $(\delta^6Li)_h$ as in Chan *et al.* (1992) and the updated $(\delta^6Li)_r$, then $(\delta^6Li)_i$ is -9.8 ‰ and α is 1.023. The lighter isotope must be preferentially incorporated into sediments with this fractionation factor if the seawater ratio, which is heavier than its sources, is to be maintained at steady state. Considering that the α for low temperature weathering of seafloor basalts is 1.019 (Chan *et al.*, 1992), the isotopic mass balance problem is still not solved. Authigenic clays are enriched in Li (200-500 ppm in smectites) relative to other rock types (igneous rocks 30 ppm, detrital clays 70-80 ppm) and could be the sink. It is worthwhile to consider if a fractionation factor of 1.023 is reasonable. Lithium fractionation during ion exchange onto zeolites was found to be 1.022 by Taylor and Urey (1938), and Dead Sea aragonite gives an apparent α of ~1.020 (Chan, unpublished).

The calculation can be done in reverse: using the value for α=1.019 determined for low temperature basalt alteration (Chan *et al.*, 1992) and other parameters as above, the hydrothermal flux can be calculated. The result (63% of total input flux, 14×10^9 mol/yr) is about twice the river flux of lithium (37%). As a comparison, the flux of lithium by emplacement of oceanic crust is also about 14×10^9 mol/yr if the basalt concentration is assumed to be 6 ppm, the crustal production rate is 3 km^2/yr (Chase, 1972), the upper 2 km of the oceanic crust is available for extraction of lithium by hydrothermal fluids and the basalt density is 2.8 g/cm^3. In terms of water, the hydrothermal flux is 3.6 to 1.4×10^{13} kg/yr using 400-1,000 µmol/kg of Li. This is comparable to the geophysical estimate of hydrothermal water flux assuming all flow is at 350°C and ignoring diffuse flow (estimated at 3-6 $\times 10^{13}$ kg/yr; Elderfield and Schultz, 1996). This estimate from lithium is only 1/3

to 1/7 of the estimates derived from the ^{3}He budget, the Sr isotopes and Mg (1 x 10^{14} kg/yr) if only the ridge-axis fluxes are considered (Edmond *et al.*, 1979; Palmer and Edmond, 1989). The Mg budget can be made compatible with a low axial hydrothermal water flux if most of the Mg is lost on the ridge flanks (Mottl and Wheat, 1994), but there is no observed evidence in DSDP/ODP cores of movement of water in ridge flank sediments at this time. The low axial heat flux can also be compatible with ^{3}He inventory if a lower global mean ^{3}He/heat ratio is used (Lupton *et al.*, 1989). But, if plumes and sediment-hosted vents, which are not representative, are excluded from the global data set, the original ^{3}He/heat estimate is quite robust (Jenkins *et al.*, 1978).

The present estimates of river and hydrothermal inputs (2.3 x 10^{10} mol/yr) almost balances the Li output from the oceans as estimated by Stoffyn-Egli and Mackenzie (1984), 0.6-1.7 x 10^{10} mol/yr.

Conclusions

(1) The Li concentration and δ^6Li in the dissolved load of the world's large rivers have been determined by the recently developed phosphate TIMS method (You and Chan, 1996). The flow-weighted mean is 215 nM and -22.9‰. The river input flux is 8.0x10^9 mol/yr and the hydrothermal flux is 1.5x10^{10} mol/yr. The residence time is 1.5 million years given the oceanic inventory of 3.6 x 10^{16} mol Li.

(2) Fluvial isotopic compositions display a large range, -6.0 to -32.2‰, comparable to the range in ^{87}Sr/^{86}Sr (0.704-0.92). There is no direct relationship between δ^6Li and lithology, but in general, evaporites are -20 to -22‰, carbonates -26 to -32‰, black shales -26‰, varied siliceous terrains -6 to -28 ‰, and shields -6.6 to -17 ‰, all lighter than seawater (-32.3‰). The lithium isotopic composition appears to be more a function of the fractionation processes during partial weathering of aluminosilicate rocks to form

neoformed clays, and in the case of evaporites, the concentration in the solution from which the secondary lithium minerals precipitated, rather than bedrock type or age.

(3) According to lithium isotope mass balance calculations based on basaltic alteration with $\alpha = 1.019$, the hydrothermal flux must be comparable to the river flux and not substantially larger as estimated on the basis of oceanic ^3He inventory. Alternatively, there must be a more efficient sink for the lighter isotope with $\alpha \approx 1.023$.

(4) Comparison with the major element and Sr isotope dataset suggests that the important processes affecting river dissolved Li isotopic compositions are isotopic fractionation between solution and secondary minerals and the degree of weathering. Overlain on this is the effect of the bedrock type making the lithium isotopic system very complicated. The dissolved Li isotope data alone are not yet sufficient to distinguish the two effects.

Acknowledgments — This study could not have been possible without the generosity of our colleagues who supplied precious river samples. We thank S. Krishnaswami and our other Indian colleagues who originally supplied the Ganges-Brahmaputra samples, K. Falkner for the Mackenzie , R. Collier for the Columbia, G. Booth and P. Swarzenski for the Mississippi and T. Buerkert for the loess sample. Rock data are from samples provided by G. Byerly, A. Katz, A. Starinsky, D. Bottomley, W. P. Leeman and N. Sturchio in association with other studies. T. Blanchard provided valuable assistance in the laboratory. The reviews of D. MacDougall and two anonymous referees greatly improved the paper. This work was supported by the MIT Student Research Fund (Y. H.) and NSF grants OCE 9314708 and EAR 9506390 to L.-H. C and NSF grants to J. M. E.

References

Anderson M. A., Bertsch P. M., and Miller W. P. (1989) Exchange and apparent fixation of lithium in selected soils and clay minerals. *Soil Science* **148**, 46-52.

Brass G. W. (1976) The variation of marine $^{87}Sr/^{86}Sr$ ratio during Phanerozoic time: interpretation using a flux model. *Geochim. Cosmochim. Acta* **40**, 721-730.

Cameron E. M., Hall G. E. M., Veizer J., and Krouse H. R. (1995) Isotopic and elemental hydrogeochemistry of a major river system: Fraser River, British Columbia, Canada. *Chem. Geol.* **122**, 149-169.

Chan L. -H. (1987) Lithium isotope analysis by thermal ionization mass spectrometry of lithium tetraborate. *Anal. Chem.* **59**, 2662-2665.

Chan L. -H. and Edmond J. M. (1988) Variations of lithium isotope composition in the marine environment: A preliminary report. *Geochim. Cosmochim. Acta* **52**, 1711-1717.

Chan L. -H., Edmond J. M., Thompson G., and Gillis K. (1992) Lithium isotopic composition of submarine basalts: implications for the lithium cycle in the oceans. *Earth Planet. Sci. Lett.* **108**, 151-160.

Chan L. -H., Edmond J. M., and Thompson G. (1993) A lithium isotope study of hot springs and metabasalts from mid-ocean ridge hydrothermal systems. *J. Geophys. Res.* **98**, 9653-9659.

Chan L. -H., Gieskes J. M., You C. -F., and Edmond J. M. (1994) Lithium isotope geochemistry of sediments and hydrothermal fluids of the Guaymas Basin, Gulf of California. *Geochim. Cosmochim. Acta* **58**, 4443-4454.

Chan L. -H., You C. -F., and Leeman W. P. (1995) Lithium isotope composition of Central American Volcanic Arc lavas; evidence of slab-derived fluids in magma genesis. Geol. Soc. Am. Annual Meeting Abstracts with Programs **27**, A-38 (abstr.).

Chan L. -H., Sturchio N. C., and Katz A. (1997) Lithium isotope study of the Yellowstone hydrothermal system. *EOS, Trans. Am. Geophys. U.* **78**, F802 (abstr.).

Chase C. G. (1972) The N plate problem of plate tectonics. *Geophys. J. Roy. Astron. Soc.* **29**, 117-122.

Cocco G., Fanfani L., and Zanazzi P. F. (1978) Lithium. In *Handbook of Geochemistry.* K. H. Wedepohl, ed. Springer, Berlin, pp. 3-A-1 - 3-A-7.

Colten V. A. and Hanor J. S. (1985) Variations in dissolved lithium in the Mississippi River and Mississippi River Estuary, Louisiana, U.S.A., during low river stage. *Chem. Geol.* **47**, 85-96.

Delaney M. L. (1986) Lithium in foraminiferal shells: Implications for high-temperature hydrothermal circulation fluxes and oceanic crustal generation rates. *Earth Planet. Sci. Lett.* **80**, 91-105.

Edmond J. M. (1992) Himalayan tectonics, weathering processes, and the strontium isotope record in marine limestones. *Science* **258**, 1594-1597.

Edmond J. M., Measures C., McDuff R. E., Chan L. H., Collier R., Grant B., Gordon L. I., and Corliss J. B. (1979) Ridge crest hydrothermal activity and the balances of the major and minor elements in the ocean: the Galapagos data. *Earth Planet. Sci. Lett.* **46**, 1-18.

Edmond J. M., Palmer M. R., Measures C. I., Grant B., and Stallard R. F. (1995) The fluvial geochemistry and denudation rate of the Guayana Shield in Venezuela, Colombia and Brazil. *Geochim. Cosmochim. Acta* **59**, 3301-3325.

Edmond J. M., Palmer M. R., Measures C. I., Brown E. T., and Huh Y. (1996) Fluvial geochemistry of the eastern slope of the northeastern Andes and its foredeep in the drainage of the Orinoco in Colombia and Venezuela. *Geochim. Cosmochim. Acta* **60**, 2949-2976.

Elderfield H. and Schultz A. (1996) Mid-ocean ridge hydrothermal fluxes and the chemical composition of the ocean. *Annu. Rev. Earth Planet. Sci.* **24**, 191-224.

Falkner K. K. *et al.* (1997) Minor and trace element chemistry of Lake Baikal, its tributaries and surrounding hot springs. *Limnol. Oceanogr.* **42**, 329-345.

Flesch G. D., Anderson A. R., Jr., and Svec H. J. (1973) A secondary isotopic standard for $^{6}Li/^{7}Li$ determinations. *Intl. J. Mass Spectrom. Ion Phys.* **12**, 265-272.

Gieskes J. M. (1983) The chemistry of interstitial waters of deep sea sediments: Interpretation of Deep Sea Drilling data. In *Chemical Oceanography*. Academic Press, London, pp. 221-269.

Goldstein S. J. and Jacobsen S. B. (1987) The Nd and Sr isotopic systematics of river-water dissolved material: Implications for the sources of Nd and Sr in seawater. *Chem. Geol. (Isotope Geosciences Section)* **66**, 245-272.

Gordeev V. V., Martin J. M., Sidorov I. S., and Sidorova M. V. (1996) A reassessment of the Eurasian river input of water, sediment, major elements and nutrients to the Arctic Ocean. *Am. J. Sci.* **296**, 664-691.

Heier N. S. and Billings G. K. (1978) Lithium. In *Handbook of Geochemistry*. K. H. Wedepohl, ed. Springer, Berlin, pp. 3-G-1—3-H-1.

Horstman E. L. (1957) The distribution of lithium, rubidium, and caesium in igneous and sedimentary rocks. *Geochim. Cosmochim. Acta* **12**, 1-28.

Hu M.-H., Stallard R. F., and Edmond J. M. (1982) Major ion chemistry of some large Chinese rivers. *Nature* **298**, 550-553.

Huh Y., Tsoi M.-Y., Zaitsev A., and Edmond J. M. (1998a) The fluvial geochemistry of the rivers of Eastern Siberia I: Tributaries of the Lena River draining the sedimentary platform of the Siberian Craton. *Geochim. Cosmochim. Acta* in press.

Huh Y., Panteleyev G., Babich D., Zaitsev A., and Edmond J. M. (1998b) The fluvial geochemistry of the rivers of Eastern Siberia II: Tributaries of the Lena, Omoloy, Yana, Indigirka, Kolyma, and Anadyr draining the collisional/accretionary zone of the Verkhoyansk and Cherskiy Ranges. *Geochim. Cosmochim. Acta* in press.

Jenkins, W. J., Edmond J. M., and Corliss J. B. (1978) Excess ^{3}He and ^{4}He in Galapagos submarine hydrothermal waters. *Nature* **272**, 156-158.

Krishnaswami S., Trivedi J. R., Sarin M. M., Ramesh R., and Sharma K. K. (1992) Strontium isotopes and rubidium in the Ganga-Brahmaputra river system: Weathering in the Himalaya, fluxes to the Bay of Bengal and contributions to the evolution of oceanic $^{87}Sr/^{86}Sr$. *Earth Planet. Sci. Lett.* **109**, 243-253.

Lupton J. E., Baker E. T., and Massoth G. J. (1989) Variable ^{3}He/heat ratios in submarine hydrothermal systems: evidence from two plumes over the Juan de Fuca ridge. *Nature* **337**, 161-164.

Morozov N. P. (1969) Geochemistry of the alkali metals in rivers. *Geochem. Int.* **6**, 585-594.

Morton J. L. and Sleep N. H. (1985) A mid-ocean ridge thermal model: constraints on the volume of axial hydrothermal heat flux. *J. Geophys. Res.* **90**, 11,345-11,353.

Mottl M. J. and Wheat C. G. (1994) Hydrothermal circulation through mid-ocean ridge flanks: Fluxes of heat and magnesium. *Geochim. Cosmochim. Acta* **58**, 2225-2237.

O'Neil J. R. (1986) Theoretical and experimental aspects of isotopic fractionation. In *Stable Isotopes in High Temperature Geological Processes.* Reviews in Mineralogy, (eds. Valley J. W., Taylor H. P., Jr., and O'Neil J. R.), Mineralogical Society of America, pp. 1-40.

Olsher U., Izatt R. M., Bradshaw J. S., and Dalley N. K.(1991) Coordination chemistry of lithium ion: A crystal and molecular structure review. *Chem. Rev.* **91**, 137-164.

Palmer M. R. and Edmond J. M. (1989) The strontium isotope budget of the modern ocean. *Earth Planet. Sci. Lett.* **92**, 11-26.

Palmer M. R. and Edmond J. M. (1992) Controls over the strontium isotope composition of river water. *Geochim. Cosmochim. Acta* **56**, 2099-2111.

Reeder S. W., Hitchon B., and Levinson A. A. (1972) Hydrogeochemistry of the surface waters of the Mackenzie River drainage basin, Canada—I. Factors controlling inorganic composition. *Geochim. Cosmochim. Acta* **36**, 825-865.

Ronov A. B., Migdisov A. A., Voskresenskaya N. T., and Korzina G. A. (1970) Geochemistry of lithium in the sedimentary cycle. *Geochem. Int.* **7**, 75-102.

Sarin M. M., Krishnaswami S., Dilli K., Somayajulu B. L. K., and Moore W. S.(1989) Major ion chemistry of the Ganga-Brahmaputra river system: Weathering processes and fluxes to the Bay of Bengal. *Geochim. Cosmochim. Acta* **53**, 997-1009.

Schumm S. A. and Winkley B. R., eds. (1994) *The Variability of Large Alluvial Rivers.* New York, ASCE Press.

Seyfried W. E., Janecky D. R., and Mottl M. J. (1984) Alteration of the oceanic crust: Implications for geochemical cycles of lithium and boron. *Geochim. Cosmochim. Acta* **48**, 557-569.

Stallard R. F. and Edmond J. M. (1983) Geochemistry of the Amazon 2. The influence of geology and weathering environment on the dissolved load. *J. Geophys. Res.* **88**, 9671-9688.

Stein C. A. and Stein S. (1994) Constraints on hydrothermal heat flux through the oceanic lithosphere from global heat flow. *J. Geophys. Res.* **99**, 3081-3095.

Stoffyn-Egli P. (1982) Conservative behavior of dissolved lithium in estuarine waters. *Estuarine, Coastal and Shelf Science* **14**, 577-587.

Stoffyn-Egli P. and Mackenzie F. T. (1984) Mass balance of dissolved lithium in the oceans. *Geochim. Cosmochim. Acta* **48**, 859-872.

Taylor T. I. and Urey H. C. (1938) Fractionation of the lithium and potassium isotopes by chemical exchange with zeolites. *J. Chem. Phys.* **6**, 429-438.

Vine J. D. (1980) Where on Earth is all the lithium? *USGS Open File Report* 80-1234.

Von Damm K. L., Edmond J. M., Grant B., Measures C. I., Walden B., and Weiss R. F. (1985) Chemistry of submarine hydrothermal solutions at 21°N, East Pacific Rise. *Geochim. Cosmochim. Acta* **49**, 2197-2220.

Wadleigh M. A., Veizer J., and Brooks C. (1985) Strontium and its isotopes in Canadian rivers: Fluxes and global implications. *Geochim. Cosmochim. Acta* **49**, 1727-1736.

Wenger M. and Armbruster T. (1991) Crystal chemistry of lithium: oxygen coordination and bonding. *Eur. J. Mineral.* **3**, 387-399.

You C. -F. and Chan L. -H. (1996) Precise determination of lithium isotopic composition in low concentration natural samples. *Geochim. Cosmochim. Acta* **60**, 909-915.

You C. -F., Chan L. -H., Spivack A. J., and Gieskes J. M. (1995) Lithium, boron, and their isotopes in sediments and pore waters of Ocean Drilling Program Site 808, Nankai Trough: Implications for fluid expulsion in accretionary prisms. *Geology* **23**, 37-40.

Zhang L. (1997) Lithium isotopes in pore waters from ODP Leg 152, offshore of Greenland: sediment-water interactions. M.S. thesis, Louisiana State University.

Table 1. Chemical data for lithium in river water samples. Original lithium data from this study are in bold type.
Li concentrations determined by ICP-MS are noted with *; the others were determined by ID-TIMS. n.d. = not determined.
Symbols for geology are: E=Evaporites, BS=Black Shales, C=Carbonates, B=Biotite, M=Metamorphics, V=Volcanics, F=Fractionated, Acid=Acid Intrusions, HH=High Himalayas, TBH=Trans-Baikal Highlands, P=Platform, Verkho=Verkhoyansk Foldbelt, A=Accretionary zone.

River Name	Station Number	Geology	Na	K	Mg	Ca	Cl	SO_4	HCO_3	Si	pH	Sr	$^{87}Sr/^{86}Sr$	Li		δ^6Li
			<			μM				>		μM		nM		‰
AMAZON [a,b]																
Amazon @ Iquitos	S302	Andes, E	225	35.5	96.7	551	156	70	1252	174	7.31	1.11	0.7086	**205**	*	**-19.6**
Madeira	S328	Andes, BS	64.5	31.1	63.6	107	12.6	35.5	304	142	6.71	0.26	0.7191	**151**	*	**-25.8**
Negro	S327	Shield, black	17.3	10.1	6.1	8.3	7.6	3.1	9	65	5.0	0.03	0.7378	**33.5**	*	**-10.5**
Amazon ab. Xingu	S336	Mouth	67.5	23.4	44.4	137	31.2	21.9	359	132	6.80	0.32	0.7109	**96.5**		**-21.6**
ORINOCO [b,c]																
Parguaza	OR309	Shield, F	19.7	15.5	1.5	4.5	5.5	0.8	7	96	5.9	16.7	0.8535	**70.7**		**-6.6**
Apure @ El Perro	OR317	Andes, C	163	47.7	139	557	15	145	1230	171	7.8	1.10	0.7124	**83.1**	*	**-32.0**
Cojedes @ Sucre	OR750	Andes, E	1410	81.7	604	2600	788	2340	2196	129	7.9	9.40	0.7098	**723**	*	**-22.1**
Orinoco@ C. Bolivar	OR451	Mouth	91.0	19.0	48.9	133	34	43	321	128	7.9	0.31	0.7182	**53.3**		**-32.2**
Caroni @ Ordaz	OR327	Shield, black	21.3	9.6	7.0	10.3	6.9	1.2	21	85	6.3	37.6	0.7322	**27.1**	*	**-17.0**
GANGES-BRAHMAPUTRA [b,d]																
Ganges @ Rishikesh	3	HH, M	145	40	239	398	42	162	1004	152	n.d.	0.80	0.7399	**471**		**-11.3**
Ganges @ Patna	17	HH+Traps	702	83	497	970	217	n.d.	3132	n.d.	n.d.	1.82	0.7245	**579**		**-22.6**
Brahmaputra @ Goalpara [e]	22	HH+Suture	80	46	148	318	29	99	884	118	n.d.	0.67	0.7197	**436**		**-19.6**
SIBERIAN RIVERS [f]																
Verkhnyaya Yazobaya	UL427	TBH, B	32.5	13.7	38.1	147	19.0	0.5	377	73	6.61	0.48	0.7406	**39.9**		**-27.6**
Timpton	UL119	Shield	46.9	4.3	43.7	105	9.2	22.3	299	110	n.d.	0.34	0.7120	**71.5**		**-18.6**
Biryuk	UL436	P, E	2780	55.4	1420	4010	2380	4460	2443	40	8.22	32.8	0.7088	**3350**	*	**-20.8**
Lena ab Aldan	UL102	P+Shield	451	14.5	141	391	544	110	675	76	n.d.	1.42	0.7102	**260**	*	**-20.6**
Aldan @ mouth	UL101	P+Sh+Verkho	44.0	11.2	149	321	15.0	44.8	891	73	n.d.	1.16	0.7113	**111**	*	**-29.0**
Sobolokh	UL602	Verkho	155	10.7	175	520	86.6	162	1132	50	7.83	2.47	0.7137	**232**	*	**-21.4**
Lena @ Klusur	UL607	Mouth	273	12.1	137	337	238	93.0	796	57	7.61	1.10	0.7105	**221**		**-21.0**
Yana ab Adycha	YN109	Verkho	76.7	19.3	98.5	180	17.6	66.4	467	79	7.16	0.95	0.7108	**125**	*	**-6.0**
Yana @ mouth	YN101	Verkho+A	54.9	19.6	103	258	17.2	106	587	66	7.69	0.84	0.7100	**101**	*	**-27.1**
Indigirka bl. B. Ercha	IG121	A	48.1	14.3	99.9	265	10.0	74.4	672	65	7.50	0.82	0.7097	**122**	*	**-25.2**
Kolyma @ head	KY103	A, V	78	9.4	82.2	203	5.5	136	356	108	7.40	0.71	0.7086	**123**	*	**-20.4**
CHINESE RIVERS [b,g]																
Yangtze	C40	P, C+H	227	34.8	318	794	159	147	2011	115	n.d.	2.05	0.7109	**573**		**-31.9**
Qiantang	C23	P, C	204	38.7	122	451	127	54	1110	76	n.d.	n.d.	n.d.	**35.1**	*	**-26.4**
BAIKAL RIVERS [h]																
Selenga		Acid, V	307	34.7	224	605	58.6	n.d.	n.d.	128	n.d.	1.92	0.7079	490		-29.9
Upper Angara		Rift, Acid	38.1	10.6	37.6	183	16.1	n.d.	n.d.	50	n.d.	0.48	0.7084	157		-26.2
Barguzin		TBH, Acid	82.9	22.3	84.3	554	13	n.d.	n.d.	n.d.	n.d.	1.17	0.7084	234		-30.7
Barguzin		TBH, Acid	105	22.6	98.3	512	n.d.	n.d.	n.d.	101	n.d.	1.31	0.7085	276		-21.5
Turka		TBH, Acid	103	11.8	57.1	405	16	n.d.	n.d.	186	5.5-6	0.56	0.7089	266		-25.1

a. Major elements data from Stallard and Edmond (1983). b. Strontium data from Palmer and Edmond (1992). c. Major elements data from Edmond *et al.* (1995, 1996).
d. Major elements data from Sarin *et al.* (1989). e. Strontium data from Krishnaswami *et al.* (1992). f. Chemical data from Huh *et al.* (in review a,b); Huh (unpublished).
g. Chemical data from Hu *et al.* (1982). h. All chemical data from Falkner *et al.* (1997).

Table 2. Additional data for lithium from "grab" samples. Original lithium data are in bold type. Li concentrations in the Mississippi and Jordan systems were determined by flame emission; others were determined by ID-TIMS. Abbreviations for geology are: PC=Precambrian, Pz=Paleozoic, Mz=Mesozoic, K=Cretaceous, Cz=Cenozoic, T=Tertiary, Sed=sedimentary, Met=metamorphic, Ig=igneous rocks, C=carbonates. n.d.=not determined.

River Name	Station Number	Geology	$^{87}Sr/^{86}Sr$	Li nM	δ^6Li ‰
MISSISSIPPI					
Lower Mssp, LA (high flow) [a]	229	Mz, Cz sand, silt clay	0.7101	450	-17.7
Lower Mssp, LA (low flow) [a]	MSR-1	Mz, Cz sand, silt clay	0.7096	1660	-15.3
Mssp @ Little Falls, MN	R1	PC Shield	0.7136	**631**	**-20.8**
Mssp @ Red Wing, MN	R2	PC Shield	0.7102	**2950**	**-16.7**
Missouri @ St Charles, MO	R5	Pz-Cz Sed	0.7092	**4070**	**-17.6**
Ohio @ Ohmsted, IL	R8	Pz Met sediments	0.7108	**707**	**-19.8**
Mssp @ Arkansas City, AR	R11		0.7098	**1560**	**-13.9**
Mssp @ St Francisville, LA	R13		0.7098	**1670**	**-16.1**
MACKENZIE [b]	69°29'	K marine sediments	0.7110	**766**	**-17.6**
	68°29'	and Ig+Met	n.d.	n.d.	**-15.5**
COLUMBIA [c]	2	complex collision zone		**244**	**-14.6**
Columbia	4		0.7108	n.d.	**-15.9**
FRASER @ Fort Langley [d]		C, Ig+Met , V	0.7120	**106**	**-28.8**
JORDAN [a]					
Jordan @ Yarmouk		basic V	n.d.	4740	-16.2
Jordan @ Allenby		C	n.d.	11700	-18.5

a. Lithium data from Chan *et al.* (1992).
b. Strontium data at median stage from Wadleigh *et al.* (1985).
c. Strontium data at median stage from Goldstein and Jacobsen (1987).
d. Strontium data at low stage from Wadleigh *et al.* (1985).

Table 3. Lithium concentration and isotopic composition of lake waters.

Name	Li (μM)	δ^6Li (‰)
Lake Tanganyika, 1410m[a]	2.1	-32.2
Caspian Sea [a]	41.2	-31.1
Dead Sea, 275m [a]	1969	-33.3
Lake Baikal [b]	294	-27.9 to -32.2

a. Chan and Edmond (1988). b. Falkner *et al.* (1997)

Table 4. δ^6Li of carbonate samples.

Sample Description	δ^6Li (‰)	Li (ppm)	Reference
Carbonates, ODP core 851A	-6.2 to -31.0[a]		You and Chan, 1996
Forams, ODP core 130-806B	-19 to -41		You and Chan, 1996
Oolite, Bahamas	-21.8	1.0	Zhang and Chan, unpublished
Carbonate ooze, MANOP C[b]	-24.3	0.4	Zhang and Chan, unpublished
Carbonate ooze, MANOP C[c]	-27.0		Chan, unpublished
Marine chalk, Judea Mt.	-12.1	1.5	Chan, unpublished
Impure limestones, Jurassic Ellis Gp.[c]	-11.0	0.6	Chan et al.,1997
Limestone, Mississippian[d]	-21.6	2.1	Chan, unpublished
Limestone, Mississippian[c]	-21.9	1.2	Chan, unpublished

[a] The values are light (-6.2‰) close to the seafloor and heavier (-31.0‰) at depth.
b leached in 0.1N HCl.
c leached in 0.5N acetic acid.
[d] total digest.

Table 5. Flux of Li and δ^6Li from major world rivers. Discharge values are from Palmer and Edmond (1989) and Gordeev et al. (1996). Drainage areas are from Schumm & Winkley (1994).

RIVER	Discharge km^3/yr	Area 10^3 km^2	Li nM	δ^6Li ‰	Li flux 10^9 mol/yr	Li Yield $mol/km^2/yr$
Amazon	6930	6,900	96.5	-21.6	0.669	96.9
Congo	1230	3,700	125		0.154	41.6
Orinoco	1100	899	53.3	-32.2	0.0586	65.2
Yangtze	900	1,943	572	-31.9	0.515	265
Brahmaputra	603	935	436	-19.6	0.263	281
Mississippi	580	3,212	813	-16.4	0.472	147
Lena	532	3,028	221	-21.0	0.118	38.8
Ganges	450	1,114	579	-22.6	0.260	234
Mackenzie	289	1,805	766	-17.6	0.221	123
Columbia	172	668	244	-14.6	0.0420	62.9
Fraser	96	233	106	-28.8	0.0102	43.6
Indigirka	61	362	122	-25.2	0.0074	20.6
Yana	34	238	101	-27.1	0.0035	14.5
Total	12977.3	25,037			2.79	
Discharge-weighted average			215	-22.9		113

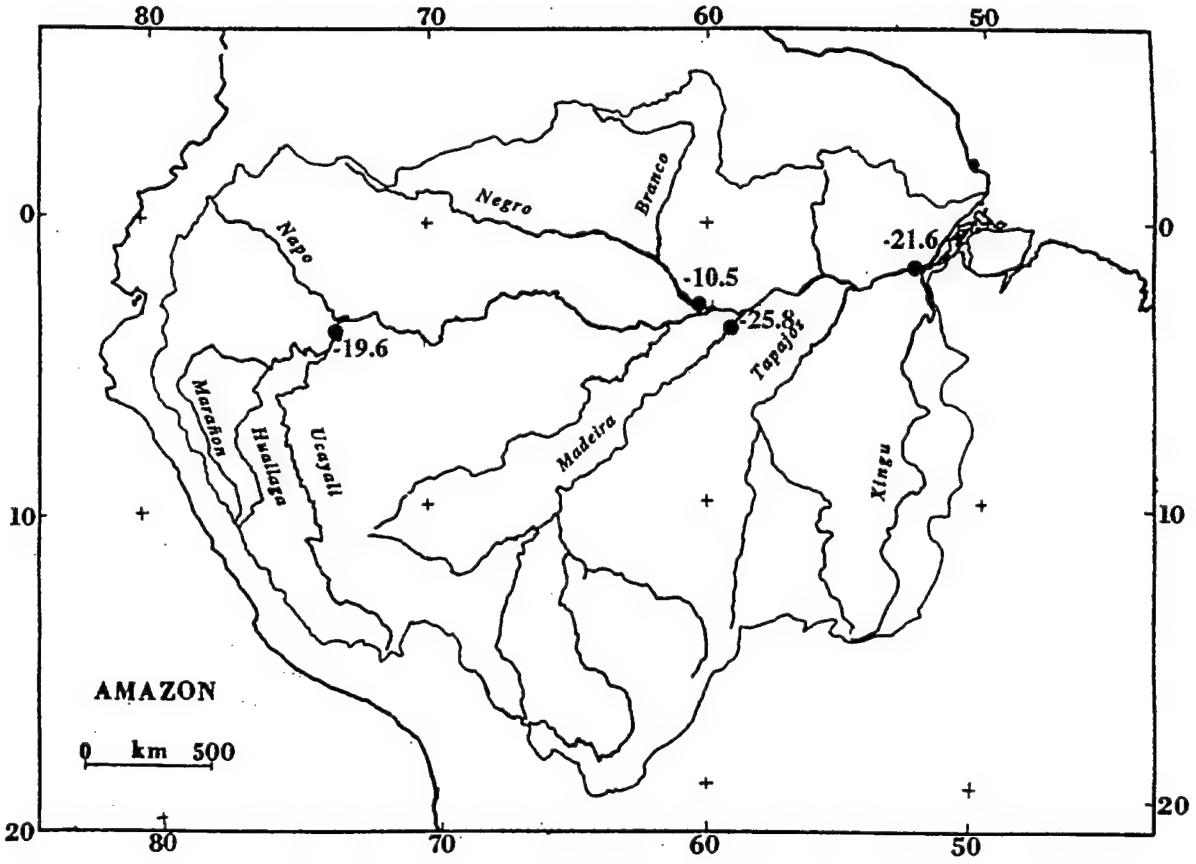

Figure 1. Location map of the samples from the Amazon basin. The sample locations are marked with the δ^6Li (‰) values. At Iquitos where the Andean tributaries come together, the δ^6Li is -19.6‰. The Negro, a black tropical shield river, gives -10.5‰. The Madeira, draining black shales and whose headwaters are in the Andes, is -25.8‰. The lower Amazon above the Xingu is -21.6‰.

Figure 2. Location map of the samples from the Orinoco basin, after Edmond *et al.* (1996). The sample locations are marked with the δ^6Li (‰) values. The Parguaza drains the extremely fractionated rapakivi granites of the Guayana Shield and is -6.6‰. Another shield river, the Caroni, is -17.0‰. The Cojedes is rich in evaporites and is -22.1‰, and the lower Orinoco at Ciudad Bolivar is -32.2‰.

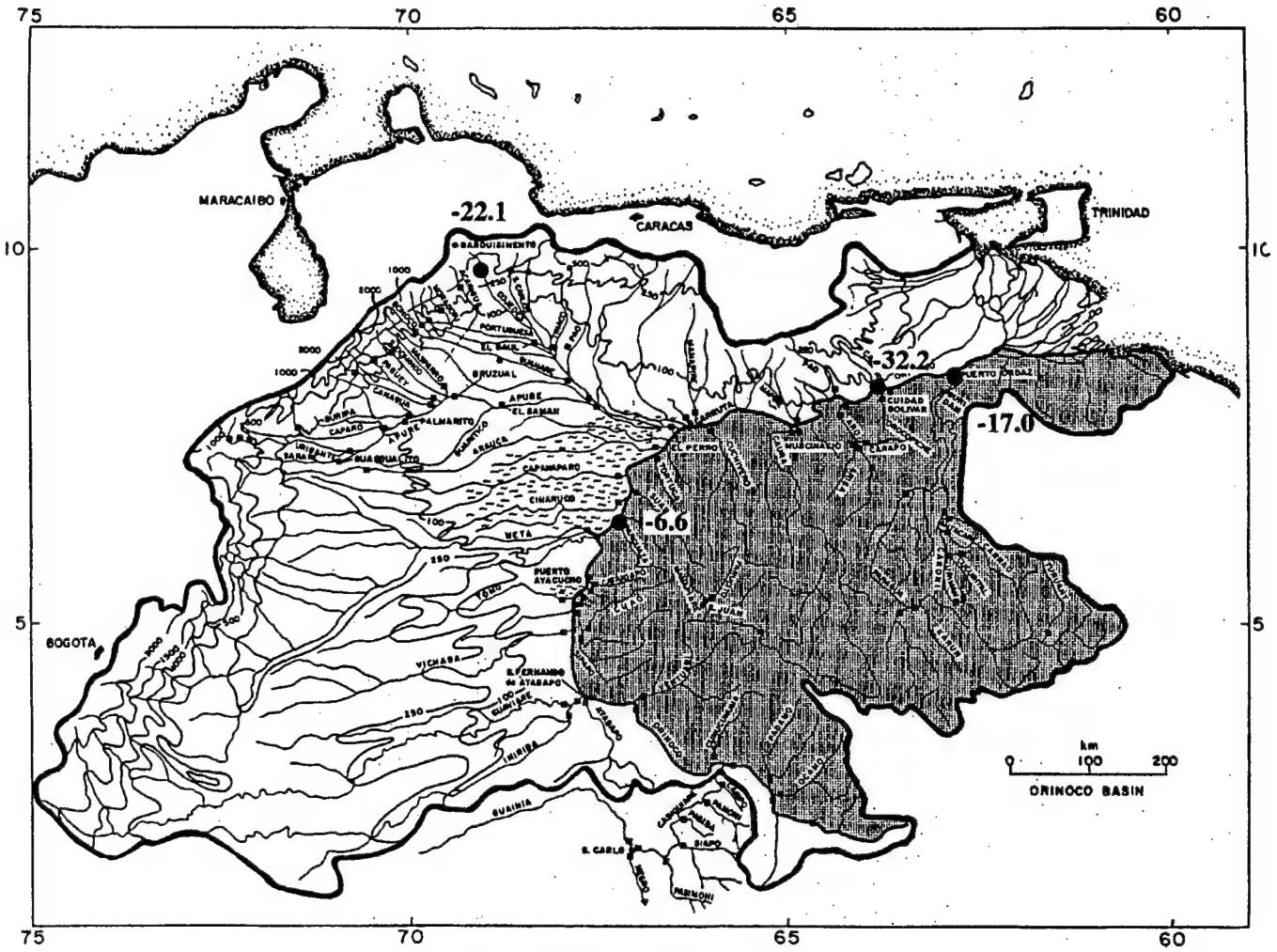

The Orinoco Basin

Figure 3. Location map of the Ganges-Brahmaputra system, after Sarin *et al.* (1989). The Ganges-Brahmaputra has very radiogenic $^{87}Sr/^{86}Sr$ in high flux owing to the present tectonics (Krishnaswami *et al.*, 1992; Edmond, 1992). The sample locations are marked with the $\delta^{6}Li$ (‰) values. The headwaters in the High Himalayas give -11.3‰, the Brahmaputra before it joins the Ganges is -19.6‰, and the Ganges downstream of additions from the Deccan Traps is -22.6‰.

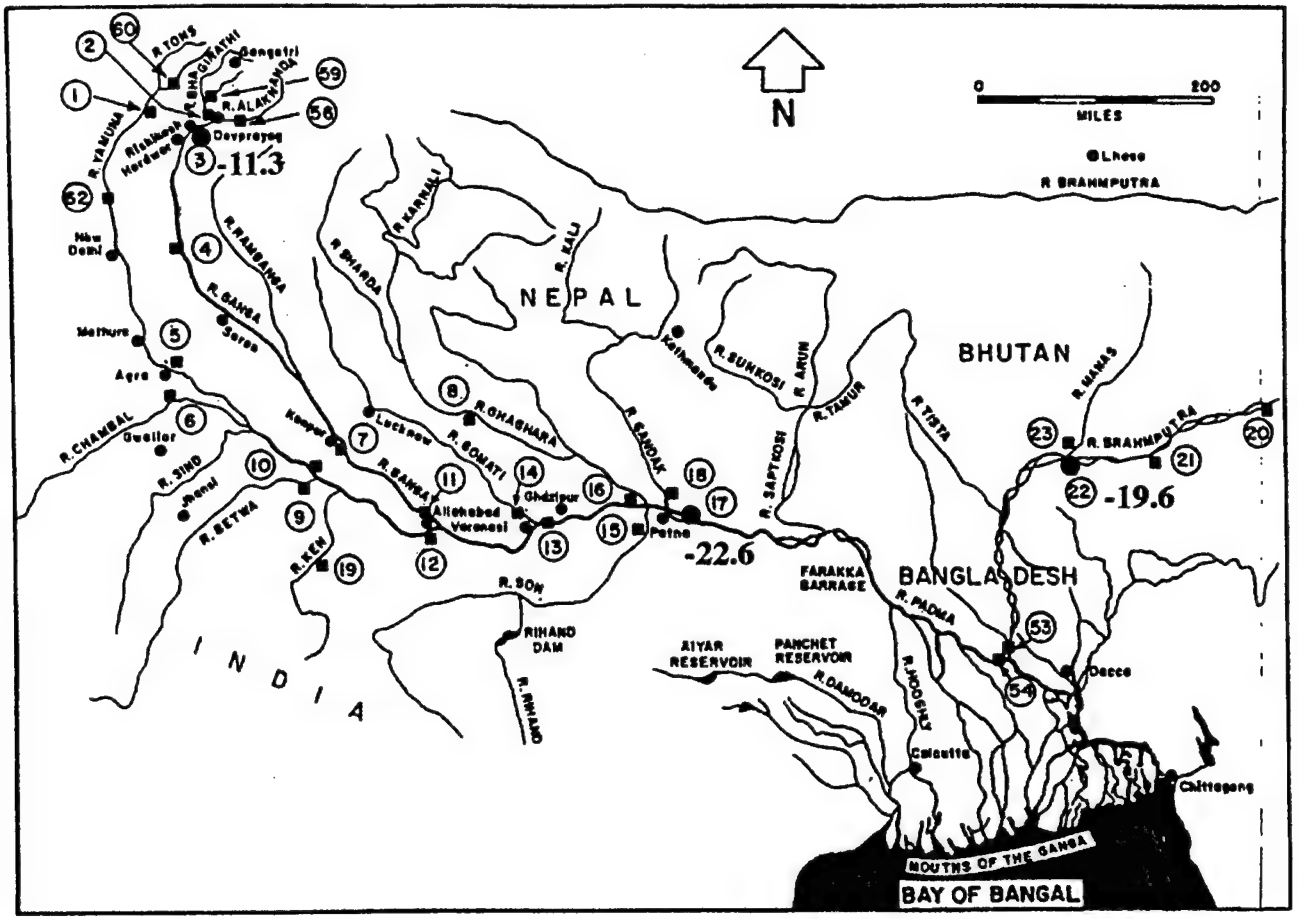
N
0
200
MILES
Lhasa
R BRAHMPUTRA
NEPAL
BHUTAN
INDIA
BANGLADESH
BAY OF BANGAL
MOUTHS OF THE GANGA
-11.3
-22.6
-19.6
R.YAMUNA
R.BHAGIRATHI
R.ALAKHNANDA
R.TONS
Gangotri
Devprayag
Rishikesh
Haridwar
New Delhi
Mathura
Agra
Gwalior
Jhansi
Kanpur
Lucknow
Allahabad
Varanasi
Ghazipur
Patna
Farakka
Barrage
Rihand
Dam
Aiyar
Reservoir
Panchet
Reservoir
Calcutta
Dacca
Chittagong
R.RAMGANGA
R.GANGA
R.SHARDA
R.KARNALI
R.KALI
R.GHAGHARA
R.GANDAK
R.SUNKOSI
R.ARUN
R.TAMUR
R.TISTA
R.MANAS
R.BRAHMPUTRA
R.CHAMBAL
R.SIND
R.BETWA
R.KEEN
R.SONATI
R.SAMGAI
R.SON
R.RIHAND
R.SAPTKOSH
R.DAMODAR
R.HOOGHLY
R.PADMA

Figure 4. Location map of the Mississippi River and its tributaries, the Missouri and Ohio Rivers. The sample locations are marked with the δ^6Li (‰) values. The upper Mississippi drains the Precambrian shield with δ^6Li of -20.8‰ and -16.7‰. The Missouri flows through sedimentary rocks of Paleozoic to Cenozoic age and is -17.6‰. The Ohio drains a mixture of metamorphic rocks and Paleozoic sediments and is -19.8‰. The lower Mississippi flows through the coastal plain underlain by interbedded sand, silt, and clay of Mesozoic and Cenozoic age, and in Louisiana δ^6Li is -16.1‰.

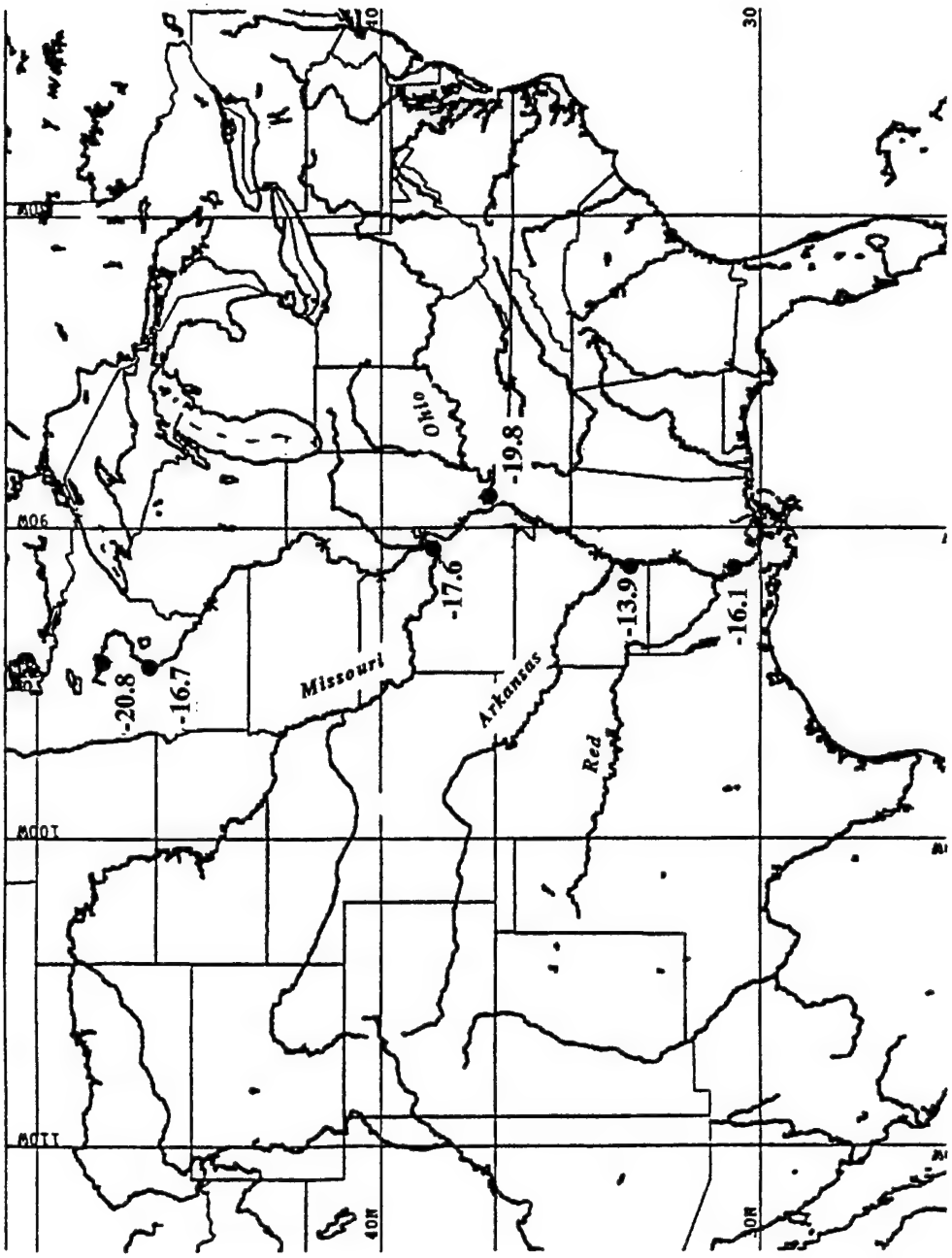
Ohio
-19.8
-17.6
-13.9
-16.1
-20.8
-16.7
Missouri
Arkansas
Red
M006
M001
M111
40N
10N

Figure 5. Location map of the Siberian rivers. The sample numbers are given with the δ^6Li (‰) values. The Siberian rivers drain a unique periglacial environment dominated by ice action but not glaciated either at present or in the past. The Lena, Yana, Indigirka, and Kolyma are the major northward flowing rivers. The Verkhnyaya Yazobaya (UL427) is a small tributary to the Vitim, a major right bank tributary of the Lena. The region is biotite-rich and the river drains exclusively the Proterozoic Trans-Baikal Highlands (TBH); the δ^6Li is -27.6‰. The Biryuk (UL436) drains the evaporitic marine carbonate sequence of the Siberian Platform and is -20.8‰. The Lena above the Aldan (UL102) is a combination of the right bank tributaries draining the TBH with a contribution from the Aldan Shield and the left bank tributaries draining the sedimentary platform; δ^6Li is -20.6‰. The Aldan is the major right bank tributary of the Lena. The headwater right bank tributaries e.g. the Timpton (UL119), drain the Aldan Shield, and the lower right bank tributaries drain the Verkhoyansk range, a collisional feature formed by the Cretaceous accretion of the Kolyma-Omolon block to the Siberian craton. The left bank tributaries drain the Vendian carbonate platform. At the mouth of the Aldan (UL101) the δ^6Li is -29.0‰. The Sobolokh (UL602) is a lower Lena tributary draining the Verkhoyansk range with -21.4‰. The Lena at Kusur (UL607) is immediately above the delta and is -21.0‰. The Yana above Adycha (YN109) is in the headwaters draining the eastern slope of the Verkhoyansk and is -6.0‰. The Yana mouth sample (YN101) is the combination of left bank tributaries draining the eastern slope of the Verkhoyansk and the right bank draining the Cherskiy Range and has a value very different from the headwaters, -27.1‰. The Indigirka (IG121) drains the complex Mesozoic accretionary structure (-25.2‰), and the Kolyma headwaters (KY103) drain the Okhotsk-Chukotka volcanic belt and the Cherskiy Range (-20.4‰). The rivers that flow into Lake Baikal drain the acid intrusives of the TBH and their values range from -21.5 to -30.7 ‰ (Falkner *et al.*, 1997).

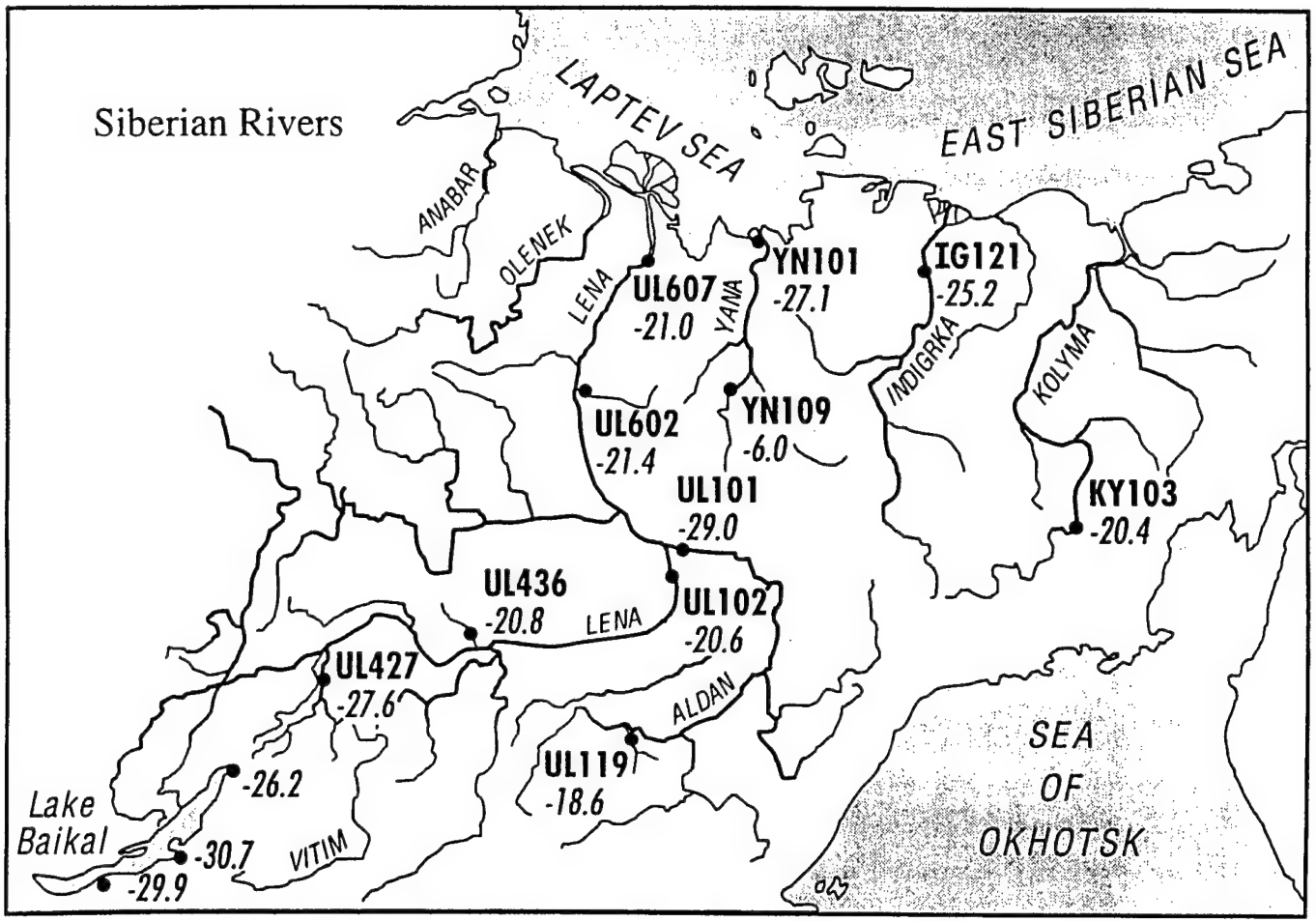
Siberian Rivers
LAPTEV SEA
EAST SIBERIAN SEA
ANABAR
OLENEK
LENA
YANA
INDIGRKA
KOLYMA
UL607
-21.0
YN101
-27.1
IG121
-25.2
UL602
-21.4
YN109
-6.0
UL101
-29.0
KY103
-20.4
UL436
-20.8
LENA
UL102
-20.6
UL427
-27.6
ALDAN
UL119
-18.6
SEA
OF
OKHOTSK
Lake
Baikal
-26.2
-30.7
-29.9
VITIM

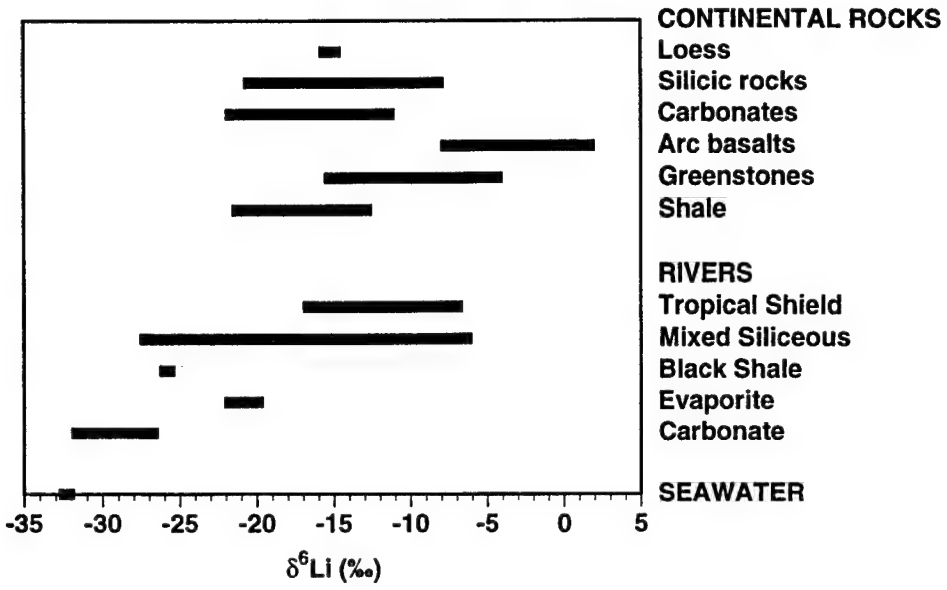

Figure 6. A summary of the known range of δ^6Li(‰) in continental rocks, rivers of different geologies, and seawater. The loess sample is from Vicksburg, MS. Silicic rocks include granitic rocks from the Barberton Greenstone Belt of South Africa, a granodiorite from the Canadian Shield and a Precambrian schist from the Yellowstone National Park. Shale samples are from calcareous shale of the Jurassic Ellis Group and Cretaceous Cody Shale (Chan *et al.*, 1997). Carbonate samples include a Senonian chalk and Lisan sediments from Israel and a Bahaman oolite. Arc basalts are from the Central American Arc (Chan *et al.*, 1995). Archean greenstones are from the Barberton Greenstone Belt, South Africa and the Yellowknife Greenstone Belt, Canada.
The ranges for rivers of different geologies are from this study. Seawater range is from Chan and Edmond (1988).

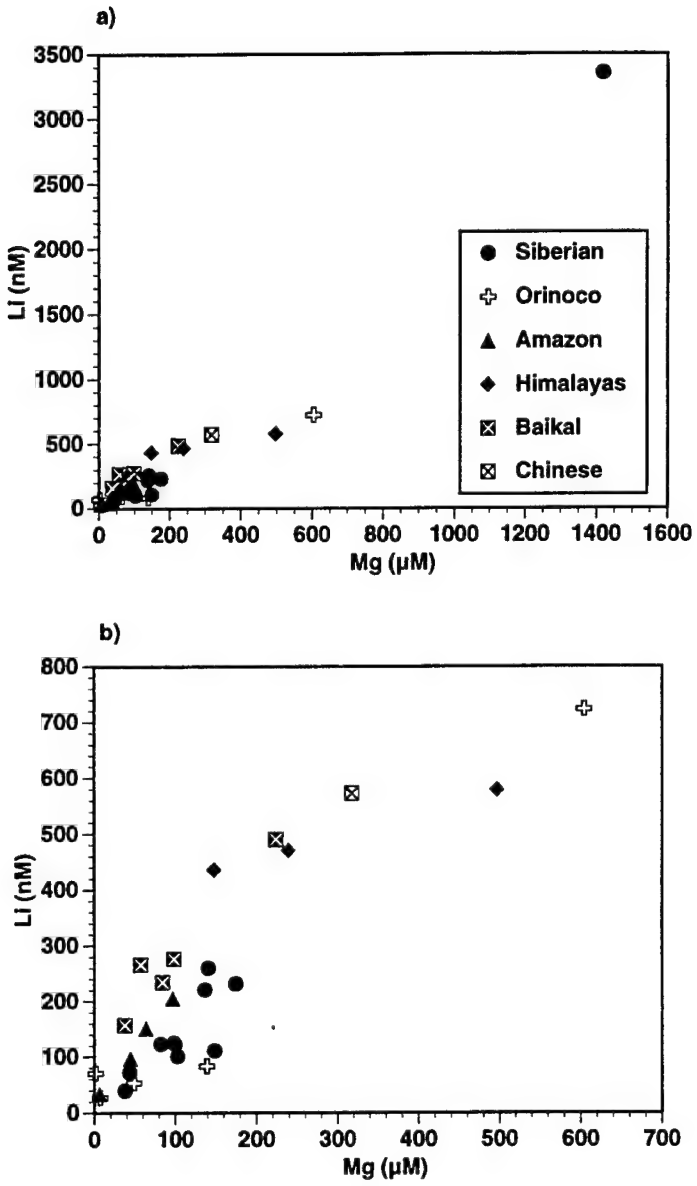

Figure 7. Li vs. Mg at (a) full scale and (b) expanded scale. The correlation is best with Mg and only diffuse with other major elements, Na, Ca, Cl, and SO_4. There is no distinguishable relationship with Si or K. Rivers listed in Table 2 are not shown on this figure due to the lack of major element data.

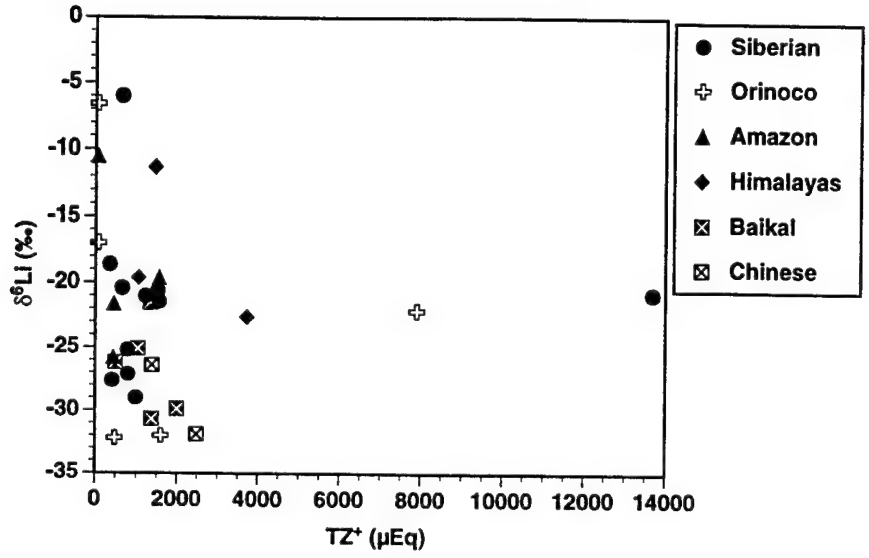

Figure 8. δ^6Li vs. TZ^+. $TZ^+ = (Na^+ + K^+ + 2Ca^{2+} + 2Mg^{2+})$ in 10^{-6} equivalents/kg. There is a similar relationship between δ^6Li and other major elements, Ca, Mg, Cl, SO_4 and to a lesser extent K. There is no relationship with Si. Rivers listed in Table 2 are not shown on this figure due to the lack of major element data.

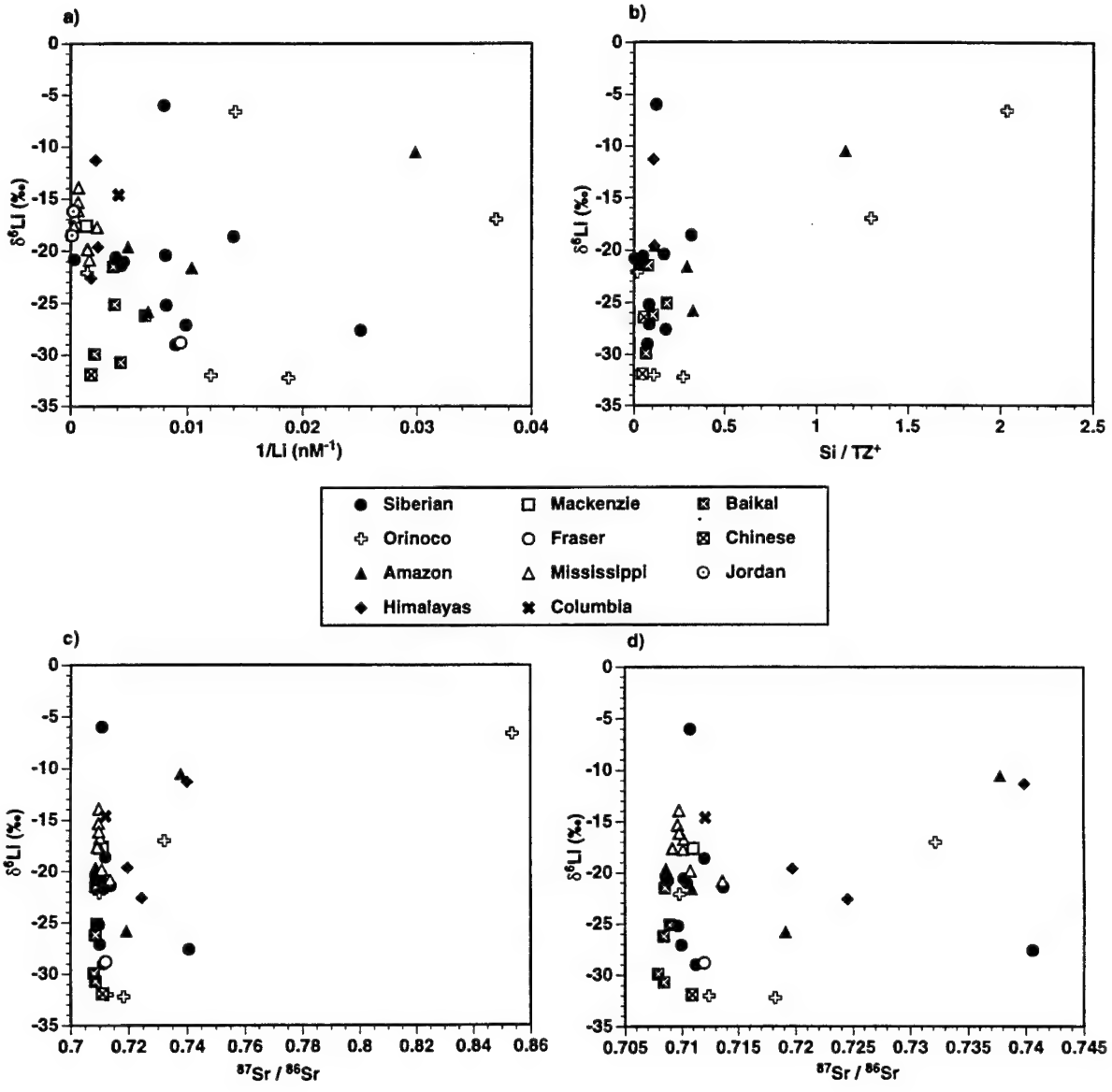

Figure 9. (a)δ^6Li (‰) vs. 1/Li (nM^{-1}). (b) δ^6Li vs. Si/TZ^+. (c) δ^6Li vs. $^{87}Sr/^{86}Sr$ full scale. (d) δ^6Li vs. $^{87}Sr/^{86}Sr$ expanded scale.

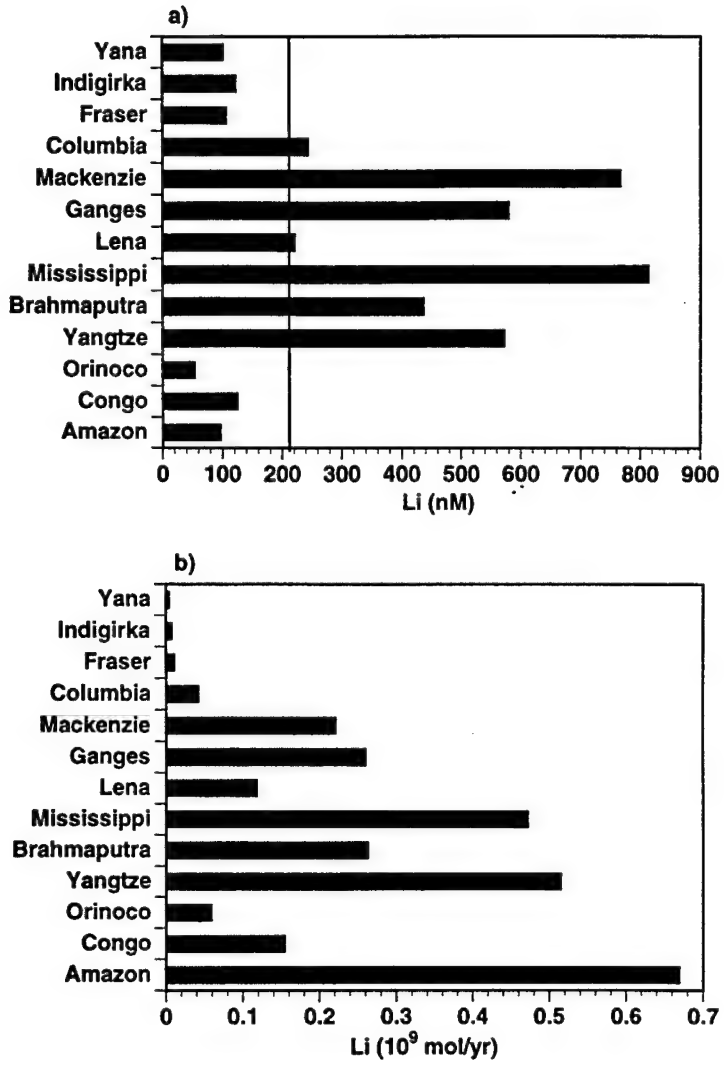

Figure 10. (a) Concentration, (b) flux of the major rivers. The line indicates the discharge-weighted mean concentration.

Chapter 6

Conclusion: Weathering and Climate—a Global Experiment

Introduction

The global carbon cycle models over geological timescales assume a climate-sensitive negative feedback through aluminosilicate weathering (Berner *et al.*, 1983). The increase in temperature due to an addition of the greenhouse gas CO_2 leads to increased vapor pressure, precipitation, runoff and weathering of aluminosilicate rocks and therefore uptake of CO_2. The Clausius-Clapeyron relationship establishing the increase of saturation vapor pressure of water with increasing temperature and the Arrhenius law indicating higher kinetic reaction rates with temperature both support the hypothesis. The two relationships have been demonstrated in the laboratory dissolution experiments (Lasaga, 1984; Lasaga *et al.*, 1994) and also in some small watershed studies (Meybeck, 1986; White and Blum, 1995). This negative feedback is necessary to explain the fact, observed in geological records, that the atmospheric CO_2 levels on the Earth have not had excursions outside the range of habitability. Because the atmosphere-ocean-biosphere reservoir is very small (~3.2×10^{18} mol CO_2) compared to the flux of CO_2 involved in the inorganic carbon cycle (~10^{19} mol/M.Y.) it is thought necessary to have a negative feedback.

The actual feedback function used in the BLAG type models is derived from the Arrhenius function with activation energies for Ca nad Mg silicate weathering determined from laboratory experiments (Brady, 1991). Assuming average temperatures of 10°C for the arctic/subarctic and 28°C for the tropics, the feedback is almost ten times higher in the tropics (Fig. 1; Berner, 1994).

To examine the viability of this hypothesis on a global scale, the scale relevant for geochemical carbon cycle models, a comparative study of the large rivers of the world at different latitudes has been carried out (Fig. 2). Unfortunately, rivers in the temperate latitudes have been impacted by human activity and most of the northern hemisphere landscapes are dominated by recent glacial action. Datasets from pristine tropical systems are available for the Amazon (Stallard and Edmond, 1983) and the Orinoco (Edmond *et al.*,

1995, 1996) draining the eastern Andes and the Guayana and Brazilian shields, the northern Congo partly draining the Congo shield (Négrel *et al.*, 1993; Dupré *et al.*, 1996), the Ganges-Brahmaputra (Sarin *et al.*, 1989; Krishnaswami *et al.*, 1992) and Indus (Pande *et al.*, 1994) draining the Himalayas. Some data are also available for the lower Yangtze and Huanghe (Hu *et al.*, 1982). The only comparable data set for the high latitudes is from the pioneering study of the Mackenzie (Reeder *et al.*, 1972), and the recent studies of the Fraser (Cameron *et al.*, 1995) and the St. Lawrence (Yang *et al.*, 1995). All three rivers are on the North American continent and have glacial overburden from outside the drainage basin which obscures the primary signal from contemporary in-situ weathering of basement rocks. Recently the fluvial geochemistry of the Siberian rivers has been studied in diverse geological regions covering the basement shield terrain, a collisional/accretionary zone of mountains with arc basalts and occluded island arcs, and a vast sedimentary platform (Huh and Edmond, 1998; Huh *et al.*, 1998a, 1998b). All major rivers from east of Lake Baikal to the Pacific coast—the Lena, Yana, Indigirka, Kolyma, Anadyr, and other smaller systems—have been sampled at every significant tributary and on the main channels at various distances above the mouth in the summers of 1994 to 1997. Archived samples from previous expeditions (1991, 1992) and "grab" samples from other investigations were also analyzed to extend coverage. The eastern Siberian rivers have the advantage of being free from extensive glaciation due to the semi-arid climate and precipitation occurring generally as rain rather than as snow. The area covered is comparable to the drainage basin of the Amazon or the contiguous US. Altogether about 300 tributaries have been sampled and greatly extend the current dataset for high latitudes and cold climates.

Rates Of CO_2 Uptake By Silicate Weathering

The methods of calculating CO_2 uptake rates by aluminosilicate weathering (ϕCO_2) from fluvial chemistry data sets are explained in detail elsewhere (Edmond and Huh,

1997). The magnitudes are shown in Fig. 3 for three different geological terranes—stable aluminosilicate basement, sedimentary platform of marine carbonates and continental detrital material, and an uplift zone of collision/accretion. The large variability in weathering rates within a latitudinal zone obscures any temperature (or latitude) dependence of ϕCO_2.

A vast platform composed of Cambrian-Ordovician carbonates, evaporites and Jurassic-Cretaceous continental sediments occupies most of the Siberian Craton. A geologically similar region in the tropics is the Chinese Platform drained by the Yangtze and the Huanghe in temperate latitudes. The range in chemical signatures of the various Siberian tributaries (~60 sampled) is large, reflecting the diversity of lithology. The total cationic charge is high (mostly < 6,000 μEq, but up to 34,800 μEq). The areal chemical fluxes (0.53-2.1 x 10^6 mol/km^2/yr) and ϕCO_2 (16-112 x 10^3 mol/km^2/yr) are dominated by the dissolution of carbonates and evaporites and are comparable to those of the Chinese rivers (0.37-2.4 x 10^6 mol/km^2/yr; 7-106 x 10^3 mol/km^2/yr) in both magnitude and composition.

The region to the east of the Siberian Platform is a geologically complex terrain formed by the Mesozoic collision and accretion of the Siberian and Kolyma plates. The total dissolved cation levels (~100 samples) are moderate (up to ~3,100 μEq), and the major ion chemistry is indicative of Ca-aluminosilicate and carbonate weathering with significant contributions from black shales in some tributaries. The Si/TZ^+*, Si/(Na*+K) (* indicates correction for evaporites), and cation ratios indicate that the weathering is superficial, i.e. only to cation-rich secondary minerals. The areal total dissolved solid fluxes range from 0.04 to 0.39 x 10^6 mol/km^2/yr, up to an order of magnitude lower than for the Amazon/Orinoco draining the Andes in the tropics (0.6-4.1 x 10^6 mol/km^2/yr). ϕCO_2 (18 to 230 x 10^3 mol/km^2/yr) is also at the lower end of the range observed in the Amazon-Orinoco headwaters (143 to 1,000 x 10^3 mol/km^2/yr). However, as the North American counterparts in similar latitudes and with comparable relief, the Mackenzie,

Yukon and Fraser draining the Rockies, also have high dissolved solids (0.2-2.9 x 10^6 mol/km^2/yr) and ϕCO_2 (19 to 1,750 x 10^3 mol/km^2/yr), these low values seem to be more a function of lithology than simply climate.

The basement of the Siberian Craton is exposed in the Aldan Shield in the south and in the Anabar Shield in the north, with Trans-Baikal Highlands forming the basement high around the southern margin of the craton. The chemical composition, especially low Si to total cation ratios, again suggests a superficially weathered system (~60 stations). The total dissolved solids fluxes are 0.39 x 10^6 mol/km^2/yr, similar to the tropical systems (0.05-0.75 x 10^6 mol/km^2/yr) and the collisional/accretionary zone of the northeastern Siberia, but a factor of 3 lower than the orogenic zones of the Americas both tropical and subarctic. The ϕCO_2 (149 x 10^3 mol/km^2/yr) also follow the same relationship (tropics 15-205 x 10^3 mol/km^2/yr).

The fluxes do not have a distinguishable relationship with discharge when comparing the global dataset. Within a smaller watershed, the upper limit shows a proportionality.

The lack of visible climatic effect in TDS and CO_2 fluxes can be ascribed to the unique non-glacial frost shattering processes which continuously expose fresh rock surfaces and thus overcome the effect of temperature inhibition on high-latitude shields and to the lateritic cover that seals in the weathering front away from the weathering agents on the tropical shields. Saprolites are preserved only in protected areas in the high latitudes, and they seem to have been generated during the warm humid Tertiary and almost none during the interglacial (LaSalle *et al.*, 1985). The scale at which frost weathering works seem to be only at large scales. Little silt-size material was observed either in the river suspended matter or overbank flows, except in the eastern rivers where unconsolidate river bank erosion resulted in high clay content in those rivers. Sand bars and mounds are found ubiquitously in the mid reaches of the Lena. Gravels and pebbles dominate the bedload in

the headwaters. Even frost shattering to pebble sized material seems to be able to overcome the inhibition by lower temperatures and drier climate.

Discussion

The implications of this large scale survey of the arctic and subarctic rivers of eastern Siberia are that the negative weathering feedback assumed in global carbon cycle models is questionable. The river data set does not support this hypothesis as a mechanism for maintaining a balance. What it does indicate is that the orogenic zones do take up much CO_2. This partly supports the idea that increases in global degassing are matched by increases in CO_2 uptake via enhanced weathering accompanying mountain uplift as in the Himalayas or the Western Cordillera of the Americas. The actual mechanism that maintains the balance between slowly varying degassing and seemingly intermittent mountain uplift is a fundamental question that remains to be answered.

There are various complications in trying to arrive at CO_2 uptake rates from river water chemistry as outlined below, but educated guesses and descriptive conclusions are possible. The weathering rates are derived from mass balance using water chemistry values at the mouth of each tributary. They represent integrated signal from the bedrock, soil, vegetation, atmospheric deposition, and floodplain storage and weathering. In essence, the comparison here is between the weathering of bedrock at high latitudes with its taiga or tundra vegetation and frozen soils and that of bedrock in the low latitudes with its rainforest and lateritic soils, and not exclusively the bedrock in two different latitudes. To the extent of comparing the two watershed in two different latitudes, this does not change the conclusion. The effect of soil is assumed to be small: in the tropical shields the complete stripping out of the cations give rise to laterite and lack of significant soil; in Siberia the soil is frozen and only a thin layer is available. The effect of vegetation on chemical weathering was surmised to be small and that on physical weathering is variable

depending on relief but hard to quantify (Drever, 1994). Floodplain storage and weathering may be temperature dependent but, at the tributary scale sampled, affects only the main channel values and not the shield comparisons. Overall, the mechanism of relief generation or exposure is determinant—passive in the laterite system of the tropics and active by frost movement in the arctic.

The heterogeneity issue should also be addressed. The lithology of a given terrain is very rarely of one rock type. If trace amounts of carbonates or evaporites in a nominally "shield" terrain were present, and erroneously all included in calculations of aluminosilicate weathering, they would give higher rates than are actually occurring. For the CO_2 cycle, the important thing is to distinguish CO_2-withdrawing weathering reactions by silicate weathering from non-CO_2 withdrawing carbonate and evaporite weathering. Sr isotope ratios were crucial for this purpose. Because carbonates and evaporites weather several orders of magnitude faster than aluminosilicates, they dominate the isotope ratio of water when they are present. In that case, Si values are used to calculate ϕCO_2 which is a conservative estimate as there seem to be substantial biogenic uptake of Si in thermokarst lakes and bogs of the northern landscapes.

The other heterogeneity issue is that of the hydrograph. The discharge of the Lena is highly seasonal with discharge limited to only a few months in summer and frozen solid in most of the reaches in winter. As we sample only in the shoulder or the secondary peak caused by summer rainfall due to access problems, it could be argued that we're missing the spring peak from ice-melt and also that the proportion of different tributaries draining different lithology may change with change in runoff, i.e. the chemistries of the water may be totally different between the ice-melt peak and the rain peak. More fundamentally, there is the error in taking annual average runoff and one point sampling to derive the fluxes. Highest weathering probably occurs at the ice melt when frost weathering is more active due to the availability of moisture and the temperature gradient established in the ground. During the summer rain, there is some dilution by the rain falling directly on the channels

and a direct runoff fraction that does not have time to react with the bedrock or soil. To the second argument, the answer is that the samples have been collected in sufficient detail that this effect is minimized, but admittedly such probability remains. In regard to the third argument, the tropical data sets have been calculated similarly, so the errors are systematic. The Amazon has also been sampled once. The Orinoco has been sampled over many times at various stages of runoff and are more representative. For the Siberian rivers, the only answer is that the samples have been collected at median stage and should be representative or low.

The next question is whether the river dissolved material is at steady state, i.e. whether sampling of water at a certain time is representative of weathering occurring at that time in the basin or whether it is only a remnant effect of the past Tertiary warm period. This is more important for the suspended material, as the storage and removal processes affects it more significantly. For the dissolved load, aside from blooms in closed reservoirs and lakes and subsequent washout during high flow, the water composition is representative of present weathering. Whether the water is interacting with fresh bedrock or "weathered" rock from warm Tertiary environments, the water chemistry represents CO_2 uptake rates from current weathering. Whatever amount is inherited from the warm period is probably not drastically different between the two latitudes.

What are the implications for weathering over historical times? My argument was that the physical exposure mechanism or the physical cover is primarily responsible for the weathering magnitude. For the present Guayana and Aldan shields this is correct. Thinking back in time and trying to deduce the importance of such mechanism versus climate in the past, we have to weigh the two. When initially fresh bedrock of low relief is exposed via uplift, presumably weathering is dependent on climate especially rainfall. Imagining a Tertiary atmosphere when both the Siberia and Guayana were relatively warm and before the buildup of significant laterite, then the weathering would initially be faster at places where there was more rainfall and higher temperatures. On the hot and humid

shield, the laterite mantle will build up faster and will sooner reach a steady state; on a cooler and drier shield it will take longer for the same amount of laterite to build up. When those are both at steady state, then the presence of mechanism to remove the lateritic mantle is the key. Before they reach that steady state, I can see there being a temperature dependent weathering rates, provided the lithology is the same. The question then is what are the timescales till a system reaches a steady state, other conditions remaining the same. The buildup of lateritic mantle on tropical shields is ~ 1m/M.Y. (Brown *et al.*, 1994; Brown *et al.*, 1995). At these rates in a few million years the laterite mantle is thick enough to seal the weathering front , a short interval on geologic and geochemical timescales.

References

Berner R. A., Lasaga A. C., and Garrels R. M. (1983) The carbonate-silicate geochemical cycle and its effect on atmospheric carbon dioxide over the past 100 million years. *Am. J. Sci.* **283**, 641-683.

Berner R. A. (1994) GEOCARB II: A revised model of atmospheric CO_2 over Phanerozoic time. *Am. J. Sci.* **294**, 56-91.

Brady P. V. (1991) The effect of silicate weathering on global temperature and atmospheric CO_2. *J. Geophys. Res.* **96**, 18101-18106.

Brown E. T., Bourlès D. L., Colin F., Sanfo Z., Raisbeck G. M., and Yiou F. (1994) The development of iron crust lateritic systems in Burkina Faso, West Africa examined with in-situ produced cosmogenic nuclides. *Earth Planet. Sci. Lett.* **124**, 19-33.

Brown E. T., Stallard R. F., Larsen M. C., Raisbeck G. M., and Yiou F. (1995) Denudation rates determined from the accumulation of in-situ produced ^{10}Be in the Luquillo Experimental Forest. *Earth Planetary Science Letters* **129**, 193-202.

Cameron E. M., Hall G. E. M., Veizer J., and Krouse H. R. (1995) Isotopic and elemental hydrogeochemistry of a major river system: Fraser River, British Columbia, Canada. *Chem. Geol.* **122**, 149-169.

Drever J. I. (1994) The effect of land plants on weathering rates of silicate minerals. *Geochim. Cosmochim. Acta* **58**, 2325-2332.

Dupré B., Gaillardet J., Rousseau D., and Allègre C. J. (1996) Major and trace elements of river-borne material: The Congo Basin. *Geochim. Cosmochim. Acta* **60**, 1301-1321.

Edmond J. M. and Huh Y. (1997) Chemical weathering yields from basement and orogenic terrains in hot and cold climates. In *Tectonic Uplift and Climate Change*. (ed. W. F. Ruddiman), Plenum Press, pp. 329-351.

Edmond J. M., Palmer M. R., Measures C. I., Brown E. T., and Huh Y. (1996) Fluvial geochemistry of the eastern slope of the northeastern Andes and its foredeep in the drainage of the Orinoco in Colombia and Venezuela. *Geochim. Cosmochim. Acta* **60**, 2949-2976.

Edmond J. M., Palmer M. R., Measures C. I., Grant B., and Stallard R. F. (1995) The fluvial geochemistry and denudation rate of the Guayana Shield in Venezuela, Colombia and Brazil. *Geochim. Cosmochim. Acta* **59**, 3301-3325.

Hu M.-H., Stallard R. F., and Edmond J. M. (1982) Major ion chemistry of some large Chinese rivers. *Nature* **298**, 550-553.

Huh Y. and Edmond J. M. (1998) The fluvial geochemistry of the rivers of eastern Siberia III: Tributaries of the Lena and Anabar draining the basement terrain of the Siberian Craton and the Trans-Baikal Highlands. *Geochim. Cosmochim. Acta* submitted, March 1998.

Huh Y., Panteleyev G., Babich D., Zaitsev A., and Edmond J. M. (1998) The fluvial geochemistry of the rivers of Eastern Siberia II: Tributaries of the Lena, Omoloy, Yana, Indigirka, Kolyma, and Anadyr draining the collisional/accretionary zone. *Geochim. Cosmochim. Acta* in press.

Huh Y., Tsoi M.-Y., Zaitsev A., and Edmond J. M. (1998) The fluvial geochemistry of the rivers of Eastern Siberia I: Tributaries of the Lena River draining the sedimentary platform of the Siberian Craton. *Geochim. Cosmochim. Acta* in press.

Krishnaswami S., Trivedi J. R., Sarin M. M., Ramesh R., and Sharma K. K. (1992) Strontium isotopes and rubidium in the Ganga-Brahmaputra river system: Weathering in the Himalaya, fluxes to the Bay of Bengal and contributions to the evolution of oceanic $^{87}Sr/^{86}Sr$. *Earth Planet. Sci. Lett.* **109**, 243-253.

Lasaga A. C. (1984) Chemical kinetics of water-rock interactions. *J. Geophys. Res.* **89**, 4009-4025.

Lasaga A. C., Soler J. M., Ganor J., Burch T. E., and Nagy K. L. (1994) Chemical weathering rate laws and global geochemical cycles. *Geochim. Cosmochim. Acta* **58**, 2361-2386.

LaSalle P., De Kimpe C. R., and Laverdiere M. R. (1985) Sub-till saprolites in southeastern Quebec and adjacent New England: Erosional, stratigraphic, and climatic significance. *Geological Society of America Special Paper* **197**, 13-20.

Meybeck M. (1986) Composition chimique des ruisseaux non pollués de France. *Sci. Geol. Bull* **39**, 3-77.

Négrel P., Allègre C. J., Dupré B., and Lewin E. (1993) Erosion sources determined by inversion of major and trace element ratios and strontium isotopic ratios in river water: The Congo Basin case. *Earth Planet. Sci. Lett.* **120**, 59-76.

Pande K., Sarin M. M., Trivedi J. R., Krishnaswami S., and Sharma K. K. (1994) The Indus river system (India-Pakistan): Major-ion chemistry, uranium and strontium isotopes. *Chem. Geol.* **116**, 245-259.

Reeder S. W., Hitchon B., and Levinson A. A. (1972) Hydrogeochemistry of the surface waters of the Mackenzie River drainage basin, Canada—I. Factors controlling inorganic composition. *Geochim. Cosmochim. Acta* **36**, 825-865.

Sarin M. M., Krishnaswami S., Dilli K., Somayajulu B. L. K., and Moore W. S. (1989) Major ion chemistry of the Ganga-Brahmaputra river system: Weathering processes and fluxes to the Bay of Bengal. *Geochim. Cosmochim. Acta* **53**, 997-1009.

Stallard R. F. and Edmond J. M. (1983) Geochemistry of the Amazon 2. The influence of geology and weathering environment on the dissolved load. *J. Geophys. Res.* **88**, 9671-9688.

White A. F. and Blum A. E. (1995) Effect of climate on chemical weathering in watersheds. *Geochim. Cosmochim. Acta* **59**, 1729-1747.

Yang C., Telmer K., and Veizer J. (1995) Chemical dynamics of the St. Lawrence riverine system: δD_{H_2O}, $\delta^{18}O_{H_2O}$, $\delta^{13}C_{DIC}$, $\delta^{34}S_{Sulfate}$, and dissolved $^{87}Sr/^{86}Sr$. *Geochim. Cosmochim. Acta* **60**, 851-866.

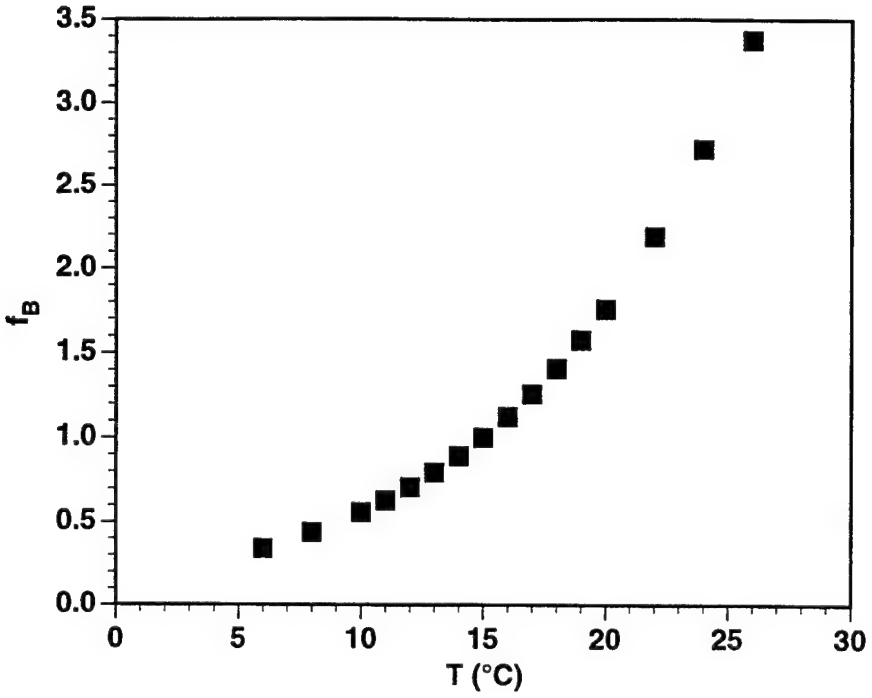

Figure 1. The dimensionless feedback function for silicates expressing the dependence of weathering on temperature, f_B. plotted against temperature (Berner, 1994).

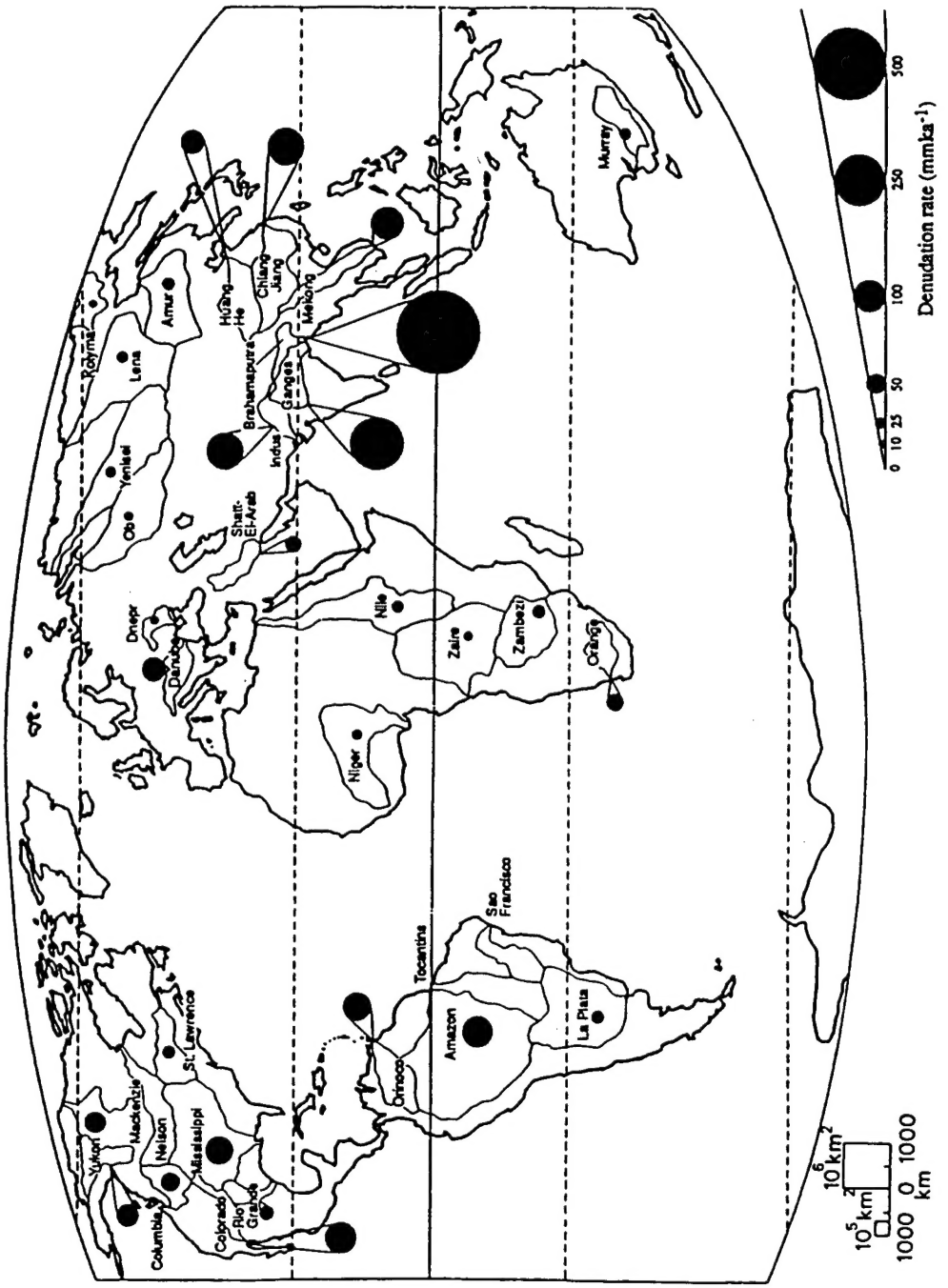

Figure 2. Locations and estimated total denudation rates for major externally drained basins. From Summerfield and Hulton (1994).

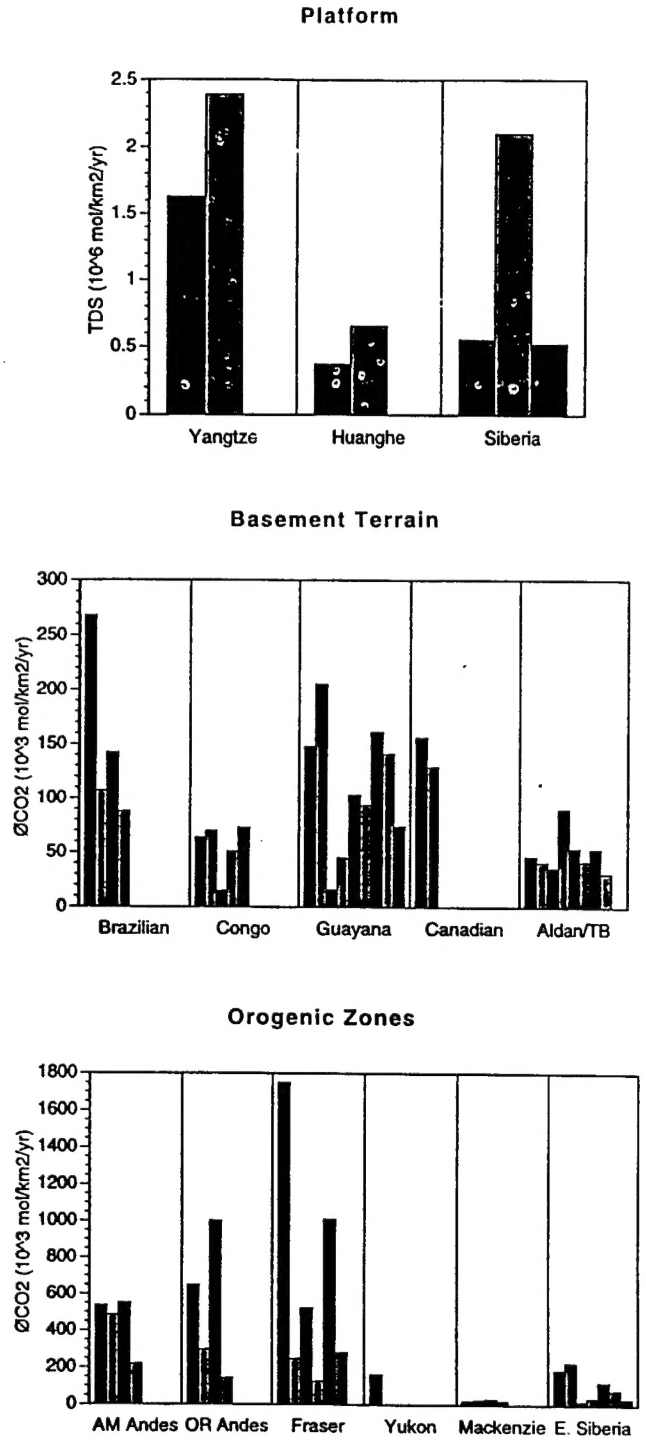

Figure 3. Fluxes of total dissolved solids (TDS) and CO_2 uptake by aluminosilicate weathering for the major world rivers of three geological regions (Huh et al., 1998a,b; Huh and Edmond, ms).

Document Library

Distribution List for Technical Report Exchange—November 1998

University of California, San Diego
SIO Library 0175C
9500 Gilman Drive
La Jolla, CA 92093-0175

Hancock Library of Biology & Oceanography
Alan Hancock Laboratory
University of Southern California
University Park
Los Angeles, CA 90089-0371

Gifts & Exchanges
Library
Bedford Institute of Oceanography
P.O. Box 1006
Dartmouth, NS B2Y 4 A2
CANADA

NOAA/EDIS Miami Library Center
4301 Rickenbacker Causeway
Miami, FL 33149

Research Library
U.S. Army Corps of Engineers
Waterways Experiment Station
3909 Halls Ferry Road
Vicksburg, MS 39180-6199

Institute of Geophysics
University of Hawaii
Library Room 252
2525 Correa Road
Honolulu, HI 96822

Marine Resources Information Center
Building E38-320
MIT
Cambridge, MA 02139

Library
Lamont-Doherty Geological Observatory
Columbia University
Palisades, NY 10964

Library
Serials Department
Oregon State University
Corvallis, OR 97331

Pell Marine Science Library
University of Rhode Island
Narragansett Bay Campus
Narragansett, RI 02882

Working Collection
Texas A&M University
Dept. of Oceanography
College Station, TX 77843

Fisheries-Oceanography Library
151 Oceanography Teaching Bldg.
University of Washington
Seattle, WA 98195

Library
R.S.M.A.S.
University of Miami
4600 Rickenbacker Causeway
Miami, FL 33149

Maury Oceanographic Library
Naval Oceanographic Office
Building 1003 South
1002 Balch Blvd.
Stennis Space Center, MS 39522-5001

Library
Institute of Ocean Sciences
P.O. Box 6000
Sidney, B.C. V8L 4B2
CANADA

National Oceanographic Library
Southampton Oceanography Centre
European Way
Southampton SO14 3ZH
UK

The Librarian
CSIRO Marine Laboratories
G.P.O. Box 1538
Hobart, Tasmania
AUSTRALIA 7001

Library
Proudman Oceanographic Laboratory
Bidston Observatory
Birkenhead
Merseyside L43 7 RA
UK

IFREMER
Centre de Brest
Service Documentation–Publications
BP 70 29280 PLOUZANE
FRANCE

50272-101

REPORT DOCUMENTATION PAGE	1. REPORT NO. MIT/WHOI 98-22	2.	3. Recipient's Accession No.

4. Title and Subtitle
The Fluvial Geochemistry of the Rivers of Eastern Siberia and Implications for the Effect of Climate on Weathering

5. Report Date
June 1998

6.

7. Author(s)
Youngsook Huh

8. Performing Organization Rept. No.

9. Performing Organization Name and Address
MIT/WHOI Joint Program in Oceanography/Applied Ocean Science & Engineering

10. Project/Task/Work Unit No.
MIT/WHOI 98-22

11. Contract(C) or Grant(G) No.
(C) EAR-9304843
(G) EAR-9627613

12. Sponsoring Organization Name and Address
National Science Foundation
Massachusetts Institute of Technology

13. Type of Report & Period Covered
Ph.D. Thesis

14.

15. Supplementary Notes
This thesis should be cited as: Youngsook Huh, 1998. The Fluvial Geochemistry of the Rivers of Eastern Siberia and Implications for the Effect of Climate on Weathering. Ph.D. Thesis. MIT/WHOI, 98-22.

16. Abstract (Limit: 200 words)

The dependence of weathering on climate (temperature and precipitation) forms the core of a negative feedback proposed to have maintained the Earth's atmospheric CO2 within habitable limits for most of its history. This hypothesis has not been proven from field results. Data for chemical compositions and fluxes of periglacial rivers of the Russian Far East—the Lena, Yana, Indigirka, Kolyma, and Anadyr—were acquired and compared to the published dataset on tropical watersheds. Three broad geological divisions are made to facilitate the comparison—the stable basement shield, region of uplift and mountain building, and the sedimentary platform. In all three geologic regions no climatic effect on the rate of uptake of CO2 by aluminosilicate weathering (ϕCO2) was observed. This appears to be due to the unique non-glacial frost shattering processes which expose fresh rock surfaces and thus overcome the effect of temperature inhibition at high-latitudes. On the tropical shields, the lateritic cover builds up due to lack of topography, seals the weathering front from the climatic agents, and lowers weathering rates. There appear to be no primary climatic effects on weathering rates on the present Earth.

17. Document Analysis a. Descriptors
Siberian Rivers
Weathering
Climate

b. Identifiers/Open-Ended Terms

c. COSATI Field/Group

18. Availability Statement	19. Security Class (This Report)	21. No. of Pages
Approved for publication; distribution unlimited.	UNCLASSIFIED	236
	20. Security Class (This Page)	22. Price

(See ANSI-Z39.18) *See Instructions on Reverse*

OPTIONAL FORM 272 (4-77)
(Formerly NTIS-35)
Department of Commerce